ALMA MATER STUDIORUM
UNIVERSITÀ DEGLI STUDI DI BOLOGNA

Dottorato di Ricerca in Ingegneria Elettronica, Informatica e delle Telecomunicazioni

Dipartimento di Ingegneria dell'Energia Elettrica e dell'Informazione "Guglielmo Marconi"

Ciclo XXV

Settore concorsuale: 09/F2 - TELECOMUNICAZIONI

Settore scientifico disciplinare: ING-INF/03 - TELECOMUNICAZIONI

CONTEXT-AWARE WIRELESS NETWORKS

Tesi presentata da:
NICOLÓ DECARLI

Coordinatore Dottorato:
Chiar.mo Prof. Ing.
ALESSANDRO VANELLI-CORALLI

Relatori:
Chiar.mo Prof. Ing.
MARCO CHIANI

Chiar.mo Prof. Ing.
DAVIDE DARDARI

ESAME FINALE 2013

INDEX TERMS

UWB

Time Delay Estimation

Localization

Relay

RFID

Contents

List of Figures

List of Tables

List of Acronyms

AcF autocorrelation function

AcR autocorrelation receiver

ADC analog-to-digital converter

AF amplify & forward

AI automatic identification

AIC Akaike information criterion

AOA angle-of-arrival

AOT approximate optimum threshold

ASNR accumulated signal-to-noise ratio

AWGN additive white Gaussian noise

BEP bit error probability

BER bit error rate

BIC Bayesian information criterion

BPAM binary pulse amplitude modulation

BPPM binary pulse position modulation

BPZF band-pass zonal filter

c.d.f. cumulative distribution function

CAIC consistent Akaike information criterion

CcF crosscorrelation function

CDMA code division multiple access

CEOT channel ensemble optimum threshold

CIR channel impulse response

CR channel response

CRB Cramér-Rao bound

CSI channel state information

CW continuous wave

DBPSK differential binary phase shift keying

DF detect & forward

DP direct path

DS-SS direct-sequence spread-spectrum

ED energy detector

EDR energy detector receiver

EIRP effective radiated isotropic power

ELP equivalent low-pass

FCC Federal Communications Commission

FIM Fisher information matrix

GLRT generalized likelihood ratio test

GPS global positioning system

HPBW half power beam width

INR interference-to-noise ratio

IR impulse radio

ISI inter-symbol interference

isi intra-symbol interference

ISNR interference-plus-signal-to-noise-ratio

ITC information theoretic criteria

JF just forward

KL Karhunen-Loéve

LEO localization error outage

LNA low-noise amplifier

LOS line-of-sight

LRT likelihood ratio test

LS least squares

MAC medium access control

MF matched filter

ML maximum likelihood

MPC multipath component

MSE mean squared error

MUI multi-user interference

NLOS non-line-of-sight

OOK on-off keying

OT optimum threshold

p.d.f. probability density function

PAM pulse amplitude modulation

PD probability of detection

PDP power delay profile

PEB position error bound

PFA probability of false alarm

PN pseudo-noise

PPM pulse position modulation

PRP pulse repetition period

PSD power spectral density

r.v. random variable

RCS radar cross section

RFID radio-frequency identification

rms root mean square

RMSE root-mean-square error

ROC receiver operating characteristic

RRC root raised cosine

RSN radar sensor network

RSSI received signal strength indicator

RTLS real time locating systems

SaG stop-and-go

SCM supply chain management

SNR signal-to-noise ratio

SPMF single-path matched filter

SQNR signal-to-quantization-noise ratio

TDE time delay estimation

TDMA time division multiple access

TDOA time difference-of-arrival

TH time-hopping

TNR threshold-to-noise ratio

TOA time-of-arrival

TR transmitted-reference

UHF ultra-high frequency

UWB ultrawide-band

VGA variable-gain amplifier

WED wall extra delay

WSN wireless sensor network

WSR wireless sensor radar

WSS wide-sense stationary

WWB Weiss-Weinstein bound

ZZB Ziv-Zakai bound

Introduction

Motivations

In the last decades the introduction of pervasive wireless technology revolutionized our daily life making available in almost any time and in any place services able to guarantee communication between people. More recently wireless devices introduced the possibility of connecting to the Internet network not only indoor when using fixed workstations, but also in mobile environments, enabling a myriad of new services capable of sharing data and providing real time information to the end user. Contextually mobile devices, for example cellphones, increased their computational capabilities and different technologies, such as global positioning system (GPS) were incorporated in the same apparatus, opening for the first time the possibility of location-based services, now more and more interconnected with the Internet world. The innovation in wireless computing did not involve the mobile devices for end users only, but also the professional market, as in the case of mobile computing for logistic applications. In this field we faced on the introduction of the concept of "Internet of Things", defined by MIT Auto-ID Labs, according to which the physical world will be mapped into the Internet space, thus enabling a potentially huge number of novel applications [1, 2, 3]. Ideally, it is expected that every object in our every-day life will be assigned to an IP address and will be responsive to the presence of people. From the technological point of view, a key enabling technology is represented by radio-frequency identification (RFID) [4].

The next technological step could be represented by the increasing of aggregation of different technologies and paradigms, enabling services strictly related to the environment in which the device is operating, whatever its nature is. This is the concept of *context-aware* networks. Context-awareness has been introduced in several fields related to wireless services, involving every stack layer, from the physical one to applications. The ideas behind context-aware computing have been presented in [5] where the author indicates a phenomenon for which computing *takes into account the natural* *human environment and allows the computers themselves to vanish into the background.* The term was firstly adopted in [6] referring to systems that *adapt according to their location of use, the collection of nearby people and objects, as well as changes to those objects over time* [7].

The context information can serve on one hand to drive, as anticipated, future applications and services, and on the other hand to improve the network efficiency itself. Examples of both applications can be find in the ideas of context-aware approaches to wireless transmission adaptation [8], context-aware wireless sensor networks [9], context-aware and adaptive security [10] and in a myriad of context-aware applications for monitoring, sensing, security, emergencies, multimedia services [11, 12, 13, 14, 15, 16, 17, 18, 19, 20].

From these works it emerges how the context-awareness, also when intended at application level, implies ad-hoc functionalities that the technology must provide [21, 8, 9, 22, 23]. In fact, context-aware applications need different kinds of information sources. In particular the two pillars are represented by the location information (from which the concept of *location-awareness* is often derived) and the sensors embedded in the devices able to provide data regarding the surrounding environment. Although available services such as GPS can provide accurate location information in outdoor environment, context-aware networking often requires the availability of this information *anywhere* and *anytime*, indoor environments included. Indoor positioning is much more challenging than outdoor and, in recent years, an important research activity has been carried out in order to design practical schemes capable of dealing with the main limitations deriving from the propagation environment and the fact that positioning must be guaranteed in many cases by already existing technologies not originally developed for this kind of service. Localization is usually realized by an infrastructure including tagged nodes (*agents* or *tags*) attached to or embedded in objects and of reference nodes (*anchors*) placed in known positions, which communicate with tags through wireless signals to determine their locations [24].

Figure 1 shows an example of context-aware network where several entities are involved. Specifically, we have a set of mobile or fixed reference nodes, whose position is known, which can communicate with active agents for exchanging information and for determining agents' position. Agents' localization can be performed by extracting some feature from the signal exchanged with reference nodes (e.g., by measuring the distance thanks to time-of-arrival (TOA) estimation or analyzing the received signal strength indicator (RSSI)) also adopting cooperative techniques according to which agents exchange messages and perform measurements among them. Moreover, relay nodes can be adopted to extend the coverage and repeat the wireless signals, to improve both the communication and the localization

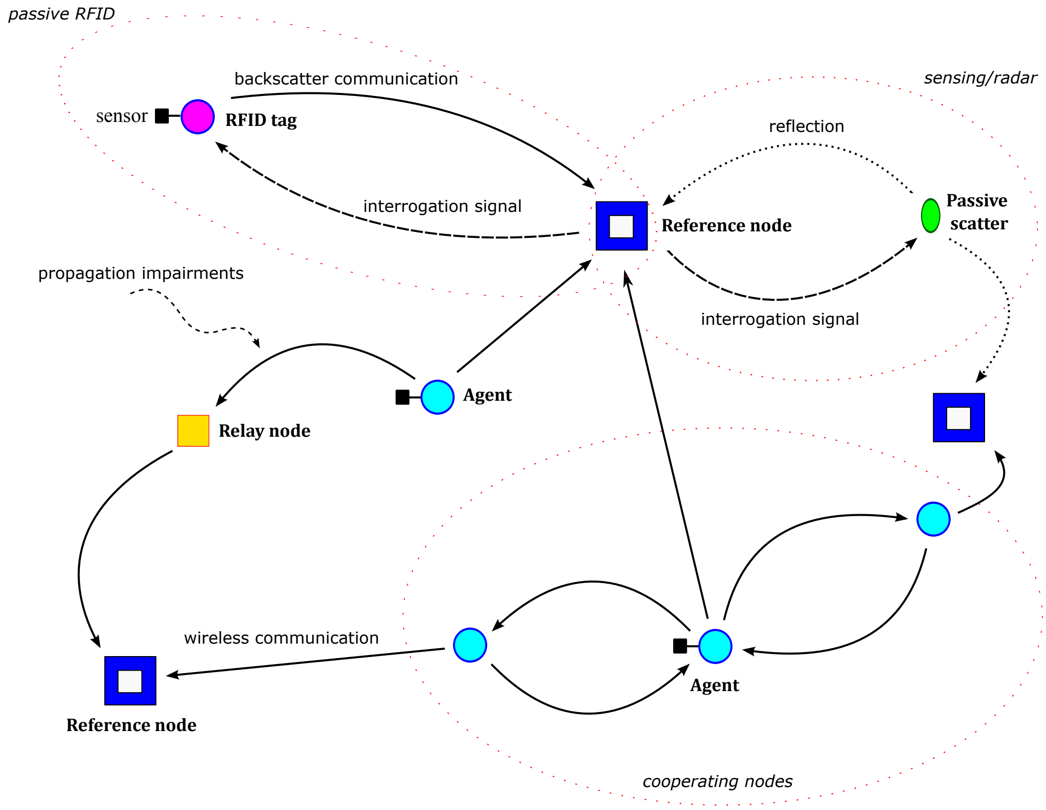

Figure 1: Context-aware wireless network.

processes. In order to exploit the environmental information sensors can be attached to agents so that their measurements are reported to the reference nodes by using wireless communication. Sensing can be performed also by reference nodes, thanks to the transmission of interrogation signals and the analysis of the environmental response from which the extraction of particular features allows detecting the presence of a certain target (a passive scatter) by using radar techniques. Furthermore, interrogation signals emitted by the reference nodes can be exploited by RFID tags capable of modulating them so that the reference node, by analyzing the variations in the interrogation signal response, can detect the presence of the tag. Thanks to the adoption of backscatter modulation a passive wireless channel can be also created between the tag and the reference node so that information can be transmitted (e.g., the data collected by a sensor attached to a tag, or the tag ID). In this example the entities composing the network have to provide communication, localization and sensing. These capabilities must be guaranteed with a reasonable complexity level and the possibility of working in presence of propagation impairments, as happens in indoor environments. Examples of application scenarios are related to wireless sensor networks (WSNs), applications for monitoring factories, security areas (e.g., to detect if intruders are present in a scenario where also authorized persons with tags embedded are moving).

This thesis investigates some topics related to *context-aware wireless networks*, focusing on technological solutions able to provide these kind of services and fulfill particular requirements such as availability of the positioning service also in challenging environments as the indoor ones. The focus is mainly related to the physical layer and to signal processing aspects, and several issues are treated such as performance analysis, algorithms development, fundamental limits and practical solutions for implementation. The applications encompass personal communications, monitoring, logistic, social networking, games, sensing and radar. Due to the demand of a technology able of guarantee both communication capability and possibility of high definition localization, also in difficult propagation environments (as indoor due to the multipath propagation) ultrawide-band (UWB) signals are chosen as candidates for certain type of applications.

The main issues related to the development of such context-aware networks and investigated, in part, in this thesis are related to:

- Propagation impairments: presence of line-of-sight (LOS)/non-line-of-sight (NLOS) channel conditions to be detected, design of localization algorithms able to cope with these situations;
- Estimation of position dependent quantities: e.g., TOA estimation, necessity of understanding the achievable accuracy also when adopting low-complexity estimation techniques and in realistic working conditions;
- Adoption of UWB technology: possibility of providing communication with the same signal adopted for localization, necessity of low-complexity demodulation techniques (non-coherent receivers) able to exploit the indoor multipath channel diversity;
- Coverage problems: introduction of relaying techniques for wireless localization and communication;
- Energy efficiency: adoption of semi-passive techniques such as RFID;
- Sensing and enhanced functionalities: integration of radar with communication and localization;
- Cooperation: exploitation of cooperation among nodes for enhanced localization and for sensing (e.g., multistatic radar).

Thesis Outline

Part I, composed of two chapters, focuses on the communication task, presenting some recent advances in the demodulation of UWB signals, with the introduction of a low-complexity architecture able to exploit the propagation environment characteristics thus improving the performance without adopting complex channel estimation schemes. Specifically, autocorrelation receivers (AcRs) and energy detector receivers (EDRs) are considered. A new method for determining the optimum integration time, to be adopted in the receiver, is proposed and characterized in terms of performance in Chapter 1. Improved receiver structures able to enhance the performance in clustered multipath channels are described and characterized in Chapter 2, also providing an analytical performance evaluation and practical solutions for the receivers optimization.

Part II moves onto the problem of time delay estimation (TDE), or TOA estimation, which is the key enabling processing from which accurate ranging information between wireless devices can be obtained. This is the first step for network localization. In particular, fundamental bounds are derived in the case the received signal is partially known or completely unknown at receiver side, as often happens in practice due to multipath propagation or the need of low-complexity solutions for TOA estimation. Moreover practical estimation schemes, such as the well known energy-based estimators, are also revised and their performance compared with the theoretical bounds. The energy detector (ED) is, in fact, well investigated also from the theoretical point of view for what concerns the detection problem, but a very few theoretical attention has been given to energy-based estimators, widely adopted in practice. The results represent fundamental limits, able to drive the design of practical algorithms for the TOA estimation problem with application to wireless localization and synchronization.

Part III, composed of two chapters, is related to positioning aspects of context-aware wireless networks. In particular Chapter 4 introduces an experimentation methodology for characterizing the performance of cooperative localization services in realistic indoor environments. Algorithms for the detection of LOS/NLOS channel conditions are presented and characterized starting from experimental measured data. It is also proposed a method for exploiting the information coming from environment maps or from channel state identification algorithms for improving the localization accuracy. In many applications cooperation among nodes cannot be exploited due to a complexity limitation demand or the impossibility of a direct communication between nodes. For such situations, Chapter 5 focuses on non-cooperative localization networks in which coverage limitations caused by NLOS channel conditions are mitigated by introducing the idea of non-regenerative relaying for network localization.

Part IV concludes the thesis presenting a broad study on a novel UWB-RFID system, which represents an example of context-aware wireless network particularly suited for logistic and security applications due to its characteristic of providing identification, communication and sensing of the environment also thanks to wireless sensor radar (WSR) methodologies. In this part four chapters analyze different aspects, from system design to implementation, problems related to interference, clutter, multiple access, and propose practical and effective solutions to make the system capable of dealing with these issues maintaining a fundamental low-complexity design. Moreover, a new theoretical derivation presents the fundamental limits in the achievable localization accuracy when adopting passive technologies, such as in the case of the mentioned RFID system or in radar applications.

Contributions

Results presented in this thesis have been, in part, published in the proceedings of international conferences and journals, and in part will be included in following up publications under preparation or revision.

The main results related to non-coherent UWB demodulation, showed in Chapter 1 and Chapter 2, in particular the integration time optimization and the new proposed receiver structure, have been presented in [25] and included in following up journal paper [26].

The new fundamental bounds for the TDE problem, derived in Chapter 3, as well as the results of the comparison with practical estimators, are part of a journal paper currently in preparation [27].

Experiments regarding cooperative localization and techniques for harnessing environmental information, presented in Chapter 4, have been included in the journal publication [28] and in the conference proceeding [29]. The novel relaying techniques for enhanced performance and coverage in network localization have been introduced in [30] and extended in a journal paper currently under review [31].

Outcomes of the case study on the novel UWB-RFID system have been presented in the conference publications [32, 33, 34, 35, 36], and are included in two following up journal papers [37, 38]. This part has been developed within the European project SELECT,[1], and thanks to the fruitful cooperation with the partners Datalogic IP Tech s.r.l.,[2] Fraunhofer Institute for

[1] `www.selectwireless.eu`
[2] `www.datalogic.com`

Integrated Circuits IIS,[3] Commissariat a l'Energie Atomique et aux Energies Alternatives Laboratory of Electronic and Information Technologies (CEA-LETI),[4] Centro de Estudios e Investigaciones Tecnicas de Gipuzkoa (CEIT),[5] Association pour la Recherche et le Développement des Méthodes et Processus Industriels (ARMINES),[6] NOVELDA AS,[7] and Iskra Sistemi.[8]

Beside the European project SELECT, the work has been carried out in the context of the European Network of Excellence in Wireless Communication NEWCOM++,[9] and the European project EUWB.[10] Several outcomes, in part included in this thesis, can be found in the project deliverables [39, 40, 41, 42, 43, 44, 45, 46].

The theoretical investigation of Part II and the experimental activity described in Part III have been developed, in part, during a visit period at Massachusetts Institute of Technology (MIT).

---

[3] `www.iis.fraunhofer.de`
[4] `www-leti.cea.fr`
[5] `www.ceit.es`
[6] `www.armines.net`
[7] `www.novelda.no`
[8] `www.iskrasistemi.si`
[9] `www.newcom-project.eu`
[10] `www.euwb.eu`

Part I

Non-Coherent Signal Demodulation

Introduction

There has been considerable interest in utilizing UWB spread-spectrum communications [47, 48] for military, homeland security, and commercial applications [49, 50]. UWB systems, in particular impulse radio (IR)-UWB systems, involve the transmission of extremely narrow pulses in conjunction with time-hopping (TH) and/or direct-sequence spread-spectrum (DS-SS) techniques to allow multiple user access, and pulse position modulation (PPM) or pulse amplitude modulation (PAM) for data transmission. One of the key peculiarities of UWB technology is related to the possibility of performing high-accuracy TOA estimation [51], opening the possibility to high-definition network localization in harsh, dense multipath environments [52, 28]. The possibility of enabling, with the same signal, both high-speed communication, even in harsh propagation environments, and high-accuracy TOA estimation, and hence positioning, appears very appealing for context-aware networking.

UWB results very robust also in dense multipath environments, (e.g. indoor), where receivers can effectively take advantage of the large number of resolvable multipath components that arise from extremely large transmission bandwidths [53, 54, 55, 56, 57]. One big issue is how to exploit this inherent system diversity. In fact, as the number of multipath components grows, conventional architectures become increasingly inadequate for capturing all the available multipath energy [58]. Furthermore optimal coherent detection of UWB signals, that is a matched filter based detection, requires complex channel estimation at the receiver to build a local reference [59]. These problems can be alleviated by using non-coherent demodulation techniques [60].

Usually, the *non-coherent* definition is referred to receivers working on signal envelope, that is, without knowledge of the signal carrier phase [61, 62, 63, 64, 65]. Non-coherent receivers have a complexity advantage since, exploiting the envelope only information, carrier recovery is avoided. When adopting IR-UWB signals a non-coherent receiver can exploit the envelope of the channel response (CR).[11] In this manner it is completely avoided the recovering of the phase, amplitude, and timing information of each multipath component (MPC) as required for ideal matched filtering. In fact, the optimum non-coherent receiver consist of a filter matched to received waveform envelope (i.e., working without the phase information), followed by an energy evaluation, or ED [66, 61]. Adopting this approach in the IR-UWB case the optimum non-coherent receiver would require a filter matched to the UWB

[11]Note that with this kind of signals the phase changes from multipath component (MPC) to MPC [60].

CR envelope prior to and ED [60]. It is obvious that this process would destroy the complexity advantage, due to the impossibility of prior knowledge of the CR envelope (as well as low-complexity estimation). Hence practical solutions have been proposed in literature, mainly based of two receiver and signaling structures: the AcR in conjunction with transmitted-reference (TR) signaling; the EDR [60].

TR technique was firstly considered in the early 1960s and involves the transmission of a reference and data signal pair, separated either in time [67] or in frequency [68].[12] Due to the simplicity of TR signaling, there is renewed interest in its use for UWB systems, in conjunction with PAM [69, 70, 71, 72, 73, 74], to exploit multipath diversity inherent in the environment without the need of channel estimation and stringent acquisition. Multiple variations of the classical TR signaling have been recently proposed in order to overcome the main limitation of the traditional scheme where a long wideband analog delay line is required at receiver side [75, 76, 77]. Differently, EDRs are based on the observation of the received signal energy, and are adopted with on-off keying (OOK) modulation or PPM [60].

Chapter 1 and 2 treat these non-coherent demodulation techniques, proposing different methodologies able to enhance the performance, by keeping low the complexity of the demodulation process.

[12]It is necessary that this pair of signals experiences the same channel, so either the time separation must be less than the channel coherence time, or the frequency separation must be less than the channel coherence bandwidth.

Chapter 1

Integration Time Optimization in Non-Coherent Receivers

1.1 Motivations

In order to achieve optimal performance in a non-coherent UWB system, the integration time T of the AcR and EDR must be optimized [78, 60]. If T is small, part of the useful multipath energy will not be collected. On the other hand, large T may result in noise accumulation where multipath is negligible or absent. In literature various works focused on integration time optimization are present, especially for the TR signaling in conjunction with EDRs. The importance of a proper setting of this parameter is underlined in [79] where the problem is addressed as a generalized likelihood hypothesis test for channel delay spread estimation or for the maximization of the effective signal-to-noise ratio (SNR) at the receiver. The major difficulty is due to the fact that the optimum integration time is not equal to the channel excess delay since the last multipath components generally exhibit a high attenuation and a consecutive high noise degradation leading, in this way, to a less significant contribution on the captured energy. For this motivation many works are based on particular assumptions on the channel characteristics: [80, 81, 82, 83] study the optimal integration time for different channel models such as IEEE 802.15.3a, Saleh-Valenzuela, and exponential power delay profile (PDP). A different approach is followed in [84] where a data-aided technique is presented. Other possibilities to improve performance are modified TR schemes, such as TR pulse cluster system [85]. In general available techniques assume a given PDP or channel model, assumptions in general too strong for a system capable of working in a real environment. In fact, in a real indoor environment, there are large variations of delay spread values as highlighted in various measurements campaigns [56].

In this chapter, a method for determining the integration time, which does not require any a-priori knowledge on the channel propagation characteristics and SNR, is proposed. The strategy is based on information theoretic criteria (ITC) for model order selection.

The discussion is here focused on the AcR with TR signaling, but can be easily extended to others non-coherent UWB demodulation techniques. Moreover, a more general and robust solution, able of further improving the performance is presented in Chapter 2.

The remainder of the chapter is organized as follows. In Section 1.2, system and channel model used for the results validation are introduced. In Sec. 1.3, the proposed integration time determination scheme is described. Some numerical results are presented in Sec. 1.4 where the bit error probability (BEP) expected for TR systems optimized with this blind approach is presented. Finally, a chapter conclusion is given in Sec. 1.5.

1.2 Signal and Channel Models

1.2.1 Transmitted-Reference Signaling

Focusing on a generic user k, the transmitted signal, according with the TR scheme, can be decomposed into a reference signal block $b_{\mathrm{r}}^{(k)}(t)$ and a data modulated signal block $b_{\mathrm{d}}^{(k)}(t)$. The transmitted signal is therefore given by

$$s(t) = \sum_{i} b_{\mathrm{r}}^{(k)}(t - iN_{\mathrm{s}}T_{\mathrm{f}}) + d_i^{(k)} b_{\mathrm{d}}^{(k)}(t - iN_{\mathrm{s}}T_{\mathrm{f}}) \tag{1.1}$$

where T_{f} is the average pulse repetition period, $d_i^{(k)} \in \{-1, 1\}$ is the ith data symbol, $N_{\mathrm{s}}T_{\mathrm{f}}$ is the symbol duration (i.e., duration of each block), and $N_{\mathrm{s}}/2$ is the number of transmitted signal pulses in each block. The reference signal and modulated signal blocks, for the conventional TR implementation, can be written as

$$\begin{aligned} b_{\mathrm{r}}^{(k)}(t) &= \sum_{j=0}^{\frac{N_{\mathrm{s}}}{2}-1} \sqrt{E_{\mathrm{p}}} a_j^{(k)} p(t - j2T_{\mathrm{f}} - c_j^{(k)} T_{\mathrm{p}}) \,, \\ b_{\mathrm{d}}^{(k)}(t) &= \sum_{j=0}^{\frac{N_{\mathrm{s}}}{2}-1} \sqrt{E_{\mathrm{p}}} a_j^{(k)} p(t - j2T_{\mathrm{f}} - c_j^{(k)} T_{\mathrm{p}} - T_{\mathrm{r}}) \end{aligned} \tag{1.2}$$

where $p(t)$ is a unit energy bandpass signal pulse with duration T_p and center frequency f_c. The energy of the transmitted pulse is then $E_\mathrm{p} = E_\mathrm{s}/N_\mathrm{s}$, where E_s is the symbol energy. Considering binary signaling the symbol energy equals the energy per bit, E_b. In order to allow multiple access and mitigate interference, DS-SS and/or TH spread-spectrum techniques can be used as accounted for in (1.2). In case of DS-SS signaling $\left\{a_j^{(k)}\right\}$ is the bipolar pseudo-random sequence of the k-th user. For the TH signaling scheme $\left\{c_j^{(k)}\right\}$ is the pseudo-random TH sequence related to the k-th user, where $c_j^{(k)}$ is an integer in the range $0 \leq c_j^{(k)} < N_\mathrm{h}$, and N_h is the maximum allowable integer shift. The duration of the received UWB pulse is $T_\mathrm{g} = T_\mathrm{p} + T_\mathrm{d}$, where T_d is the maximum excess delay of the channel. To preclude inter-symbol interference (ISI) and intra-symbol interference (isi), we assume that $T_\mathrm{r} \geq T_\mathrm{g}$ and $N_\mathrm{h} T_\mathrm{p} + T_\mathrm{r} \leq 2T_\mathrm{f} - T_\mathrm{g}$, where T_r is the time separation between each pair of data and reference pulses.

1.2.2 Channel Model

The received signal can be written as[1]

$$r(t) = s(t) \otimes h(t) + n(t) \tag{1.3}$$

where $h(t)$ is the channel impulse response (CIR) and $n(t)$ is zero-mean, white Gaussian noise with two-sided power spectral density $N_0/2$. We consider a linear time-invariant multipath channel with CIR $h(t) = \sum_{l=1}^{L} \alpha_l \delta(t - \tau_l)$, where $\delta(\cdot)$ is the Dirac-delta distribution, L is the number of multipath components, and α_l and τ_l respectively denote the amplitude and delay of the l-th path.

1.2.3 Autocorrelation Receiver Structure

Without loss of generality, we consider now a single user system, therefore we omit the index k in the rest of the chapter. As shown in Fig. 1.1, the conventional AcR first passes the received signal through an ideal band-pass zonal filter (BPZF) with center frequency f_c to eliminate out-of-band noise. If the bandwidth W of the BPZF is wide enough, signal distortions and consequently ISI and i.s.i. caused by filtering is negligible.

The received signal at the output of the BPZF can be written as

[1] The notation $\otimes$ stands for continuous-time convolution.

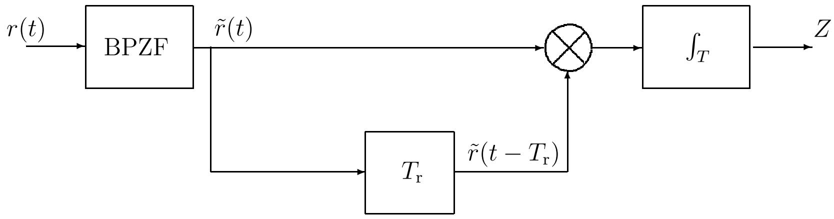

Figure 1.1: Conventional autocorrelation receiver.

$$
\begin{aligned}
\widetilde{r}(t) &= s(t) \otimes h(t) \otimes h_{\mathrm{ZF}}(t) + \widetilde{n}(t) \\
&= \sum_{i} \sum_{j=0}^{\frac{N_s}{2}-1} \sum_{l=1}^{L} \sqrt{E_{\mathrm{p}}} \alpha_l a_j p(t - iN_{\mathrm{s}}T_{\mathrm{f}} - j2T_{\mathrm{f}} - c_j^{(k)} T_{\mathrm{p}} - \tau_l) \\
&+ \sqrt{E_{\mathrm{p}}} \alpha_l a_j d_i p(t - iN_{\mathrm{s}}T_{\mathrm{f}} - j2T_{\mathrm{f}} - c_j^{(k)} T_{\mathrm{p}} - T_{\mathrm{r}} - \tau_l) + \widetilde{n}(t) \\
&= \widetilde{w}(t) + \widetilde{n}(t), \qquad (1.4)
\end{aligned}
$$

where $h_{\mathrm{ZF}}(t)$ is the impulse response of the BPZF and $\widetilde{n}(t)$ is the filtered thermal noise.

The filtered received signal is then passed through a correlator with integration interval T, as shown in Fig. 1.1. Under the hypothesis of perfect synchronization, considering the detection of the data symbol at $i = 0$, the decision statistic for TR signaling is then given by

$$
Z = \sum_{j=0}^{\frac{N_{\mathrm{s}}}{2}-1} \int_{j2T_{\mathrm{f}}+T_{\mathrm{r}}+c_jT_{\mathrm{p}}}^{j2T_{\mathrm{f}}+T_{\mathrm{r}}+c_jT_{\mathrm{p}}+T} \widetilde{r}(t)\, \widetilde{r}(t - T_{\mathrm{r}})\, dt\,. \qquad (1.5)
$$

In the next section we propose a strategy to determine the optimum integration time T.

1.3 Integration Time Determination

The aim of this section is to present a totally blind approach to determine the value of the integration time T that allows the receiver to approach the best compromise between the useful captured energy and the excessive noise accumulation caused by the reference signal.

Figure 1.2 represents the block diagram of the receiver for the integration time determination. The filtered received signal is firstly passed in an ED to

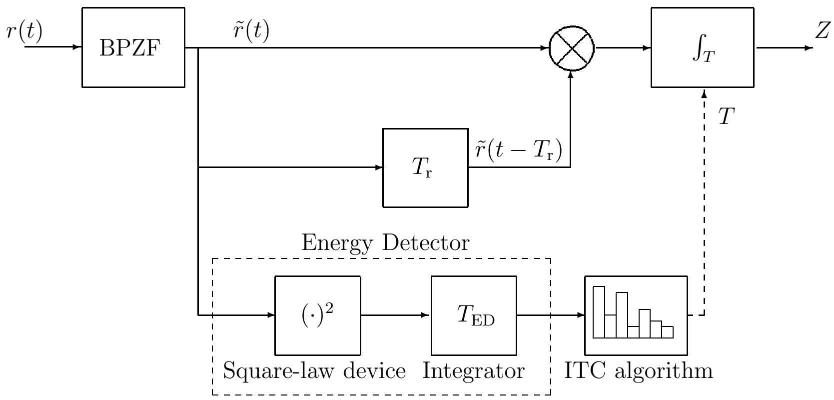

Figure 1.2: AcR with proposed integration time estimation.

collect signal energy in a certain time slot (or bin) of duration T_{ED} within the observation interval $T_{\text{ob}} \le T_{\text{r}}$. The ED is composed of a square-law device followed by an integrate-and-dump device whose integration time is T_{ED}, thus $N_{\text{bin}} = \lfloor T_{\text{ob}}/T_{\text{ED}} \rfloor$ consecutive energy samples (named energy profiles) are collected.

Suppose now to collect N_{ob} received signal energy profiles assuming that the channel is invariant for the entire acquisition time. The collected energy samples can be arranged in a $N_{\text{ob}} \times N_{\text{bin}}$ matrix, denoted by $\mathbf{Y}$, with elements

$$y_{l,n} = \int_{t_n}^{t_{n+1}} \widetilde{r}^2(t)\, dt \tag{1.6}$$

for $n = 0, \ldots, N_{\text{bin}} - 1$ and $l = 0, \ldots, N_{\text{ob}} - 1$. Integration intervals t_n are chosen to ensure the alignment of the received pulses, for example considering $N_{\text{s}} = 2$ we have $t_n = c_0 T_{\text{p}} + l2T_{\text{f}} + T_{\text{r}} + nT_{\text{ED}}$.

The probability density function (p.d.f.) of the random variable (r.v.) (1.6) can be evaluated using the equivalent low-pass (ELP) representation of $\widetilde{r}(t)$ and the sampling theorem as presented in [86]. In particular, it is possible to show that (1.6) is a non-central Chi-square distributed r.v. with $\nu = 2WT_{\text{ED}}$ degrees of freedom, that is with p.d.f. [86]

$$f(y; \lambda_n, \sigma^2) = \frac{W}{\sigma^2} \left(\frac{y}{\lambda_n}\right)^{\frac{\nu-2}{4}} \exp\left(-\frac{(y+\lambda_n)}{\sigma^2/W}\right) I_{\frac{\nu}{2}-1}\left(\frac{2\sqrt{y\lambda_n}}{\sigma^2/W}\right) \tag{1.7}$$

with $y \ge 0$, where $\sigma^2 = N_0 W$ represents the noise power, $I_m(\cdot)$ is the m-th order modified Bessel function of the first kind, λ_n is the non-centrality parameter representing the energy of the noise-free received waveform in T_{ED} given by

$$\lambda_n = \int_{t_n}^{t_{n+1}} \widetilde{w}(t)^2 \, dt. \tag{1.8}$$

In the case that a bin contains only noise, (1.7) reduces to a central Chi-square distribution with p.d.f. given by [86]

$$f(y;\sigma^2) = \left(\frac{W}{\sigma^2}\right)^{\frac{\nu}{2}} \frac{y^{\frac{\nu}{2}-1}}{\Gamma(\frac{\nu}{2})} \exp\left(-\frac{Wy}{\sigma^2}\right), \qquad y \geq 0 \tag{1.9}$$

where $\Gamma(\cdot)$ is the Gamma function.

Received signal energy profiles contained in the matrix $\mathbf{Y}$ are then analyzed to detect the last energy bin that contains an useful amount of energy from which the optimum integration time T is determined. The algorithm used to decide if significant energy is present in a certain bin is based on ITC typically adopted in model order selection problems [87, 88].

The rationale behind the use of model order selection strategy to find the integration time is the following. We define a family of models to fit observed data. The family of models is chosen in a way that for each model, the number of free adjusted parameters (unknown parameters) is univocally related to the number of signal-plus-noise bins.[2] Model order selection chooses the model that best fit the data, which results in a model with the number of unknown parameters that allows to determine the effective sets of signal-plus-noise bins and noise-only bins, respectively [89]. Once the set of signal-plus-noise bins is known, the integration time can be readily calculated from the index of the last bin in this set.

Having defined a family of models to fit the observed data (in our case represented by a matrix $\mathbf{X}$) dependent on a certain unknown number k of parameters, $\boldsymbol{\Theta}^{(k)}$, a model order selection rule has the purpose of choosing the number $\widehat{k}$ of parameters (in our case the number of bins containing useful energy) that allows to best fit the data.

Formalizing the problem, the ITC chooses as $\widehat{k}$ the value that minimizes the function

$$\mathrm{ITC}(k) = -2 \ln f\left(\mathbf{X}; \widehat{\boldsymbol{\Theta}}^{(k)}\right) + \mathcal{L}(k) \tag{1.10}$$

where $f(\cdot;\cdot)$ is the likelihood of observed data $\mathbf{X}$, $\widehat{\boldsymbol{\Theta}}^{(k)}$ is the vector of the estimated parameters under k-th model order hypothesis, and $\mathcal{L}(k)$ is a penalty factor associated to the specific model order selection rule as defined later.

[2]Since we assume that the noise variance is not known, one of the free adjusted parameters is the noise variance.

In order to exploit this model order selection strategy for our problem, we proceed with an approach similar to that presented in [89] which can be summarized in the following steps.

1. Starting from the collected energy samples $\mathbf{Y}$ construct the vector $\mathbf{d}$, adopted for unknown parameters estimation, by column averaging

$$d_n = \sum_{l=0}^{N_{\text{ob}}-1} y_{l,n}\,, \quad n = 0, \ldots, N_{\text{bin}} - 1\,. \tag{1.11}$$

2. Sort the vector $\mathbf{d}$ in decreasing order obtaining $\mathbf{z}$. We indicate with $\boldsymbol{\pi} = (\pi_0, \pi_1, \ldots, \pi_{N_{\text{bin}}-1})$ a vector of permutation indexes, so that $z_n = d_{\pi_n}$. Then, define the matrix of observed data, $\mathbf{X}$, that contains the columns of $\mathbf{Y}$ re-arranged according to the same ordering, that is, $x_{l,n} = y_{l,\pi_n}$.

3. In the k-th model order hypothesis, perform estimation of the parameters vector

$$\widehat{\boldsymbol{\Theta}}^{(k)} = \Big(\underbrace{\widehat{\lambda}_0^{(k)}, \ldots, \widehat{\lambda}_{k-1}^{(k)}}_{k \text{ bins with energy}}, \underbrace{0, \ldots\ldots\ldots\ldots, 0}_{N_{\text{bin}}-k \text{ noise-only bins}}, \widehat{\sigma}^2_{(k)} \Big) \tag{1.12}$$

where[3]

$$\widehat{\lambda}_n^{(k)} = \left(z_n - \frac{\nu \widehat{\sigma}^2_{(k)}}{2W} \right)^+, \quad n = 0, \ldots, k-1\,, \tag{1.13}$$

is the non-centrality parameter estimate (i.e., signal energy estimate) of the n-th ordered bin, and $\widehat{\sigma}^2_{(k)}$ is the maximum likelihood (ML) estimate of noise power σ^2, that is,

$$\widehat{\sigma}^2_{(k)} = \frac{1}{T_{\text{ED}}} \frac{\sum_{q=k}^{N_{\text{bin}}-1} z_q}{N_{\text{bin}} - k}\,. \tag{1.14}$$

4. Evaluate ITC(k) for $k = 1, \ldots, N_{\text{bin}} - 1$ and take as $\widehat{k}$ the value of k which minimize (1.10), that is

$$\widehat{k} = \underset{k \in \{1,..,N_{\text{bin}}-1\}}{\text{argmin}} \; \text{ITC}(k) \tag{1.15}$$

[3]The operator $(x)^+$ stands for the positive part of x, that is $(x)^+ = \max(0, x)$. Note that the maximum likelihood (ML) estimator of the non-centrality parameter of a Chi-square r.v. cannot be expressed in closed-form. However, in [90] it is shown that (1.13) is a good approximation of the ML estimate when $\nu > 1$.

5. Now $\widehat{k}$ is an estimate of the number of bins, in the received signal, containing useful energy. Then, the integration time T in the AcR can be set from the permutation vector $\boldsymbol{\pi}$ as

$$T = T_{\mathrm{ED}} \cdot \max_{i=0 \dots \widehat{k}-1} \{\pi_i\} \, . \tag{1.16}$$

The joint p.d.f. of the matrix $\mathbf{X}$ in (1.10) can be calculated considering that the output of the energy detector consists of independent random variables in $n = 0, \dots, N_{\mathrm{bin}} - 1$ and $l = 0, \dots, N_{\mathrm{ob}} - 1$. Therefore we have

$$-2 \ln f\left(\mathbf{X}; \widehat{\mathbf{\Theta}}^{(k)}\right) = -2 \sum_{l=0}^{N_{\mathrm{ob}}-1} \sum_{n=0}^{N_{\mathrm{bin}}-1} \ln f\left(x_{l,n}; \widehat{\Theta}_n^{(k)}, \widehat{\sigma}^2_{(k)}\right) \tag{1.17}$$

where $f(\cdot;\cdot)$ is given by (1.7) for the first k bins containing the useful signal and by (1.9) for the last $N_{\mathrm{bin}} - k$ bins containing only noise.

The algorithm assumes that, under the model order hypothesis k, the first k bins contains useful energy and therefore are represented by (1.7), and the last $N_{\mathrm{bin}} - k$ bins are noise-only bins so they are represented by (1.9). Then, the model that best fit the data is chosen as the estimate, $\widehat{k}$, of the number of signal-plus-noise bins. The complexity in evaluating (1.17) can be drastically reduced using approximations of the statistical distribution of energy samples, $y_{l,n}$, without significant performance loss, as shown in [89].

Note that, equation (1.7) returns an indeterminate form in the case the estimated parameter (1.13) is equal to zero. However, the noise power estimation is performed on the bins taken from the ordered vector $\mathbf{z}$, hence $\widehat{\sigma}^2_{(k)}$ is always smaller than, or equal to, the energy of the presumed signal-plus-noise bin, guaranteeing that $\widehat{\lambda}_n^{(k)} > 0$, $n = 0, \dots, k-1$.

As far as the penalty factor $\mathcal{L}(k)$ is concerned, it is related to the number $k+1$ of free adjusted parameters, and the number of observations N_{ob}. Different penalty factors are proposed in literature depending on their capability to correctly estimate the model order. In this work we considered three penalty factors widely adopted in the literature [87, 88, 91]:

- $\mathcal{L}(k) = 2(k+1)$ (Akaike information criterion (AIC));
- $\mathcal{L}(k) = (k+1) \log N_{\mathrm{ob}}$ (Bayesian information criterion (BIC));
- $\mathcal{L}(k) = (k+1)(\log N_{\mathrm{ob}} + 1)$ (consistent Akaike information criterion (CAIC)).

The performance of a TR-AcR with integration time estimation based on these penalty factors will be compared in the next section.

1.4 Numerical Results

In this section, numerical results are presented to illustrate the performance of the proposed blind integration time estimation scheme. For BEP analysis we have followed the approach presented in [78] using semi-analytical Monte Carlo simulations with 300 different channel realizations for each channel model analyzed. In particular, we consider a TR-AcR scheme that adopts $N_\mathrm{s} = 2$ pulses per information bit; root raised cosine (RRC) pulses[4] with pulse width parameter $T_\mathrm{w} = 0.95\,\mathrm{ns}$, roll-off factor $\nu = 0.6$, center frequency $f_\mathrm{c} = 3.95\,\mathrm{GHz}$, and an ideal BPZF with bandwidth $W = 1/T_\mathrm{w}$ centered at frequency f_c. Results are given for two different multipath channel models. The first one is a tapped-delay line channel model with an exponential PDP [78] with $L = 100$ independent paths spaced apart of T_p, each with Nakagami-m distributed amplitudes with parameter $m = 2$, a probability $a = 0.8$ of having a path in a given time slot and a power decay factor $G = 0.09$. The second one is the IEEE 802.15.4a CM4 type (indoor office, NLOS) model [92]. Channel impulse responses have been truncated to $T_\mathrm{g} = 100\,\mathrm{ns}$ since, with the parameters specified, after T_g seconds the channel impulse response vanishes and does not provide significant energy. For the ITC algorithms an energy detection time $T_\mathrm{ED} = 5T_\mathrm{p}$, $N_\mathrm{ob} = 128$ channel observations and $T_\mathrm{ob} = T_\mathrm{g}$ have been adopted.

Figure 1.3 compares the BEP for the AcR with fixed integration time and for the AcR with the proposed blind integration time determination algorithm. In particular the curve in dot-dashed line ($- \cdot$) is related to the receiver with fixed integration time which captures all the multipath components (integration time equal to the maximum excess delay $T_\mathrm{d} = 100\,\mathrm{ns}$). The dashed curve (- -) is for the receiver with the *channel ensemble optimum integration time*: this one has been found *a-posteriori* for the considered channel model as the value that minimize the BEP for each SNR. The continuous curves (–) in the same figure represent the performance of the proposed blind integration time estimation scheme, where for each channel realization, the integration time is determined by the receiver observing N_ob energy profiles. The results obtained show that AIC tends to overestimate the useful channel length resulting in noise accumulation that produces performance comparable to that of the fixed (maximum) integration time. Better results are given by the BIC, while CAIC determines the best integration time for the AcR receiver. Despite the proposed algorithm is completely blind, the performance of CAIC is coincident to that with the channel ensemble optimum integration time.

[4] See (3.63) for the definition.

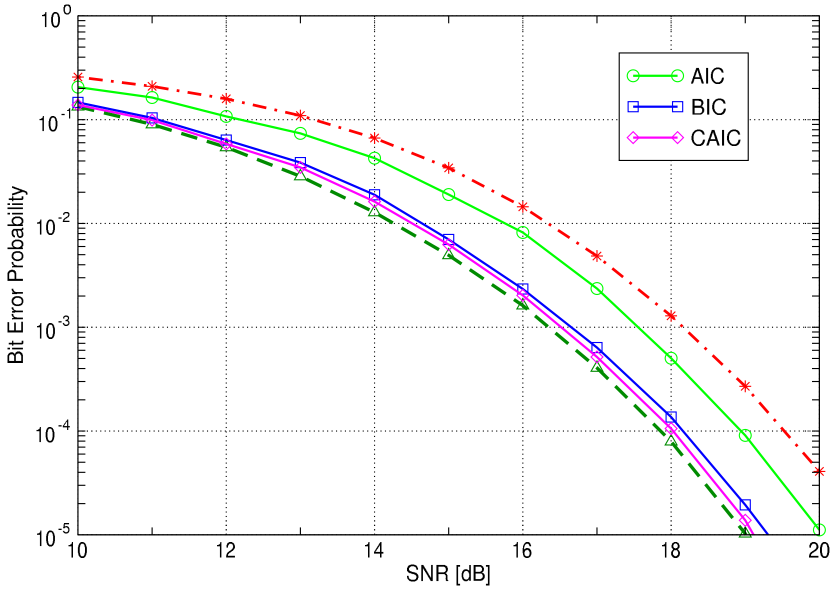

Figure 1.3: BEP for the TR AcR as a function of the SNR for exponential PDP channel model, considering different strategies for the integration time determination.

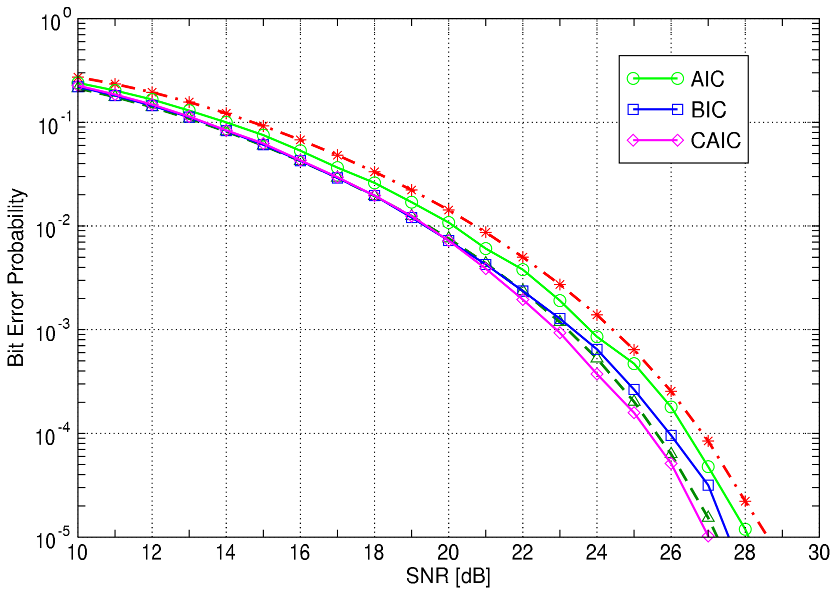

Figure 1.4: BEP for the TR AcR as a function of the SNR for IEEE 802.15.4a CM4 channel model, considering different strategies for the integration time determination.

Figure 1.4 shows the performance of the same system for the IEEE 802.15.4a CM4 channel model. The behavior of the TR-AcR with various integration time determination are essentially the same as in Fig. 1.3. Note that here, the performance obtained with CAIC are in some cases slightly better than the channel ensemble optimum integration time: this is due to the fact that the channel ensemble optimum integration time is an average value determined *a-posteriori* for the given channel model while the ITC algorithm estimates the optimal integration time T for each channel realization.

In both cases it is possible to see that the integration time determined with the proposed algorithm can give about 2 dB gain at 10^{-4} BEP over the fixed integration time equal to the channel maximum excess delay. Higher gains for the proposed scheme are expected in real environments where the channel delay spread can exhibits significant variations.

1.5 Conclusion

In this chapter, a blind algorithm for the integration time determination in TR-AcRs has been proposed. The algorithm is based on information theoretic criteria for model order selection, and is able to find the portion of the received signal that contains useful energy minimizing the collection of noise energy. The algorithm analyzes the energy profile of the received signal and identifies the appropriate integration time without the need of any additional hypothesis on the channel statistics, noise power, and SNR. Simulation results show that the proposed blind algorithm provides at least the same performance as that achievable by the channel ensemble optimum integration time which is determined *a-posteriori* having specified a channel model. The proposed approach requires, in general, synchronization at the receiver side, and presents good performance in dense multipath channels. When the CIR includes clustered multipath, an important improvement can be achieved with the novel solution presented in Chapter 2.

Chapter 2

Stop-and-Go Receivers

2.1 Motivations

In Chapter 1 it has been shown how the integration time T plays a fundamental role on the performance achievable by non-coherent UWB demodulation schemes, as well known from the literature [25, 82, 79, 80, 81, 85, 83, 84, 93]. However, when the channel PDP involves multipath clusters, the collection of excessive noise is unavoidable regardless of the choice of T since a certain amount of the integrated signal is composed of noise only. In order to enhance the effective SNR of non-coherent receivers, different weighting strategy have been proposed for both AcRs and EDRs [94, 95, 96, 97, 98, 99], based on assigning small weights to those portions of the received signal containing a small amount of multipath energy. The main drawback of these techniques is the need of a-priori channel knowledge or a potentially complex weights selection procedure that requires parameters estimation and functions minimization at the receiver.

In this chapter, a low complexity strategy, based on the work [100] and capable of alleviating excessive noise accumulation, for non-coherent UWB demodulation is introduced. The proposed stop-and-go (SaG) scheme allows the AcR and the EDR to stop integrating whenever there is no significant signal energy present in the channel output. The main advantages of the proposed scheme over conventional AcR and EDR are:

- The maximum integration time T can be kept as large as possible (e.g., equal to the maximum expected channel excess delay) without noise penalty;
- No a-priori channel information is required to optimize the performance;

- Better performance than conventional TR-AcR and EDR, even when adopting integration time optimization, in the presence of clustered multipath.

The analysis is here carried out considering the classical TR-binary pulse amplitude modulation (BPAM) implementation with the reference and data pulses separated in time domain when adopting the AcR, and binary pulse position modulation (BPPM) when adopting the EDR: however the proposed scheme can be applied to different non-coherent UWB demodulators and different signaling formats such as code-multiplexed TR [76], OOK-EDR or M-PPM-EDR [60].

The remainder of the chapter is organized as follows. In Sec. 2.2, the system and the channel model are introduced. In Sec. 2.3, the proposed scheme is described. In Sec. 2.4, performance in terms of BEP for both AcR with TR BPAM and EDR with BPPM are analyzed. The sampling expansion approach originally proposed in [101] is adopted to analyze the SaG receiver schemes. In particular a semi-analytical method to evaluate the BEP of the SaG exploitable for any kind of multipath channel is derived. Section 2.5 shows different strategies to optimize the performance of the proposed SaG receivers. Numerical results are presented in Sec. 2.6 to show the performance gain of the SaG receivers in comparison with a classical AcR or EDR. Finally, a conclusion is given in Sec. 2.7.

2.2 Signal and Channel Model

2.2.1 TR-BPAM

In TR-BPAM signaling, the transmitted signal for a generic user[1] can be decomposed into a reference signal block $b_\mathrm{r}(t)$ and a data modulated signal block $b_\mathrm{d}(t)$. The band-pass transmitted signal is given by

$$s_\mathrm{TR}(t) = \sum_i b_\mathrm{r}(t - iT_\mathrm{s}) + d_i b_\mathrm{d}(t - iT_\mathrm{s}) \tag{2.1}$$

where $T_\mathrm{s} = N_\mathrm{s} T_\mathrm{f}^\mathrm{TR}$ is the symbol time, with T_f^TR the average pulse repetition period, $d_i \in \{-1, 1\}$ the ith data symbol, and where $N_\mathrm{s}/2$ is the number of transmitted signal pulses in each block [69, 102, 70]. The reference signal

[1] Without loss of generality we focus on a single user system to simplify the mathematical notation.

and the modulated signal blocks can be written as[2]

$$
\begin{aligned}
b_{\mathrm{r}}(t) &= \sum_{j=0}^{\frac{N_{\mathrm{s}}}{2}-1} \sqrt{E_{\mathrm{p}}^{\mathrm{TR}}}\, a_j\, p(t - j2T_{\mathrm{f}}^{\mathrm{TR}} - c_j T_{\mathrm{p}}) \,, \\
b_{\mathrm{d}}(t) &= \sum_{j=0}^{\frac{N_{\mathrm{s}}}{2}-1} \sqrt{E_{\mathrm{p}}^{\mathrm{TR}}}\, a_j\, p(t - j2T_{\mathrm{f}}^{\mathrm{TR}} - c_j T_{\mathrm{p}} - T_{\mathrm{r}})
\end{aligned}
\tag{2.2}
$$

where $p(t)$ is the normalized band-pass signal pulse with duration T_{p}, center frequency f_{c} and unit energy. The energy of the transmitted pulse is then $E_{\mathrm{p}}^{\mathrm{TR}} = E_{\mathrm{s}}^{\mathrm{TR}}/N_{\mathrm{s}}$, where $E_{\mathrm{s}}^{\mathrm{TR}}$ is the symbol energy associated with TR signaling. In the case of binary signaling that we are considering, the symbol energy equals the energy per bit, E_{b}. Note that the transmitted energy is equally allocated among $N_{\mathrm{s}}/2$ reference pulses and $N_{\mathrm{s}}/2$ modulated pulses. To enhance the robustness of TR systems against interference and to allow multiple access, DS-SS and/or TH spread-spectrum techniques can be used as shown in (2.2). In case of DS-SS signaling $\{a_j\}$ is the bipolar pseudo-random sequence of the user. For the TH signaling $\{c_j\}$ is the pseudo-random TH sequence related to the user, where c_j is an integer in the range $0 \le c_j < N_{\mathrm{h}}$, and N_{h} is the maximum allowable integer shift. The duration of the received UWB pulse is $T_{\mathrm{g}} = T_{\mathrm{p}} + T_{\mathrm{d}}$, where T_{d} is the maximum excess delay of the channel. To preclude ISI and isi, we assume that $T_{\mathrm{r}} \ge T_{\mathrm{g}}$ and $N_{\mathrm{h}} T_{\mathrm{p}} + T_{\mathrm{r}} \le 2T_{\mathrm{f}}^{\mathrm{TR}} - T_{\mathrm{g}}$, where T_{r} is the time separation between each pair of data and reference pulses. We consider perfect synchronization at the receiver side although, as shown later, the proposed receiver is more robust to synchronization errors with respect to conventional TR.[3]

2.2.2 BPPM

In this case, the transmitted signal can be expressed as

$$
s_{\mathrm{BPPM}}(t) = \sum_i \left[\frac{(1+d_i)}{2} b_1(t - iT_{\mathrm{s}}) + \frac{(1-d_i)}{2} b_2(t - iT_{\mathrm{s}})) \right] \tag{2.3}
$$

where $d_i \in \{-1, 1\}$ is the ith data symbol, $T_{\mathrm{s}} = \frac{N_{\mathrm{s}}}{2} T_{\mathrm{f}}^{\mathrm{ED}}$ is the symbol duration with N_{s} and $T_{\mathrm{f}}^{\mathrm{ED}}$ denoting the number of pulses per symbol and the average

[2]Note that other combinations of data and reference pulses are also possible. For simplicity, and without loss of generality, we have adopted the conventional TR signaling, in which the number of reference and data pulses are equal[69].

[3]The sensitivity analysis to synchronization errors, however, is beyond the scope of this work. See, e.g., [103, 104].

pulse repetition period, respectively [73].[4] The transmitted signal for $d_i = +1$ and $d_i = -1$ can be written, respectively, as

$$
\begin{aligned}
b_1(t) &= \sum_{j=0}^{\frac{N_\mathrm{s}}{2}-1} \sqrt{E_\mathrm{p}^\mathrm{ED}}\, a_j\, p(t - jT_\mathrm{f}^\mathrm{ED} - c_j T_\mathrm{p})\,, \\
b_2(t) &= \sum_{j=0}^{\frac{N_\mathrm{s}}{2}-1} \sqrt{E_\mathrm{p}^\mathrm{ED}}\, a_j\, p(t - jT_\mathrm{f}^\mathrm{ED} - c_j T_\mathrm{p} - \Delta)
\end{aligned}
\tag{2.4}
$$

where Δ is the time shift between two different data symbols and the other terms are defined as in (2.2). The energy of the transmitted pulse is $E_\mathrm{p}^\mathrm{ED} = 2E_\mathrm{s}^\mathrm{ED}/N_\mathrm{s}$, where E_s^ED is the symbol energy. Note that, adopting the position modulation, the transmitted energy is allocated among $N_\mathrm{s}/2$ modulated pulses. To preclude ISI and isi we assume $\Delta > T_\mathrm{g}$ and $N_\mathrm{h} T_\mathrm{p} + \Delta \leq T_\mathrm{f}^\mathrm{ED} - T_\mathrm{g}$.

2.2.3 Channel Model

The received signal can be written as $r_\mathrm{TR}(t) = s_\mathrm{TR}(t) \otimes h(t) + n(t)$ and $r_\mathrm{BPPM}(t) = s_\mathrm{BPPM}(t) \otimes h(t) + n(t)$ for TR-BPAM and for BPPM, respectively, where $h(t)$ is the CIR and $n(t)$ is zero-mean, additive white Gaussian noise (AWGN) with two-sided power spectral density (PSD) $N_0/2$. We consider the linear time-invariant channel model which CIR can be written as $h(t) = \sum_{l=1}^{L} \alpha_l \delta(t - \tau_l)$ where $\delta(\cdot)$ is the Dirac-delta function, L is the number of multipath components, and α_l and τ_l denote the amplitude and delay of the lth path, respectively [57].

2.3 Stop-and-Go Receivers

2.3.1 Conventional AcR

As shown in Fig. 2.1a, the conventional AcR first passes the received signal through an ideal band-pass filter with center frequency f_c to eliminate out-of-band noise. If the bandwidth W of the filter is wide enough, then the signal passes through undistorted, so ISI and isi caused by filtering is negligible. The received signal at the output of the band-pass filter is denoted by

$$
\widetilde{r}_\mathrm{TR}(t) = \sum_i \breve{b}_\mathrm{r}(t - iT_\mathrm{s}) + d_i \breve{b}_\mathrm{d}(t - iT_\mathrm{s}) + \widetilde{n}(t) \tag{2.5}
$$

[4] We set $T_\mathrm{f}^\mathrm{TR} = \frac{T_\mathrm{f}^\mathrm{ED}}{2}$ so that the two signaling scheme present the same symbol duration.

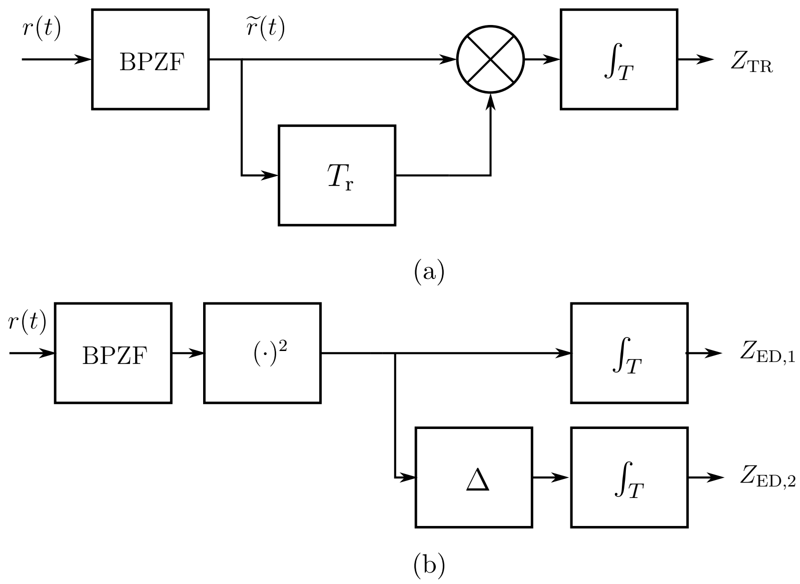

Figure 2.1: Conventional non-coherent receivers. (a) AcR. (b) EDR.

where $\breve{b}_{\mathrm{r}}(t) = b_{\mathrm{r}}(t) \otimes h(t) \otimes h_{\mathrm{ZF}}(t)$ and $\breve{b}_{\mathrm{d}}(t) = b_{\mathrm{d}}(t) \otimes h(t) \otimes h_{\mathrm{ZF}}(t)$, $h_{\mathrm{ZF}}(t)$ is the filter impulse response, and the term $\widetilde{n}(t)$ is a zero-mean, Gaussian random process with autocorrelation function $R_{\widetilde{n}}(\tau) = W N_0 \operatorname{sinc}(W\tau)\cos(2\pi f_{\mathrm{c}}\tau)$, with $\operatorname{sinc}(x) = \sin(\pi x)/(\pi x)$. Note that, when $|\tau|$ is a multiple of $1/W$, noise samples are statistically independent, and when $|\tau| \gg 1/W$, that is, $|\tau| \geq T_{\mathrm{g}}$, noise samples can be reasonably considered as statistically independent. The filtered received signal is passed through a correlator with integration interval T, as shown in Fig. 2.1a. The incoming signal is correlated with a delayed version of the reference signal, thus collecting the received signal energy. The integration interval T determines the number of multipath components (or equivalently, the amount of energy) captured by the receiver, as well as the amount of noise energy accumulated. Hence, for the conventional TR signaling, $T_{\mathrm{p}} \leq T \leq T_{\mathrm{g}}$.

Focusing on the data symbol at $i = 0$, the decision statistic generated at the AcR is then given by

$$Z_{\mathrm{TR}} = \sum_{j=0}^{\frac{N_{\mathrm{s}}}{2}-1} \int_{j2T_{\mathrm{f}}^{\mathrm{TR}}+T_{\mathrm{r}}+c_jT_{\mathrm{p}}}^{j2T_{\mathrm{f}}^{\mathrm{TR}}+T_{\mathrm{r}}+c_jT_{\mathrm{p}}+T} \widetilde{r}_{\mathrm{TR}}(t)\,\widetilde{r}_{\mathrm{TR}}(t-T_{\mathrm{r}})\,dt\,. \tag{2.6}$$

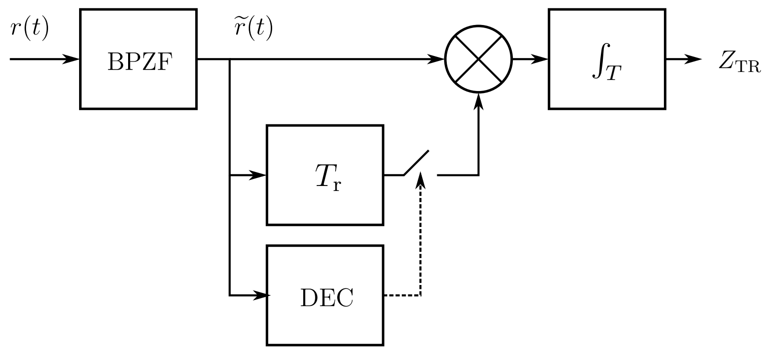

(a)

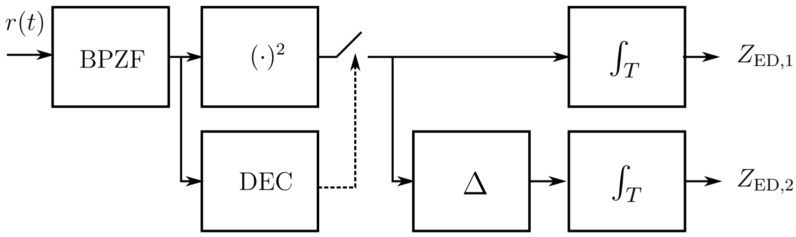

(b)

Figure 2.2: Stop-and-go receivers. (a) SaG-AcR. (b) SaG-EDR.

2.3.2 Conventional EDR

As shown in Fig. 2.1b, similarly to the AcR, the conventional EDR first passes the received signal through an ideal band-pass filter with center frequency f_{c} to eliminate out-of-band noise. The received signal at the output of the band-pass filter can be written as

$$\widetilde{r}_{\mathrm{BPPM}}(t) = \sum_i \left[\frac{(1+d_i)}{2} \breve{b}_1(t - iT_{\mathrm{s}}) + \frac{(1-d_i)}{2} \breve{b}_2(t - iT_{\mathrm{s}}) \right] + \widetilde{n}(t) \qquad (2.7)$$

where $\breve{b}_1(t) = b_1(t) \otimes h(t) \otimes h_{\mathrm{ZF}}(t)$ and $\breve{b}_2(t) = b_2(t) \otimes h(t) \otimes h_{\mathrm{ZF}}(t)$, and the other terms are defined as in (2.5). The filtered received signal is passed through a couple of EDs, with integration interval T, that measure the energy in two different time windows separated of Δ. As for the AcR, the integration interval T determines the number of multipath components captured by the receiver, as well as the amount of noise energy accumulated.

Focusing on the data symbol at $i = 0$, the decision statistic generated at

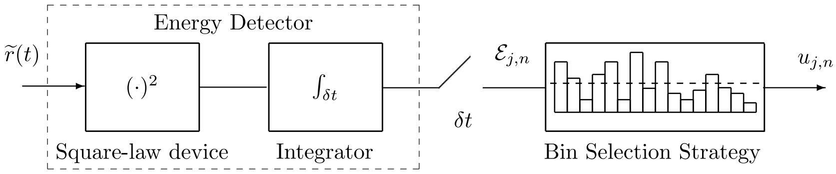

Figure 2.3: Decision device (DEC).

the EDR is then given by

$$\begin{aligned} Z_{\mathrm{ED}} = & \underbrace{\sum_{j=0}^{\frac{N_{\mathrm{s}}}{2}-1} \int_{jT_{\mathrm{f}}^{\mathrm{ED}}+c_j T_{\mathrm{p}}}^{jT_{\mathrm{f}}^{\mathrm{ED}}+c_j T_{\mathrm{p}}+T} \left(\widetilde{r}_{\mathrm{BPPM}}(t)\right)^2 \, dt}_{Z_{\mathrm{ED},1}} \\ & - \underbrace{\sum_{j=0}^{\frac{N_{\mathrm{s}}}{2}-1} \int_{jT_{\mathrm{f}}^{\mathrm{ED}}+c_j T_{\mathrm{p}}+\Delta}^{jT_{\mathrm{f}}^{\mathrm{ED}}+c_j T_{\mathrm{p}}+T+\Delta} \left(\widetilde{r}_{\mathrm{BPPM}}(t)\right)^2 \, dt}_{Z_{\mathrm{ED},2}} \, . \end{aligned} \tag{2.8}$$

2.3.3 SaG Receivers

As described earlier, the integration interval T of the conventional AcR and EDR must be suitably designed to avoid excessive noise energy accumulation, while capturing the maximum energy from the desired signal. However, in the presence of clustered multipaths [105], an optimal choice of T may still lead to excessive noise energy accumulation due to time gaps (inter-cluster intervals) in the received signal that do not contain useful energy. To alleviate this problem, we propose the SaG-AcR shown in Fig. 2.2a and the SaG-EDR shown in Fig. 2.2b. The proposed SaG receivers include a decision device (DEC) composed of an ED (see Fig. 2.3) to detect which portions of the received signal contain useful energy. In particular, the idea is to decompose the integration interval into N_{bin} short time slots (or bins) of duration $T_{\mathrm{ED}} = T/N_{\mathrm{bin}}$, and to select among them only those which contain significant energy from the desired signal. When no significant signal energy is detected in a given bin, that bin is not used by the correlator in the SaG-AcR or not integrated in the SaG-EDR, preventing noise energy accumulation.

The ED adopted for the decision regarding the bins to be integrated operates on the delay path in the case of AcR, or in one of the two branches of the EDR, when a training sequence is transmitted.[5] We denote the energy

[5]In case of BPPM the receiver needs to operate in the specific time window where the signal is effectively present, so the presence of a training sequence is assumed. Moreover,

samples at the output of the ED resulting from the jth received pulse with

$$\mathcal{E}_{j,n} = \int_{t_{n-1}^{\mathrm{TR}}}^{t_n^{\mathrm{TR}}} \widetilde{r}_{\mathrm{TR}}^{2}(t - T_{\mathrm{r}})\, dt, \qquad n = 1, 2, \ldots, N_{\mathrm{bin}} \tag{2.9}$$

for the SaG-AcR, with $t_n^{\mathrm{TR}} = j2T_{\mathrm{f}}^{\mathrm{TR}} + c_j T_{\mathrm{p}} + T_{\mathrm{r}} + nT_{\mathrm{ED}}$. In the case of SaG-EDR we consider that the energy samples adopted for the demodulation of the jth received pulse are collected on the previous data symbol that we suppose part of the known training sequence, that is[6]

$$\mathcal{E}_{j,n} = \int_{t_{n-1}^{\mathrm{ED}}}^{t_n^{\mathrm{ED}}} \widetilde{r}_{\mathrm{BPPM}}^{2}(t - T_{\mathrm{s}})\, dt, \qquad n = 1, 2, \ldots, N_{\mathrm{bin}} \tag{2.10}$$

with $t_n^{\mathrm{ED}} = jT_{\mathrm{f}}^{\mathrm{ED}} + c_j T_{\mathrm{p}} + nT_{\mathrm{ED}}$.

The energy samples $\mathcal{E}_{j,n}$ are then used to select the desired bins through the variable $u_{j,n}$ which represents the state of the switch in the nth bin of the jth pulse. Such a variable is generated by the *bin selection strategy* as described in Section 2.5. Note that for the generic received pulse j, N_{bin} binary decisions $u_{j,1}, \ldots, u_{j,N_{\mathrm{bin}}}$ are produced by the decision device. For notational convenience, in the following we will use the continuous-time switch signal $u_j(t)$ that commands the switching at the jth pulse defined as

$$u_j^{\mathrm{TR}}(t) = \sum_{n=1}^{N_{\mathrm{bin}}} u_{j,n} \,\mathrm{rect}\left(\frac{t - t_{n-1}^{\mathrm{TR}} - T_{\mathrm{ED}}/2}{T_{\mathrm{ED}}}\right) \tag{2.11}$$

for the SaG-AcR, and

$$u_j^{\mathrm{ED}}(t) = \sum_{n=1}^{N_{\mathrm{bin}}} u_{j,n} \,\mathrm{rect}\left(\frac{t - t_{n-1}^{\mathrm{ED}} - T_{\mathrm{ED}}/2}{T_{\mathrm{ED}}}\right) + \sum_{n=1}^{N_{\mathrm{bin}}} u_{j,n} \,\mathrm{rect}\left(\frac{t - t_{n-1}^{\mathrm{ED}} - \Delta - T_{\mathrm{ED}}/2}{T_{\mathrm{ED}}}\right) \tag{2.12}$$

for the SaG-EDR, where $\mathrm{rect}(t/T_{\mathrm{ED}})$ is a unit-amplitude rectangular pulse with duration T_{ED} centered at the origin. The parameter T_{ED} determines the ability to separate time intervals containing paths from those containing noise only. Small T_{ED} results in high temporal resolution but larger N_{bin}; hence, a trade-off between receiver performance and complexity is expected.

after a first phase, it is possible to operate with a decision-feedback approach, similarly to what presented in [95].

[6]Without loss of generality we considerer a training sequence of all +1 so that the channel response is concentrated in the first part each pulse repetition period is divided in.

Note that with the SaG strategy the maximum integration time T can be kept as large as possible (e.g., equal to the maximum expected channel excess delay) without noise penalty; moreover, in case of imperfect synchronization, noise-only bins preceding the signal TOA do not produce further penalty since they are discarded by the switch driven by the decision device.

2.4 Performance Evaluation

2.4.1 SaG-AcR

Considering the presence of the switching signal $u_j^{\mathrm{TR}}(t)$, the decision variable Z_{TR} in (2.6) can be rewritten as[72, 102]

$$Z_{\mathrm{TR}} = \sum_{j=0}^{\frac{N_\mathrm{s}}{2}-1} \int_0^T \tilde{u}_j^{\mathrm{TR}}(t)\Big(\breve{b}_\mathrm{r}(t+j2T_\mathrm{f}^{\mathrm{TR}}+c_jT_\mathrm{p})+\widetilde{n}(t+j2T_\mathrm{f}^{\mathrm{TR}}+c_jT_\mathrm{p})\Big) \\ \times\Big(d_0\breve{b}_\mathrm{d}(t+j2T_\mathrm{f}^{\mathrm{TR}}+c_jT_\mathrm{p}+T_\mathrm{r})+\widetilde{n}(t+j2T_\mathrm{f}^{\mathrm{TR}}+c_jT_\mathrm{p}+T_\mathrm{r})\Big)\,dt \tag{2.13}$$

where $\tilde{u}^{\mathrm{TR}}(t) = u^{\mathrm{TR}}(t+j2T_\mathrm{f}^{\mathrm{TR}}+c_jT_\mathrm{p}+T_\mathrm{r})$. Note that if the symbol duration is less than the channel coherence time, all pairs of separated pulses will experience the same channel condition, implying that $\breve{b}_\mathrm{r}(t+j2T_\mathrm{f}^{\mathrm{TR}}+c_jT_\mathrm{p}) = \breve{b}_\mathrm{d}(t+j2T_\mathrm{f}^{\mathrm{TR}}+c_jT_\mathrm{p}+T_\mathrm{r})$ for all $t\in[0,T]$. Therefore, we can significantly simplify the expression in (2.13) as follows:

$$Z_{\mathrm{TR}} = \sum_{j=0}^{\frac{N_\mathrm{s}}{2}-1} \int_0^T \tilde{u}_j^{\mathrm{TR}}(t)\big(w_j(t)+\eta_{1,j}(t)\big)\big(d_0w_j(t)+\eta_{2,j}(t)\big)\,dt = \sum_{j=0}^{\frac{N_\mathrm{s}}{2}-1} V_j \tag{2.14}$$

where $w_j(t) \triangleq \breve{b}_\mathrm{r}(t+j2T_\mathrm{f}^{\mathrm{TR}}+c_jT_\mathrm{p})$, $\eta_{1,j}(t) \triangleq \widetilde{n}(t+j2T_\mathrm{f}^{\mathrm{TR}}+c_jT_\mathrm{p})$ and $\eta_{2,j}(t) \triangleq \widetilde{n}(t+j2T_\mathrm{f}^{\mathrm{TR}}+c_jT_\mathrm{p}+T_\mathrm{r})$ defined over the interval $[0,T]$. With the position made on the T_r value to avoid ISI and isi, the noise samples are then spaced by $T_\mathrm{r} > T_\mathrm{g}$ so they can be considered as independent, regardless of c_j.[7] We further observe that V_j represents the integrator output corresponding to the jth received modulated pulse.

Since the received signal is a real band-pass signal of bandwidth W, it can be sampled at a frequency greater than or equal to $2W$ [86]. Sampling

[7] Hence, no further assumption on c_j is required in our analysis.

the received signal at rate $2W$ in the interval $[0,T]$ is then represented by $2WT$ real samples.[8] Following this approach, we can represent V_j as [72, 102]

$$V_j = \frac{1}{2W}\sum_{m=1}^{2WT}\tilde{u}_j^{\mathrm{TR}}\left(\frac{m}{2W}\right)\cdot\Big(d_0 w_{j,m}^2 + w_{j,m}\eta_{2,j,m} + d_0 w_{j,m}\eta_{1,j,m} + \eta_{1,j,m}\eta_{2,j,m}\Big) \tag{2.15}$$

where the mth samples in the interval $[0,T]$ of $w_j(t)$, $\eta_{1,j}(t)$ and $\eta_{2,j}(t)$ in (2.14) are respectively denoted as $w_{j,m}$, $\eta_{1,j,m}$ and $\eta_{2,j,m}$. We can now express (2.15) conditioned on d_0 and $a_j=+1$ in the form of a summation of squares

$$\begin{aligned}
V_{j|d_0=+1} &= \sum_{m=1}^{2WT}\tilde{u}_j^{\mathrm{TR}}\left(\frac{m}{2W}\right)\left[\left(\frac{1}{\sqrt{2W}}w_{j,m}+\beta_{1,j,m}\right)^2-\beta_{2,j,m}^2\right], \\
V_{j|d_0=-1} &= \sum_{m=1}^{2WT}\tilde{u}_j^{\mathrm{TR}}\left(\frac{m}{2W}\right)\left[-\left(\frac{1}{\sqrt{2W}}w_{j,m}-\beta_{2,j,m}\right)^2+\beta_{1,j,m}^2\right]
\end{aligned} \tag{2.16}$$

where $\beta_{1,j,m} = \frac{1}{2\sqrt{2W}}(\eta_{2,j,m}+\eta_{1,j,m})$ and $\beta_{2,j,m} = \frac{1}{2\sqrt{2W}}(\eta_{2,j,m}-\eta_{1,j,m})$ are statistically independent Gaussian r.v.s with variance $N_0/4$. Due to the statistical symmetry in (2.16) of V_j with respect to d_0 and $\{a_j\}$, we simply need to calculate the BEP conditioned on $d_0=+1$ and $a_j=+1$. For notational simplicity, we define the normalized r.v.s $Y_{\mathrm{TR},1}$, $Y_{\mathrm{TR},2}$, $Y_{\mathrm{TR},3}$, and $Y_{\mathrm{TR},4}$ as

$$\begin{aligned}
Y_{\mathrm{TR},1} &= \frac{2}{N_0}\sum_{j=0}^{\frac{N_s}{2}-1}\sum_{m=1}^{2WT}\tilde{u}_j^{\mathrm{TR}}\left(\frac{m}{2W}\right)\cdot\left(\frac{1}{\sqrt{2W}}w_{j,m}+\beta_{1,j,m}\right)^2, \\
Y_{\mathrm{TR},2} &= \frac{2}{N_0}\sum_{j=0}^{\frac{N_s}{2}-1}\sum_{m=1}^{2WT}\tilde{u}_j^{\mathrm{TR}}\left(\frac{m}{2W}\right)\cdot\beta_{2,j,m}^2, \\
Y_{\mathrm{TR},3} &= \frac{2}{N_0}\sum_{j=0}^{\frac{N_s}{2}-1}\sum_{m=1}^{2WT}\tilde{u}_j^{\mathrm{TR}}\left(\frac{m}{2W}\right)\cdot\left(\frac{1}{\sqrt{2W}}w_{j,m}-\beta_{2,j,m}\right)^2, \\
Y_{\mathrm{TR},4} &= \frac{2}{N_0}\sum_{j=0}^{\frac{N_s}{2}-1}\sum_{m=1}^{2WT}\tilde{u}_j^{\mathrm{TR}}\left(\frac{m}{2W}\right)\cdot\beta_{1,j,m}^2.
\end{aligned} \tag{2.17}$$

Notice that in the summation, $\tilde{u}_j^{\mathrm{TR}}\left(\frac{m}{2W}\right)\in\{0,1\}$ and accounts for the inclusion of the mth sample resulting from the ED decision. It is thus convenient

[8]For convenience it is assumed that $2WT$ is an integer.

to define

$$N_{\mathrm{u}}^{\mathrm{TR}} = \sum_{j=0}^{\frac{N_{\mathrm{s}}}{2}-1} \sum_{m=1}^{2WT} \tilde{u}_j^{\mathrm{TR}} \left(\frac{m}{2W}\right) \leq N_{\mathrm{s}} WT \tag{2.18}$$

as the total number of signal samples accumulated during T, related to a symbol.

Conditioned on the channel, $Y_{\mathrm{TR},1}$ and $Y_{\mathrm{TR},3}$ are non-central Chi-square r.v.s with $N_{\mathrm{u}}^{\mathrm{TR}}$ degrees of freedom, whereas $Y_{\mathrm{TR},2}$ and $Y_{\mathrm{TR},4}$ are central Chi-square r.v.s with the same degrees of freedom as $Y_{\mathrm{TR},1}$ and $Y_{\mathrm{TR},3}$. Both $Y_{\mathrm{TR},1}$ and $Y_{\mathrm{TR},3}$ have the same non-centrality parameter $2\gamma^{\mathrm{TR}}$, where

$$\gamma^{\mathrm{TR}} = \frac{1}{N_0} \sum_{j=0}^{\frac{N_{\mathrm{s}}}{2}-1} \sum_{m=1}^{2WT} \tilde{u}_j^{\mathrm{TR}} \left(\frac{m}{2W}\right) \cdot \frac{w_{j,m}^2}{2W} = \frac{1}{N_0} \sum_{j=0}^{\frac{N_{\mathrm{s}}}{2}-1} \int_0^T \tilde{u}_j^{\mathrm{TR}}(t) \cdot w_j^2(t)\, dt \tag{2.19}$$

which, according to (2.11), can be rewritten as

$$\gamma^{\mathrm{TR}} = \frac{1}{N_0} \sum_{j=0}^{\frac{N_{\mathrm{s}}}{2}-1} \sum_{n=1}^{N_{\mathrm{bin}}} u_{j,n}\, \lambda_{j,n}^{\mathrm{TR}} \tag{2.20}$$

where

$$\lambda_{j,n}^{\mathrm{TR}} = \int_{(n-1)T_{\mathrm{ED}}}^{nT_{\mathrm{ED}}} w_j^2(t)\, dt, \qquad n = 1, 2, \ldots, N_{\mathrm{bin}} \tag{2.21}$$

represents the energy of the noise-free received waveform in the nth bin. Also, (2.20) suggests that the non-centrality parameter is proportional to the accumulated energy from selected bins (where selection is operated by $u_{j,n}$) of the $N_{\mathrm{s}}/2$ received modulated pulses that form a symbol. More precisely, the parameter γ^{TR} represents the instantaneous SNR obtained by accumulating the energy from a fraction of the received signal bins, hence named accumulated signal-to-noise ratio (ASNR). In fact, γ^{TR} is in general different from the SNR measured at the input of the AcR, due to the possible suppression of certain paths by the bin selection strategy.

The p.d.f.s of $Y_{\mathrm{TR},1}$, conditioned on γ^{TR}, and $Y_{\mathrm{TR},2}$ are then given by $f_{Y_{\mathrm{TR},1}|\gamma^{\mathrm{TR}}}(y_1) = f_{\mathrm{NC}}(y_1, 2\gamma^{\mathrm{TR}}, N_{\mathrm{u}}^{\mathrm{TR}}/2)$ and $f_{Y_{\mathrm{TR},2}}(y_2) = f_{\mathrm{C}}(y_2, N_{\mathrm{u}}^{\mathrm{TR}}/2)$ where

$$f_{\mathrm{NC}}(y, \mu, \nu) = e^{-(y+\mu)} \left(\frac{y}{\mu}\right)^{\frac{(\nu-1)}{2}} I_{\nu-1}(2\sqrt{y\mu}), \quad y \geq 0, \tag{2.22}$$

$$f_{\mathrm{C}}(y, \nu) = \frac{y^{(\nu-1)}}{\Gamma(\nu)}\, e^{-y}, \quad y \geq 0 \tag{2.23}$$

with $I_\kappa(\cdot)$ the κth order modified Bessel function of the first kind [106, ch. 9, p. 374] and $\Gamma(\cdot)$ the Gamma function [106, ch. 6, p. 255].

Using the approach presented in [72, 102], the BEP of TR signaling with SaG-AcR conditioned on the single CIR realization and the decisions $u_{j,n}$ is given by $\mathbb{P}\{Y_{\mathrm{TR},1} < Y_{\mathrm{TR},2}|d_0 = +1\}$. Thus, after some mathematical derivations, the BEP can be expressed in the closed-form $P_{\mathrm{e,TR}} = P_{\mathrm{e}}(\gamma^{\mathrm{TR}}, N_{\mathrm{u}}^{\mathrm{TR}})$, where[9]

$$P_{\mathrm{e}}(\gamma, N_{\mathrm{u}}) = \frac{e^{-\gamma}}{2^{\frac{N_{\mathrm{u}}}{2}}} \sum_{i=0}^{\frac{N_{\mathrm{u}}}{2}-1} \frac{\gamma^i}{i!} \sum_{k=i}^{\frac{N_{\mathrm{u}}}{2}-1} \frac{1}{2^k} \frac{(k + N_{\mathrm{u}}/2 - 1)!}{(k-i)!(N_{\mathrm{u}}/2 + i - 1)!} \,. \tag{2.24}$$

2.4.2 SaG-EDR

Considering the presence of the switching signal $u_j^{\mathrm{ED}}(t)$, the decision variable Z_{ED} in (2.8) can be rewritten as [73][10]

$$\begin{aligned} Z_{\mathrm{ED}} = & \sum_{j=0}^{\frac{N_{\mathrm{s}}}{2}-1} \int_0^T \tilde{u}_j^{\mathrm{ED}}(t) \left(\frac{(1+d_0)}{2} \breve{b}_1(t + jT_{\mathrm{f}}^{\mathrm{ED}} + c_j T_{\mathrm{p}}) + \widetilde{n}(t + jT_{\mathrm{f}}^{\mathrm{ED}} + c_j T_{\mathrm{p}}) \right)^2 dt \\ & - \sum_{j=0}^{\frac{N_{\mathrm{s}}}{2}-1} \int_0^T \tilde{u}_j^{\mathrm{ED}}(t) \left(\frac{(1-d_0)}{2} \breve{b}_2(t + jT_{\mathrm{f}}^{\mathrm{ED}} + c_j T_{\mathrm{p}} + \Delta) + \widetilde{n}(t + jT_{\mathrm{f}}^{\mathrm{ED}} + c_j T_{\mathrm{p}} + \Delta) \right)^2 dt \end{aligned} \tag{2.25}$$

where $\tilde{u}^{\mathrm{ED}}(t) = u^{\mathrm{ED}}(t + jT_{\mathrm{f}}^{\mathrm{ED}} + c_j T_{\mathrm{p}})$. We can now rewrite (2.25) as follows:

$$\begin{aligned} Z_{\mathrm{ED}} = & \sum_{j=0}^{\frac{N_{\mathrm{s}}}{2}-1} \underbrace{\int_0^T \tilde{u}_j^{\mathrm{ED}}(t) \left(\frac{(1+d_0)}{2} w_{1,j}(t) + \eta_{1,j}(t) \right)^2 dt}_{V_{j,1}} \\ & - \sum_{j=0}^{\frac{N_{\mathrm{s}}}{2}-1} \underbrace{\int_0^T \tilde{u}_j^{\mathrm{ED}}(t) \left(\frac{(1-d_0)}{2} w_{2,j}(t) + \eta_{2,j}(t) \right)^2 dt}_{V_{j,2}} = \sum_{j=0}^{\frac{N_{\mathrm{s}}}{2}-1} V_{j,1} - \sum_{j=0}^{\frac{N_{\mathrm{s}}}{2}-1} V_{j,2} \end{aligned} \tag{2.26}$$

where $w_{1,j}(t) \triangleq \breve{b}_1(t + jT_{\mathrm{f}}^{\mathrm{ED}} + c_j T_{\mathrm{p}})$, $w_{2,j}(t) \triangleq \breve{b}_2(t + jT_{\mathrm{f}}^{\mathrm{ED}} + c_j T_{\mathrm{p}} + \Delta)$, $\eta_{1,j}(t) \triangleq \widetilde{n}(t + jT_{\mathrm{f}}^{\mathrm{ED}} + c_j T_{\mathrm{p}})$ and $\eta_{2,j}(t) \triangleq \widetilde{n}(t + jT_{\mathrm{f}}^{\mathrm{ED}} + c_j T_{\mathrm{p}} + \Delta)$ defined over the interval $[0, T]$.

[9]See also Appendix 3.D for the derivation.

[10]Note that $\left(u_j^{\mathrm{ED}}(t)\right)^2 = u_j^{\mathrm{ED}}(t)$ and $\tilde{u}_j^{\mathrm{ED}}(t + \Delta) = \tilde{u}_j^{\mathrm{ED}}(t)$ for $t \in [0, T]$.

Following the approach adopted for the SaG-AcR we can exploit the sampling expansion representing $V_{j,1}$ and $V_{j,2}$ as

$$V_{j,1} = \frac{1}{2W} \sum_{m=1}^{2WT} \tilde{u}_j^{\mathrm{ED}} \left(\frac{m}{2W}\right) \cdot \left(\frac{(1+d_0)}{2} w_{1,j,m} + \eta_{1,j,m}\right)^2 ,$$
$$V_{j,2} = \frac{1}{2W} \sum_{m=1}^{2WT} \tilde{u}_j^{\mathrm{ED}} \left(\frac{m}{2W}\right) \cdot \left(\frac{(1-d_0)}{2} w_{2,j,m} + \eta_{2,j,m}\right)^2 \tag{2.27}$$

where the mth samples in the interval $[0, T]$ of $w_{1,j}(t)$, $w_{2,j}(t)$, $\eta_{1,j}(t)$ and $\eta_{2,j}(t)$ in (2.26) are respectively denoted as $w_{1,j,m}$, $w_{2,j,m}$, $\eta_{1,j,m}$ and $\eta_{2,j,m}$. For mathematical convenience, we define the normalized r.v.s $Y_{\mathrm{ED},1}$, $Y_{\mathrm{ED},2}$, $Y_{\mathrm{ED},3}$, and $Y_{\mathrm{ED},4}$ as

$$\begin{aligned}
Y_{\mathrm{ED},1} &= \frac{1}{N_0} \sum_{j=0}^{\frac{N_s}{2}-1} V_{j,1|d_0=+1} = \frac{1}{N_0} \sum_{j=0}^{\frac{N_s}{2}-1} \sum_{m=1}^{2WT} \tilde{u}_j^{\mathrm{ED}} \left(\frac{m}{2W}\right) \cdot \frac{(w_{1,j,m} + \eta_{1,j,m})^2}{2W} , \\
Y_{\mathrm{ED},2} &= \frac{1}{N_0} \sum_{j=0}^{\frac{N_s}{2}-1} V_{j,2|d_0=+1} = \frac{1}{N_0} \sum_{j=0}^{\frac{N_s}{2}-1} \sum_{m=1}^{2WT} \tilde{u}_j^{\mathrm{ED}} \left(\frac{m}{2W}\right) \cdot \frac{\eta_{2,j,m}^2}{2W} , \\
Y_{\mathrm{ED},3} &= \frac{1}{N_0} \sum_{j=0}^{\frac{N_s}{2}-1} V_{j,1|d_0=-1} = \frac{1}{N_0} \sum_{j=0}^{\frac{N_s}{2}-1} \sum_{m=1}^{2WT} \tilde{u}_j^{\mathrm{ED}} \left(\frac{m}{2W}\right) \cdot \frac{\eta_{1,j,m}^2}{2W} , \\
Y_{\mathrm{ED},4} &= \frac{1}{N_0} \sum_{j=0}^{\frac{N_s}{2}-1} V_{j,2|d_0=-1} = \frac{1}{N_0} \sum_{j=0}^{\frac{N_s}{2}-1} \sum_{m=1}^{2WT} \tilde{u}_j^{\mathrm{ED}} \left(\frac{m}{2W}\right) \cdot \frac{(w_{2,j,m} + \eta_{2,j,m})^2}{2W} .
\end{aligned} \tag{2.28}$$

Again, in the summation, $\tilde{u}_j^{\mathrm{ED}} \left(\frac{m}{2W}\right) \in \{0, 1\}$ and accounts for the inclusion of the mth sample resulting from the ED decision. It is thus convenient to define

$$N_{\mathrm{u}}^{\mathrm{ED}} = \sum_{j=0}^{\frac{N_s}{2}-1} \sum_{m=1}^{2WT} u_j^{\mathrm{ED}} \left(\frac{m}{2W}\right) \leq N_s WT \tag{2.29}$$

as the total number of signal samples accumulated during T, related to a symbol.

Conditioned on the channel, $Y_{\mathrm{ED},1}$ and $Y_{\mathrm{ED},4}$ are non-central Chi-square r.v.s with $N_{\mathrm{u}}^{\mathrm{ED}}$ degrees of freedom, whereas $Y_{\mathrm{ED},2}$ and $Y_{\mathrm{ED},3}$ are central Chi-square r.v.s with the same degrees of freedom as $Y_{\mathrm{ED},1}$ and $Y_{\mathrm{ED},4}$. Since, given the channel $h(t)$, $w_{1,j}(t) = w_{2,j}(t) = w_j(t)$ (i.e., $w_{1,j,m} = w_{2,j,m} = w_{j,m}$), both

$Y_{\mathrm{ED},1}$ and $Y_{\mathrm{ED},4}$ have the same non-centrality parameter $2\gamma^{\mathrm{ED}}$, where

$$\gamma^{\mathrm{ED}} = \frac{1}{2N_0} \sum_{j=0}^{\frac{N_s}{2}-1} \sum_{m=1}^{2WT} \tilde{u}_j^{\mathrm{ED}} \left(\frac{m}{2W}\right) \cdot \frac{w_{j,m}^2}{2W} = \frac{1}{2N_0} \sum_{j=0}^{\frac{N_s}{2}-1} \int_0^T \tilde{u}_j^{\mathrm{ED}}(t) \cdot w_j^2(t)\, dt \tag{2.30}$$

which, according to (2.12), can be rewritten as

$$\gamma^{\mathrm{ED}} = \frac{1}{2N_0} \sum_{j=0}^{\frac{N_s}{2}-1} \sum_{n=1}^{N_{\mathrm{bin}}} u_{j,n}\, \lambda_{j,n}^{\mathrm{ED}} \tag{2.31}$$

where

$$\lambda_{j,n}^{\mathrm{ED}} = \int_{(n-1)T_{\mathrm{ED}}}^{nT_{\mathrm{ED}}} w_j^2(t)\, dt, \qquad n = 1, 2, \ldots, N_{\mathrm{bin}} \tag{2.32}$$

represents the energy of the noise-free received waveform in the nth bin. As for the SaG-AcR, the parameter γ^{ED} is the ASNR.

The BEP of the SaG-EDR, conditioned on the single CIR realization and the decisions $u_{j,n}$, is then given by $\mathbb{P}\{Y_{\mathrm{ED},1} < Y_{\mathrm{ED},2} | d_0 = +1\}$. Since $E_{\mathrm{p}}^{\mathrm{TR}} = \frac{1}{2}E_{\mathrm{p}}^{\mathrm{ED}}$, we have that $\lambda_{j,n}^{\mathrm{TR}} = \frac{1}{2}\lambda_{j,n}^{\mathrm{ED}}$, so $\gamma^{\mathrm{TR}} = \gamma^{\mathrm{ED}}$, fixed the CIR realization and the decisions $u_{j,n}$ (i.e., the same ASNR and $N_{\mathrm{u}}^{\mathrm{TR}} = N_{\mathrm{u}}^{\mathrm{ED}}$). Hence the the BEP of the EDR with BPPM $P_{\mathrm{e,ED}} = P_{\mathrm{e}}(\gamma^{\mathrm{ED}}, N_{\mathrm{u}}^{\mathrm{ED}})$, where $P_{\mathrm{e}}(\gamma, N_{\mathrm{u}})$ is given by (2.24), equals the BEP of the SaG-AcR with TR-BPAM as for conventional AcR and EDR [107, 73, 60]. For this reason in the rest of the chapter we will refer generically to γ and N_{u}.

In Fig. 2.4, the conditional BEP is plotted as a function of γ for different values of N_{u}. Fixing the amount of energy captured, or equivalently the ASNR, the performance is worse for dispersive channels that have a long impulse response. In fact, a long CIR implies a high N_{u} and consequently more noise is accumulated, as expected in a non-coherent scheme. To obtain the BEP of the SaG receivers, (2.24) can be used in a semi-analytical Monte-Carlo approach that requires the generation of the CIR only and the evaluation of N_{u} and γ based on the bin selection strategies described in the following section.

2.5 Bin Selection Strategies for the SaG Receivers

The analysis of the SaG receivers has shown how the performance is related to the number of accumulated samples N_{u} and to the ASNR γ, both dependent

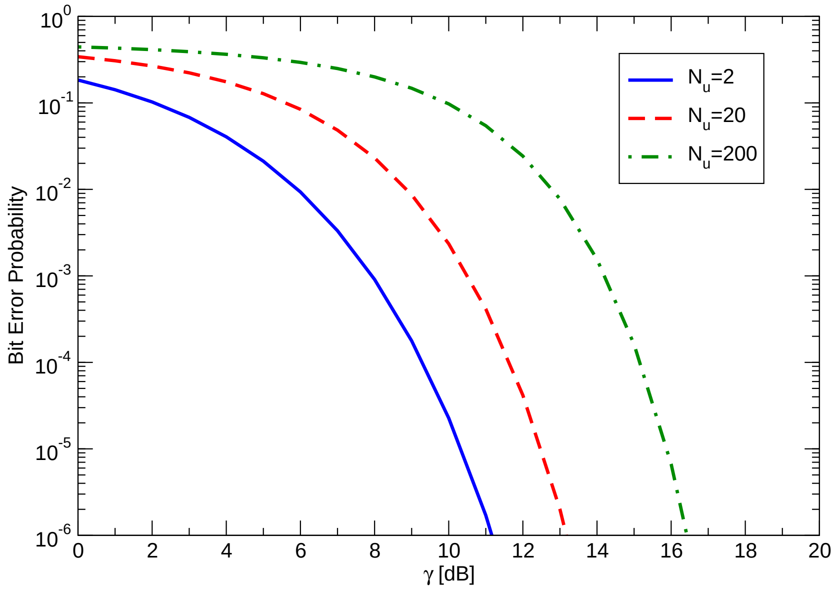

Figure 2.4: Conditional BEP of the SaG receiver as a function of the ASNR for different number of samples accumulated N_{u}.

on the bin selection strategy. To perform bin selection related to the jth pair of pulses, we consider the observation of N_{a} previous reference pulses for the SaG-AcR, or N_{a} pulses in the training sequence for SaG-EDR,[11] collecting the energy samples $\mathcal{E}_{j,n}, \mathcal{E}_{j-1,n}, \dots, \mathcal{E}_{j-N_{\mathrm{a}}+1,n}$ for $n = 1, \dots, N_{\mathrm{bin}}$. Without loss of generality and to simplify the notation, in the rest of the chapter we suppress the index j, and we define $\mathcal{E}_{q,n} = \mathcal{E}_{j-q+1,n}$ with $q = 1, \dots, N_{\mathrm{a}}$ and $n = 1, \dots, N_{\mathrm{bin}}$. Moreover, for notational convenience, let us arrange the energy samples $\mathcal{E}_{q,n}$ in a $N_{\mathrm{a}} \times N_{\mathrm{bin}}$ matrix $\boldsymbol{\mathcal{E}}$ and define the vector $\boldsymbol{\varepsilon} = (\varepsilon_1, \dots, \varepsilon_{N_{\mathrm{bin}}})$ obtained by accumulation of N_{a} previous energy samples, where the nth element of the vector is computed as[12]

$$\varepsilon_n = \frac{1}{N_{\mathrm{a}}} \sum_{q=1}^{N_{\mathrm{a}}} \mathcal{E}_{q,n} \qquad n = 1, \dots, N_{\mathrm{bin}} \,. \tag{2.33}$$

Since it is advantageous to start collecting energy from bins with the higher energy (and thus most probably those containing the useful signal), we define a vector $\boldsymbol{\varepsilon}' = (\varepsilon'_1, \dots, \varepsilon'_{N_{\mathrm{bin}}})$ obtained by sorting $\boldsymbol{\varepsilon}$ in decreasing order. In particular, indicating with $\boldsymbol{\pi} = (\pi_1, \pi_2, ..., \pi_{N_{\mathrm{bin}}})$ the vector of permutation indexes to sort $\boldsymbol{\varepsilon}$ in decreasing order, we have $\varepsilon'_n = \varepsilon_{\pi_n}$. Similarly, we denote

[11] Provided that the CIR remains constant during the time interval $2N_{\mathrm{a}}T_{\mathrm{f}}^{\mathrm{TR}}$ for the SaG-AcR, and $N_{\mathrm{a}}T_{\mathrm{f}}^{\mathrm{ED}}$ for the SaG-EDR, so that $\lambda_{j,n}^{\mathrm{TR}} = \lambda_n^{\mathrm{TR}}$ and $\lambda_{j,n}^{\mathrm{ED}} = \lambda_n^{\mathrm{ED}}$, $\forall j$.

[12] This corresponds to column averaging of $\boldsymbol{\mathcal{E}}$.

with $\boldsymbol{\lambda}'$ the ordered version of the vector $\boldsymbol{\lambda} = (\lambda_1, \ldots, \lambda_{N_{\text{bin}}})$, with elements $\lambda'_n = \lambda_{\pi_n}$ defined in (2.21) and (2.32) , and unknown at the receiver.[13] Their estimation can be performed having in mind that λ_n is the non-centrality parameter of the Chi-square distributed r.v. $\mathcal{E}_{q,n}$ [86, 89]. Unfortunately, the ML estimator of the non-centrality parameter of a Chi-square r.v. cannot be expressed in closed-form [90].[14] Thus, instead of the ML, we use the simpler estimator [90][15]

$$\widehat{\lambda}'_n = \left(\varepsilon'_n - \sigma^2 T_{\text{ED}}\right)^+ \tag{2.34}$$

with $\sigma^2 = N_0 W$.

2.5.1 Threshold-Based Bin Selection Strategy

A simple way to implement a bin selection strategy is to compare each sample ε_n with a threshold, to make a binary decision regarding the presence of significant useful energy. Intuitively, and in accordance to numerical results, there is an optimum threshold that minimizes the BEP. In fact, if the threshold is zero, all energy samples collected are used in the demodulation process and the scheme is equivalent to conventional AcR or EDR. Conversely, if the threshold is too high, only very few samples contribute to the demodulation process resulting in a drastic reduction of the ASNR. Therefore, in this section we analyze the problem of designing a proper threshold for the SaG receivers, proposing various schemes with different complexities and performance. In a threshold-based SaG receiver the bin selection strategy output is the variable u_n which represents the state of the switch in the nth bin (of the jth pulse), according to the following rule

$$u_n = \begin{cases} 1, & \text{if } \varepsilon_n > \xi \ , \\ 0, & \text{otherwise} \end{cases} \tag{2.35}$$

where ξ represents the threshold. Due to noise averaging in (2.33), more reliable decisions u_n are expected increasing N_{a}.

Optimum Threshold

To find the optimum threshold (OT), which guarantees minimum BEP, we calculate the corresponding number of bins to be collected, by analyzing

[13]Here λ_n refers indistinctly to λ_n^{TR} or λ_n^{ED}.

[14]The maximization of the likelihood function leads to a numerical solution of an equation involving modified Bessel functions.

[15]The operator $(x)^+$ stands for the positive part of x, that is $(x)^+ = \max(0, x)$. In [90] it has been shown that the ML estimate is dominated by the simplified estimator (2.34) with squared error as the loss function. As will be shown in Section 2.6 such simple estimator gives satisfactory results.

the vector of ordered average energy samples $\boldsymbol{\varepsilon}'$. In particular, since every collected bin gives a contribution, in terms of accumulated samples, equal to $N_\mathrm{s} W T_\mathrm{ED}$, the total number of samples collected by k bins is ${N_\mathrm{u}}^{(k)} = k N_\mathrm{s} W T_\mathrm{ED}$.[16] Considering the ordered vectors $\boldsymbol{\varepsilon}'$ and $\boldsymbol{\lambda}'$, the ASNR (2.20) or (2.31) corresponding to the selection of the first k ordered bins can be rewritten as

$$\gamma^{(k)} = \frac{N_\mathrm{s}}{2N_0} \sum_{n=1}^{k} \lambda'_n \tag{2.36}$$

for the SaG-AcR and

$$\gamma^{(k)} = \frac{N_\mathrm{s}}{4N_0} \sum_{n=1}^{k} \lambda'_n \tag{2.37}$$

for SaG-EDR. Therefore, the optimum number of bins can be expressed as

$$\widehat{k} = \underset{k \in \{1, \ldots, N_\mathrm{bin}\}}{\operatorname{argmin}} \; P_e\left(\gamma^{(k)}, {N_\mathrm{u}}^{(k)}\right) \tag{2.38}$$

where $P_e(\gamma^{(k)}, {N_\mathrm{u}}^{(k)})$ is given by (2.24). Once $\widehat{k}$ is calculated, the threshold ξ in (2.35) can be set as

$$\xi = \frac{\varepsilon'_{\widehat{k}} + \varepsilon'_{\widehat{k}+1}}{2}\,. \tag{2.39}$$

Note that the minimum search in (2.38) can be stopped when the BEP starts increasing since the energy samples are considered in decreasing order.[17]

This optimal approach for the threshold setting requires the knowledge of the ASNR and the noise PSD N_0. In general, $\gamma^{(k)}$ is not known a-priori therefore it has to be estimated through (2.36) or (2.37) by substituting λ'_n with $\widehat{\lambda'}_n$ calculated by (2.34). Similarly, if N_0 is not known, it needs to be estimated as explained in Section 2.5.1.

Approximate Optimum Threshold

Analyzing the properties of (2.24), it is possible to avoid its direct evaluation and minimization in (2.38) by an alternative solution which consists on the search for an approximate optimum threshold (AOT) through an iterative approach. For instance, suppose to perform the minimization (2.38) and to

[16] The notations $A^{(k)}$ and $A_{(k)}$ indicates that the quantity A refers to the case where only the first k out of N_bin bins with indexes $\pi_1, \ldots, \pi_k$ are selected.

[17] This leads to a function with only one absolute minimum.

be at step k having already collected the $k-1$ strongest bins: if we add another bin there is an increase of $\Delta N_{\mathrm{u}} = N_{\mathrm{s}} W T_{\mathrm{ED}}$ collected samples. This increment is favorable only if the corresponding ASNR variation, indicated with $\Delta\gamma$, is such that $P_{\mathrm{e}}(\gamma^{(k-1)} + \Delta\gamma, {N_{\mathrm{u}}}^{(k-1)} + \Delta N_{\mathrm{u}}) < P_{\mathrm{e}}(\gamma^{(k-1)}, {N_{\mathrm{u}}}^{(k-1)})$. Since the increment ΔN_{u} depends only on receiver parameters (i.e., W and T_{ED}), it is possible to define the function

$$\Delta P_{\mathrm{e}}(\gamma, \Delta\gamma, N_{\mathrm{u}}) = P_{\mathrm{e}}(\gamma + \Delta\gamma, N_{\mathrm{u}} + \Delta N_{\mathrm{u}}) - P_{\mathrm{e}}(\gamma, N_{\mathrm{u}}) \tag{2.40}$$

which represents the variation of the BEP from step k to step $k+1$. This function can be numerically inverted, by setting $\Delta P_{\mathrm{e}}(\gamma, \Delta\gamma, N_{\mathrm{u}}) = 0$, finding the ASNR variation $\Delta\gamma \triangleq g(\gamma, N_{\mathrm{u}})$ required to decrease the BEP. The particularity that leads us to this approach is the fact that $g(\gamma, N_{\mathrm{u}})$ is, with good approximation, not function of γ and N_{u} individually but of the ratio γ/N_{u}, that is, equivalently $g(\gamma N_{\mathrm{u}}, N_{\mathrm{u}})$ is only function of γ. To prove this, in Fig. 2.5 we shows the curves $g(\gamma N_{\mathrm{u}}, N_{\mathrm{u}})$ as a function of γ, varying N_{u}; in particular we consider $N_{\mathrm{u}} = 10$ (blue lines with $\circ$) and $N_{\mathrm{u}} = 50$ (red lines with $\triangle$), and different increments of the number of samples collected, that is, $\Delta N_{\mathrm{u}} = 2$, $\Delta N_{\mathrm{u}} = 4$, $\Delta N_{\mathrm{u}} = 8$ and $\Delta N_{\mathrm{u}} = 16$. The figure confirms only a very weak dependence of $g(\gamma N_{\mathrm{u}}, N_{\mathrm{u}})$ from N_{u}, hence the above approximation appears reasonable. As further confirmed by numerical results in Section 2.6, such an approximation is more than satisfactory, especially for small ΔN_{u}. Therefore, for a given ΔN_{u} we define a new function, $\widetilde{g}(s) \approx g(s\bar{N}_{\mathrm{u}}, \bar{N}_{\mathrm{u}})$, reflecting the approximation, where $\bar{N}_{\mathrm{u}}$ is a fixed value,[18] such that now $\Delta\gamma \approx \widetilde{g}(\gamma/N_{\mathrm{u}})$. This function $\widetilde{g}(s)$ is so represented by the curves of Fig. 2.5 substituting γ with $s = \gamma/N_{\mathrm{u}}$ in the horizontal axis.

Starting from these considerations it is possible to find the optimum number of bins to be collected with the following iterative algorithm:[19]

$k = 0$
repeat
  $k = k + 1$
  calculate $\Delta\gamma = \gamma^{(k)} - \gamma^{(k-1)}$
until $\Delta\gamma < \widetilde{g}\big(\gamma^{(k-1)}/N_{\mathrm{u}}^{(k-1)}\big)$
set $\widehat{k} = k - 1$

where $\gamma^{(k)}$ is given by (2.36) or (2.37), depending on the receiver, and assuming $\gamma^{(0)} = 0$, $N_{\mathrm{u}}^{(0)} \neq 0$. Once found $\widehat{k}$ the threshold ξ can be set according to (2.39). As for the OT scheme it is necessary to estimate the ASNR and, the noise PSD.

[18] The value does not affect the result.

[19] The function $\widetilde{g}(s)$ can be stored in a lookup table.

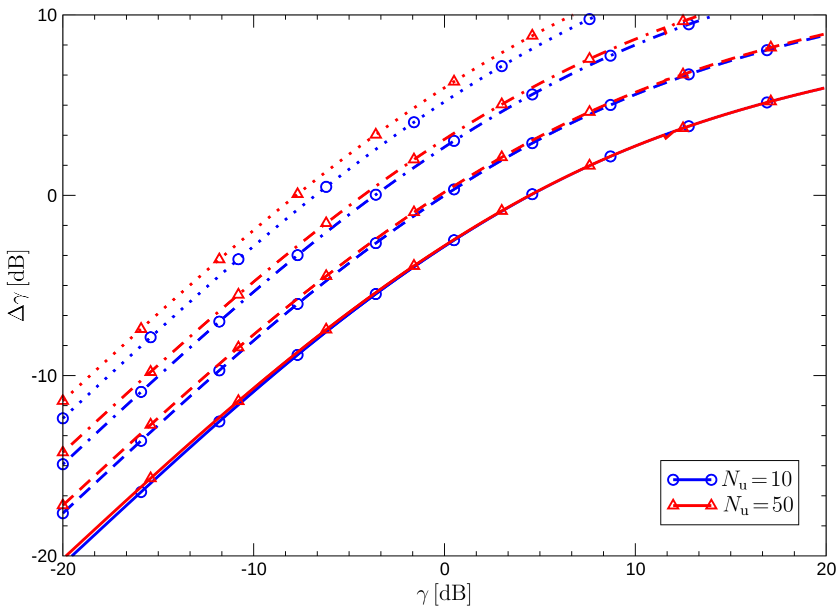

Figure 2.5: Required ASNR improvement $\Delta\gamma$ as function of the ASNR γ for different N_u. Continuous lines (–) are for $\Delta N_u = 2$, dashed lines (- -) are for $\Delta N_u = 4$, dot-dashed lines (·-) are for $\Delta N_u = 8$, dotted lines (··) are for $\Delta N_u = 16$.

Channel Ensemble Optimum Threshold

A third method for setting the threshold is based on the a-posteriori analysis of the average BEP, that is, averaged over several CIRs, as a function of the threshold-to-noise ratio (TNR) $\mathsf{TNR} = \xi/N_0$. More precisely, we define the channel ensemble optimum threshold (CEOT), as the one that minimizes the average BEP for each average SNR and for the considered channel model. Such definition is motivated by the numerical results in Section 2.6 showing that the TNR giving the minimum average BEP for the SaG receivers has a weak dependence on the channel model and on the SNR. Therefore, by the use of such curves, it is possible to derive the optimum TNR and consequently the CEOT, once the noise PSD is known. Note that, such threshold is fixed for a given channel and average SNR, and does not guarantee optimal performance for each channel response realization as the OT presented in Section 2.5.1 or the AOT search in Section 2.5.1, but it produces the minimum BEP on average over the channel ensemble. The advantage is that once the optimal TNR is known, it does not need any further calculation unless the system parameters are changed, leading to a rather simple implementation.

Noise Power Estimation

All threshold-based proposed SaG receivers require noise power knowledge, hence if N_0 is not known a-priori, it must be estimated. A simple method to perform noise power estimation is to consider the average energy of the last $\widetilde{k}$ bins taken from the vector $\boldsymbol{\varepsilon}'$ of ordered energy samples, that likely contain noise only. In this manner the estimator for N_0 is given by

$$\widehat{N}_0 = \frac{\sum_{n=\widetilde{k}+1}^{N_{\text{bin}}} \varepsilon'_n}{\left(N_{\text{bin}} - \widetilde{k}\right) W T_{\text{ED}}}. \tag{2.41}$$

Obviously the estimation accuracy is related to $\widetilde{k}$, N_{a} and availability of at least $\widetilde{k}$ noise-only bins. Therefore, the parameter $\widetilde{k}$ needs to be chosen carefully to avoid the presence of signal-plus-noise bins in the last $\widetilde{k}$ elements of $\boldsymbol{\varepsilon}'$. Such information requires in general some a-priori knowledge of the CIR duration. If not available, the blind bin selection strategy described in the next section can represent a very robust and viable solution.

2.5.2 Blind Bin Selection Strategy

To derive a bin selection strategy that does not require any a-priori knowledge about the ASNR and the noise PSD, and does not need to set-up a threshold, we propose an approach based on ITC for model order selection problems [108, 87, 109, 88]. The key idea is the same as the one already presented for the integration time determination problem in Sec.1.3, and involves determining the bins containing noise only by using model order selection methods. In this way, the decision device in Fig. 2.3 acts as a non-linear excision filter, which allows the deletion of the noise-only bins [89, 110]. In particular, we define a family of models to fit the observed data $\boldsymbol{\mathcal{E}}$. The family of models is defined in a way that for each model, the number of free adjusted parameters is equal to the number of signal-plus-noise bins. With model order selection we then choose the model that best fits the data, which corresponds to the model with the number of free adjusted parameters equal to the actual number of signal-plus-noise bins. Once the bins containing the desired signal are detected, noise-only bins can be deleted by the switch.

Formalizing the problem, the ITC chooses as $\widehat{k}$ the value that minimizes the function [87]

$$\mathsf{ITC}(k) = -2 \ln f\left(\boldsymbol{\mathcal{E}}; \widehat{\boldsymbol{\Theta}}^{(k)}\right) + \mathcal{L}(k) \tag{2.42}$$

where $f(\cdot;\cdot)$ is the likelihood function of observed data $\boldsymbol{\mathcal{E}}$ conditioned on the vector of estimated parameters, $\widehat{\boldsymbol{\Theta}}^{(k)}$, under model order hypothesis k, and

$\mathcal{L}(k)$ is a penalty term that depends on the specific model order selection rule as shown later.

To exploit the model order selection strategy (2.42) the p.d.f.s of the r.v.s representing the observations is required. The energy sample $\mathcal{E}_{q,n}$ at the output of the ED is a non-central Chi-square distributed r.v. whose p.d.f. is [86, 111]

$$f_{\mathrm{S}}(\varepsilon;\lambda_n,\sigma^2)=\frac{W}{\sigma^2}f_{\mathrm{NC}}\left(\frac{W}{\sigma^2}\varepsilon,\frac{W}{\sigma^2}\lambda_n,\bar{\nu}\right),\qquad \varepsilon\geq 0 \tag{2.43}$$

with $\bar{\nu}=2WT_{\mathrm{ED}}$ degrees of freedom.[20] For those bins containing noise only, (2.43) reduces to a central Chi-square distribution with p.d.f. [86, 111]

$$f_{\mathrm{N}}(\varepsilon;\sigma^2)=\left(\frac{W}{\sigma^2}\right)^{\frac{\bar{\nu}}{2}}f_{\mathrm{C}}\left(\frac{W}{\sigma^2}\varepsilon,\bar{\nu}\right),\qquad \varepsilon\geq 0\,. \tag{2.44}$$

In the k-th model order hypothesis the parameter vector is

$$\widehat{\boldsymbol{\Theta}}^{(k)}=\Big(\underbrace{\widehat{\lambda'}_1^{(k)},\ldots\ldots,\widehat{\lambda'}_k^{(k)}}_{k\,\text{signal-plus-noise bins}},\underbrace{0,\ldots\ldots\ldots\ldots,0}_{N_{\mathrm{bin}}-k\text{ noise-only bins}},\sigma^2_{(k)}\Big) \tag{2.45}$$

where $\widehat{\lambda'}_n^{(k)}>0$ represents the non-centrality parameter estimate, obtained by (2.34) where σ^2 is replaced by its ML estimate, $\widehat{\sigma}^2_{(k)}$, under the hypothesis of having $N_{\mathrm{bin}}-k$ noise-only bins, that is

$$\widehat{\sigma}^2_{(k)}=\frac{1}{T_{\mathrm{ED}}}\frac{\sum_{n=k+1}^{N_{\mathrm{bin}}}\varepsilon'_n}{N_{\mathrm{bin}}-k}\,. \tag{2.46}$$

Then,

$$\widehat{k}=\underset{k\in\{1,\ldots,N_{\mathrm{bin}}\}}{\operatorname{argmin}}\ \mathsf{ITC}(k) \tag{2.47}$$

and the corresponding switch state to allow deletion of noise-only bins during symbol detection is $u_{\pi_n}=1$ for $n=1,\ldots,\widehat{k}$ and $u_{\pi_n}=0$ elsewhere.

The joint p.d.f. of the matrix $\boldsymbol{\mathcal{E}}$ in (2.42) can be calculated considering that the output of the energy detector produces independent random variables in $q=1,\ldots,N_{\mathrm{a}}$ and $k=1,\ldots,N_{\mathrm{bin}}$ [89]. Therefore, the log-likelihood

[20] For convenience it is assumed that $2WT_{\mathrm{ED}}$ is an integer.

function of observed data becomes[21]

$$\ln f\left(\boldsymbol{\mathcal{E}};\widehat{\Theta}^{(k)}\right)=\sum_{q=1}^{N_\mathrm{a}}\left[\sum_{n=1}^{k}\ln f_\mathrm{S}\left(\mathcal{E}_{q,\pi_n};\widehat{\Theta}_n^{(k)},\widehat{\sigma}^2_{(k)}\right)+\sum_{n=k+1}^{N_\mathrm{bin}}\ln f_\mathrm{N}\left(\mathcal{E}_{q,\pi_n};\widehat{\sigma}^2_{(k)}\right)\right]. \tag{2.48}$$

Finally, the term $\mathcal{L}(k)$ in (2.42) is a penalty term which has different expressions according to the model order selection rule. For the AIC [108, 91] it is $\mathcal{L}(k)=2(k+1)$, since $k+1$ is the number of parameters under the hypothesis k (k non-centrality parameters for the k signal-plus-noise bins, plus the noise variance $\widehat{\sigma}^2_{(k)}$). For the BIC [112] it is $\mathcal{L}(k)=(k+1)\log N_\mathrm{a}$.

2.6 Numerical Results

In this section, we compare the SaG receivers with the conventional AcR and EDR. In particular, we consider $N_\mathrm{s}=2$ and transmitted pulses compliant with the IEEE 802.15.4a standard [113]: RRC pulses[22] with pulse width parameter $T_\mathrm{w}=1\,\mathrm{ns}$,[23] roll-off factor $\nu=0.6$, center frequency $f_\mathrm{c}=4\,\mathrm{GHz}$ are adopted. At the receiver, an ideal band-pass filter with bandwidth $W=2\,\mathrm{GHz}$ centered at frequency f_c is considered.[24] Performance analysis is proposed in the IEEE 802.15.4a multipath channel model [114] and, if not otherwise stated, the channel model CM1 is considered, with channel responses duration truncated up to 150 ns. For both conventional AcR and EDR, and SaG receivers we consider a time-bandwidth product $WT=300$, which guarantees to capture the entire CIRs. The BEP, averaged on different channel realizations, as function of the average SNR, is adopted as performance metric.

Figure 2.6 presents the averaged BEP of the proposed SaG receivers as function of N_a considering the OT bin selection strategy (Section 2.5.1) with perfect knowledge of the noise power and of the non-centrality parameters

[21] Note that, because of the ordering imposed to the parameter vector $\boldsymbol{\lambda}'$ (and as a consequence on the non-centrality parameters in (2.45)) the column indexes in $\boldsymbol{\mathcal{E}}$ are permutated accordingly to $\boldsymbol{\pi}$. Equation (2.43) returns an indeterminate form in the case the non-centrality parameter estimate $\widehat{\lambda'}_n^{(k)}$ is equal to zero; this fact seems to occur since we adopt the estimator (2.34) that subtracts the average noise energy from each energy sample. However the noise power estimation is performed on the last $N_\mathrm{bin}-k$ energy samples of $\boldsymbol{\varepsilon}'$, hence $\widehat{\sigma}^2_{(k)}$ is always smaller than, or equal to, the energy of the signal-plus-noise bins, guaranteeing that $\widehat{\lambda'}_n^{(k)}>0$ for $n=1,\dots,k$.

[22] See (3.63) for the definition.

[23] The correspondent pulse duration is $T_\mathrm{p}\approx 3T_\mathrm{w}$.

[24] The value of the receiving filter bandwidth $W=2/T_\mathrm{w}=2\,\mathrm{GHz}$ ensures that the signal spectrum of bandwidth $(1+\beta)T_\mathrm{w}=1.6\,\mathrm{GHz}$ passes undistorted.

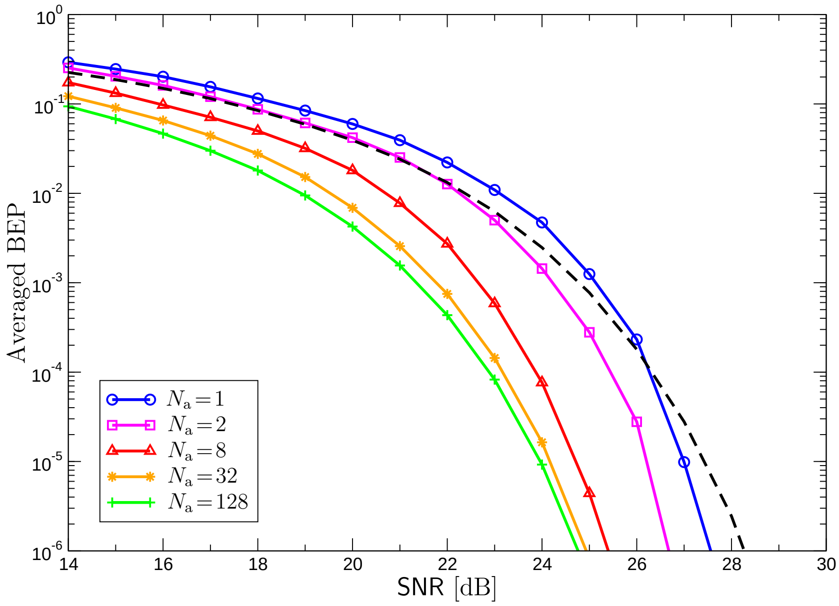

Figure 2.6: Performance of the proposed SaG receivers as function of the number of accumulations N_a with optimal threshold. Dashed line (--) is for the conventional AcR and EDR.

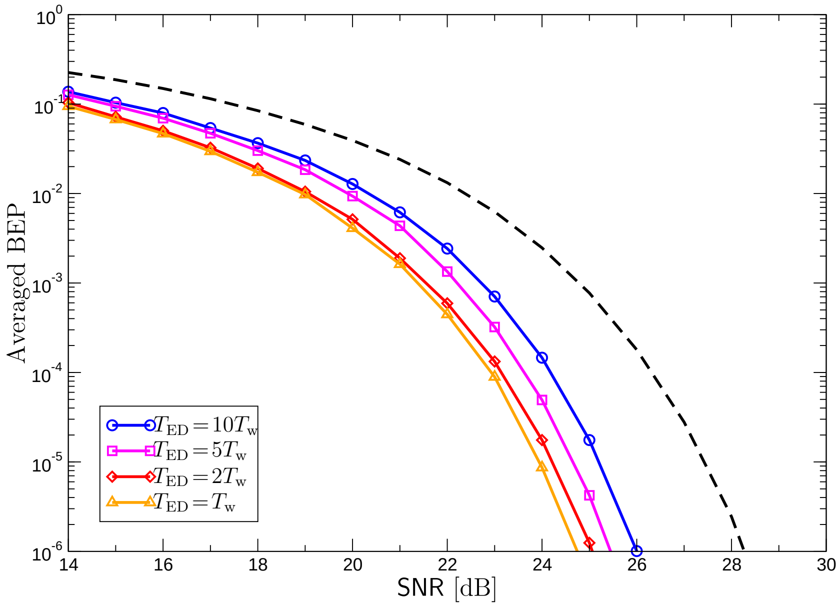

Figure 2.7: Performance of the proposed SaG receivers as function of the integration time T_{ED} of DEC with optimal threshold. Dashed lines dashed line (--) is for the conventional AcR and EDR.

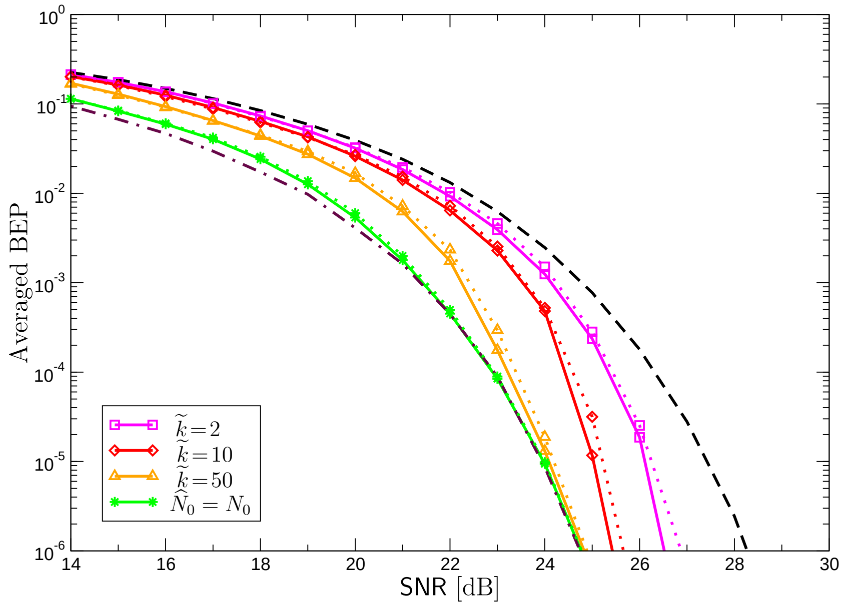

Figure 2.8: Performance of the proposed SaG-AcR for different number $\widetilde{k}$ of bins considered for noise PSD estimation. Continuous lines (–) are for the receiver with OT, dotted lines (··) are for the receiver with AOT. Dashed line (--) is for the conventional AcR. Dot-dashed line (-·) is for the prior knowledge of N_0 and the non-centrality parameters λ_n (ideal receiver).

λ_n (ideal receiver). An ED integration time $T_{\mathrm{ED}} = T_{\mathrm{w}}$ is considered. For comparison, the performance of the conventional AcR is reported. The figure shows that the proposed scheme presents a gain of about 3–4 dB with respect to the conventional AcR if a proper number of accumulations on the energy profile is adopted (e.g., $N_{\mathrm{a}} > 8$). In the following, a value $N_{\mathrm{a}} = 128$ is considered. The impact of a different ED integration time T_{ED} of DEC is reported in Fig. 2.7. As expected, the best BEP is achieved for a T_{ED} comparable to the pulse duration ($T_{\mathrm{ED}} = T_{\mathrm{w}}$), but significant gains are also present for longer integration times with a consequent decrease of the receiver complexity. In the following results we will assume $T_{\mathrm{ED}} = T_{\mathrm{w}}$.

We now focus the analysis on the effects of the different bin selection strategies. In the following we consider the SaG-AcR.[25] Figure 2.8 presents the performance of the SaG-AcR with OT (in continuous lines), for different number of bins $\widetilde{k}$ considered for noise PSD estimation operated by (2.41).

[25]It has been demonstrated that the BEP is the same for SaG-AcR and SaG-EDR. However, the EDR performs the bin selection with an effective SNR 3 dB higher than the AcR, due to the fact that $E_{\mathrm{p}}^{\mathrm{TR}} = \frac{1}{2} E_{\mathrm{p}}^{\mathrm{ED}}$. The effective performance of the SaG-EDR is then improved due to the possibility of taking more reliable decisions on the bins to be integrated.

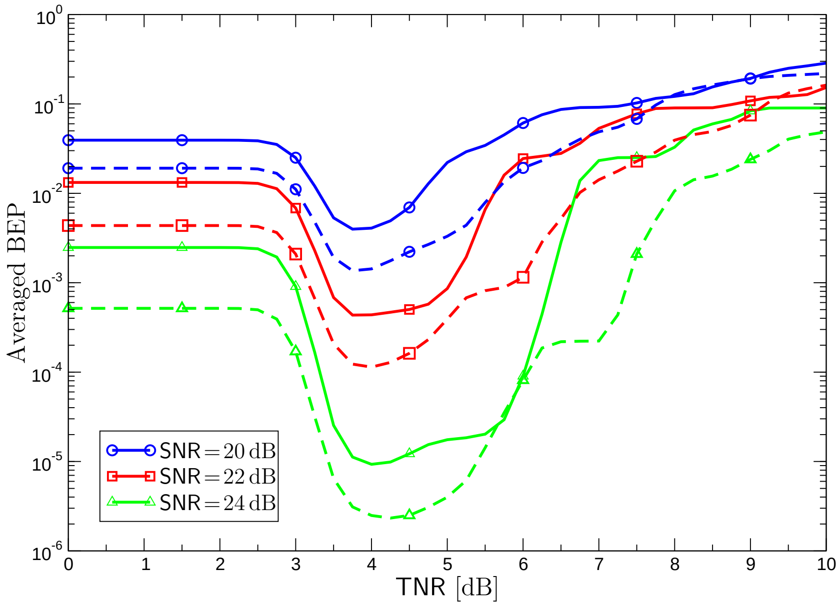

Figure 2.9: Performance of the proposed SaG-AcR with fixed threshold ξ as function of TNR for different SNRs. Continuous lines (–) are for the CM1 channel model, dashed lines (--) are for the CM5 channel model.

From the estimate $\widehat{N}_0$, the non-centrality parameters $\widehat{\lambda}'_n$ are obtained by (2.34). Comparison with the case of perfect noise PSD knowledge and estimation of λ_n, as well as perfect knowledge of both noise power and λ_n is also provided. In the same plot the results obtained with AOT are also reported (in dotted lines). Regarding the AOT, given the adopted N_s, W and T_ED, we have $\Delta N_\mathrm{u} = 4$ for the threshold calculation.[26] A realistic implementation accounting for a quantization step of 0.1 dB for $s = \gamma / N_\mathrm{u}$ in the lookup table containing $\widetilde{g}(s)$ is considered. As we can see, increasing $\widetilde{k}$ decreases the variance of noise power estimate with a corresponding performance improvement. The value $\widetilde{k} = 50$ allows obtaining a performance almost comparable to the one of the receiver with perfect parameter knowledge at high SNR, while a loss of about 1 dB is present at medium SNR correspondent to a BEP of 10^{-3}. It is important to remark that a significant gain is in any case present with respect to the conventional AcR, and the estimation of the non-centrality parameters λ_n adopting the simplified estimator (2.34) does not significantly worsen the performance. Moreover, the adoption of the AOT results in a minimum performance loss with respect to the OT. It is important to remark that in this case the threshold setting procedure is significantly simplified.

[26] The curve corresponding to $N_\mathrm{u} = 10$ in Fig. 2.5 is adopted.

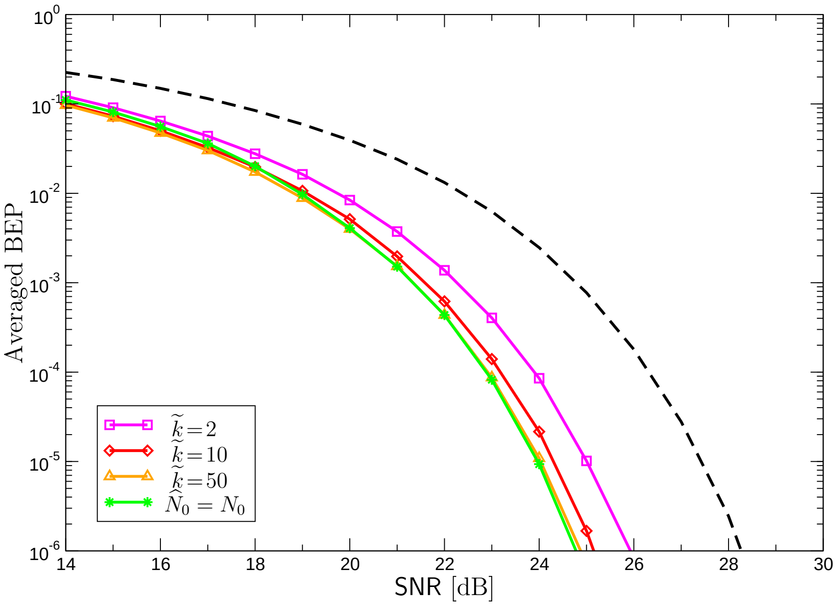

Figure 2.10: Performance of the proposed SaG-AcR with fixed threshold $\mathsf{TNR} = 4\,\text{dB}$ for different number $\widetilde{k}$ of bins considered for noise PSD estimation. Dashed line (--) is for the conventional AcR.

We now consider on the CEOT described in Section 2.5.1. Figure 2.9 shows the averaged BEP as function of the TNR for different average SNRs and considering the CM1 and the CM5 channel models. For high TNRs the performance worsens as the bin selection reduces the amount of signal energy at the input of the integrator, while when the TNR is below 2 dB the performance is that of the conventional AcR. For the parameter T_{ED} considered, there is an optimum TNR value between 4 to 4.5 dB, which minimizes the averaged BEP irrespectively, with good approximation, of the SNR and channel model. Hence, it is possible to set-up a threshold that depends on N_0 and the receiver parameters, in particular the integration time T_{ED}. Adopting this approach the only estimation of $\widehat{N}_0$ is necessary with a significant reduction of the receiver complexity.[27] In Fig. 2.10, the averaged BEP of the proposed receiver with $\mathsf{TNR} = 4\,\text{dB}$ and that of the conventional AcR are reported as a function of the number $\widetilde{k}$ of bins considered for noise power estimation. It is important to underline how in this case with $\widetilde{k}=10$ only the performance is significantly close to the one of the receiver with perfect noise power knowl-

[27]The value of $\mathsf{TNR}=4\,\text{dB}$ which results in a minimum BEP is also easily explainable: a noise-only bin has an average energy $N_0 W T_{\text{ED}}$, which corresponds to $2N_0$ since we considered $T_{\text{ED}} = T_{\text{w}}$ and $W = 2/T_{\text{w}}$, as a consequence the threshold ξ is just 1 dB above the average energy of noise bins, enough to remove noise-only bins and preserve signal-plus-noise bins.

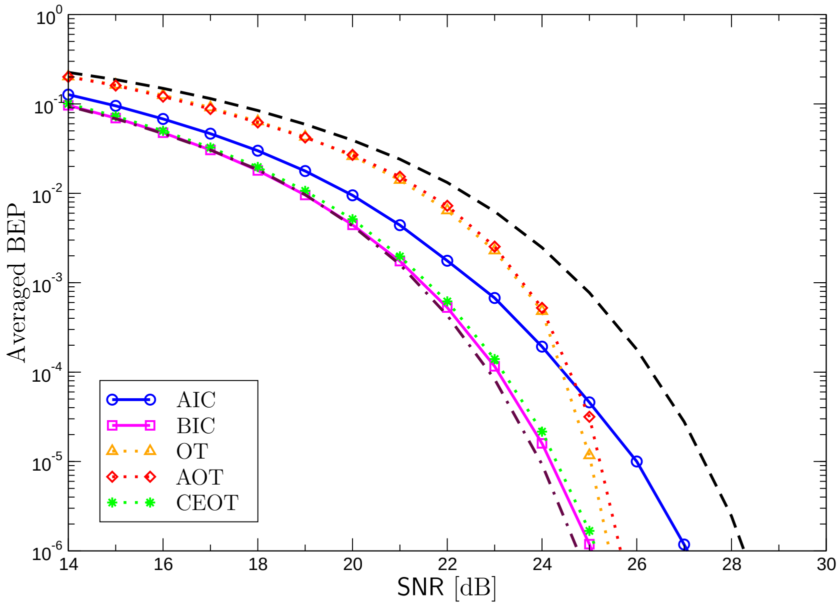

Figure 2.11: Performance of the SaG-AcR with different bin selection strategies. Continuous lines (–) are for the blind selection strategy. Dotted lines (··) are for the threshold-based strategies with $\widetilde{k} = 10$. Dashed line (--) is for the conventional AcR. Dot-dashed line (-·) is for the SaG-AcR with optimum threshold and prior parameter knowledge (ideal receiver).

edge: this fact can be explained since adopting this threshold setting method the estimation of the non-centrality parameters λ_n operated starting from $\widehat{N}_0$ is avoided, with a consequent prevention of estimation errors propagation.

Finally, the performance of the SaG-AcR receiver with the blind bin selection strategy presented in Section 2.5.2, is reported in Fig. 2.11. For comparison, the results regarding threshold-based bin selection strategies with $\widetilde{k} = 10$ are reported. Analyzing the curves we can conclude that the AIC criterion is not the best choice to properly select the bins, especially at high SNR: this is mainly due to the fact that AIC tends to overestimate the model order, that is, the number of bins containing useful multipath energy, hence collecting energy also from noise-only bins [87]. On the contrary the BIC is a consistent criterion and for a sufficient number of observations, N_a, it properly selects the signal-plus-noise bins. Adopting the BIC criterion the performance of the proposed receiver with blind selection strategy is very close to that of the receiver adopting the CEOT and the ideal receiver with OT and a-priori parameters knowledge, and performs better than OT and AOT when noise power and non-centrality parameters λ_n need to be estimated. It is interesting to remark despite the CEOT is optimal for the channel ensemble while the OT and AOT are optimized for (hence dependent on) each CIR, CEOT performs better for intermediate SNRs. This behavior can be explained considering that while CEOT requires only noise power estimation, OT and AOT need also non-centrality parameters estimation, therefore CEOT results to be more robust at low and medium SNRs, where estimation errors can be relevant.

2.7 Conclusion

In this chapter, novel AcR and EDR schemes for UWB BPAM-TR and BPPM, called SaG receivers have been introduced. They are based on energy detection, that avoid noise energy collection from those intervals of the received signal that do not contain useful energy. The proposed strategy is easy to implement and therefore is attractive for robust low-complexity communication systems. First, a closed-form semi-analytical expression, which provides insight into the impact of noise and energy collection on system performance has been derived. Starting from this, different bin selection strategies with different complexities and performance have been investigated. Finally, the numerical comparison of the proposed receivers with the conventional AcR and EDR and for different bin selection strategies highlights the performance gain that can be obtained adopting the SaG strategy, with a potential extension of the benefits to other non-coherent UWB signaling techniques.

Part II

Time-Delay Estimation

Introduction

Time-delay estimation (TDE), also referred to as *epoch* estimation or TOA estimation, is a classical signal processing problem and a fundamental operation in different context [115, 116, 117, 118, 119, 120, 121, 122, 51, 123]. TDE is necessary for timing digital receivers, audio processing and source localization [124, 125, 126] radar and sonar target distance estimation [127, 128, 129, 130, 131], synchronization of wired or wireless systems [132, 133], and it is one of the functionalities enabling localization, key feature of context-aware wireless networks [134, 135, 51].

In fact, among different localization techniques, those based on distance estimation (ranging) are more suitable for high localization accuracy.[28] Starting from TOA measurements, that is starting from the knowledge of the propagation time between two devices, it is in fact possible to recover directly the distance (i.e., the range) by simple multiplication for the speed of light. It is well known that ranging accuracy is directly proportional to the signal bandwidth and hence the use of wideband or UWB signals is attractive for ranging applications. In particular, UWB technology offers the potential of achieving high ranging accuracy even in harsh environments [51, 139, 134, 140, 138], due to its ability to resolve multipath [53, 54, 55]. Ranging techniques based on TOA estimation of the first arriving signal path are mainly affected by noise, multipath components, pulse distortion, obstacles, interference, and clock drift [141, 51, 134, 140, 142]. These problems, mainly due to the propagation environment, especially when indoor, pose several limitations on the achievable performance in terms of accuracy since the received signal has embedded some unknown parameters or, in the worst case, must be considered almost totally unknown. In these cases practical estimation techniques have been proposed. Unfortunately, the known bounds are very optimistic when compared to the performance of these practical estimators [51].

The aim of this part is presenting some novel results on performance bounds for TDE when signals are partially known or unknown at the receiver, with applications to the various contexts already remarked and with a particular emphasis on the problem of ranging for location determination.

[28]We refer the reader to [24, 52] for more information on the variety of localization techniques and to [136, 137, 138] for the fundamentals bounds.

Chapter 3

Bounds on Time-Delay Estimation for Partially Known and Unknown Signals

3.1 Motivations

Several papers address the TOA estimation problem in the presence of multipath such as [55, 59], where amplitudes and delays of the multipath components are jointly estimated using the ML approach [55, 59] or the generalized ML based technique analyzed in [143] (see for example the survey [51] and the references therein).

Such kind of estimators rely on coherent correlation, that is, they assume local knowledge of the received pulse template, and offer in theory the best performance. However their design and implementation is not always practical for several reasons. In fact the waveform shape estimation might be computationally intensive when signals are distorted by the channel. Even with perfect knowledge of the waveform, especially adopting UWB signals, pulse overlap due to multipath might result in strong signal distortion. In addition, the waveform could not be completely well specified at the transmitter side due to random phase of the local oscillator, as will be clarified later. For these reasons a plethora of approaches with different levels of complexity and performance have been developed in the literature. Among them, of particular interest when dealing with low complexity receivers and unknown waveforms, are those relying on energy measurements [144, 51, 145, 132, 146, 147, 148, 135, 149]. In many of these approaches the energy of the received signal is evaluated in time slots with duration T comparable with the pulse duration. Several techniques are proposed to identify the index of the time slot containing the first arriving signal components. Unfortunately one drawback of these approaches is that a floor on estimation mean squared error (MSE), equal to $T^2/12$, arises due to time discretization.

Moreover, although energy detection is widely investigated both from the practical and from the theoretical point of view for the signal detection problem, especially when in presence of unknown deterministic signals [86, 150, 151, 152, 153, 111, 154, 155, 156], a general lack of theoretical foundation is present for the TOA estimation problem, despite the broad application of the technique.

Besides specific TOA estimation algorithms, estimation error bounds play a fundamental role since they serve as useful performance benchmarks for the design of TOA estimators.

Cramér-Rao bound (CRB) has been widely used as a performance benchmark for assessing the estimator error [157, 122, 158, 51, 159, 160]. Its use is justified by asserting that the performance of the ML estimator approaches asymptotically to the CRB for sufficiently high SNRs [66]. It is well known, however, that the CRB is not accurate at low and moderate SNR. In fact, the performance of the TOA estimator, as all non-linear estimators, is characterized by the presence of distinct SNR regions (i.e., low, medium, and high SNRs) corresponding to different modes of operation. This behavior is referred to as the *threshold effect* [161] and it has been studied in a variety of contexts (e.g., [116, 162, 117, 163, 118, 119]). In a low SNR region (also known as the *a priori region*), the MSE is close to that obtained solely from the a priori information about the TOA and signal observations provide little additional information. In a high SNR region (also known as the *asymptotic region*), the MSE is accurately predicted by the CRB. Between these two extremes, there may be an additional region (also known as the *transition region* or *ambiguity region*) where observations are subject to ambiguities that are not accounted for by the CRB [66].

Although CRB accurately predicts the MSE in asymptotic region, operating conditions in such a region are often impractical due to the requirements on emitted power level typical in short-range systems. In addition, the CRB cannot be derived in certain conditions [66]. Therefore other bounds, which are more complicated but tighter than the CRB, have been proposed in the literature. In particular, the Barankin bound identifies the SNR values (thresholds) that distinguish the ambiguity region [164, 165]. The Ziv-Zakai bound (ZZB) [166], with its improved versions such as the Bellini-Tartara bound [167] and the Chazan-Zakai-Ziv bound [168], as well as the Weiss-Weinstein bound (WWB) [163] are more accurate than the Barakin bound. They can be applied to a wider range of SNRs and account for both ambiguity effects and a priori information of the parameter to be estimated. However, they may not be analytically tractable in many cases or require more complicated evaluations compared to the CRB, especially when operating in the presence of multipath [169, 170, 171, 172].

In [173] the expression of the CRB for multipath environments is given starting from the joint estimation of channel parameters. In [172] the approach developed in [116, 162] for the estimation of the relative delay between two sensors emitting noise-like signals is extended to that emitting UWB signals. The work [174] evaluates the ZZB for Gaussian signals assuming perfect channel knowledge at the receiver. A few results are present for the case where the receiver has a partial or no knowledge about the channel [170, 171]. In particular, in [170] the ZZB using measured data as well as Monte Carlo generated CRs is investigated, whereas [171] derives the ZZB using second order statistics approach by modeling the received signal as non-stationary Gaussian random process.

The aim of this chapter is to investigate ZZBs on the MSE associated with the TOA estimation of partially known and unknown signals. These bounds represent the performance limits of any TOA estimator dealing with the same hypothesis about signal knowledge. To allow for a comprehensive overview of the problems, some previous results are also revised and discussed when necessary.

The key contributions of the chapter can be summarized as follows:

- Derivation of the ZZB for TOA estimation for signals with unknown phase;
- Derivation of the ZZB for TOA estimation for unknown deterministic signals;
- Comparison of the ZZBs and CRBs with the performance of the revised and derived ML estimators under the same hypothesis on the signal knowledge.

The remainder of the chapter is organized as follows. In Sec. 3.2 the signal and channel models are introduced. The ZZB is reviewed briefly in Sec. 3.3. The bound is then derived in Sec. 3.4 and it is compared to the CRB in the ideal AWGN scenario. Section 3.5 extends the classical ZZB for the case of partially known signals, in particular signals with unknown carrier phase. Section 3.6 derives new fundamental bounds for the case of unknown deterministic signals. For the derivations several tools such as series expansion of signals are revised and extended to particular cases of interest in the appendices. In Sec. 3.7 classical TOA estimators are reviewed considering the results obtained during the derivation of the bounds. Numerical results are then presented in Sec. 3.8 providing a comparison between the bounds and the estimators performance.

3.2 Signal Model

We consider, as transmitted signal, a time-limited waveform $p(t)$ with duration T_{p}. When $p(t)$ has a bandpass nature, we denote by f_{c} its central frequency and we refer, for convenience, to its ELP as $\tilde{p}(t)$ so that

$$p(t) = \Re\left\{\tilde{p}(t)\, e^{\jmath 2\pi f_{\mathrm{c}} t}\right\} . \tag{3.1}$$

Bandpass signals are usually generated starting from in-phase and in-quadrature baseband components $p_I(t)$ and $p_Q(t)$ that are further used as input to a quadrature modulator adopting a local oscillator with carrier frequency f_{c} and initial phase ϕ, that is, $\tilde{p}(t) = \tilde{p}_0(t)\, e^{\jmath\phi}$, with $\tilde{p}_0(t) = p_I(t) + \jmath p_Q(t)$.

Note that every physically realizable signal is time-limited, and hence, rigorously, not limited in bandwidth. However, in practice, the signal bandwidth can be truncated to a suitable value W so that the energy contribution of out-of-band signal components is negligible. More rigorously, we consider $p(t)$ *band-limited at level* ϵ with bandwidth W, if W is the smallest value for which[1]

$$\int_{|f|>W} |P(f)|^2\, df < \epsilon \tag{3.2}$$

where $P(f)$ is the Fourier transform of $p(t)$ and the energy ϵ lying outside the frequency range is less than the smallest amount we are able to detect by any means in the real world [175].

Signal $p(t)$ is transmitted through a channel and the received signal can be expressed as

$$r(t) = s(t-\tau) + n(t) \tag{3.3}$$

where $s(t) = p(t) \otimes h(t)$ is the CR, $h(t)$ is the CIR, τ is the TOA of the received signal to be estimated, and $n(t)$ is AWGN with zero mean and two-sided spectral density $N_0/2$ in the signal band of width W.[2] We consider the delay introduced by the channel de-embedded from $h(t)$ and accounted for by τ. The duration of the received CR $s(t)$ is $T_{\mathrm{s}} = T_{\mathrm{p}} + T_{\mathrm{d}}$, where T_{d} is the

[1] When $p(t)$ has a bandpass nature, the integration in (3.2) is performed over the interval $|f| > \left\{f_{\mathrm{c}} + \frac{W}{2}\right\} \cup \left\{|f| < f_{\mathrm{c}} - \frac{W}{2}\right\}$.

[2] We consider the presence of a zonal filter that removes all the noise components outside W.

maximum excess delay of the channel. In the absence of other information, we assume the TOA τ to be unknown and randomly distributed in the interval $[0, T_\mathrm{a}]$. The goal is to obtain the estimate $\hat{\tau}$ of τ by observing $r(t)$ in the interval $[0, T_\mathrm{ob}]$, with $T_\mathrm{ob} > T_\mathrm{a} + T_\mathrm{s}$, with partial (even statistical) or no knowledge on $s(t)$ available.

For further convenience, we make use of orthonormal series expansion representations of signals in $[0, T_\mathrm{ob}]$ [66, p. 178] using a suitable complete orthonormal basis $\{\Phi_m(t)\}_{m=1}^{M}$, as detailed in Appendix 3.A. Specifically we can write

$$r(t) = \sum_{m=1}^{M} r_m \, \Phi_m(t), \quad 0 \leq t \leq T_\mathrm{ob} \tag{3.4}$$

and

$$n(t) = \sum_{m=1}^{M} n_m \, \Phi_m(t), \quad 0 \leq t \leq T_\mathrm{ob} \tag{3.5}$$

with $M = \lfloor 2WT_\mathrm{ob} \rfloor + 1$ for lowpass signals and $M = 2(\lfloor WT_\mathrm{ob} \rfloor + 1)$ for bandpass signals [176]. Adopting the classical Karhunen-Loéve (KL) expansion (see Appendix 3.A.1 and 3.A.2) we have that $n_m = c_m \, \sigma_n$, with $\sigma_n^2 = \frac{N_0}{2}$, where coefficients $\{c_m\}$ are independent zero mean Gaussian r.v.s with unitary variance. According to the previous series expansion, signals $r(t)$ and $n(t)$ are fully represented by the coefficients vectors $\mathbf{r} = [r_1, r_2, \ldots, r_M]^T \in \mathbb{R}^M$, and $\mathbf{n} = [n_1, n_2, \ldots, n_M]^T \in \mathbb{R}^M$, respectively.

Signal $s(t)$, instead, is by definition time-limited in $0 \leq t \leq T_\mathrm{s}$, therefore it can be conveniently expanded, as reported in Appendix 3.A.3 and 3.A.4), using an orthonormal basis $\{\Psi_n(t)\}_{n=1}^{N}$[3]

$$s(t) = \sum_{n=1}^{N} s_n \, \Psi_n(t) \,, \quad 0 \leq t \leq T_\mathrm{s} \tag{3.6}$$

where $N = \lfloor 2WT_\mathrm{s} \rfloor + 1$ for lowpass signals and $N = 2(\lfloor WT_\mathrm{s} \rfloor + 1)$ for bandpass signals. Since $T_\mathrm{s} < T_\mathrm{ob}$, the dimensionality of coefficients vector $\mathbf{s} = [s_1, s_2, \ldots, s_N]^T \in \mathbb{R}^N$ is less than that of $\mathbf{r}$, that is, $N < M$.

It is possible to express $y(t) = s(t - \tau)$ in (3.3) over the orthonormal basis

[3] There is complete freedom on the choice of the orthonormal base. If the same base leading to the KL expansion of random signals is adopted, it has to be remarked that functions $\{\Phi_m(t)\}$ are different from the ones considered in the expansion $\mathbf{n}$ of the noise, since they are function of the signal duration (see Appendix 3.A.1). Differently, if the basis leading to the sampling expansion, as reported in (3.77), is adopted, the same basis can be used for expanding signals of different duration.

$\{\Phi_m(t)\}_{m=1}^{M}$ as follows

$$y(t) = s(t-\tau) = \sum_{n=1}^{N} s_n\, \Psi_n(t-\tau) = \sum_{m=1}^{M} y_m\, \Phi_m(t) \tag{3.7}$$

where

$$y_m = \sum_{n=1}^{N} s_n \int_0^{T_{\text{ob}}} \Psi_n(t-\tau)\, \Phi_m(t)\, dt = \sum_{n=1}^{N} s_n\, h_{m,n}^{(\tau)} \tag{3.8}$$

and

$$h_{m,n}^{(\tau)} = \int_0^{T_{\text{ob}}} \Psi_n(t-\tau)\, \Phi_m(t)\, dt\,. \tag{3.9}$$

Defining the matrix $\mathbf{H}^{(\tau)} = \{h_{m,n}^{(\tau)}\} \in \mathbb{R}^{M\times N}$, expression (3.3) can be expressed equivalently in the following form

$$\mathbf{r} = \mathbf{H}^{(\tau)}\, \mathbf{s} + \mathbf{n} = \mathbf{y} + \mathbf{n}\,. \tag{3.10}$$

In particular, vector $\mathbf{y}$ lies in a N-dimensional subspace of $\mathbb{R}^M$ denoted by $\langle \mathbf{H}^{(\tau)} \rangle$,[4] with $N < M$. In particular, given a vector $\mathbf{x} \in \mathbb{R}^M$ containing the series expansion coefficient of a generic signal $x(t)$, the orthogonal projection of $\mathbf{x}$ onto $\langle \mathbf{H}^{(\tau)} \rangle$ is denoted by $\mathbf{P}_{\mathbf{H}^{(\tau)}}\, \mathbf{x}$, where $\mathbf{P}_{\mathbf{H}^{(\tau)}}$ is the orthogonal projection matrix (or projector) $\mathbf{P}_{\mathbf{H}^{(\tau)}} = \mathbf{H}^{(\tau)} \left(\mathbf{H}^{(\tau)T} \mathbf{H}^{(\tau)} \right)^{-1} \mathbf{H}^{(\tau)T}$. Note that the orthogonal projection of $\mathbf{x}$ onto $\langle \mathbf{H}^{(\tau)} \rangle$ corresponds to the projection of $x(t)$ onto the interval $[\tau, \tau + T_{\text{s}}]$, that is, the signal $x(t) \cdot \Pi\left(\frac{t-\tau}{T_{\text{s}}}\right)$, for $t \in [0, T_{\text{ob}}]$, with $\Pi(x) \triangleq 1$ for $0 < x < 1$, and zero otherwise.[5] The vector $\hat{\mathbf{y}} = \mathbf{P}_{\mathbf{H}^{(\tau)}} \mathbf{r}$ is, in fact, the estimation of the noise-free received signal $\mathbf{y}$ [177, p. 368],[6] and since we are making the hypothesis of a delay τ through $\mathbf{H}^{(\tau)}$, this estimation must be equal to the received signal itself for the portion containing the useful signal, and zero otherwise [178, p. 250]. In addition it can be shown that

$$\mathbf{x}^T \mathbf{P}_{\mathbf{H}^{(\tau)}} \mathbf{x} = \int_{-\infty}^{\infty} x^2(t)\, \Pi\left(\frac{t-\tau}{T_{\text{s}}}\right)\, dt = \int_{\tau}^{\tau+T_{\text{s}}} x^2(t)\, dt \tag{3.11}$$

[4] This is the span of the column vectors composing $\mathbf{H}^{(\tau)}$.

[5] See the proof of (3.11).

[6] The matrix $\mathbf{P}_{\mathbf{H}^{(\tau)}}$ is, in fact, singular, otherwise it would be possible to recover the received signal $\mathbf{r}$ from his projection $\hat{\mathbf{y}}$, that is clear impossible since different $\mathbf{r}$ can have the same projection $\hat{\mathbf{y}}$.

which represents the energy of $x(t)$ in the interval $[\tau, \tau + T_{\mathrm{s}}]$.

Proof of (3.11) See Appendix 3.B.

The conditional p.d.f. of $\mathbf{r}$ is given by[7]

$$p\{\mathbf{r}|\tau\} = \frac{1}{\left(\sqrt{2\pi\sigma^2}\right)^M} \exp\left\{-\frac{1}{2\,\sigma^2}\left\|\mathbf{r} - \mathbf{H}^{(\tau)}\,\mathbf{s}\right\|^2\right\} \tag{3.12}$$

with $\sigma^2 = N_0 W$.

In the rest of the chapter we will consider different models for $s(t)$. The simplest is the model of known deterministic signal for which the shape $\mathbf{s}$ is exactly known. As partially known signal we consider the case of a deterministic signal for which the shape is not completely known, for example because $s(t)$ has embedded some unknown parameters, such as the carrier phase when it is a bandpass signal. As last we consider an unknown but deterministic signal, for which the shape of the signal $s(t)$ is totally unknown. In this case the only information available on the signal is its bandwidth W, (its nature of lowpass or bandpass signal) and its duration T_{s}. For the deterministic signal case (known, partially known or unknown) we define the SNR as $\mathsf{SNR} = \frac{E_{\mathrm{s}}}{N_0}$, having indicated with E_{s} the energy of $s(t)$.

3.3 The Ziv-Zakai Lower Bound

For reader convenience, we begin with a brief review of the ZZB.[8] It can be derived starting from the following general identity for MSE estimation[9]

$$\mathrm{MSE} = \mathbb{E}\left\{\epsilon_\tau^2\right\} = \frac{1}{2}\int_0^\infty z \cdot \mathbb{P}\left\{|\epsilon| \ge \frac{z}{2}\right\} dz \tag{3.13}$$

where $\epsilon_\tau \triangleq \hat{\tau} - \tau$ represents the estimation error, and then by finding a lower bound on $\mathbb{P}\{|\epsilon_\tau| \ge z/2\}$ [167]. It can be easily shown that

$$\begin{aligned}
&\mathbb{P}\left\{|\epsilon_\tau| \ge \frac{z}{2}\right\} = \\
&\int_{-\infty}^{\infty}\left[p_\tau(\tau)\,\mathbb{P}\left\{\hat{\tau} \ge \tau + \frac{z}{2}\middle|\tau\right\} + p_\tau(\tau+z)\,\mathbb{P}\left\{\hat{\tau} \le \tau + \frac{z}{2}\middle|\tau + z\right\}\right] d\tau
\end{aligned} \tag{3.14}$$

[7] $\|\mathbf{x}\|^2 = \mathbf{x}^T\mathbf{x}$.

[8] Actually, the Bellini-Tartara improved ZZB version [167] is here considered and the correct name should be BTZZB, however we will continue to refer to ZZB for conciseness.

[9] Here the expectation is with respect to τ and $\mathbf{r}$.

where $p_\tau(\tau)$ is the p.d.f. of the TOA τ. The previous expression can be lower-bounded by

$$\begin{aligned} &2\int_{-\infty}^{\infty} \min\left\{p_\tau(\tau), p_\tau(\tau+z)\right\} \\ &\times \left[\frac{1}{2}\mathbb{P}\left\{\hat{\tau} \geq \tau + \frac{z}{2}\middle|\tau\right\} + \frac{1}{2}\mathbb{P}\left\{\hat{\tau} \leq \tau + \frac{z}{2}\middle|\tau+z\right\}\right] d\tau\,. \end{aligned} \tag{3.15}$$

The term in square brackets in (3.15) represents the probability of error for testing of two equally probable hypothesis

$$\begin{aligned} &\mathcal{H}_1 : \; r(t) = s(t-\tau) + n(t) \quad \text{or} \quad \mathbf{r} = \mathbf{H}^{(\tau)}\,\mathbf{s} + \mathbf{n}\,, \\ &\mathcal{H}_2 : \; r(t) = s(t-\tau-z) + n(t) \quad \text{or} \quad \mathbf{r} = \mathbf{H}^{(\tau+z)}\,\mathbf{s} + \mathbf{n} \end{aligned} \tag{3.16}$$

using a suboptimum decision rule in which the parameter is first estimated and a decision is made according to minimum distance between τ and $\tau+z$ as described in [168]. Then (3.15) can be further lower-bounded by replacing the term in square brackets with the error probability $P_{\min}(\tau, z)$ corresponding to the optimum decision rule based on the log-likelihood ratio test (LRT) [66, p. 26]

$$l(\mathbf{r}) = \ln \frac{p\left\{\mathbf{r}|\tau\right\}}{p\left\{\mathbf{r}|\tau+z\right\}} \underset{\mathcal{H}_2}{\overset{\mathcal{H}_1}{\gtrless}} 0\,. \tag{3.17}$$

In general $P_{\min}(\tau, z)$ does not depend on the delay τ thus the bound is formulated with respect to $P_{\min}(z)$ [168]. When τ is uniformly distributed in $[0, T_\mathrm{a}]$ (most ignorance case), the ZZB is given by [167, 168]

$$\mathsf{ZZB} = \frac{1}{T_\mathrm{a}}\int_0^{T_\mathrm{a}} z\left(T_\mathrm{a} - z\right) P_{\min}(z)\; dz\,. \tag{3.18}$$

The main challenge in (3.18) is to design the optimum binary detection scheme based on (3.17) and to derive a tractable expression for its performance $P_{\min}(z)$. It is interesting to observe that the ZZB is obtained by recognizing that the performance evaluation of an estimation problem can be transformed to a binary detection problem. We will exploit this observation in successive sections to obtain the ZZB for the cases of interest.

3.4 ZZB for Known Signals

As explained in Sec. 3.3, the ZZB requires the evaluation of the error probability $P_{\min}(z)$ corresponding to the optimum binary detector (3.17). Whatever test we design can never be better than a "genie test" in which the genie provides the receiver with perfect CR $s(t)$, or equivalently $\mathbf{s}$, and then the receiver performs the optimum likelihood ratio test conditioned on that CR. This is equivalent to evaluate the error probability $P_{\min}\left(z\middle|\mathbf{s}\right)$, conditioned on $\mathbf{s}$, corresponding to a classical coherent binary communication system employing the waveforms $s(t-\tau)$ and $s(t-\tau-z)$ for hypothesis $\mathcal{H}_1$ and $\mathcal{H}_2$, respectively, with known $s(t)$. It is well known [66, p. 254] that the optimum binary detector passes its input $r(t)$ through a filter matched to the signal $s(t-\tau)-s(t-\tau-z)$ and samples its output at time $t=T_{\mathrm{ob}}$. If the output is positive, it chooses hypothesis $\mathcal{H}_1$; if negative, hypothesis $\mathcal{H}_2$. Therefore, the error probability is given by [65, p. 129]

$$P_{\min}\left(z\middle|\mathbf{s}\right) = Q\left(\sqrt{\mathsf{SNR}\left(1-\rho_{\mathrm{s}}(z)\right)}\right) \tag{3.19}$$

where $Q\left(\cdot\right)$ is the Gaussian Q-function, and we have defined $\rho_{\mathrm{s}}(z)$ the normalized auto-correlation function of $s(t)$ as

$$\rho_{\mathrm{s}}(z) = \frac{1}{E_{\mathrm{s}}}\int_{-\infty}^{\infty} s(t)\, s(t-z)\, dt\,. \tag{3.20}$$

By replacing in (3.18) $P_{\min}\left(z\right)$ with $P_{\min}\left(z\middle|\mathbf{s}\right)$, we obtain the ZZB conditioned on $s(t)$

$$\mathsf{ZZB}\Big|_{\mathbf{s}} = \frac{1}{T_{\mathrm{a}}}\int_{0}^{T_{\mathrm{a}}} z\left(T_{\mathrm{a}}-z\right) P_{\min}\left(z\middle|\mathbf{s}\right)\, dz\,. \tag{3.21}$$

It is known that in this case for large SNRs the ZZB converges to the CRB given by [168]

$$\mathsf{CRB} = \left[-\mathbb{E}\left\{\frac{\partial^2}{\partial\tau^2}\ln p\left\{\mathbf{r}|\tau\right\}\right\}\right]^{-1} = \frac{N_0/2}{(2\,\pi)^2 E_{\mathrm{s}}\,\beta^2} = \frac{1}{8\,\pi^2\,\beta^2\,\mathsf{SNR}} \tag{3.22}$$

where β is the *effective bandwidth* of $s(t)$ defined by

$$\beta^2 = \frac{\int_{-\infty}^{\infty} f^2 |S(f)|^2\, df}{E_{\mathrm{s}}} \tag{3.23}$$

and $S(f)$ is the Fourier transform of $s(t)$. Moreover, indicating with $\tilde{s}(t)$ the ELP of $s(t)$, in the particular but common case where $\tilde{s}(t)=s_0(t)$ is an even function, (3.23) can be rewritten as $\beta^2 = f_{\mathrm{c}}^2+\beta_0^2$ where

$$\beta_0^2 = \frac{\int_{-\infty}^{\infty} f^2 |S_0(f)|^2\, df}{2E_{\mathrm{s}}} \tag{3.24}$$

and $S_0(f)$ is the Fourier transform of $s_0(t)$.

Notice that the denominator of (3.22) is proportional to the energy in the signal, where the constant β depends on the shape of the signal and the skewness of its spectrum through (3.23). Having large values of β, that is, a signal with wide transmission bandwidth and/or large center frequency f_c, is beneficial for time-delay estimation.

3.4.1 Average ZZB

In the presence of a frequency selective channel, $s(t)$ is characterized statistically according to some channel model and it belongs in general to a random process $S(t)$ modeling the channel characteristics. The unconditional (average) ZZB can be evaluated by averaging (3.21) on $S(t)$, that is,

$$\mathsf{ZZB} = \mathbb{E}\left\{\mathsf{ZZB}\big|_{S(t)}\right\} = \frac{1}{T_{\rm a}} \int_0^{T_{\rm a}} z\,(T_{\rm a} - z)\, P_{\min}^{(\rm av)}(z)\, dz \qquad (3.25)$$

where

$$P_{\min}^{(\rm av)}(z) \triangleq \mathbb{E}\left\{P_{\min}\left(z\middle|S(t)\right)\right\} \qquad (3.26)$$

and the statistical expectation is taken with respect to the realizations of $S(t)$.

We want to stress that the bound in (3.25) assumes that the receiver has perfect knowledge of the CR. This approach was first proposed in [170] for UWB multipath channels. Note that (3.26) can be seen as the average BEP for coherent detection of a ideal binary PPM Rake receiver in the presence of multipath assuming perfect channel state information. Such BEP expressions are known in the literature [179, 180, 174] and can be exploited to derive the ZZB through (3.25).

3.5 ZZB for Signals with Unknown Phase

In Section 3.2 we mentioned that usually signal $s(t)$ is obtained through modulation of a baseband component $\tilde{p}_0(t)$. In most cases, the initial phase ϕ of the carrier is uncontrolled (*non-coherent transmitter*), for example, because the local oscillator is free-running and not synchronized with the generator of the baseband signal $\tilde{p}_0(t)$. This means that the shape of the transmitted bandpass signal $p(t)$ is not completely determined at the transmitted side and hence coherent TOA estimation at the receiver does not add any additional information on the TOA, as will be clearer later.

The ZZB in (3.21) and the CRB in (3.22) are meaningful when $s(t)$ is completely recovered at the receiver (corresponding to the adoption of a coherent estimator) and the carrier phase ϕ of the transmitted pulse is perfectly controlled at the transmitted (i.e., a coherent transmitter is adopted). As already anticipated, when the initial phase ϕ of the carrier is uncontrolled, it does not carry any additional information on TOA. Hence, the TOA estimation must rely on the signal envelope $|\tilde{s}(t)|$ only.

To evaluate the ZZB, the optimum detector can be derived from the following log-LRT[10] [178, p. 200],[66, p. 87]

$$l(\mathbf{r}) = \ln \frac{\int_0^{2\pi} p\left\{\mathbf{r}|\tau, \phi\right\} p_\Phi(\phi)\, d\phi}{\int_0^{2\pi} p\left\{\mathbf{r}|\tau + z, \phi\right\} p_\Phi(\phi)\, d\phi} \underset{\mathcal{H}_2}{\overset{\mathcal{H}_1}{\gtrless}} 0 \tag{3.27}$$

where the marginal p.d.f.s are evaluated with respect to the uniform distribution $p_\Phi(\phi) = 1/2\pi$ in $[0, 2\pi]$ of the r.v. Φ (most ignorance assumption). In this case the optimum detector corresponds to the envelope detector for binary, equally-energy correlated signals [66, p. 341], which error probability expression is given by [61, p. 312]

$$P_{\min}(z) = Q_1(a(z), b(z)) - \frac{1}{2} e^{-\mathsf{SNR}/2} I_0(a(z)\, b(z)) \tag{3.28}$$

with

$$\begin{aligned} a(z) &= \sqrt{\frac{\mathsf{SNR}}{2}\left(1 - \sqrt{1 - |\rho_0(z)|^2}\right)}, \\ b(z) &= \sqrt{\frac{\mathsf{SNR}}{2}\left(1 + \sqrt{1 - |\rho_0(z)|^2}\right)} \end{aligned} \tag{3.29}$$

and where

$$\rho_0(z) = \frac{1}{2E_\mathrm{s}} \int_0^{T_\mathrm{s}} \tilde{s}^*(t)\, \tilde{s}(t - z)\, dt \tag{3.30}$$

is the normalized complex-valued correlation coefficient between the ELP $\tilde{s}(t - \tau)$ and $\tilde{s}(t - \tau - z)$. $Q_1(a, b)$ denotes the Marcum Q function and $I_0(x)$ is the modified Bessel function of first kind of order zero [106, p. 374]. When $z > T_\mathrm{s}$, $\tilde{s}(t-\tau)$ and $\tilde{s}(t-\tau-z)$ are orthogonal and $P_{\min}(z) = P_{\min} = \frac{1}{2} e^{-\mathsf{SNR}/2}$, that is, it corresponds to the performance of the optimum envelope detector with orthogonal signals [61, p. 311].

[10] Some authors refers to this test as average-LRT (ALRT) [181].

3.5.1 Asymptotic ZZB

In Appendix 3.C it is shown that for large SNR, the asymptotic behavior of $P_{\min}(z)$ in (3.28) is

$$P_{\min}(z) \simeq \sqrt{\frac{1-|\rho_0(z)|}{2|\rho_0(z)|}}\, Q\left(\sqrt{\mathsf{SNR}(1-|\rho_0(z)|)}\right) \approx Q\left(\sqrt{\mathsf{SNR}\,(1-|\rho_0(z)|)}\right). \tag{3.31}$$

Equation (3.31) is formally identical to (3.19), therefore by following the same approach as in [168] it can be shown that, for high SNR,

$$\mathsf{ZZB} \simeq \frac{1}{8\,\pi^2\,\beta_0^2\,\mathsf{SNR}} \tag{3.32}$$

where β_0 is the effective bandwidth of the baseband envelope $|\tilde{s}(t)|$ defined in (3.24). The result in (3.32) tells us that the ZZB tends to the corresponding CRB evaluated considering the received signal ELP instead of the bandpass signal.[11] Contrary to the bounds (3.21) and (3.22), this bound depends on the signal ELP effective bandwidth only and not on the center frequency f_c. This is one of the motivation that justifies the adoption of wideband or, better yet, UWB signals to achieve accurate ranging. Adopting a wideband signal, it is possible to achieve high-accuracy time-delay estimation also without exploiting the phase information, through non-coherent estimation techniques and also in the presence of a non-coherent transmitters. Vice versa, to obtain high TOA estimation accuracy with narrowband signals, coherent transmitters as well as coherent receivers are necessary.

Notice that, in the high-SNR region, the SNR gap between the case between a coherent and a non-coherent estimator is $\Delta\mathsf{SNR} = 10\log_{10}\left(1+\frac{f_c^2}{\beta_0^2}\right)$dB.

3.6 ZZB for Unknown Deterministic Signals

We consider now $s(t)$ be a deterministic but unknown signal. Note that in the absence of additional hypothesis on $s(t)$, it is not possible to identify uniquely the TOA because the starting and ending instants of $s(t)$ would not be defined. Therefore the only assumption we consider is that $s(t)$ is zero outside the interval $[0, T_s]$, and so it can be represented according to the series expansions presented in Section 3.2. The estimation of the TOA has to embed the estimation of the received waveform $s(t)$ by means of its series expansion coefficients $\mathbf{s}$ that have to be treated as nuisance parameters.

[11]The CRB resulting from a phase uncertainty on the received signal, hence related to the ELP, is evaluated in [182, p. 278].

3.6.1 Detector Design

In the absence of any statistical characterization of the nuisance parameters (i.e., in presence of an unknown deterministic signal), the test design procedure to determine $P_{\min}(z)$ in (3.18) is not uniquely defined. A possibility could be the adoption of the detector presented in Section 3.4 assuming perfect knowledge of the received waveform.[12] However, as will be shown in the numerical results, the corresponding ZZB would be in general quite loose with respect the actual performance of realistic estimators.

A practical and usual approach for this kind of problem is to design the detector performing the generalized likelihood ratio test (GLRT) [178, p. 200][66, p. 88]. Unfortunately we cannot state the optimality of the GLRT, then the corresponding ZZB expression is not in general a lower bound. However further considerations about the optimality can be done, considering invariance properties of the detector [183], and will be included in a following up work.

The log-GLRT is obtained by replacing the nuisance parameters $\mathbf{s}$ by their ML estimates $\hat{\mathbf{s}}_1$ and $\hat{\mathbf{s}}_2$, respectively, under hypothesis $\mathcal{H}_1$ and $\mathcal{H}_2$ true [66, p. 92]

$$l(\mathbf{r}) = \ln \frac{p\left\{\mathbf{r}|\tau, \hat{\mathbf{s}}_1\right\}}{p\left\{\mathbf{r}|\tau+z, \hat{\mathbf{s}}_2\right\}} \underset{\mathcal{H}_2}{\overset{\mathcal{H}_1}{\gtrless}} 0 \tag{3.33}$$

where the ML estimates $\hat{\mathbf{s}}_1$ and $\hat{\mathbf{s}}_2$, obtained as least squares (LS) solutions, are given by

$$\begin{aligned} \hat{\mathbf{s}}_1 &= \left(\mathbf{H}^{(\tau)^T}\mathbf{H}^{(\tau)}\right)^{-1} \mathbf{H}^{(\tau)^T}\, \mathbf{r}\,, \\ \hat{\mathbf{s}}_2 &= \left(\mathbf{H}^{(\tau+z)^T}\mathbf{H}^{(\tau+z)}\right)^{-1} \mathbf{H}^{(\tau+z)^T}\, \mathbf{r}\,. \end{aligned} \tag{3.34}$$

As a consequence from (3.12), the statistics $l(\mathbf{r})$ in (3.33) becomes

$$l(\mathbf{r}) = \left\|\mathbf{r} - \mathbf{H}^{(\tau+z)}\,\hat{\mathbf{s}}_2\right\|^2 - \left\|\mathbf{r} - \mathbf{H}^{(\tau)}\,\hat{\mathbf{s}}_1\right\|^2 = \|\bar{\mathbf{n}}_2\|^2 - \|\bar{\mathbf{n}}_1\|^2 \tag{3.35}$$

where

$$\begin{aligned} \bar{\mathbf{n}}_1 &= \mathbf{r} - \mathbf{H}^{(\tau)}\,\hat{\mathbf{s}}_1 = \left(\mathbf{I}_M - \mathbf{P}_{\mathbf{H}^{(\tau)}}\right)\mathbf{r}\,, \\ \bar{\mathbf{n}}_2 &= \mathbf{r} - \mathbf{H}^{(\tau+z)}\,\hat{\mathbf{s}}_2 = \left(\mathbf{I}_M - \mathbf{P}_{\mathbf{H}^{(\tau+z)}}\right)\mathbf{r} \end{aligned} \tag{3.36}$$

[12] This leads, for the detector performance evaluation, to the perfect measurement bound [66, p. 88].

having defined the projectors $\mathbf{P}_{\mathbf{H}^{(\tau)}} = \mathbf{H}^{(\tau)} \left(\mathbf{H}^{(\tau)^T}\mathbf{H}^{(\tau)}\right)^{-1} \mathbf{H}^{(\tau)^T}$ and $\mathbf{P}_{\mathbf{H}^{(\tau+z)}} = \mathbf{H}^{(\tau+z)} \left(\mathbf{H}^{(\tau+z)^T}\mathbf{H}^{(\tau+z)}\right)^{-1} \mathbf{H}^{(\tau+z)^T}$, with $\mathbf{I}_M$ the Mth order identity matrix. The GLRT is therefore

$$l(\mathbf{r}) = \mathbf{r}^T\, \mathbf{P}_{\mathbf{H}^{(\tau)}}\, \mathbf{r} - \mathbf{r}^T\, \mathbf{P}_{\mathbf{H}^{(\tau+z)}}\, \mathbf{r} = \mathbf{r}^T\, \mathbf{G}\, \mathbf{r} \underset{\mathcal{H}_2}{\overset{\mathcal{H}_1}{\gtrless}} 0 \tag{3.37}$$

where $\mathbf{G} = \mathbf{P}_{\mathbf{H}^{(\tau)}} - \mathbf{P}_{\mathbf{H}^{(\tau+z)}}$.

Proof of (3.37). Recalling that $\|\mathbf{x}\|^2 = \mathbf{x}^T\mathbf{x}$ we have from (3.35) and (3.36) that $l(\mathbf{r}) = \mathbf{r}^T\mathbf{Q}^T_{\mathbf{H}^{(\tau+z)}}\mathbf{Q}_{\mathbf{H}^{(\tau+z)}}\mathbf{r} - \mathbf{r}^T\mathbf{Q}^T_{\mathbf{H}^{(\tau)}}\mathbf{Q}_{\mathbf{H}^{(\tau)}}\mathbf{r}$ where $\mathbf{Q}_{\mathbf{H}^{(\tau)}} = \mathbf{I}_M - \mathbf{P}_{\mathbf{H}^{(\tau)}}$ and $\mathbf{Q}_{\mathbf{H}^{(\tau+z)}} = \mathbf{I}_M - \mathbf{P}_{\mathbf{H}^{(\tau+z)}}$ are projectors in the spaces $\langle\mathbf{H}^{(\tau)}\rangle^\perp$ and $\langle\mathbf{H}^{(\tau+z)}\rangle^\perp$, respectively [177]. This imply that $\mathbf{Q}^T_{\mathbf{H}^{(\tau)}} = \mathbf{Q}_{\mathbf{H}^{(\tau)}}$, $\mathbf{Q}^T_{\mathbf{H}^{(\tau+z)}} = \mathbf{Q}_{\mathbf{H}^{(\tau+z)}}$ and $\mathbf{Q}^2_{\mathbf{H}^{(\tau)}} = \mathbf{Q}_{\mathbf{H}^{(\tau)}}$, $\mathbf{Q}^2_{\mathbf{H}^{(\tau+z)}} = \mathbf{Q}_{\mathbf{H}^{(\tau+z)}}$, so that $l(\mathbf{r}) = \mathbf{r}^T\mathbf{Q}_{\mathbf{H}^{(\tau+z)}}\mathbf{r} - \mathbf{r}^T\mathbf{Q}_{\mathbf{H}^{(\tau)}}\mathbf{r}$, which gives immediately the result (3.37).

According to (3.11) it results that

$$l(\mathbf{r}) = \int_{\tau}^{\tau+T_\mathrm{s}} r^2(t)\, dt - \int_{\tau+z}^{\tau+z+T_\mathrm{s}} r^2(t)\, dt \underset{\mathcal{H}_2}{\overset{\mathcal{H}_1}{\gtrless}} 0\,. \tag{3.38}$$

3.6.2 Detector Performance

The GLRT performance is given by the BEP

$$P_{\min}(z) = \frac{1}{2}\,\mathrm{P}\left\{l(\mathbf{r}|\mathcal{H}_1) < 0\right\} + \frac{1}{2}\,\mathrm{P}\left\{l(\mathbf{r}|\mathcal{H}_2) > 0\right\} \tag{3.39}$$

where $l(\mathbf{r}|\mathcal{H}_1)$ and $l(\mathbf{r}|\mathcal{H}_2)$ denote the GLRT (3.38) specified in the case of $\mathcal{H}_1$ true and $\mathcal{H}_2$ true, respectively.

Considering that, under $\mathcal{H}_1$, $s(t-\tau)$ is by definition zero outside the interval $[\tau, \tau+T_\mathrm{s}]$, it is

$$\begin{aligned} l(\mathbf{r}|\mathcal{H}_1) &= \int_{\tau}^{\tau+T_\mathrm{s}} (s(t-\tau)+n(t))^2\, dt - \int_{\tau+z}^{\tau+z+T_\mathrm{s}} (s(t-\tau)+n(t))^2\, dt \\ &= \begin{cases} \int_{\tau}^{\tau+T_\mathrm{s}} (s(t-\tau)+n(t))^2\, dt - \int_{\tau+z}^{\tau+z+T_\mathrm{s}} n^2(t)\, dt\,, & z \geq T_\mathrm{s}\,, \\ \int_{\tau}^{\tau+z} (s(t-\tau)+n(t))^2\, dt - \int_{\tau+T_\mathrm{s}}^{\tau+z+T_\mathrm{s}} n^2(t)\, dt\,, & 0 \leq z < T_\mathrm{s}\,. \end{cases} \end{aligned} \tag{3.40}$$

After similar considerations, under $\mathcal{H}_2$, $s(t-\tau-z)$ is by definition zero outside the interval $[\tau + z, \tau + z + T_s]$, so that

$$
\begin{aligned}
l(\mathbf{r}|\mathcal{H}_2) &= \int_{\tau}^{\tau+T_s} (s(t-\tau-z)+n(t))^2\,dt - \int_{\tau+z}^{\tau+z+T_s} (s(t-\tau-z)+n(t))^2\,dt \\
&= \begin{cases} -\int_{\tau+z}^{\tau+z+T_s}(s(t-\tau-z)+n(t))^2\,dt + \int_{\tau}^{\tau+T_s} n^2(t)\,dt\,, & z \geq T_s\,, \\ -\int_{\tau+T_s}^{\tau+z+T_s}(s(t-\tau-z)+n(t))^2\,dt + \int_{\tau}^{\tau+z} n^2(t)\,dt\,, & 0 \leq z < T_s. \end{cases}
\end{aligned}
\tag{3.41}
$$

We now proceed with the evaluation of this $P_{\min}(z)$ in (3.39), corresponding to the detector (3.38). Note that $P_{\min}(z)$ corresponds to the error probability of a PPM demodulator with partial pulses overlap and energy detection receiver. In the following we make use of the series expansions detailed in Sec. 3.2 and Appendix 3.A, considering separately the case $z \geq T_s$ and $0 \leq z < T_s$. Moreover, as will be detailed in the derivation, it is necessary to resort to different approaches when z is small, depending on the signal type. Specifically, we define the value ξ, so that a different derivation in the detector performance is followed if $z < \xi$ and if $z \geq \xi$. In particular, as will be clarified afterward, we have $\xi = 1/2W$ for lowpass signals, and $\xi = 1/W$ for bandpass signals.

1) Evaluation of $P_{\min}(z)$ for $z \geq T_s$

Making use of the orthonormal expansions detailed in Appendix 3.A we define the r.v.s

$$
\begin{aligned}
Y_1 &= \frac{2}{N_0}\int_{\tau}^{\tau+T_s}(s(t-\tau)+n(t))^2\,dt = \frac{2}{N_0}\int_0^{T_s}(s(t)+n(t+\tau))^2\,dt \\
&= \sum_{m=1}^{N}\left(\sqrt{\frac{2}{N_0}}\eta_m + c_{1,m}\right)^2, \\
Y_2 &= \frac{2}{N_0}\int_{\tau+z}^{\tau+z+T_s} n^2(t)\,dt = \frac{2}{N_0}\int_0^{T_s} n^2(t+\tau+z)\,dt = \sum_{m=1}^{N} c_{2,m}^2\,, \\
Y_3 &= \frac{2}{N_0}\int_{\tau+z}^{\tau+z+T_s}(s(t-\tau-z)+n(t))^2\,dt = \frac{2}{N_0}\int_0^{T_s}(s(t)+n(t+\tau+z))^2\,dt \\
&= \sum_{m=1}^{N}\left(\sqrt{\frac{2}{N_0}}\eta_m + c_{2,m}\right)^2, \\
Y_4 &= \frac{2}{N_0}\int_{\tau}^{\tau+T_s} n^2(t)\,dt = \frac{2}{N_0}\int_0^{T_s} n^2(t+\tau)\,dt = \sum_{m=1}^{N} c_{1,m}^2
\end{aligned}
\tag{3.42}
$$

where N has been defined in Section 3.2, $\{c_{1,m}\}$, $\{c_{2,m}\}$ are related, respectively, to the series expansion coefficients of $\sqrt{\frac{2}{N_0}}n(t+\tau)$ and $\sqrt{\frac{2}{N_0}}n(t+\tau+z)$ and η_m are the series expansion coefficients of $s(t)$ for $t \in [0, T_\mathrm{s}]$.[13] According to the signal model considered, $\{c_{1,m}\}$, $\{c_{2,m}\}$ are statistically independent Gaussian r.v.s with zero mean and unit variance. As a consequence Y_1 and Y_3 are non-central Chi-square distributed r.v.s, whereas Y_2 and Y_4 are central Chi-square distributed r.v.s, each having $p = N$ degrees of freedom.[14] The non-centrality parameter μ of Y_1 and Y_3 is given by $\mu = 2\gamma$, where

$$\gamma = \frac{1}{N_0}\sum_{m=1}^{N}\eta_m^2 = \frac{1}{N_0}\int_0^{T_\mathrm{s}} s^2(t)\,dt = \frac{E_\mathrm{s}}{N_0} \tag{3.43}$$

is the received SNR. In addition Y_1, Y_2, Y_3 and Y_4 do not depend on z, then the probability of error $P_{\min}(z)$ results independent on z. Making use of (3.42) we can express the $P_{\min}$ in (3.39), for $>\geq T_\mathrm{s}$ as

$$P_{\min}^{(\mathrm{I})} = \frac{1}{2}\mathbb{P}\left\{Y_1 < Y_2\right\} + \frac{1}{2}\mathbb{P}\left\{Y_3 < Y_4\right\}\,. \tag{3.44}$$

Due to statistical symmetry in (3.42), the BEP can be evaluated as[15]

$$P_{\min}^{(\mathrm{I})} = \mathbb{P}\left\{Y_1 < Y_2\right\} = P_Y(\gamma, \lceil p/2 \rceil) \tag{3.45}$$

where

$$P_Y(\gamma, q) = \frac{\exp(-\gamma/2)}{2^q}\sum_{i=0}^{q-1}\frac{(\gamma/2)^i}{i!}\sum_{j=i}^{q-1}\frac{(j+q-1)!}{2^j(j-i)!(q+i-1)!} \tag{3.46}$$

whose derivation is given in Appendix 3.D.

---

[13] For bandpass signals η_m are for odd m (even m) the series expansion coefficients of the in-phase (in-quadrature) components of the ELP $\tilde{s}(t)$ of $s(t)$.

[14] The p.d.f.s of these r.v.s are reported in (3.89).

[15] Since it is required $2q$ to be even (i.e., $q \in \mathbb{N}$) in the error probability expression (3.46), the ceiling operator $\lceil\cdot\rceil$ is adopted on $p/2$ in (3.45).

2) Evaluation of $P_{\min}(z)$ for $\xi \le z < T_\mathrm{s}$

We now define the r.v.s

$$
\begin{aligned}
Y_1 &= \frac{2}{N_0}\int_{\tau}^{\tau+z} (s(t-\tau)+n(t))^2\,dt = \frac{2}{N_0}\int_0^z (s(t)+n(t+\tau))^2\,dt \\
&= \sum_{m=1}^{p(z)} \left(\sqrt{\frac{2}{N_0}}\eta_{1,m} + c_{1,m}\right)^2, \\
Y_2 &= \frac{2}{N_0}\int_{\tau+T_\mathrm{s}}^{\tau+z+T_\mathrm{s}} n^2(t)\,dt = \frac{2}{N_0}\int_0^z n^2(t+\tau+T_\mathrm{s})\,dt = \sum_{m=1}^{p(z)} c_{2,m}^2\,, \\
Y_3 &= \frac{2}{N_0}\int_{\tau+T_\mathrm{s}}^{\tau+z+T_\mathrm{s}} (s(t-\tau-z)+n(t))^2\,dt \\
&= \frac{2}{N_0}\int_0^z (s(t-z+T_\mathrm{s})+n(t+\tau+T_\mathrm{s}))^2\,dt \\
&= \sum_{m=1}^{p(z)} \left(\sqrt{\frac{2}{N_0}}\eta_{2,m} + c_{2,m}\right)^2, \\
Y_4 &= \frac{2}{N_0}\int_{\tau}^{\tau+z} n^2(t)\,dt = \frac{2}{N_0}\int_0^z n^2(t+\tau)\,dt = \sum_{m=1}^{p(z)} c_{1,m}^2
\end{aligned}
\tag{3.47}
$$

where $p(z) = \lfloor 2\,W\,z \rfloor + 1$ for lowpass signals and $p(z) = 2(\lfloor W\,z \rfloor + 1)$ for bandpass signals,[16] and $\{c_{1,m}\}$, $\{c_{2,m}\}$ are related, respectively, to the series expansion coefficients of $\sqrt{\frac{2}{N_0}}n(t+\tau)$ and $\sqrt{\frac{2}{N_0}}n(t+\tau+T_\mathrm{s})$ for $t \in [0,z]$, while $\eta_{1,m}$ and $\eta_{2,m}$ are the series expansion coefficients of $s(t)$ for $t \in [0,z]$ and $t \in [T_\mathrm{s}-z, T_\mathrm{s}]$, respectively.[17] Again, $\{c_{1,m}\}$, $\{c_{2,m}\}$ are statistically independent Gaussian r.v.s with unit variance. As a consequence Y_1 and Y_3 are non-central Chi-square distributed r.v.s, whereas Y_2 and Y_4 are central Chi-square distributed r.v.s, each having $q(z)$ degrees of freedom. The non-centrality parameter $\mu_1(z)$ and $\mu_2(z)$ of Y_1 and Y_3 are given by $\mu_1(z) = 2\gamma_1(z)$

[16]This corresponds to the representation with at least two elements for a lowpass signal, and with at least two elements for the in-phase and in-quadrature components of the ELP of a bandpass signal.

[17]For bandpss signals $\eta_{1,m}$ and $\eta_{2,m}$ are for odd m (even m) the series expansion coefficients of the in-phase (in-quadrature) components of the ELP $\tilde{s}(t)$ of $s(t)$.

and $\mu_2(z) = 2\gamma_2(z)$, where

$$\gamma_1(z) = \frac{1}{N_0} \sum_{m=1}^{p(z)} \eta_{1,m}^2 = \frac{1}{N_0} \int_0^z s^2(t)\, dt\,, \tag{3.48}$$

$$\gamma_2(z) = \frac{1}{N_0} \sum_{m=1}^{p(z)} \eta_{2,m}^2 = \frac{1}{N_0} \int_{T_\mathrm{s}-z}^{T_\mathrm{s}} s^2(t)\, dt \tag{3.49}$$

now both dependent on z. Note that (3.48) and (3.49) represent the SNR captured in the intervals $[0, z]$ and $[T_\mathrm{s} - z, T_\mathrm{s}]$, respectively, under the two hypothesis. The probability of error results[18]

$$\begin{aligned} P_{\min}^{(\mathrm{II})}(z) =& \frac{1}{2}\mathbb{P}\{Y_1 < Y_2\} + \frac{1}{2}\mathbb{P}\{Y_3 < Y_4\} \\ =& \frac{1}{2}P_Y\left(\gamma_1(z), \lceil p(z)/2 \rceil\right) + \frac{1}{2}P_Y(\gamma_2(z), \lceil p(z)/2 \rceil)\,. \end{aligned} \tag{3.50}$$

3) Evaluation of $P_{\min}(z)$ for $z < \xi$

When $z < \xi$, a lowpass signal is represented, according to Appendix 3.A, with one only element, while a bandpass signal with one element in each of the two components of its ELP. In the following we specify the resulting detector for these two cases.

[18] In the presence of a waveform with even symmetry with respect to $T_\mathrm{s}/2$ it is $\gamma_1(z) = \gamma_2(z)$, hence $P_{\min}^{(\mathrm{II})}(z) = P_Y(\gamma_1(z), \lceil p(z)/2 \rceil)$.

Lowpass signals For $2\,z\,W < 1$ we use the result (3.70) in Appendix 3.A. Define the r.v.s

$$\begin{aligned}
Y_1 &= \frac{2}{N_0}\int_{\tau}^{\tau+z} (s(t-\tau)+n(t))^2\,dt = \frac{2}{N_0}\int_0^z (s(t)+n(t+\tau))^2\,dt \\
&= \frac{2}{N_0}\left(\eta_{1,1}+\sqrt{N_0\,W\,z}\,c_{1,1}\right)^2 , \\
Y_2 &= \frac{2}{N_0}\int_{\tau+T_\mathrm{s}}^{\tau+z+T_\mathrm{s}} n^2(t)\,dt = \frac{2}{N_0}\int_0^z n^2(t+\tau+T_\mathrm{s})\,dt = 2\,W\,z\,c_{2,1}^2 , \\
Y_3 &= \frac{2}{N_0}\int_{\tau+T_\mathrm{s}}^{\tau+z+T_\mathrm{s}} (s(t-\tau-z)+n(t))^2\,dt \\
&= \frac{2}{N_0}\int_0^z (s(t-z+T_\mathrm{s})+n(t+\tau+T_\mathrm{s}))^2\,dt \\
&= \frac{2}{N_0}\left(\eta_{2,1}+\sqrt{N_0\,W\,z}\,c_{2,1}\right)^2 , \\
Y_4 &= \frac{2}{N_0}\int_{\tau}^{\tau+z} n^2(t)\,dt = \frac{2}{N_0}\int_0^z n^2(t+\tau)\,dt = 2\,W\,z\,c_{1,1}^2
\end{aligned} \tag{3.51}$$

where $c_{1,1}$ and $c_{2,1}$ are related to the series expansion coefficients of $\sqrt{\frac{2}{N_0}}n(t+\tau)$ and $\sqrt{\frac{2}{N_0}}n(t+\tau+T_\mathrm{s})$ for $t\in[0,z]$, while $\eta_{1,1}$ and $\eta_{2,1}$ are the series expansion coefficients of $s(t)$ for $t\in[0,z]$ and $t\in[T_\mathrm{s}-z,T_\mathrm{s}]$, respectively. Again, $c_{1,1}$ and $c_{2,1}$ are statistically independent Gaussian r.v.s with unit variance. Now $\sqrt{Y_1}$ and $\sqrt{Y_2}$ are Gaussian r.v.s, with mean, respectively, $\sqrt{\mu_1(z)}=\sqrt{2\gamma_1(z)}$ and $\sqrt{\mu_2(z)}=\sqrt{2\gamma_2(z)}$, where $\gamma_1(z)$ and $\gamma_2(z)$ are given by (3.48) and (3.49), and variance $2\,W\,z$. Differently, $\sqrt{Y_2}$ and $\sqrt{Y_4}$ are Gaussian r.v.s with zero mean and variance $2\,W\,z$. The BEP results

$$\begin{aligned}
P_{\min}^{(\mathrm{III})}(z) &= \frac{1}{2}\mathbb{P}\left\{\sqrt{Y_1}<\sqrt{Y_2}\right\}+\frac{1}{2}\mathbb{P}\left\{\sqrt{Y_3}<\sqrt{Y_4}\right\} \\
&= \frac{1}{2}Q\left(\sqrt{\frac{\gamma_1(z)}{2\,W\,z}}\right)+\frac{1}{2}Q\left(\sqrt{\frac{\gamma_2(z)}{2\,W\,z}}\right) .
\end{aligned} \tag{3.52}$$

Bandpass signals For $z\,W < 1$ we use the result (3.76) in Appendix 3.A. Define the r.v.s

$$
\begin{aligned}
Y_1 &= \frac{2}{N_0}\int_{\tau}^{\tau+z}(s(t-\tau)+n(t))^2\,dt = \frac{2}{N_0}\int_0^z (s(t)+n(t+\tau))^2\,dt \\
&= \frac{2}{N_0}\left[\left(\eta_{1,1,1}+\sqrt{\frac{N_0\,W\,z}{2}}\,c_{1,1,1}\right)^2+\left(\eta_{1,2,1}+\sqrt{\frac{N_0\,W\,z}{2}}\,c_{1,2,1}\right)^2\right], \\
Y_2 &= \frac{2}{N_0}\int_{\tau+T_\mathrm{s}}^{\tau+z+T_\mathrm{s}} n^2(t)\,dt = \frac{2}{N_0}\int_0^z n^2(t+\tau+T_\mathrm{s})\,dt = W\,z\,(c_{2,1,1}^2+c_{2,2,1}^2), \\
Y_3 &= \frac{2}{N_0}\int_{\tau+T_\mathrm{s}}^{\tau+z+T_\mathrm{s}}(s(t-\tau-z)+n(t))^2\,dt \\
&= \frac{2}{N_0}\int_0^z (s(t-z+T_\mathrm{s})+n(t+\tau+T_\mathrm{s}))^2\,dt \\
&= \frac{2}{N_0}\left[\left(\eta_{2,1,1}+\sqrt{\frac{N_0\,W\,z}{2}}\,c_{2,1,1}\right)^2+\left(\eta_{2,2,1}+\sqrt{\frac{N_0\,W\,z}{2}}\,c_{2,2,1}\right)^2\right], \\
Y_4 &= \frac{2}{N_0}\int_{\tau}^{\tau+z} n^2(t)\,dt = \frac{2}{N_0}\int_0^z n^2(t+\tau)\,dt = W\,z\,(c_{1,1,1}^2+c_{1,2,1}^2).
\end{aligned} \tag{3.53}
$$

Now $c_{1,1,1}$ ($c_{1,2,1}$) and $c_{2,1,1}$ ($c_{2,2,1}$) are related to the series expansion coefficients of the in-phase (in-quadrature) components of the ELP $\sqrt{\frac{2}{N_0}}\tilde{n}(t+\tau)$ and $\sqrt{\frac{2}{N_0}}\tilde{n}(t+\tau+T_\mathrm{s})$ of $\sqrt{\frac{2}{N_0}}n(t+\tau)$ and $\sqrt{\frac{2}{N_0}}n(t+\tau+T_\mathrm{s})$, for $t\in[0,z]$, where, in $c_{i,j,k}$, index i defines the signal (delayed of τ for $i=1$ or $\tau+T_\mathrm{s}$ for $i=2$), j defines the in-phase or in-quadrature component, and $k=1$ since one only coefficient is not zero. Coefficients $\eta_{1,1,1}$ ($\eta_{1,2,1}$) and $\eta_{2,1,1}$ ($\eta_{2,2,1}$) are the series expansion coefficients of the in-phase (in-quadrature) components of the ELP $\tilde{s}(t)$ and $\tilde{s}(t-\tau-z)$ of $s(t)$ and $s(t-\tau-z)$, for $t\in[0,z]$. Consequently, $\sqrt{Y_1}$ and $\sqrt{Y_2}$ are Ricean r.v.s, that is, $\sqrt{Y_1}\sim\mathsf{Rice}\left(\sqrt{\mu_1(z)},\sqrt{W z}\right)$ and $\sqrt{Y_3}\sim\mathsf{Rice}\left(\sqrt{\mu_2(z)},\sqrt{W z}\right)$, whereas $\sqrt{Y_2}$ and $\sqrt{Y_4}$ are Rayleigh r.v.s that is, $\sqrt{Y_2}\sim\mathsf{Rayleigh}\left(\sqrt{W z}\right)$ and $\sqrt{Y_4}\sim\mathsf{Rayleigh}\left(\sqrt{W z}\right)$.[19] Recognizing that the detector under analysis is analogous to the envelope detector with orthogonal signals already known in the literature [61, p. 307], the BEP

[19]We have $X\sim\mathsf{Rice}(\nu,\sigma)$ with p.d.f. $f_X(x)=\frac{x}{\sigma^2}\exp\left\{\frac{-(x^2+\nu^2)}{2\sigma^2}\right\}I_0\left(\frac{x\nu}{\sigma^2}\right)$, and $X\sim\mathsf{Rayleigh}(\sigma)$ with p.d.f. $f_X(x)=\frac{x}{\sigma^2}e^{-\frac{x^2}{2\sigma^2}}$, for $x\geq 0$.

results

$$\begin{aligned} P_{\min}^{(\mathrm{III})}(z) &= \frac{1}{2}\mathbb{P}\left\{\sqrt{Y_1} < \sqrt{Y_2}\right\} + \frac{1}{2}\mathbb{P}\left\{\sqrt{Y_3} < \sqrt{Y_4}\right\} \\ &= \frac{1}{4}\exp\left\{-\frac{\gamma_1(z)}{2\,W\,z}\right\} + \frac{1}{4}\exp\left\{-\frac{\gamma_2(z)}{2\,W\,z}\right\}. \end{aligned} \tag{3.54}$$

By substituting (3.45), (3.50), and (3.52) (or (3.54) for bandpass signals) in (3.18), we get the ZZB on TOA estimation MSE with unknown deterministic signal, that is

$$\begin{aligned} \mathsf{ZZB} =& \frac{1}{T_\mathrm{a}}\int_0^{\xi} z(T_\mathrm{a}-z)P_{\min}^{(\mathrm{III})}(z)\;dz + \frac{1}{T_\mathrm{a}}\int_{\xi}^{T_\mathrm{a}} z(T_\mathrm{a}-z)P_{\min}^{(\mathrm{II})}(z)\;dz \\ &+ \left(\frac{T_\mathrm{a}^2}{6} - \frac{T_\mathrm{s}^2}{2} + \frac{T_\mathrm{s}^3}{3T_\mathrm{a}}\right) P_{\min}^{(\mathrm{I})}\,. \end{aligned} \tag{3.55}$$

The importance of this bound lies in the fact that the evaluation of the CRB is not possible because its derivation requires that the p.d.f. respects some “goodness” conditions not satisfied in our case [66].

3.6.3 Asymptotic ZZB

For large SNR, and in accordance with numerical results, the dominant term in (3.55) is the first one, related to the integral including $P_{\min}^{(\mathrm{III})}(z)$ which considers $P_{\min}^{(\mathrm{III})}(z)$ defined for small values of z. This corresponds to the error probability of distinguishing between $s(t)$ and a slightly shifted version of itself.

Lowpass signals

In this case, for lowpass signals, we have

$$\mathsf{ZZB} \simeq \frac{1}{T_\mathrm{a}}\int_0^{1/2W} z(T_\mathrm{a}-z)\,Q\left(\sqrt{\frac{\mathsf{SNR}\,\eta(z)}{2Wz}}\right)\,dz \tag{3.56}$$

with[20]

$$\eta(z) = \frac{1}{E_\mathrm{s}}\int_0^z s^2(t)\,dt\,. \tag{3.57}$$

[20] We consider, for convenience, a symmetric waveform so that $\gamma_1(z) = \gamma_2(z)$.

Adopting the approximation for the Gaussian Q function presented in Appendix 3.C we obtain

$$\begin{aligned}\mathsf{ZZB} &\simeq \frac{1}{T_\mathrm{a}} \int_0^{1/2W} z(T_\mathrm{a} - z) \sqrt{\frac{W z}{\pi\, \mathsf{SNR}\, \eta(z)}} \exp\left\{-\frac{\mathsf{SNR}\, \eta(z)}{4Wz}\right\} dz \\ &= \frac{e^{-\mathsf{SNR}}}{\sqrt{\mathsf{SNR}}} \int_0^{1/2W} \sqrt{\frac{W z^3}{\pi\ \eta(z)}} \exp\left\{-\frac{\eta(z)}{4Wz}\right\} dz\,. \end{aligned} \tag{3.58}$$

Note that, for high SNR, the slope of the ZZB with respect to the SNR is the same as the CRB and ZZB considering perfect signal knowledge, since the detector performance is expressed in the form $P_{\min}(z) = Q\left(\sqrt{k(z) \cdot \mathsf{SNR}}\right)$, with $k(z)$ a positive constant.

Bandpass signals

In this case, for bandpass signals, we have

$$\begin{aligned}\mathsf{ZZB} &\simeq \frac{1}{2T_\mathrm{a}} \int_0^{1/W} z(T_\mathrm{a} - z) \exp\left\{-\frac{\mathsf{SNR}\, \eta(z)}{2Wz}\right\} dz \\ &= \frac{e^{-\mathsf{SNR}}}{2} \int_0^{1/W} z \exp\left\{-\frac{\eta(z)}{2Wz}\right\} \end{aligned} \tag{3.59}$$

with $\eta(z)$ defined in (3.57).

From these results it can be noted that the asymptotic ZZB is affected by the behavior of $s^2(t)$ in the first ξ seconds (edge behavior).

3.7 ML TOA Estimators

3.7.1 ML TOA Estimation of Known Signals

This is a classic non-linear parameter estimation problem where the corresponding ML estimator, which is asymptotically efficient, is simply composed of a filter matched to the signal $s(t)$ (or equivalently of a correlator with template $s(t)$). Therefore the ML TOA estimate can be obtained by evaluating the following classical expression [66]

$$\hat{\tau} = \underset{\tau}{\operatorname{argmax}} \ln p\left\{\mathbf{r}|\tau\right\} = \underset{\tau}{\operatorname{argmax}} \int_{T_\mathrm{ob}} r(t)\, s(t-\tau)\, dt\,. \tag{3.60}$$

The TOA estimation is performed by looking at the time instant corresponding to the peak output of the filter matched to $s(t)$.

3.7.2 ML TOA Estimation of Signals with Unknown Phase

Supposing the phase as unknown and statistically averaging its values under the hypothesis of most ignorance as presented in (3.27) (Bayesian approach), the result deals with correlations operated on the signal envelope as given by [182, p. 277]

$$\hat{\tau} = \underset{\tau}{\operatorname{argmax}} \int_{2\pi} \ln p\left\{\mathbf{r}|\tau,\phi\right\}\, d\phi = \underset{\tau}{\operatorname{argmax}} \left| \int_{T_{\text{ob}}} \tilde{r}(t)\, \tilde{s}^{*}(t-\tau)\, dt \right| \tag{3.61}$$

where $\tilde{r}(t)$ and $\tilde{s}(t)$ are respectively, the ELP of $r(t)$ and $s(t)$. In this case, TOA estimation is performed by looking at the time instant corresponding to the peak output of the filter matched to $\tilde{s}(t)$, having as input the ELP of the received signal.

3.7.3 ML TOA Estimation of Unknown Deterministic Signals

Modeling the signal as unknown but deterministic, the log-likelihood function (3.33) can be used to derive the ML estimate, that is

$$\hat{\tau} = \underset{\tau,\mathbf{s}}{\operatorname{argmax}} \ln p\left\{\mathbf{r}|\tau,\mathbf{s}\right\} = \underset{\tau}{\operatorname{argmax}} \int_{\tau}^{\tau+T_{\text{s}}} r^{2}(t)\, dt\,. \tag{3.62}$$

It is important to remark that estimator (3.62) requires a pre-filtering of the received signals to reduce the out-of-band noise since TOA estimation relies on energy measurements without operating correlations.

3.8 Numerical Results

To better highlight the impact on the performance of main signal parameters we analyze the theoretical performance limits of TOA estimation in AWGN channels. As example we consider a RRC received pulse [113], that is

$$\tilde{g}(t) = \frac{4\,\nu}{\pi\sqrt{T_{\text{w}}}} \frac{\cos\left((1+\nu)\pi t/T_{\text{w}}\right) + \sin\left((1-\nu)\pi t/T_{\text{w}}\right)/(4\nu t/T_{\text{w}})}{1-(4\nu t/T_{\text{w}})^{2}}\,, \tag{3.63}$$

where parameter T_{w} and roll-off factor ν determine the transmitted signal bandwidth $W = (1+\nu)/T_{\text{w}}$. In particular, as first example, we consider the lowpass signal $g(t) = \tilde{g}(t)$, and as second example the bandpass signal $g(t) = \tilde{g}(t)\cos(2\pi f_{\text{c}} t)$, with $T_{\text{w}} = 3.2\,\text{ns}$, $\nu = 0.6$ and $f_{\text{c}} = 4\,\text{GHz}$. The

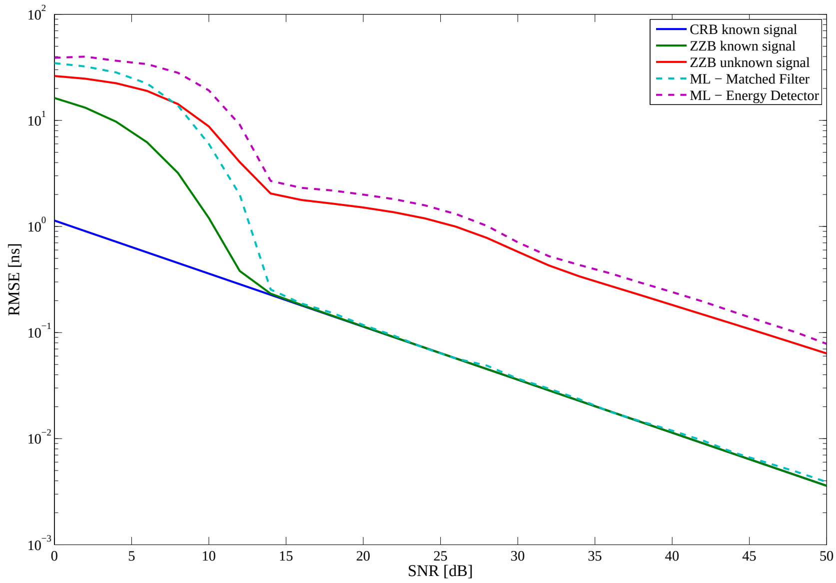

Figure 3.1: Results for lowpass signals.

signal (3.63) is exactly band-limited, so its time-limited version is obtained by cutting it to its main two lobes.

Figure 3.1 shows the root-mean-square error (RMSE) for CRBs and ZZBs considering the indicated lowpass signal. In particular, the CRB (3.22), and the ZZBs (3.18) with (3.19) and (3.55), where the bound for unknown signal is obtained considering the BEP of the lowpass case (3.52), are reported. A receiver bandwidth $W = 8/T_{\mathrm{w}}$ is considered to make signal distortion negligible. For comparison, the performance of ML estimators (3.60), and (3.62) is depicted in the figure with dashed lines.

The presence of the threshold effect is evident from the ZZB. In fact, the a priori region can be observed in the ZZB which approaches to $T_{\mathrm{a}}/\sqrt{12}$ for low SNR values. On the other hand this behavior cannot be observed in the CRB. For high SNRs, that is in the asymptotic region, the estimator is able to lock onto the correct peak of the matched filter (MF) output and the estimation error approaches that predicted by the CRB.

Figure 3.2 shows the RMSE for CRBs and ZZBs using the indicated bandpass signal. In particular, CRBs (3.22), (3.32) and the ZZBs (3.18) with (3.19) and (3.28) and (3.55), where the bound for unknown signal is obtained considering the BEP of the lowpass case (3.54), are reported. A receiver bandwidth $W = 8/T_{\mathrm{w}}$ is considered. For comparison, the performance of ML estimators (3.60), (3.61) and (3.62) is depicted in the figure with dashed lines.

As expected the resulting non-coherent bounds increase significantly as

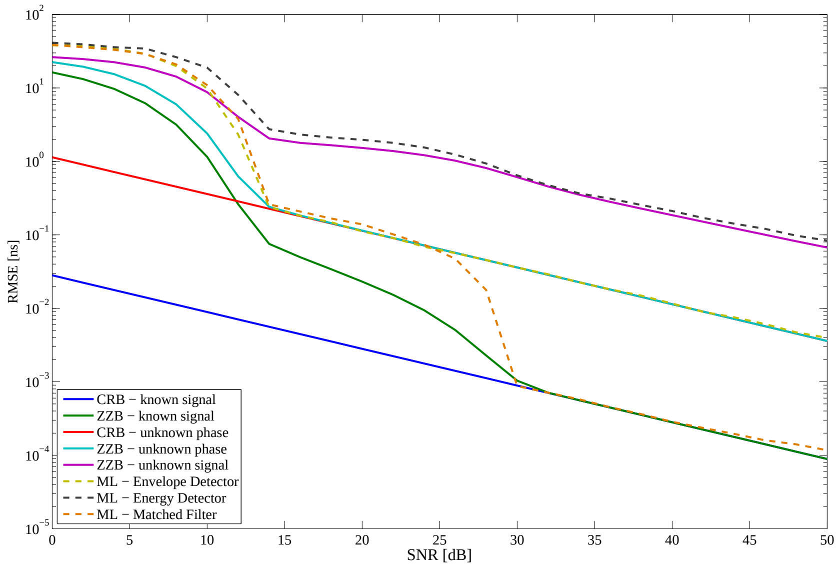

Figure 3.2: Results for lowpass signals.

they depend only on pulse bandwidth and not on f_c. Note that a constant RMSE gap between the ZZB and the CRB can be observed in the ambiguity region between 12 dB and 30 dB for a RRC pulse with $\tau_p = 3.2$ ns. In general, the RMSE gap depends on the ratio between the central frequency f_c and the signal bandwidth W as observed also in [162, 172] considering signal with rectangular spectrum.

In both results related to lowpass and bandpass signals the CRBs and ZZBs obtained with the hypothesis of known signals (also with unknown phase) are very loose, also in the high SNR region. This shows that they are not suitable for performance comparison of non-coherent estimators assuming an unknown signal, as the estimator (3.62). In this case the new expression (3.55) provides a very tight and more realistic bound for all the range of SNR, representing a fundamental tool for the comparison of practical algorithms and for providing design criteria. The importance is even more pronounced by the fact that the CRB for unknown signal is not defined.

3.9 Conclusion

In this chapter we have presented new bounds for TDE of partially known and unknown deterministic signals. These bounds represent the performance limit of any practical estimator operating under the same conditions. The ZZB for unknown signals is particularly interesting since the corresponding CRB does not exist for this kind of problem. The derived ZZBs foresee the presence of different regions, clearly showing the SNRs threshold values of the ambiguity region, where the signal observation adds a little contribution to the estimation performance, and of the asymptotic region, where the estimator performance is correctly predicted by the CRB (when exists). Moreover the proposed new bound for unknown signals results very tight considering the real performance of ML estimators based on energy measurements on the received signal, as it is the usual approach for the case of unknown signal shape.

3.A Series Expansions of Signals

In this appendix, orthonormal series expansions are used to express the signals, both random and deterministic, as a linear combination of terms, providing a good approximation of the signal energy in a time-limited interval T. When representing random processes, the classical KL expansion, leading to uncorrelated coefficients, is adopted [66, 184]. These expansions allow characterizing the signal energy in a time-limited interval, in the presence of Gaussian noise, with the Chi-square distribution, and their adoption is justified by the resulting good accuracy when $WT \gg 1$. In [185] it has been shown that the accuracy is quite good also for moderate and small WT. In this chapter we adopt the conventional expansion also for small WT, extending the derivation to the case $2WT < 1$ for lowpass signals and $WT < 1$ for bandpass signals.

3.A.1 Series Expansion of Baseband Random Signals

Consider a zero mean, wide-sense stationary (WSS), Gaussian random process $n(t)$ with a flat power spectral density $N_0/2$ in $[-W, W]$ observed in $t \in [0, T]$. Its autocorrelation function is $R_n(\tau) = N_0 W \text{sinc}\,(2W\tau)$, with $\text{sinc}\,(x) \triangleq \frac{\sin(\pi x)}{\pi x}$ for $x \neq 0$ and $\text{sinc}\,(0) \triangleq 1$.

The classical KL series expansion of $n(t)$ over the interval $[0, T]$ is[21]

$$n(t) = \sum_{m=1}^{\infty} \sqrt{\lambda_m}\, c_m\, \Phi_m(t) \tag{3.64}$$

where $\{c_m\}$ are independent zero mean Gaussian r.v.s with unitary variance, whereas $\Phi_m(t)$ and λ_m are, respectively, the eigenfunctions and eigenvalues

[21]The equality in (3.64) means mean square convergence, i.e., $\lim\limits_{M\to\infty} \mathbb{E}\left\{\left|n(t) - \sum_{m=1}^{M} \sqrt{\lambda_m}\, c_m\, \Phi_m(t)\right|^2\right\} = 0$.

of the integral equation [66, p. 180]

$$\int_0^T R_n(t-\tau)\,\Phi_m(\tau)\,d\tau = \lambda_m\,\Phi_m(t)\,. \tag{3.65}$$

The eigenfunctions of (3.65), which form a set of complete orthonormal functions $\{\Phi_m(t)\}$ with support $[0,T]$,[22] are prolate spheroidal wave functions [186, 187], whereas the corresponding eigenvalues are given by

$$\lambda_m = N_0\,W\,T\left[R_{0m}^{(1)}(\pi W\,T,1)\right]^2 \tag{3.66}$$

being $R_{0m}^{(1)}(x,1)$ the radial prolate spheroidal function [186]. The coefficient $\lambda_m\,c_m^2$ corresponds to the energy along the coordinate function $\Phi_m(t)$ of a particular random process sample. Therefore the energy of a sample of $n(t)$ is

$$E_n = \int_0^T n^2(t)\,dt = \sum_{m=1}^{\infty}\lambda_m\,c_m^2\,. \tag{3.67}$$

It has been shown in [186, 188, 189] that for $2WT \gg 1$ the eigenvalues λ_m rapidly drops to zero for $m > \lfloor 2WT \rfloor + 1$, leading to the well-known "2WT-theorem" [190, 191],[192, p.128], according to which the series can be truncated to the first $N = \lfloor 2WT \rfloor + 1$ terms. Moreover it is $\lambda_m \approx \frac{N_0}{2}$ for $1 \le m \le 2WT$, and zero otherwise, so that

$$n(t) \approx \sqrt{\frac{N_0}{2}}\sum_{m=1}^{N} c_m\,\Phi_m(t) \tag{3.68}$$

and [86][23]

$$E_n = \int_0^T n^2(t)\,dt \approx \frac{N_0}{2}\sum_{m=1}^{N} c_m^2\,. \tag{3.69}$$

Approximations (3.64) and (3.69) get less accurate as $2WT$ approaches one, and if $N \le 1$ (i.e., $T < 1/2W$), these approximations are no longer valid. In such a case it is possible to see [188] that $\lambda_m \approx 0$ for $m > 1$ and [188] suggests the approximation $\lambda_1 \approx \frac{N_0}{2}\frac{2}{\pi}c\left(1-\frac{c^2}{9}\right)$, with $c = \pi WT$. Considering the case of very small WT, where effectively only $\lambda_1 \neq 0$, we adopt here the approximation $\lambda_1 \approx \frac{N_0}{\pi}\,c$ (i.e., $R_{01}^{(1)}(\pi W\,T,1) \approx 1$), so that $\lambda_1 \approx N_0\,W\,T$, and then

$$E_n = \int_0^T n^2(t)\,dt \approx N_0\,W\,T\,c_1^2\,. \tag{3.70}$$

[22] Even if not explicitly specified, functions $\{\Phi_m(t)\}$ depends on WT.

[23] Hence we have that the expected received energy in T is given by $\mathbb{E}\left\{\int_0^T n^2(t)\,dt\right\} = \mathbb{E}\left\{\sum_{m=1}^{\infty}\lambda_m\,c_m^2\right\} = N_0WT$ [66, p. 181].

3.A.2 Series Expansion of Bandpass Random Signals

Consider $n(t)$ to be a bandpass, zero-mean, WSS, Gaussian random process with a flat power spectral density $N_0/2$ for $|f| \in [-f_c - W/2, f_c + W/2]$ observed in $t \in [0,T]$. We have that a sample function $n(t)$ of the random process can be written as $n(t) = V(t)\cos(2\pi f_c t + \phi(t))$. Using the conventional approach it is [184, p.159]

$$n(t) = n_I(t)\,\cos(2\pi f_c\,t) - n_Q(t)\,\sin(2\pi f_c\,t) \tag{3.71}$$

where $n_I(t)$ and $n_Q(t)$ are, respectively, the in-phase and in-quadrature baseband components of $n(t)$. In this manner we have $n_I(t) = V(t)\cos(\phi(t))$ and $n_Q(t) = V(t)\sin(\phi(t))$. Moreover, the random processes related to $n_I(t)$ and $n_Q(t)$ are statistically independent, zero-mean Gaussian processes.[24] It can be shown that their spectral densities are confined to the region $|f| < W/2$ with intensity N_0. The baseband components can be expanded in orthonormal series as previously discussed

$$\begin{aligned} n_I(t) &\approx \sqrt{N_0}\sum_{m=1}^{N/2} c_{1,m}\,\Phi_m(t)\,, \\ n_Q(t) &\approx \sqrt{N_0}\sum_{m=1}^{N/2} c_{2,m}\,\Phi_m(t) \end{aligned} \tag{3.72}$$

with $c_{1,m}$ and $c_{2,m}$ independent zero mean Gaussian r.v.s with unitary variance, and $N = 2(\lfloor WT \rfloor + 1)$. Therefore

$$E_n = \int_0^T n^2(t)\,dt \approx \frac{1}{2}\int_0^T n_I^2(t)\,dt + \frac{1}{2}\int_0^T n_Q^2(t)\,dt = \frac{N_0}{2}\sum_{m=1}^{N} c_m^2 \tag{3.73}$$

having defined $c_{2m-1} = c_{1,m}$ and $c_{2m} = c_{2,m}$ for $m = 1, 2, \ldots, N/2$. Note that this expression is identical to (3.69). This means that all the analysis carried out for baseband signals still applies for bandpass signals when $WT \gg 1$.

When if $N \leq 2$ (i.e., $T < 1/W$), the hypothesis of *large* T appears difficult

[24]This requires that spectral density is narrow with respect to the central frequency, i.e., the envelope $V(t)$ and the phase $\phi(t)$ are slowly varying functions of the time, and the observation time T is large enough [184, p. 158].

to validate. In fact, this corresponds to the assumption that

$$\begin{aligned}E_n &= \int_0^T n^2(t)\,dt = \int_0^T n_I^2(t)\cos^2(2\pi f_c t)\,dt + \int_0^T n_Q^2(t)\sin^2(2\pi f_c t)\,dt \\ &\quad - 2\int_0^T n_I(t)\,n_Q(t)\,\cos(2\pi f_c t)\,\sin(2\pi f_c t)\,dt \\ &\approx \frac{1}{2}\int_0^T n_I^2(t)\,dt + \frac{1}{2}\int_0^T n_Q^2(t)\,dt\,. \end{aligned} \tag{3.74}$$

If (3.74) is verified with satisfactory approximation,[25] we have that the approach followed for lowpass signals in Appendix 3.A.1 still applies. In this case we obtain

$$\begin{aligned}E_{n_I} &= \int_0^T n_I^2(t)\,dt \approx N_0\,W\,T\,c_{1,1}^2\,, \\ E_{n_Q} &= \int_0^T n_Q^2(t)\,dt \approx N_0\,W\,T\,c_{2,1}^2 \end{aligned} \tag{3.75}$$

and

$$E_n = \int_0^T n^2(t)\,dt \approx \frac{N_0\,W\,T}{2}\left(c_{1,1}^2 + c_{2,1}^2\right) = \frac{N_0\,W\,T}{2}\left(c_1^2 + c_2^2\right)\,. \tag{3.76}$$

3.A.3 Series Expansion of Baseband Deterministic Signals

In the case of a deterministic signal $s(t)$ observed in the interval $[0, T]$, there is a complete degree of freedom in choosing the orthonormal basis. Often the sampling expansion, considering the orthonormal base $\Psi_n(t) = \sqrt{2W}\mathrm{sinc}\,(2Wt - n)$,[26] is adopted [190, 191]

$$s(t) \simeq \frac{1}{\sqrt{2W}}\sum_{n=1}^{N} s_n\,\Psi_n(t) \tag{3.77}$$

where $s_n = s(n/2W)$ are the samples of $s(t)$ taken at Nyquist rate $2W$ over the interval $[0, T]$. Also in this case, for $2WT \gg 1$ the following approxima-

[25] We will show in the numerical result that, for our problem, approximation (3.74) is satisfactory also for wideband signals.

[26] Note that, differently from $\{\Phi_m(t)\}$, the base $\{\Psi_n(t)\}$ is not concentrated in the interval $[0, T]$.

tion for the energy of $s(t)$ in the interval $[0, T]$ holds [190, 176, 86][27]

$$\int_0^T s^2(t)\, dt \approx \frac{1}{2W} \sum_{n=1}^{N} s_n^2 \,. \tag{3.78}$$

In the detector derivation presented in Sec. 3.6.2, it results necessary to represent the signal in a portion $[0, z]$ of the interval $[0, T]$, with $z < T$. In order to obtain a satisfactory approximation also when $z < 1/2W$, it is important to adopt the basis $\{\Phi_m(t)\}$, where now $\{\Phi_m(t)\}$ is related to the interval $W\, z$, obtaining

$$s(t) \approx \sum_{m=1}^{M} \eta_m \, \Phi_m(t) \,. \tag{3.79}$$

3.A.4 Series Expansion of Bandpass Deterministic Signals

Consider the signal $s(t)$ as deterministic and bandpass, with non-zero Fourier transform in $|f| \in [-f_c - W/2, f_c + W/2]$, observed in $t \in [0, T]$. We can represent it by its ELP $\tilde{s}(t)$, that is $s(t) = \Re\left\{\tilde{s}(t)\, e^{\jmath 2\pi f_c t}\right\}$. The ELP can be decomposed as $\tilde{s}(t) = s_I(t) + \jmath s_Q(t)$, therefore we obtain

$$s(t) = s_I(t) \cos(2\pi f_c t) - s_Q(t) \sin(2\pi f_c t) \,, \tag{3.80}$$

where the in-phase and in-quadrature baseband components $s_I(t)$ and $s_Q(t)$ have a spectrum confined to $|f| \leq W/2$. We can then apply all the derivation presented in Appendix 3.A.3 to each of the two baseband components, adopting the expansions

$$s_I(t) \approx \sum_{m=1}^{M} \eta_{1,m} \, \Phi_m(t) \tag{3.81}$$

$$s_Q(t) \approx \sum_{m=1}^{M} \eta_{2,m} \, \Phi_m(t) \tag{3.82}$$

with $\eta_{1,m}$ and $\eta_{2,m}$ the series expansion coefficients of $s_I(t)$ and $s_Q(t)$ for $t \in [0, T]$.

[27] However, the representation error obtained when adopting $\{\Psi_n(t)\}$ is higher than with $\{\Phi_n(t)\}$ that lead to the best approximation in $t \in [0, T]$ [176].

3.B Proof of Equation (3.11)

Recalling (3.10) we have that $\mathbf{r} = \mathbf{H}^{(\tau)}\,\mathbf{s} + \mathbf{n} = \mathbf{y} + \mathbf{n}$. Consider a different orthonormal bases for $r(t)$ according to which the series expansion coefficients are written as $\tilde{\mathbf{r}} = \mathbf{S}^{(\tau)}\,\mathbf{s} + \tilde{\mathbf{n}} = \tilde{\mathbf{y}} + \tilde{\mathbf{n}}$. In order to prove that $\mathbf{H}^{(\tau)}\left(\mathbf{H}^{(\tau)^T}\mathbf{H}^{(\tau)}\right)^{-1}\mathbf{H}^{(\tau)^T}\mathbf{r}$ corresponds to the expansion of the signal $r(t)\,\Pi\left(\frac{t-\tau}{T_\mathrm{s}}\right)$ for $t \in [0, T_\mathrm{ob}]$, we can try to recover the same results from the expansion $\mathbf{S}^{(\tau)}\left(\mathbf{S}^{(\tau)^T}\mathbf{S}^{(\tau)}\right)^{-1}\mathbf{S}^{(\tau)^T}\tilde{\mathbf{r}}$. It is now convenient to choose $\mathbf{S}^{(\tau)}$ so that $\tilde{\mathbf{r}}$ represents the samples of the received signal in $[0, T_\mathrm{ob}]$, and $\mathbf{s}$ represents the samples of the transmitted signal in $[0, T_\mathrm{s}]$. In this case it is easy to show that $\mathbf{S}^{(\tau)}$ has the block structure

$$\mathbf{S}^{(\tau)} = \left[\mathbf{0}_{T,N}, \mathbf{I}_N, \mathbf{0}_{M-N-T,N}\right]^T \tag{3.83}$$

with $T = \lceil \tau/2W \rceil$,[28] $\mathbf{0}_{A,B}$ the $A \times B$ null matrix and $\mathbf{I}_N$ the Nth order identity matrix. Moreover, matrix $\mathbf{S}^{(\tau)}$ contains N linearly independent vectors (it forms an orthonormal basis), and $\mathbf{P}_{\mathbf{S}^{(\tau)}} = \mathbf{S}^{(\tau)}\left(\mathbf{S}^{(\tau)^T}\mathbf{S}^{(\tau)}\right)^{-1}\mathbf{S}^{(\tau)^T} = \mathbf{S}^{(\tau)}\mathbf{S}^{(\tau)^T}$. It is immediate to show that

$$\mathbf{P}_{\mathbf{S}^{(\tau)}} = \begin{bmatrix} \mathbf{0}_{T,T} & \mathbf{0}_{T,N} & \mathbf{0}_{T,M-N-T} \\ \mathbf{0}_{N,T} & \mathbf{I}_N & \mathbf{0}_{N,M-N-T} \\ \mathbf{0}_{M-N-T,T} & \mathbf{0}_{M-N-T,N} & \mathbf{0}_{M-N-T,M-N-T} \end{bmatrix} \tag{3.84}$$

and $\mathbf{P}_{\mathbf{S}^{(\tau)}}\mathbf{r} = \left[\mathbf{0}_T, \mathbf{r}[T+1], \mathbf{r}[T+2], \mathbf{r}[T+N], \mathbf{0}_{M-N-T}\right]^T$, from which results the quadratic form $\mathbf{r}^T\mathbf{P}_{\mathbf{S}^{(\tau)}}\mathbf{r} = \int_\tau^{\tau+T_\mathrm{s}} r^2(t)\,dt$, that is (3.11) where $r(t)$ is a generic $x(t)$.[29]

3.C Asymptotic Expression of $P_{\min}(z)$

Adopting, as approximation, the lower bound derived in [193] for the Marcum Q-function[30]

$$Q_1(\alpha, \beta) \geq e^{-\frac{\alpha^2+\beta^2}{2}} I_0(\alpha\beta) \tag{3.85}$$

we obtain

$$P_{\min}(z) \simeq \frac{1}{2} e^{-\frac{\mathsf{SNR}}{2}} I_0\left(\frac{\mathsf{SNR}}{2}|\rho_0(z)|\right) \tag{3.86}$$

[28] We consider, for convenience, the lowpass signal case.

[29] Note that $\mathbf{P}_{\mathbf{S}^{(\tau)}}$ is positive definite.

[30] This bound, valid for $\beta > \alpha$ is very tight especially for high β (i.e., high SNR), see also [194].

since $a^2(z)+b^2(z) = \mathsf{SNR}$ and $a(z)b(z) = \frac{\mathsf{SNR}}{2}|\rho_0(z)|$. Considering that $I_0(x) \simeq \frac{e^x}{\sqrt{2\pi x}}$ for large x [106, p. 377] we obtain

$$P_{\min}(z) \simeq \frac{1}{\sqrt{4\pi \mathsf{SNR}|\rho_0(z)|}} \exp\left\{-\frac{\mathsf{SNR}}{2}(1-|\rho_0(z)|)\right\}. \tag{3.87}$$

Adopting now the approximation for the Gaussian Q-function[195]

$$Q(x) \simeq \frac{1}{\sqrt{2\pi x^2}} e^{-\frac{x^2}{2}} \tag{3.88}$$

we obtain (3.31).

3.D Derivation of $\mathbb{P}\{Y_1 < Y_2\}$

In this appendix we derive $\mathbb{P}\{Y_1 < Y_2\}$. Y_1 and Y_2 are defined in 3.6 with, respectively, non-central Chi-square p.d.f. $f_{\text{NC}}(y,\mu,\nu)$, and central Chi-square p.d.f. $f_{\text{C}}(y,\nu)$, where $\mu = 2\gamma$ is the non-centrality parameter and $\nu = 2q$ are the degrees of freedom, that is

$$\begin{aligned} f_{\text{NC}}(y,\mu,\nu) &= \frac{1}{2} e^{-\frac{y+\mu}{2}} \left(\frac{y}{\mu}\right)^{\frac{\nu-2}{4}} I_{\frac{\nu}{2}-1}(\sqrt{y\mu}), \quad y \geq 0, \\ f_{\text{C}}(y,\nu) &= \frac{y^{(\frac{\nu}{2}-1)}}{2^{\frac{\nu}{2}}\Gamma\left(\frac{\nu}{2}\right)} e^{-\frac{y}{2}}, \quad y \geq 0 \end{aligned} \tag{3.89}$$

with $I_\kappa(\cdot)$ the κth order modified Bessel function of the first kind [106, p. 374] and $\Gamma(\cdot)$ the Gamma function [106, p. 255].

Consider two new r.v.s R_1 and R_2 where $R_1 = \sqrt{Y_1}$ and $\sqrt{Y_2}$. The p.d.f.s of R_1 and R_2 can be found using the r.v.s transformation rule as follows

$$\begin{aligned} f_{R_1}(r_1) &= 2\,r_1 f_{\text{NC}}(r_1^2,\mu,\nu), \\ f_{R_2}(r_2) &= 2\,r_2 f_{\text{C}}(r_2^2,\nu). \end{aligned} \tag{3.90}$$

From (3.90), the cumulative distribution function (c.d.f.) of R_2 can be obtained as

$$F_{R_2}(r_2) = \int_0^{r_2} 2t \frac{t^{2(q-1)}}{2^q\,\Gamma(q)} e^{-\frac{t^2}{2}}\, dt. \tag{3.91}$$

Adopting the transformation $\frac{t^2}{2} = \xi$ we obtain

$$F_{R_2}(r_2) = \frac{1}{\Gamma(q)} \int_0^{\frac{r_2^2}{2}} \xi^{(q-1)} e^{-\xi}\, d\xi = \frac{1}{\Gamma(q)} \gamma\left(q, \frac{r_2^2}{2}\right) \tag{3.92}$$

where $\gamma(\cdot,\cdot)$ is the lower incomplete gamma function [106, p. 260].
Since $\gamma(n,x) = \Gamma(n)\left(1 - e^{-x}\sum_{i=0}^{n-1}\frac{x^i}{i!}\right)$ we get

$$F_{R_2}(r_2) = 1 - e^{-\frac{r_2^2}{2}}\sum_{i=0}^{q-1}\frac{1}{i!}\left(\frac{r_2^2}{2}\right)^i. \tag{3.93}$$

By using (3.90) and (3.93), we can rewrite $\mathbb{P}\{Y_1 < Y_2\}$ as

$$\begin{aligned}
\mathbb{P}\{Y_1 < Y_2\} &= \mathbb{P}\{R_1 < R_2\} = 1 - \mathbb{P}\{R_2 < R_1\} \\
&= 1 - \int_0^\infty F_{R_2}(r_1) f_{R_1}(r_1)\, dr_1 \\
&= 1 - \int_0^\infty \left[1 - e^{-\frac{r_1^2}{2}}\sum_{i=0}^{q-1}\frac{1}{i!}\left(\frac{r_1^2}{2}\right)^i\right] f_{R_1}(r_1)\, dr_1 \\
&= \int_0^\infty r_1^q\, e^{-\frac{r_1^2+\mu}{2}}\,\mu^{-\frac{q-1}{2}} I_{q-1}\left(r_1\sqrt{\mu}\right)\, e^{-\frac{r_1^2}{2}}\sum_{i=0}^{q-1}\frac{1}{i!}\left(\frac{r_1^2}{2}\right)^i dr_1 \\
&= e^{-\frac{\mu}{2}}\mu^{-\frac{q-1}{2}}\sum_{i=0}^{q-1}\frac{1}{i!\,2^i}\int_0^\infty r^{q+2i}e^{-r^2} I_{q-1}\left(r\sqrt{\mu}\right)\, dr. \qquad (3.94)
\end{aligned}$$

The following integral is given in [196][31]

$$\begin{aligned}
\int_0^\infty x^{m-1}\exp\left(-a^2x^2\right) I_n(bx)\, dx =& \frac{b^n\Gamma(\frac{m+n}{2})}{2^{(n+1)}a^{(m+n)}\Gamma(n+1)}\exp\left(\frac{b^2}{4a^2}\right) \\
&\times {}_1F_1\left(\frac{n-m}{2}+1; n+1; -\frac{b^2}{4a^2}\right)
\end{aligned} \tag{3.95}$$

where ${}_1F_1(\cdot;\cdot;\cdot)$ is the confluent hypergeometric function of the first kind[32] [106, ch. 13] that is

$${}_1F_1(c_1; c_2; x) \triangleq \sum_{k=0}^\infty \frac{(c_1)_k}{(c_2)_k}\frac{x^k}{k!} \tag{3.96}$$

where $(d)_k \triangleq \Gamma(d+k)/\Gamma(d)$ is the Pochhammer symbol [106, p. 256]. By substituting (3.95) in (3.94), we obtain

$$\mathbb{P}\{Y_1 < Y_2\} = \frac{e^{-\frac{\mu}{4}}}{2^q\,\Gamma(q)}\sum_{i=0}^{q-1}\frac{\Gamma(q+i)}{i!\,2^i}{}_1F_1\left(-i; q; -\frac{\mu}{4}\right). \tag{3.97}$$

[31] The expression is derived from [197, p. 394]. An equivalent expression in given in [106, p. 486].

[32] Also referred as Kummer's function [106, p. 504].

The function ${}_1F_1\left(-c_1; c_2; x\right)$ for $c_1 > 0$ and $c_2 > 0$, as in this case, can be rewritten as a finite summation [106, p. 509], that is

$$ {}_1F_1\left(c_1; c_2; x\right) = \frac{c_1!}{(c_2)_{c_1}} L_{c_1}^{(c_2-1)}(x) \tag{3.98} $$

having indicated with $L_n^{\alpha}(x)$ the associated Laguerre polynomial given by[33]

$$ L_n^{\alpha}(x) \triangleq \sum_{m=0}^{n} (-1)^m \frac{(n+\alpha)!}{(n-m)!(\alpha+m)!m!} x^m \,. \tag{3.99} $$

This leads to the following expression

$$ \mathbb{P}\left\{Y_1 < Y_2\right\} = \frac{e^{-\frac{\mu}{4}}}{2^q} \sum_{i=0}^{q-1} \frac{1}{2^i} \sum_{j=0}^{i} \frac{(i+q-1)!}{(i-j)!(j+q-1)!j!} \left(\frac{\mu}{4}\right)^j \,. \tag{3.100} $$

We can now rearrange (3.100) obtaining the final formulation

$$ \mathbb{P}\left\{Y_1 < Y_2\right\} = \frac{e^{-\frac{\mu}{4}}}{2^q} \sum_{i=0}^{q-1} \frac{\left(\frac{\mu}{4}\right)^i}{i!} \sum_{k=i}^{q-1} \frac{(k+q-1)!}{2^k(k-i)!(k+q-1)!} \,. \tag{3.101} $$

[33] Also referred as generalized Laguerre polynomial [106, p. 775].

Part III

Location-Awareness

Introduction

High-accuracy network localization is essential for a variety of wireless applications including logistic, search and rescue, automotive, medical services, security tracking and military systems, and results one of the key enabling features of context-aware networks [52]. Network localization is usually realized by an infrastructure including tagged nodes (*agents* or *tags*) attached to or embedded in objects and of reference nodes (*anchors*) placed in known positions, which communicate with tags through wireless signals to determine tags' location [198, 199, 24].

Common methods to determine the position of tags are based on features measurement from received waveforms, such as TOA, time difference-of-arrival (TDOA), RSSI, and angle-of-arrival (AOA). The choice of the features affects significantly the localization accuracy [24].

Future real time locating systems (RTLS) are expected to provide reliable and secure high-accuracy localization of objects while maintaining low power consumption and costs. This is challenging especially in harsh propagation environments such as indoor and urban canyon. In this perspective, UWB technology offers the potential of achieving high ranging accuracy through signal TOA measurements due to its ability to resolve multipath [47, 51]. Other advantages of UWB include, low power consumption at the transmitter side, robustness to multipath, low detection probability, and large numbers of devices that can coexist in the same area. These properties encouraged the adoption of UWB radio for *active tags* (i.e., devices equipped with a radio transmitter), in localization systems [134, 200, 201]. *Passive tags* based on backscattered signaling have been recently proposed for next generation RFID and low-cost localization systems [50] and will be analyzed in the last part of this thesis.

The presence of obstacles in real propagation environments generates NLOS channel conditions that may severely degrade ranging accuracy due to direct path blockage, direct path excess delay, lowering of the SNR [202, 28]. NLOS conditions can also disable ranging, leading to a limitation of the area covered by the localization system. Several NLOS mitigation approaches have been presented in the literature to improve the localization accuracy in NLOS conditions [203, 204, 205]. All these methods and similar assume that, even in NLOS, a signal exchange between nodes is possible with certain amount of degradation. Unfortunately in many scenarios the signal might be completely obstructed by obstacles thus making the above-mentioned techniques not effective.

In the presence of severe NLOS conditions, a typical solution consists in increasing the number of anchors at the expense of higher infrastructure and deployment costs.[34] Despite the possibility of increasing the number of anchors, several different approaches can be adopted for improved network localization in these situations. First of all, the possibility of cooperation among tags can be considered [137, 52, 28, 206].

Chapter 4 presents the results of several experimentation campaign oriented to investigate the advantages of cooperation between nodes, of the prior knowledge of the environment and of the identification of the channel state (i.e., LOS/NLOS) in the positioning process.

Unfortunately cooperation can be exploited only by active tags equipped with sufficient computational capability, often in contrast with low cost requirements. In addition, it has to be remarked that area coverage for localization systems is more demanding than area coverage in communication systems because at least three anchors must be visible simultaneously by a tag in each position to make tag localization in two-dimension feasible without ambiguity. On the other hand, many applications pose several constraints on infrastructure cost, thus a reduction of the number of anchors is desirable regardless the presence of NLOS conditions. To address this issue and enable localization with satisfactory performance also in non-cooperative networks, Chapter 5 introduces the idea of relaying techniques for localization, providing practical solutions and performance analysis.

[34] Note also that anchors have to be tightly time synchronized if time-based positioning approaches are adopted.

Chapter 4

Experimentation for Cooperative Localization

4.1 Motivations

Cooperation among peer nodes at the physical layer can significantly expand the capabilities of wireless networks [207, 208, 209, 210]. In context-aware networks cooperation between nodes can be successfully exploited to improve the performance and to reduce the outages due to an insufficient number of anchors in visibility of a certain node [137, 211]. The performance of such networks depends on the conditions of each link, and thus the experimental characterization of channels associated with all links is essential for the design of cooperative wireless networks.

For what concerns the characterization of cooperative location-aware networks, the following two kinds of measurements are necessary for all links:[1]

- *range measurements* for estimating the link distance between each pair of nodes; and
- *waveform measurements* for estimating the range and channel state associated with each link,

both of which are used as inputs to the localization algorithms. Network experimentation based on waveform measurements enables the characterization of cooperative wireless networks for various applications. While there have been numerous works on measurements and models of wireless environments

[1]In principle range information can be extracted from received waveforms. However, this could require network synchronization. In our experimental setting, this is alleviated by radios that enable the collection of range and waveform measurements simultaneously.

[212, 213, 214, 215, 216, 217, 218, 56, 55, 114, 219, 105, 57], they have mainly focused on point-to-point channels.

Providing location-awareness in cluttered environments is challenging primarily due to multipath, LOS blockage, and excess propagation delays through materials.[2] UWB technology [47, 48, 220] can provide accurate localization [136, 134, 24] in such environments [200, 138, 221, 222, 134] due to its ability to resolve multipath and penetrate obstacles [54, 53, 218, 56, 55, 114]. UWB signals provide fine delay resolution, enabling precise TOA measurements for range estimation between two nodes [135, 223, 224, 51]. However, the accuracy and reliability of range-based localization techniques typically degrade in cluttered environments, where multipath, LOS blockage, and excess propagation delays through materials lead to positively-biased range measurements [51, 225].

We consider in this chapter the problem of network localization in realistic indoor environments, involving anchors (also referred to as beacons) and agents (also referred to as tags or targets). In a noncooperative setting, each agent estimates the distances from neighboring anchors, which are then used as inputs to a localization algorithm for determining its own position. In a cooperative setting, each agent estimates the distances from neighboring agents in addition to that from neighboring anchors. The localization process consists of a measurement phase where agents perform measurements with anchors and others agents (in a cooperative setting), and a location update phase where agents infer their position based on prior knowledge and new measurements. The performance of localization algorithms depends mainly on two factors: (i) the geometric configuration of the network described by the positions of anchors and agents, and (ii) the quality of measurements affected by the propagation conditions of the environment [134, 51, 137]. Localization performance can be improved significantly by selecting appropriate anchors [138, 137, 226] and mitigating the effects of unreliable range measurements [227, 204].

In this chapter, results of several measurement campaigns are presented, providing a methodology particularly suited for cooperative wireless networks. This enables the performance evaluation of various network localization algorithms under a common setting. The key contributions of the chapter can be summarized as follows:

- Development of experimentation methodology for the characterization of cooperative wireless networks in realistic environments;

[2] In these environments (e.g., inside buildings, in urban canyons, under tree canopies, and in caves), the global positioning system (GPS) is often inaccessible.

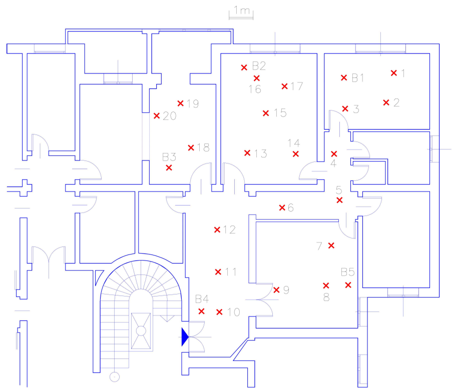

(a) Environment A: Wireless Communications Laboratory at Univ. of Bologna.

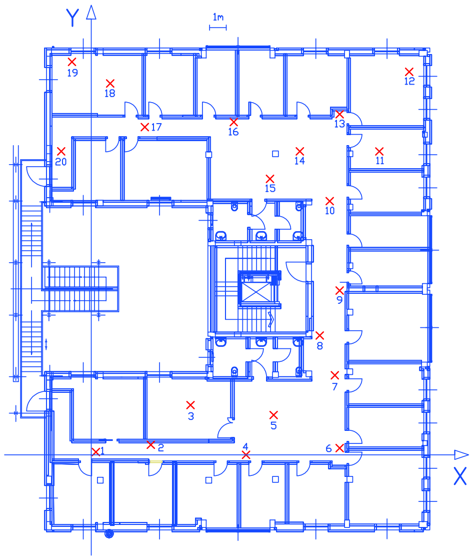

(b) Environment B: Engineering Faculty at Univ. of Bologna (Cesena campus).

Figure 4.1: The experimentation environments.

- Establishment of database with range and waveform measurements for cooperative wireless channels; and
- Presentation of experimental results related to localization in LOS and NLOS conditions.

The remainder of the chapter is organized as follows. The experimentation methodology for cooperative location-aware networks is presented in Sec. 4.2. In Sec. 4.3, a range error model is introduced. Section 4.4 describes techniques for range error mitigation and position refinement. Finally, a conclusion is given in Sec. 4.5.

4.2 Network Experimentation Methodology

We now describe the network experiments for design and analysis of cooperative location-aware networks under a common set of measurements. The performance of such networks is dominated by the behavior of range errors. Range estimates based on TOA measurements are typically corrupted by thermal noise, multipath fading, direct path (DP) blockage, and DP excess delay [51]. A range measurement is referred to as a DP measurement if it is obtained from a signal traveling along a straight line between the two nodes. A measurement is non-DP if the DP signal is completely obstructed (i.e., DP

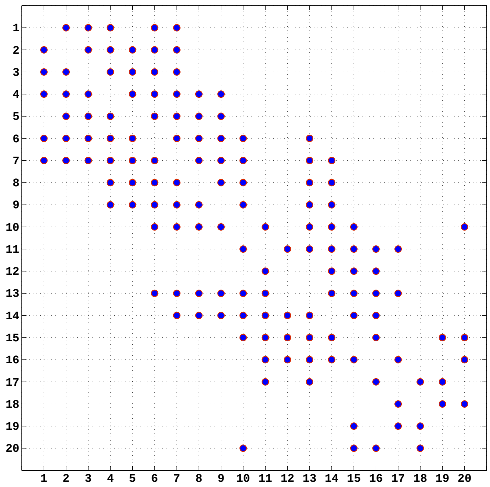

Figure 4.2: Connectivity matrix for the environment B.

blockage) and the first signal to arrive at the receiver comes from reflected paths only. Another source of error is the DP excess delay caused by the propagation of a partially obstructed DP components that travels through different obstacles (e.g., walls in buildings).[3]

An important observation to be made is that DP blockage and DP excess delay have the same effects on range measurements: they both add a positive bias to the true distance between the nodes. These measurements are referred to as NLOS measurements. A LOS measurement occurs when the signal travels along an unobstructed DP.

The geometry of the network, the measurements of all links, and measurements through obstacles, all of which affect the performance of cooperative wireless networks, are described in the following.

4.2.1 Network Geometry

We consider wireless networks in realistic indoor environments with a geometric configuration consisting of N_{b} anchors deployed in known positions to determine the unknown positions of N_{a} agents. In particular, we chose a set

[3]Given a homogeneous material with relative electrical permittivity ϵ_{r}, the speed of the electromagnetic wave traveling inside materials is slowed down by a factor $\sqrt{\epsilon_{\mathrm{r}}}$ with respect to the speed of light c. Hence the extra delay introduced by a wall of thickness d_{W} is $\Delta \simeq \left(\sqrt{\epsilon_{\mathrm{r}}}-1\right) d_{\mathrm{W}}/c$ (considering wideband signals, since ϵ_{r} is frequency-dependent, a signal distorsion is also present).

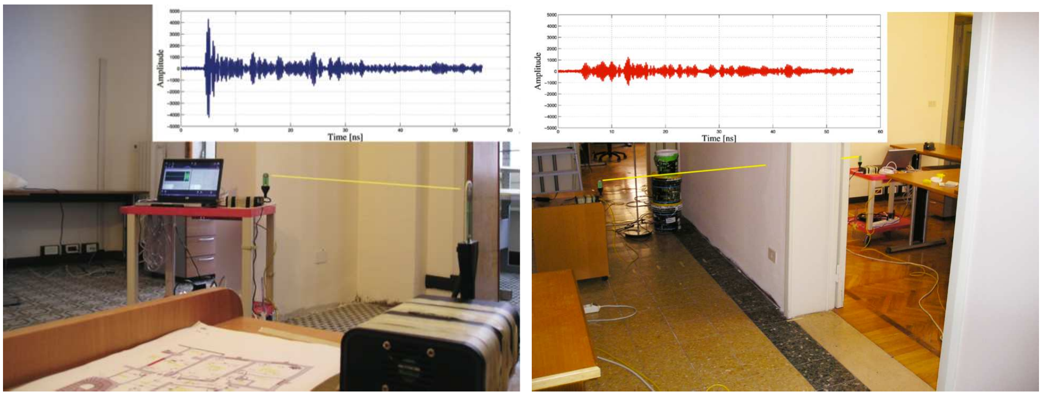

(a) A view of measurement setup.

(b) Through a wall measurement.

Figure 4.3: A typical apartment in Bologna, Italy, serving as the network experimentation environment.

of positions for anchors and agents, and performed simultaneous range and waveform measurements for all possible links between pairs of nodes.[4] Two measurement campaigns have been carried out: (i) in a typical apartment with furniture and concrete walls with thickness of 15 and 30 cm (environment A); and (ii) in a typical office indoor environment with furniture and drywall with thickness of 10 cm (environment B). In the environment A, $N_\mathrm{p} = 25$ possible node positions of which $N_\mathrm{b} = 5$ are anchors (labeled B1-B5) and $N_\mathrm{a} = 20$ are agents (numbered 1-20) are considered. In the environment B, $N_\mathrm{p} = 20$ possible nodes positions (numbered 1-20) are considered, despite the adoption as anchors or agents.

As example, considering environment A, range and waveform measurements for each pair of anchor and agent were made for a noncooperative setting (i.e., 5×20 possible links). In addition, measurements between each pair of agents were also made for a cooperative setting (i.e., additional $\binom{20}{2}$ possible links). A total of 1500 measurements were collected for each pair of nodes in both environments, whose maps are reported in Fig. 4.1.

Note that NLOS situations can significantly reduce the SNR at receiver side so that, in some situations, a link between two nodes cannotexist, due to the impossibility of detecting the presence of the signal by the receiving radio. In this case the number of connections is obviously less than in a fully connected network. Figure 4.2 shows this fact presenting, as example, the connectivity matrix related to measurements performed in environment B.

[4]In general, the selection of nodes positions can be based on a grid or by choosing key positions in the environment (e.g., particular places in a room or in a corridor).

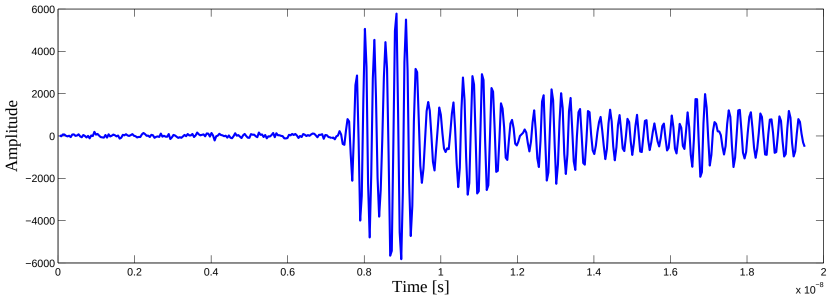

(a) LOS

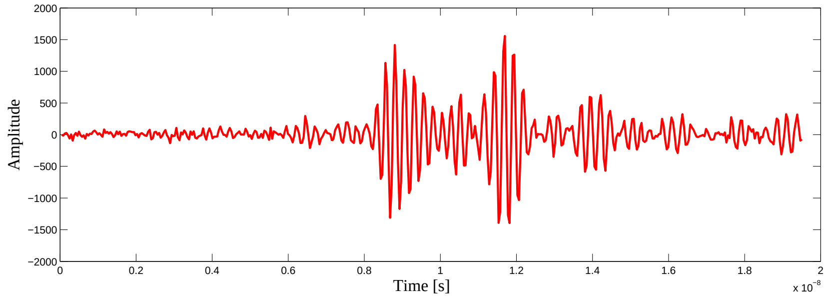

(b) NLOS

Figure 4.4: Example of measured waveforms.

4.2.2 Links Characterization

The characterization of cooperative wireless networks requires measurements for all links between pairs of nodes (agent and anchor or two cooperating agents). Such measurements were performed using UWB radios operating in the $3.2 - 7.4$ GHz band. These commercial radios can provide (i) range measurements through TOA estimation based on thresholding techniques,[5] and (ii) samples of received signal waveforms. Waveform measurements are the CRs to the transmitted signals. When adopting IR-UWB signals these CRs are closely related to the CIRs. Measurement setup examples for LOS and NLOS conditions are shown in Fig. 4.3(a) and Fig. 4.3(b), considering the environment A.

A pair of nodes can be in LOS or NLOS condition depending on their relative positions within the environment. Figure 4.4 shows typical waveform measurements collected, representing channel pulse responses in LOS and NLOS conditions, respectively, in the experimentation environment A. It can be seen from the figures that LOS and NLOS conditions give rise to different behaviors of waveform measurements. The presence of multipath,

[5]A survey on ranging techniques and performance limits is given in [51].

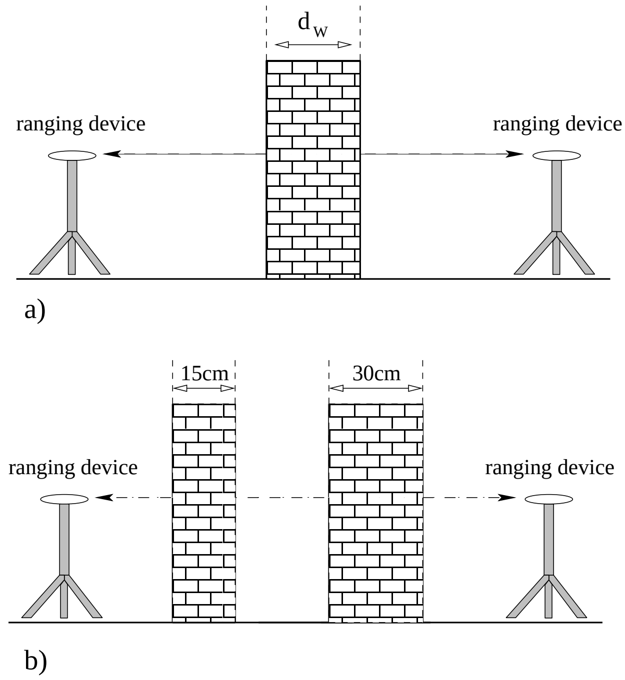

Figure 4.5: Obstacles characterization setup [228].

typical of indoor environments, is also noticeable in both waveforms. The knowledge of the NLOS condition can be exploited to mitigate ranging errors to significantly improve the performance of the localization algorithms.

Let $d_{i,j}$ denotes the Euclidean distance between two nodes (i.e., an agent and a reference node, which can be either an anchor or a cooperative agent) in positions $\mathbf{p}_i$ and $\mathbf{p}_j$, respectively. Note that UWB radios provide ranging accuracy on the order of a few centimeters, and thus the true distance between each pair of nodes must be measured with an accuracy better than a centimeter. On the other hand, measuring the true distance between two nodes with obstacles (e.g., walls) in between can be difficult even using laser-based ranging devices. This difficulty is alleviated by using a 3D computer-aided design software.

4.2.3 Obstacles Characterization

To characterize the bias of ranging errors due to obstacles, additional range measurements were collected in the environment. The transmitting and receiving nodes were placed in several positions, such that one or two walls with different thicknesses were present between the two nodes, according to

Layout, d_{W} [cm]	mean bias [cm]	std dev [cm]
1 wall, 15.5	16.4	3.7
1 wall, 30	29.5	3.2
2 walls, 15.5+30	45.2	3

Table 4.1: Mean and standard deviation of ranging bias for different wall thicknesses.

Fig. 4.5. Range measurements were collected using UWB radios located in five sets of short distances (i.e., 20, 40, 60, 80, and 100 cm from both sides of the walls) to isolate the effects of excess delay from those of multipath. A view of the measurement setup is given in Fig. 4.3(b). By using the collected range measurements ensemble (5×1500 measurements in total), the mean (bias) and standard deviation of range errors were calculated respectively as: 16.4 cm and 3.7 cm for one wall with thickness $d_{\mathrm{W}} = 15.5$ cm; 29.5 cm and 3.2 cm for one wall with $d_{\mathrm{W}} = 30.0$ cm; and 45.2 cm and 3.0 cm for two walls with total $d_{\mathrm{W}} = 15.5 + 30.0$ cm (see also Tab. 4.1).

As can be noted, the bias appears to increase with the thickness of the wall. The low value of the standard deviation indicates that the range errors are dominated by the effects of excess delay rather than those of multipath and thermal noise. From the collected ensemble of measurements we observe that $\Delta \simeq d_{\mathrm{W}}/c$, thus $\epsilon_{\mathrm{r}} \simeq 4$.[6]

In the following sections, the measurements from our network experiments will be used to model ranging errors as well as to analyze signal processing techniques able to improve the localization performance.

4.3 Range Error Model

Understanding the behavior of range errors is essential for the development of cooperative localization techniques. In the following, range model based on measurements in Sec. 4.2.2 and range error bias model based on measurements in Sec. 4.2.3 will be developed.

We start by categorizing these link measurements in Section 4.2.2 in terms of the channel state (e.g., the state $\mathcal{H}_i$ indicates i walls between a pair of nodes with $i = 0, 1, ..., 4$). Figure 4.6 shows the range error bias (i.e., average range error over 1500 measurements) for each link as a function of the true distance, in LOS ($\mathcal{H}_0$) and NLOS ($\mathcal{H}_1$, $\mathcal{H}_2$, $\mathcal{H}_3$, and $\mathcal{H}_4$) conditions. Note that the bias depends strongly on the total thickness of the walls. Range

[6]The value of ϵ_{r}, which depends on the material of the wall, is confirmed by a similar result obtained in [229]. See also [230] for a more accurate wall behavior characterization.

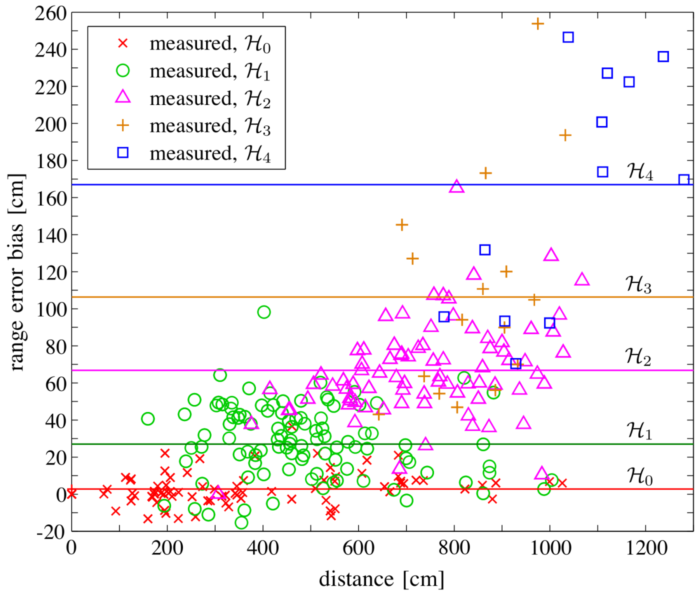

Figure 4.6: Range error bias as a function of distance for nodes pairs in LOS or NLOS conditions.

measurements described in Sec. 4.2.2 also show that the range $r_{i,j}$ between the pair of nodes i and j, in both LOS and NLOS conditions, can be modeled as

$$r_{i,j} = d_{i,j} + b_{i,j} + \epsilon_{i,j} \tag{4.1}$$

where $d_{i,j}$ is the true distance and $b_{i,j}$ is the range error bias. The quantity $\epsilon_{i,j}$ is modeled as a zero mean r.v., independent of $b_{i,j}$, with variance $\sigma^2_{i,j}$ [228]. Our link measurements show that $b_{i,j}$ and $\sigma^2_{i,j}$ depend on the obstacles (e.g., the number of walls) between nodes i and j. Equation (4.1) was also used in [225, 138], where $b_{i,j}$ and $\sigma^2_{i,j}$ were modeled as a function of true distance.

We expect the bias $b_{i,j}$ to vary more in a cluttered environment (with many walls, machines, and furniture such as a typical office building) than in an open environment.

When the environmental information (e.g., the number of walls and the excess delay) is available, $b_{i,j}$ in (4.1) can be modeled as a function of excess delay, namely

$$b_{i,j} = c \sum_{k=1}^{N_{\mathrm{w}}(i,j)} n_k^{(i,j)} \Delta_k \tag{4.2}$$

where c is the speed of light, the summation is over the $N_{\mathrm{w}}(i,j)$ different extra delay values, and $n_k^{(i,j)}$ is the number of walls that result in the same

Condition	mean bias [cm]	std dev [cm]	frequency
$\mathcal{H}_0$ (LOS)	1.7	6.9	0.27
$\mathcal{H}_1$ (1 wall)	32.4	13.9	0.35
$\mathcal{H}_2$ (2 walls)	64.6	23.3	0.28
$\mathcal{H}_3$ (3 walls)	N.A.	N.A.	0.05
$\mathcal{H}_4$ (4 walls)	N.A.	N.A.	0.03

Table 4.2: Mean bias, standard deviation and frequency in different wall conditions.

extra delay value Δ_k (e.g., the number of walls with the same material and thickness). We refer to this model as wall extra delay (WED) bias model. The total number of walls between the two nodes is

$$n^{(i,j)} = \sum_{k=1}^{N_{\mathrm{w}}(i,j)} n_k^{(i,j)} \,. \tag{4.3}$$

When every wall in the scenario has the same thickness and composition (i.e., $\Delta_k = \Delta$ for each k), (4.2) simplifies to

$$b_{i,j} = c\, n^{(i,j)} \Delta \,. \tag{4.4}$$

Mean bias, standard deviation and frequency for different number of wall conditions are reported in Tab. 4.2.

We will show in Sec. 4.4 that the WED bias model can be used to mitigate range errors, resulting in significant improvement of localization performance.

4.4 Harnessing Environmental Information

The knowledge of the environment can be harnessed to mitigate range errors, and thus to improve localization accuracy. Such knowledge can be obtained from environmental information or by processing the received waveforms using channel state identification techniques. These two cases will be referred to as WED bias model with environmental information (the number of walls is known) and WED bias model with channel state identification (the number of walls is estimated), respectively. Supposing that no estimation is performed on the receiving signal, but there is availability of the environmental information (i.e., the building map) we have the following algorithm for improved localization performance:

1. *Initial position estimate:* obtain an initial position estimate $\hat{\mathbf{p}}^{(1)}$ based on the range measurements;

2. *Range error mitigation:* mitigate bias of the range error from measurements according to the bias model and the initial position estimate $\hat{\mathbf{p}}^{(1)}$;

3. *Position refinement:* update the position estimate $\hat{\mathbf{p}}^{(2)}$ with the corrected range values.

Specifically the step (2) consists in subtract, from the ranging estimates, the bias provided by the number of walls which the signal is supposed to has crossed given the position estimate $\hat{\mathbf{p}}^{(1)}$.[7]

Differently, if prior knowledge of the environment map is not available, but it is possible to estimate the number of walls from the receiving signal we have the algorithm:

1. *Range error correction:* mitigate bias of the range error from measurements according to the bias model and the estimated channel conditions;

2. *Position refinement:* obtain the position estimate $\hat{\mathbf{p}}$ with the corrected range values.

It is clear how, in this case, the first position estimation is avoided. However, although the reduced complexity in the positioning algorithm, there is an increase in the signal processing part due to the waveform elaboration necessary for extracting environmental conditions information (i.e., estimation of the number of walls). Note that, in this case, range measurements are processed according to the estimation results performed on the received waveforms. In the following section an example of this estimation process, with numerical results obtained exploiting the described measurements campaigns, is provided.

4.4.1 Previous Works

Several techniques have been proposed recently in order to identify channel conditions in terms of obstruction [203, 231, 232, 233, 234, 235, 236, 237, 238, 239, 240, 241, 242, 204, 243]. Obstruction detection is generally performed by extracting a certain feature from the received waveform that varies with different channel conditions. For example in [238] the identification is based on the first peak amplitude of the received signal and delay between the first

[7] Obviously, in case of a high estimation error in the initial position estimate $\hat{\mathbf{p}}^{(1)}$ the number of walls can be erroneously detected with consequent error propagation.

and the strongest path. In [232, 233], root mean square (rms) delay-spread, mean excess delay and kurtosis parameters are used for that purpose. The detection can also be realized without observing the received waveform directly, which is the case of the non-parametric approach proposed in [231]. This work assumes that multiple and independent TOA measurements between agents and anchors are available and that the change in location of the agents during such measurements is negligible. In these conditions, the p.d.f. of distance estimates between agent and anchor is obtained from the measurements and is compared with the p.d.f. corresponding to LOS propagation. If the distance between the p.d.f.s is less than a given threshold, the channel is declared as LOS, otherwise it is stated as NLOS. Others recent non-parametric solutions based on machine learning can be found in [242, 204, 243]. Here some existing and new channel LOS/NLOS identification algorithms are presented and compared under common conditions.

We consider here the problem of detecting the LOS and NLOS propagation conditions. However, it has been shown in [28] how it is possible, with a similar procedure, to discriminate between the presence of one or more walls.

4.4.2 Channel State Identification Algorithms

Classic Identification Approach

Most of the LOS/NLOS identification techniques proposed in the literature can be summarized according to the following classic binary detection scheme, where the detection is performed by extracting a certain number N of features $\boldsymbol{\gamma} = \{\gamma_1, \gamma_2, \ldots, \gamma_N\}$ from the received signal and applying the classical decision theory with a LRT:

$$\frac{p(\boldsymbol{\gamma}|\,\mathrm{LOS})}{p(\boldsymbol{\gamma}|\,\mathrm{NLOS})} \underset{\mathcal{H}_1}{\overset{\mathcal{H}_0}{\gtrless}} \frac{p(\mathrm{NLOS})}{p(\mathrm{LOS})} \tag{4.5}$$

where $p(\boldsymbol{\gamma}|\,\mathrm{LOS})$ and $p(\boldsymbol{\gamma}|\,\mathrm{NLOS})$ are, respectively, the joint p.d.f.s of the set of features $\{\gamma_1, \gamma_2, \ldots, \gamma_N\}$ under LOS and NLOS conditions, $p(\mathrm{LOS})$ and $p(\mathrm{NLOS})$ are the prior probabilities of the LOS and NLOS events, respectively, $\mathcal{H}_0$ denotes the hypothesis of a LOS condition and $\mathcal{H}_1$ the presence of a certain obstruction.

Different techniques are then often distinguished by different choice of the set $\boldsymbol{\gamma}$ of signal features. When more than one parameter are extracted from the signal, for example γ_1 and γ_2, obtaining the joint p.d.f. can be difficult. A sub-optimal approach is to consider γ_1 and γ_2 as independent random variables. Then, the decision rule becomes

$$\frac{p(\gamma_1, \gamma_2|\,\text{LOS})}{p(\gamma_1, \gamma_2|\,\text{NLOS})} = \frac{p(\gamma_1|\,\text{LOS})}{p(\gamma_1|\,\text{NLOS})}\,\frac{p(\gamma_2|\,\text{LOS})}{p(\gamma_2|\,\text{NLOS})} \underset{\mathcal{H}_1}{\overset{\mathcal{H}_0}{\gtrless}} \frac{p(\text{NLOS})}{p(\text{LOS})}\ . \tag{4.6}$$

In many practical cases, nodes that are estimating their relative distance perform several consecutive measurements; hence, a large set of waveforms is usually available. In this case, we can decide for one or the other hypothesis observing the complete set of collected waveforms (assuming a quasi-stationary scenario), considering in (4.5) or (4.6) the average value of the parameter(s).

Distribution-Based Identification Approach

In this chapter we propose a different method for exploiting the complete set of waveforms instead of taking decision on the single waveform. The idea is to provide an estimation of the probability distribution of the parameter of interest, and to compare it with the reference ones corresponding to LOS and NLOS propagation. The decision is taken in favor of the hypothesis for which the estimated distribution is at minimum "distance" to the reference one. The distance between distributions has to be defined according to a certain metric. Examples of such metrics are the Euclidean distance and the relative entropy or Kullback-Leibler distance. The decision criterion is then given by

$$\frac{D(\widehat{p}_{\boldsymbol{\gamma}}\|p_{\boldsymbol{\gamma}}^{(\text{nlos})})}{D(\widehat{p}_{\boldsymbol{\gamma}}\|p_{\boldsymbol{\gamma}}^{(\text{los})})} \underset{\mathcal{H}_1}{\overset{\mathcal{H}_0}{\gtrless}} \frac{p(\text{NLOS})}{p(\text{LOS})} \tag{4.7}$$

where $\widehat{p}_{\boldsymbol{\gamma}}$ denotes the estimated joint distribution while $p_{\boldsymbol{\gamma}}^{(\text{los})}$ and $p_{\boldsymbol{\gamma}}^{(\text{nlos})}$ are the reference distributions of the two hypotheses. For $N = 1$ and equal prior probabilities for the two channel states, we have

$$D(\widehat{p}_{\gamma}\|{p_{\gamma}}^{(\text{nlos})}) \underset{\mathcal{H}_1}{\overset{\mathcal{H}_0}{\gtrless}} D(\widehat{p}_{\gamma}\|p_{\gamma}^{(\text{los})})\ . \tag{4.8}$$

The experimental results related to this identification method presented in Sec. 4.4.3 are obtained by using as metric of comparison the Euclidean distance given by

$$D(p\|q) = \sqrt{\int_{-\infty}^{+\infty} [p(x) - q(x)]^2 dx}\ . \tag{4.9}$$

Features choice

A fundamental step in designing (4.5) or (4.7) is the choice of the features $\boldsymbol{\gamma}$, extracted by observing the received signal $r(t)$ in a certain observation interval T, which are usually more affected by channel conditions.

The first parameter taken into account is the rms delay spread that captures the temporal dispersion of the energy in a signal. It is defined as

$$\tau_{\text{rms}} = \sqrt{\frac{\int_0^\infty (t-\tau_{\text{m}})^2 |r(t)|^2 dt}{\int_0^\infty |r(t)|^2 dt}} \tag{4.10}$$

where τ_{m} is the mean excess delay given by

$$\tau_{\text{m}} = \frac{\int_0^\infty t|r(t)|^2 dt}{\int_0^\infty |r(t)|^2 dt} \,. \tag{4.11}$$

In case of LOS propagation, the strongest path is typically the first one, while in NLOS conditions it is common to have the strongest path preceded by some other smaller echoes resulting in a larger value of the delay-spread. When distributions in (4.5) are unimodal and $p(\text{LOS})=p(\text{NLOS})$[1], then (4.5) is equivalent comparing γ to a suitable threshold λ corresponding to the intersection between $p(\boldsymbol{\gamma}|\,\text{LOS})$ and $p(\boldsymbol{\gamma}|\,\text{NLOS})$. In the delay-spread case the decision rule takes the form

$$\text{Decide} : \begin{cases} \text{LOS} \,, & \text{if } \tau_{\text{rms}} \leq \lambda_\tau \\ \text{NLOS} \,, & \text{if } \tau_{\text{rms}} > \lambda_\tau \end{cases} . \tag{4.12}$$

Another parameter taken into account is the kurtosis, defined by

$$\kappa = \frac{1}{\sigma_{|r|}^4 T} \int_T \left(|r(t)| - \mu_{|r|}\right)^4 dt \tag{4.13}$$

where $\mu_{|r|} = \frac{1}{T}\int_T |r(t)|dt$ and $\sigma_{|r|}^2 = \frac{1}{T}\int_T (|r(t)| - \mu_{|r|})^2 dt$. LOS waveforms usually produce a higher value for the kurtosis. For this reason the decision is taken as

$$\text{Decide} : \begin{cases} \text{NLOS} \,, & \text{if } \kappa < \lambda_k \\ \text{LOS} \,, & \text{if } \kappa \geq \lambda_k \end{cases} \tag{4.14}$$

where λ_k is the threshold value for the detection performed with this scheme. Parameters τ_{rms} and κ are strongly related to the shape of the waveform. A

[1] This assumption is usually considered when no a priori information is available.

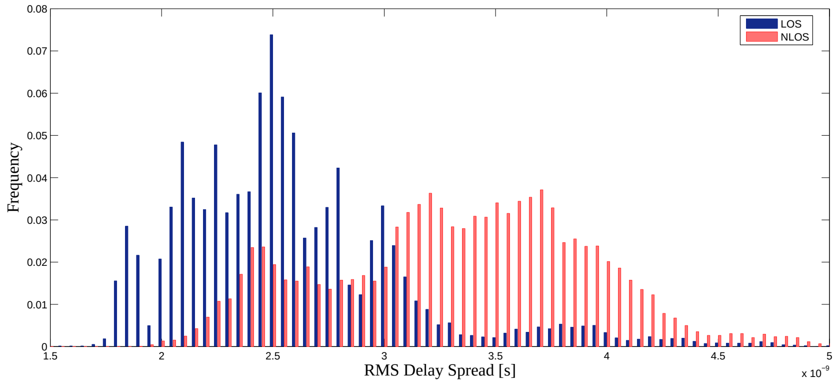

Figure 4.7: Example of relative frequency for delay spread in LOS and NLOS conditions derived from experimental data.

different feature exploitable for the identification is the energy of the received signal given by

$$\mathcal{E}_r = \int_T |r(t)|^2 dt \ . \tag{4.15}$$

In this case we decide for the NLOS hypothesis if this energy is below a certain threshold due to walls, objects attenuation and reflections, and decide LOS otherwise.

4.4.3 Experimental Results

The identification methods have been tested with real waveforms obtained from measurements collected in environment B. The totality of collected waveforms has been split in two disjoined sets: a *training set* and a *validation set*. The former is used for the computation of the reference probability distributions under LOS and NLOS hypotheses and the choice of the thresholds $\lambda_\tau, \lambda_k, \ldots$, the latter is used for testing the identification algorithms. In Fig. 4.7 an example of relative frequency distributions for τ_{rms} in LOS and NLOS conditions is shown; from that probability distributions are approximated. Each of the two sets contains 500 waveforms collected for each pair of nodes. In this manner we have four disjointed sets; the training set and the validation set for nodes in LOS conditions and the same for nodes in NLOS conditions. In the case of classic identification approaches parameters τ_{rms}, κ and $\mathcal{E}_r$ are first computed from the waveform under test; then a decision based on (4.5) or (4.6) is taken. The percentage of agreements is considered as an indicator of the quality of the identification method. Even though the parameters τ_{rms} and κ have been already proposed in other chap-

Decision	τ_{rms}	κ	Joint τ_{rms}-κ	$\mathcal{E}_r$
$\mathcal{H}_0\|\mathcal{H}_0$	0.77	0.74	0.88	0.96
$\mathcal{H}_1\|\mathcal{H}_1$	0.79	0.77	0.79	0.87
Error Rate	0.22	0.25	0.17	0.09

Table 4.3: Classical identification approach.

Decision	τ_{rms}	κ	Joint τ_{rms}-κ
$\mathcal{H}_0\|\mathcal{H}_0$	0.81	0.96	0.93
$\mathcal{H}_1\|\mathcal{H}_1$	0.76	0.71	0.82
Error Rate	0.22	0.17	0.13

Table 4.4: Distribution-based identification approach.

ters by considering waveforms drawn from the IEEE 802.15.4a channel model characterized by long channel responses (often > 100 ns) [232, 233], here the same approach is tested on real data often characterized by shorter channel responses (about 20 ns).

In the case of distribution-based identification approach, the observation is taken, instead of on the single waveform, on a certain number of waveforms belonging to the validation set related to the same pair of nodes. Specifically the decision is taken according to (4.8), having previously built the reference distributions through the training set of waveforms, and again the percentage of agreements is taken as an indicator of the quality.

For the identification based on delay-spread and kurtosis, waveforms have been filtered with a band-pass filter compliant with spectral emission of the devices used during measurements; subsequently they have been normalized to have unitary energy. In this manner only the shape of the signal plays a role in the identification. For the identification based on received energy, waveforms have been clearly only filtered without any other type of processing.

Table 4.3 shows the rate of correct and incorrect channel condition identification using classical detecting schemes. As can be noted, τ_{rms} and κ features give similar results. The third column considers the joint distribution (4.6) which leads to an improvement in the detection performance. Results related to the energy parameter (4.15) are reported in column 4 of Table 4.3. Surprising, the performance obtained is remarkable. Probably this result is strictly related to the particular environment under investigation where there is a tight correlation between low SNR and NLOS conditions.

Table 4.4 refers to the proposed distribution-based approach and shows again the rate of correct and incorrect channel condition identification. For each couple of nodes the distribution is computed using 100 waveforms of the validation set. We can observe how this approach gives in general better results especially when using the kurtosis as parameter. Even in this case using the joint distribution instead of considering a single parameter improves the detection performance.

4.5 Conclusion

The notion of network experimentation and an experimentation methodology particularly suited for cooperative wireless networks have been introduced. Based on this methodology extensive measurement campaigns, including ranges and waveforms measurements, have been performed. The collected measurements enable the modeling of range errors for both LOS and NLOS conditions and the development of channel state identification and range error mitigation techniques. The detection of the LOS/NLOS conditions was performed with a classical binary hypothesis test using rms delay spread and kurtosis of the received waveforms as features for the identification. The two classifiers based on these parameters provide about the same results in terms of correct identifications. The performance can be improved using the two parameters jointly for the test.

Further performance analysis and comparison between localization algorithms harnessing channel state information can be found in [28].

Chapter 5

Relaying Techniques for Network Localization

5.1 Motivations

When cooperation among nodes is not feasible due to the low-complexity requirements (or the impossibility of a direct communication between pair nodes), relaying techniques can be adopted to deal with NLOS channel conditions.

Communication coverage can be increased by using regenerative relays called detect & forward (DF) [210, 244, 245, 209, 246, 247]. Localization coverage extension has been addressed in [248, 249, 250] for locating and tracking passive point scatterers or regenerative relays using UWB signals. An UWB localization system with a single anchor is proposed in [251] where the knowledge of the room geometry is exploited to map the signal reflections onto a set of virtual anchors. This approach requires accurate electromagnetic knowledge of the environment, which is often not available. The adoption of regenerative relays was proposed in [252] with the purpose to reduce the overhead and scaling inefficiencies of conventional two-way ranging approaches. A similar approach based on secondary anchors performing ranging is described in [253], while in [254] regenerative relays are employed in ad hoc networks composed of master and secondary active nodes for localization without need for prior synchronization between the nodes.

A fundamental issue to be addressed to make relaying approaches for localization appealing is the complexity that must be considerably lower than that of the anchor nodes. The above approaches for regenerative relays require the same complexity of anchors because TOA estimation and data communication capabilities are needed for the scheme to work properly.

Moreover, the design of regenerative relays depends on the specific signal format adopted by the localization system. This prevents the possibility to use the same infrastructure to extend the coverage of systems adopting simultaneously active tags, passive tags (based on backscatter modulation), or UWB WSRs for tracking moving untagged nodes.

The above-mentioned limitations can be overcome by using UWB *non-regenerative relays* where neither modulator nor demodulator sections are present in the relay and the signal is repeated as is. Non-regenerative relays can be active, also called *amplify & forward (AF)*, or completely passive, namely *just forward (JF)* (also referred to as *cold repeaters*). Non-regenerative relaying is well known in communication networks; for example JF relays are adopted as gap fillers in broadcast systems and Wi-Fi, to cover shadowed areas, especially in indoor environments. Passive relay solutions in [255, 256, 257, 258] are adopted to increase the coverage of RFID systems in harsh propagation environments such as inside a metal container, pallet or a product container. JF relays are usually composed of a couple of interconnected directive antennas and take advantage of antenna directivity gain to mitigate the additional path-loss caused by obstacles [258]. Non-regenerative relay based systems present in the literature are oriented to improve communication and are not oriented to localization.

This chapter provides the basis for the design and analysis of localization systems with non-regenerative relaying. Both AF and JF are considered for coverage extension and performance improvement in harsh propagation environments (e.g., indoor environment with NLOS propagation conditions). ML position estimators accounting also for relayed signals are designed in order to assess the feasibility of the approach. The benefits of the proposed solution are quantified, enabling a direct comparison between performance of non-relaying versus JF and AF relaying. The key contributions of the chapter can be summarized as follows:

- Introduction of the concept of non-regenerative relaying for localization systems;
- Analysis and design of localization systems with relays accounting for nodes deployment, propagation environment, and channel state information (CSI);
- Quantification of benefits given by relaying techniques on localization performance.

This chapter is organized as follows. Section 5.2 presents non-regenerative relaying, Sec. 5.3 analyzes network localization with non-regenerative relays.

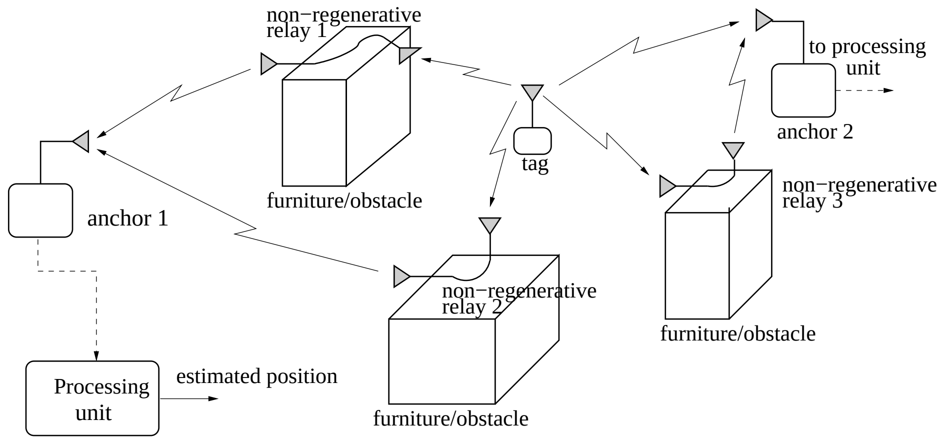

Figure 5.1: Example of localization system employing non-regenerative relays.

Section 5.4 quantifies the impact of the proposed relaying technique for a case study, and a conclusion is given in Sec. 5.5.

5.2 System Model

We consider (see Fig. 5.1) a localization system with an infrastructure composed of N_a anchors located in known positions $\mathbf{p}_n^{(\mathrm{A})}$, for $n = 1, 2, \ldots, N_\mathrm{a}$, a set of N_r non-regenerative unidirectional relays deployed in known positions $\mathbf{p}_i^{(\mathrm{R})}$, for $i = 1, 2, \ldots, N_\mathrm{r}$, and a generic tag in unknown position $\mathbf{p}$ to be determined. Anchors are supposed to be part of a network controlled by the central processing unit and to have a common time scale (i.e., synchronized).

5.2.1 Non-Regenerative Relays

The purpose of relays is to repeat the signal exchange between tags and anchors. Non-regenerative relays can be passive (JF) or active (AF). With reference to Fig. 5.2a, the JF relay is composed of a weak directional antenna (antenna A), an electrical cable and a high gain directional antenna (antenna B). The phenomenon exploited by the relay is the partial compensation of the additional path-loss caused by the two-hop link thanks to the directional properties of the antennas. Relays can be implemented in several ways. Unidirectional relays are sufficient when operating in a localization system with active tags adopting a one-way ranging protocol (e.g., TDOA) [24]. More complex bi-directional relays are necessary in case of two-way ranging protocols in order to ensure two-directional transmission capabilities. In this chapter we focus the attention on unidirectional relays due to their intrinsic

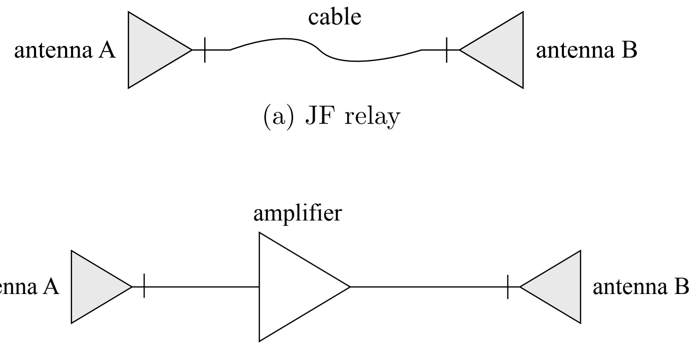

(a) JF relay

(b) AF relay

Figure 5.2: Non-regenerative relays.

lower complexity. In Fig. 5.2b an example of one-way AF relay is depicted. The difference with respect to the JF relay is the insertion of an amplifier in between antenna A and antenna B to reinforce the signal. Mutual coupling between antennas must be controlled through proper isolation and device deployment in order to avoid unstable loops caused by positive feedback that could arise. This effect might cause a limitation on the maximum tolerable signal amplification level. A more complex architecture that adopts echo cancelers can be also adopted in order to increase the robustness against feedback. Other similar solutions can be considered to this purpose (e.g., [259]), even though they still require an external synchronization signal.

A characteristic of non-regenerative relays is the additional thermal noise generation. More specifically, if $T_{\mathrm{a}} = 290\,\mathrm{K}$ is the antenna temperature, and G the gain of the relay ($G < 1$ in JF relays), the equivalent single-side noise PSD results $N_R = k_b\,F_R$, where k_b is the Boltzmann's constant and F_R is the relay noise figure ($F_R = 1/G$ in JF relays).

As general guideline, the relays are deployed in such a way that antenna B is in LOS condition with respect to one preferred anchor, and antenna A is LOS with respect to all the possible tag positions of interest intended to be covered by the repeater (e.g., a shadowed area).

5.2.2 Signal Model

Tags emit a signal $s(t)$ which may be received by one or more anchors through a direct path (when LOS), through reflections from walls and obstacles, as well as through non-regenerative relays. Tags can coexist in the same environment by a suitable channelization method or a medium access control (MAC) procedure. Consider the transmitted impulse-radio UWB ranging packet $s(t)$. It is, in general, composed of a sequence of N_{s} UWB pulses modulated according to a TH sequence $\{c_k\}$, with $c_k \in \{0, 1, \ldots H-1\}$, and/or a direct spreading sequence $\{d_k\} \in \{-1, 1\}$ to make the transmitted signal unique for each specific tag [47]. The transmitted ranging packet can be written as[1]

$$s(t) = \sum_{k=0}^{N_\mathrm{s}-1} d_k \, p(t - kT_\mathrm{f} - c_k T_\mathrm{h} - t_0) \tag{5.1}$$

where T_f identifies the pulse repetition period (PRP), typically chosen larger than the channel excess delay, T_h is the TH time slot, usually chosen so that $H\,T_\mathrm{h} < T_\mathrm{f}$, and t_0 represents the time offset of the tag's internal clock with respect to that of the anchors. The transmission time instant t_0 is not known to the anchors since, in general, tags and anchors are asynchronous. However, in some system configurations tags can be partially synchronized through a dedicated conventional control channel (e.g., at 2.4 GHz or ultra-high frequency (UHF)) [264]. In such a case the initial uncertainty on t_0 can be significantly reduced.

We define for notational convenience the quantities:

$$a_{l,m}(\mathbf{p}) = \begin{cases} w(\mathbf{p}, \mathbf{p}_m^{(\mathrm{A})}) & \text{for } l = 1\,, \\ w(\mathbf{p}, \mathbf{p}_{l-1}^{(\mathrm{R})}) \sqrt{G_{l-1}}\, w(\mathbf{p}_{l-1}^{(\mathrm{R})}, \mathbf{p}_m^{(\mathrm{A})}) & \text{for } l = 2, \ldots, L\,, \end{cases} \tag{5.2}$$

$$\tau_{l,m}(\mathbf{p}, t_0) = \begin{cases} \tau(\mathbf{p}, \mathbf{p}_m^{(\mathrm{A})}) + t_0 & \text{for } l = 1\,, \\ \tau(\mathbf{p}, \mathbf{p}_{l-1}^{(\mathrm{R})}) + \delta^{(\mathrm{R})} + \tau(\mathbf{p}_{l-1}^{(\mathrm{R})}, \mathbf{p}_m^{(\mathrm{A})}) + t_0 & \text{for } l = 2, \ldots, L \end{cases} \tag{5.3}$$

where $L = N_\mathrm{r} + 1$ is the number of signal replicas potentially present at the anchor, $\tau(\mathbf{p}_1, \mathbf{p}_2) \triangleq ||\mathbf{p}_1 - \mathbf{p}_2||/c$ is the travel time taken by the signal to reach position $\mathbf{p}_2$ from $\mathbf{p}_1$ being c the speed of light (time-of-flight), G_i is the gain of the ith relay, and $\delta^{(\mathrm{R})}$ is the delay introduced by the relay mainly caused by the presence of the electrical cable and/or the amplifier. When a path between generic positions $\mathbf{p}_1$ and $\mathbf{p}_2$ exists, the coefficient $w(\mathbf{p}_1, \mathbf{p}_2)$ accounts for the transmitted power, antenna gains and path-loss. Especially this coefficients can be expressed as:

$$w(\mathbf{p}_1, \mathbf{p}_2) = \sqrt{\frac{1}{L(\mathbf{p}_1, \mathbf{p}_2)}} \tag{5.4}$$

where

$$L(\mathbf{p}_1, \mathbf{p}_2) = L_0 \, ||\mathbf{p}_1 - \mathbf{p}_2||^\beta \Psi(\mathbf{p}_1, \mathbf{p}_2) \tag{5.5}$$

[1]Through a proper design of the spreading sequence $\{d_k\}$, $\{c_k\}$ it is possible to reduce the multi-user interference in a multi-tag scenario. The analysis of multi-user interference is beyond the scope of this chapter and well investigated in the literature [260, 261, 262, 263].

is the intrinsic channel path-loss, with path-loss exponent β, and L_0 is the channel path-loss at 1 meter. The term $\Psi(\mathbf{p}_1, \mathbf{p}_2)$ is a comprehensive coefficient which accounts for antennas' radiation patterns.[2] In the absence of a path (severe NLOS propagation condition) it is $w(\mathbf{p}_1, \mathbf{p}_2) = 0$. Note that the information about radio visibility can be derived from the environment knowledge [28].

The received signal at the mth anchor takes the form

$$r_m(t) = s_m(t) + n_m(t) \tag{5.6}$$

where the term $n_m(t) = \sum_{i=0}^{N_\mathrm{R}} n_{i,m}(t)$ accounts for all noise components. In particular, $n_{i,m}(t)$, for $i = 1, \ldots, N_\mathrm{r}$ is the thermal noise, with PSD $N_{i,m}$, due to the ith relay as seen by the mth anchor, and $n_{0,m}(t)$ is the thermal noise due to the anchor with PSD $N_{0,m} = N_0$. The useful term $s_m(t)$ can be expressed as

$$s_m(t) = \sum_{l=1}^{L} a_{l,m}(\mathbf{p})\, g_{l-1,m}(t - \tau_{l,m}(\mathbf{p}, t_0)) \tag{5.7}$$

where $g_{i,m}(t)$, for $i = 1, 2, \ldots N_\mathrm{r}$, are the CRs to $s(t)$ related to the link $\{\text{tag} \rightarrow i\text{th relay} \rightarrow m\text{th anchor}\}$, whereas $g_{0,m}(t)$ is the channel response to $s(t)$ related to the link $\{\text{tag} \rightarrow m\text{th anchor}\}$. They account for multipath propagation effects as well as for signal distortion that might be caused by antennas and circuits frequency selectivity. In this formulation multiple hop paths between relays are neglected, since they are expected to be strongly mitigated by directive antenna radiation patterns. The terms for $l > 1$ in the summation in (5.7) account for all signals repeated by the relays, whereas the term for $l = 1$ accounts for the direct path between the tag and the anchor (even through environmental multipath). In the following we will refer to the complete set of L signals at anchor m with the name *replicas*.

For the sake of illustration, in Fig. 5.3 an example of signal structure received by anchors A and B in the scenario of Fig. 5.1 is depicted supposing the presence of $N_\mathrm{r} = 3$ relays and $N_\mathrm{a} = 2$ anchors located in known positions and AWGN channels. Consider the tag is in NLOS condition with respect to anchor 1, e.g., $w\left(\mathbf{p}, \mathbf{p}_1^{(\mathrm{A})}\right) = 0$. In addition we suppose in the example that $w\left(\mathbf{p}_1^{(\mathrm{A})}, \mathbf{p}_3^{(\mathrm{R})}\right) = w\left(\mathbf{p}_1^{(\mathrm{R})}, \mathbf{p}_2^{(\mathrm{A})}\right) = w\left(\mathbf{p}_2^{(\mathrm{R})}, \mathbf{p}_2^{(\mathrm{A})}\right) = 0$. $\delta^{(\mathrm{R})} = 0$ is assumed for simplicity. As can be seen, the impulse emitted by the tag at time $t = t_0$ is received by relay 1 after $\tau\left(\mathbf{p}, \mathbf{p}_1^{(\mathrm{R})}\right)$ seconds and then repeated. The repeated

[2]Antenna frequency selectivity is included in the CRs $g_{i,m}(t)$ defined later.

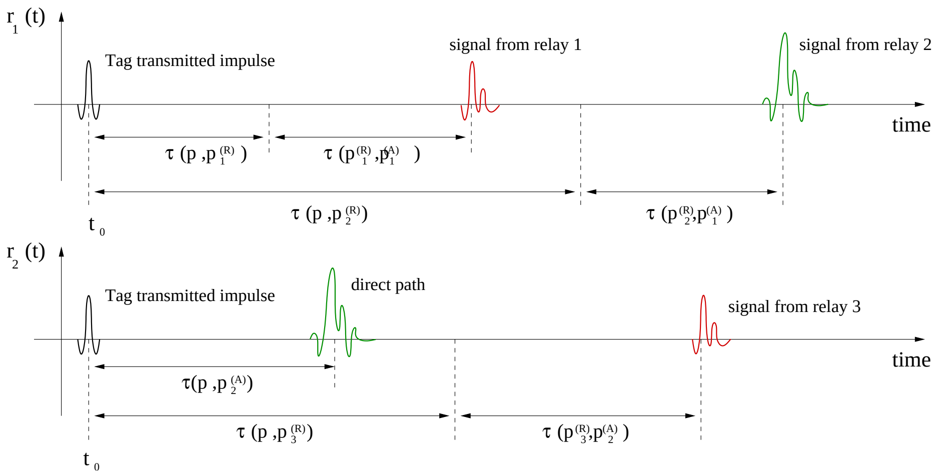

Figure 5.3: Example of signal structure in a scenario adopting active tags. $\delta^{(\mathrm{R})} = 0$. $r_1(t)$ and $r_2(t)$ are the signals received by anchors 1 and 2, respectively.

signal arrives at anchor 1 after $\tau\left(\mathbf{p}, \mathbf{p}_1^{(\mathrm{R})}\right) + \tau\left(\mathbf{p}_1^{(\mathrm{R})}, \mathbf{p}_1^{(\mathrm{A})}\right)$ seconds. It has to be remarked that the delay $\tau\left(\mathbf{p}_1^{(\mathrm{R})}, \mathbf{p}_1^{(\mathrm{A})}\right)$ is known since the positions of anchors and relays are a priori known.

5.3 Localization with Non-Regenerative Relays

In this section, ML position estimation is addressed with the purpose of assessing the feasibility of localization enhancement through the adoption of non-regenerative relays. It has to be remarked that the proposed architecture based on non-regenerative relays is not limited to ML position estimators. Although other state-of-the-art approaches for TOA and position estimation could be adopted [24, 51], with proper adaptation to include the presence of relays, ML estimators have been chosen because of their asymptotic efficiency and wide adoption. In the following, different ML estimators are derived for different CSI availability.

5.3.1 ML Localization with Perfect CSI (Estimator A)

In the following the ML tag's position estimator is derived considering perfect CSI, that is, a perfect knowledge of the CRs $g_{i,m}(t)$ as well as of the channel gain coefficients $w(\cdot, \cdot)$. Obviously, perfect CSI cannot be obtained in practice,[3] but results obtained are still useful as performance benchmark of other estimators operating under more realistic assumptions.

Considering N_{a} anchors, the likelihood function related to position $\mathbf{p}$ of the tag and ranging packet starting time t_0 is

$$\Lambda(\mathbf{p}, t_0) = \prod_{m=1}^{N_{\mathrm{a}}} k \exp\left\{-\frac{1}{N_m}\int_{T_{\mathrm{ob}}} \left[r_m(t) - s_m(t; \mathbf{p}, t_0)\right]^2 \, dt\right\} \tag{5.8}$$

where T_{ob} is the observation interval that has to be chosen for accommodating all the useful signal replica, $N_m = \sum_{i=0}^{N_{\mathrm{r}}} N_{i,m}$ represents the overall noise PSD at each anchor, k is a constant including all the terms not dependent on $\mathbf{p}$ and t_0, and where we have made explicit the dependence of $s_m(t)$ on the position $\mathbf{p}$ and t_0. Taking the logarithm and discarding all the terms that do not contribute to the maximization, the log-likelihood function to be maximized with respect to $\mathbf{p}$ and t_0 becomes:

$$l(\mathbf{p}, t_0) = \sum_{m=1}^{N_{\mathrm{a}}} \frac{2}{N_m}\int_{T_{\mathrm{ob}}} r_m(t)\, s_m(t; \mathbf{p}, t_0)\, dt - \sum_{m=1}^{N_{\mathrm{a}}} \frac{1}{N_m}\int_{T_{\mathrm{ob}}} s_m^2(t; \mathbf{p}, t_0)\, dt\,. \tag{5.9}$$

The last integral in (5.9) returns the energy of $s_m(t; \mathbf{p}, t_0)$ which does not depend on t_0 but only on $\mathbf{p}$. The ML position estimate $\hat{\mathbf{p}}$ of the tag is therefore

$$\hat{\mathbf{p}} = \underset{(\mathbf{p}, t_0)}{\operatorname{argmax}}\, l(\mathbf{p}, t_0)\,. \tag{5.10}$$

In particular, by replacing (5.7) in (5.9) we obtain

$$l(\mathbf{p}, t_0) = \sum_{m=1}^{N_{\mathrm{a}}} \left\{\frac{2}{N_m}\left[\sum_{l=1}^{L} a_{l,m}(\mathbf{p})\, \chi_{l,m}\left(\tau_{l,m}(\mathbf{p}, t_0)\right)\right] - \frac{E_m(\mathbf{p})}{N_m}\right\} \tag{5.11}$$

where we have defined the correlation term

$$\chi_{l,m}(\xi) \triangleq \int_{T_{\mathrm{ob}}} r_m(t)\, g_{l-1,m}(t - \xi)\, dt \tag{5.12}$$

and the energy term

$$E_m(\mathbf{p}) \triangleq \int_{T_{\mathrm{ob}}} s_m^2(t; \mathbf{p}, t_0)\, dt\,. \tag{5.13}$$

[3] In this scenario obtaining CSI is a more challenging task with respect to conventional communication systems, due to the presence of relayed components in the received signal.

The ML estimator invole passing, at each anchor, the received signal through a bank of filters matched to $g_{i,m}(t)$, and observing their weighted outputs in proper time instants depending on the position $\mathbf{p}$ under hypothesis. Obviously the implementation can be drastically simplified by adopting filters matched to a template waveform equal, for example, to the transmitted signal $p(t)$. Notice that, in (5.11), correlators outputs are optimally weighted by the noise PSD N_m at each anchor, in order to take into account the different noise level due to the particular anchor-relay distances.

5.3.2 ML Localization with Partial CSI

We now want to relax the assumption of perfect CSI, considering different levels of knowledge available at the receiver. We first derive the ML estimator in case of unknown received signal amplitude; in this case the localization capability is related to the delay-distance dependence of signal TOA only. Secondly, the possibility of adopting a position estimator that does not require the knowledge of the CRs $g_{i,m}(t)$, but exploits both the information on RSSI and TOA is investigated. As last, a blind position estimator that does not require the knowledge of the CRs and exploits the only information of TOA is derived. In these last two cases we assume, for the estimator design purpose, the CRs $g_{i,m}(t)$ as unknown deterministic signals.

For the derivation of the corresponding estimators, we use the well-known result according to which a band-limited signal $x(t)$, with bandwidth W, observed in the time-limited interval $(0, T_{\text{ob}})$ is described with good approximation (if $WT_{\text{ob}} \gg 1$) by a set of $M = 2\lceil WT_{\text{ob}} \rceil$ samples[4] obtained by sampling the original signal at times $\delta t = 1/2W$ apart (sampling time). Specifically, it is $x(t) = \sum_{n=1}^{\infty} x_n \operatorname{sinc}(2Wt - n)$, where $\operatorname{sinc}(t) = \sin(\pi t)/(\pi t)$, for $t \neq 0$ and 1 for $t = 0$, and we associate to $x(t)$, $t \in (0, T_{\text{ob}})$, the vector of coefficients $\mathbf{x} = \{x_n\}_{n=1}^{M}$, with $x_n = x(n\delta t)$. Adopting this representation we have also[5] [86]

$$\int_{T_{\text{ob}}} x^2(t)\, dt \simeq \frac{1}{2W} \|\mathbf{x}\|^2 . \tag{5.14}$$

[4]The operator $\lceil x \rceil$ denotes the smallest integer larger than x.
[5]$\|\mathbf{x}\|^2 = \mathbf{x}^T \mathbf{x}$.

Therefore we have the following associations:

$$
\begin{array}{lll}
r_m(t) \quad t \in (0, T_{\text{ob}}) & \rightarrow \mathbf{r}^{(m)} \in \mathbb{R}^N \text{ with elements } r_n^{(m)} = r_m(n\delta t)\,, \\
n_m(t) \quad t \in (0, T_{\text{ob}}) & \rightarrow \mathbf{n}^{(m)} \in \mathbb{R}^N \text{ with elements } n_n^{(m)} = n_m(n\delta t)\,, \\
s_m(t) \quad t \in (0, T_{\text{ob}}) & \rightarrow \mathbf{s}^{(m)} \in \mathbb{R}^N \text{ with elements } s_n^{(m)} = s_m(n\delta t)\,, \\
g_{i,m}(t) \quad t \in (0, T_{\text{p}}^{(i,m)}) & \rightarrow \mathbf{g_l}^{(m)} \in \mathbb{R}^{M^{(l,m)}} \text{ with elements } g_{l,n}^{(m)} = g_{l-1,m}(n\delta t)
\end{array}
\tag{5.15}
$$

where $N = \lceil T_{\text{ob}}/\delta t \rceil$ and $M^{(l,m)} = \left\lceil T_{\text{p}}^{(l,m)}/\delta t \right\rceil$, having denoted $T_{\text{p}}^{(l,m)}$ the duration of the l-th replica of the received signal at the m-th anchor.

Known Signal, TOA-based ML Position Estimation (Estimator B1)

We now derive the position estimator considering in (5.10) and (5.11) the channel coefficients $w(\cdot,\cdot)$ unknown quantities. First we define the vector of channel amplitudes

$$\mathbf{a}^{(m)} = \left[a_{1,m}(\mathbf{p}), a_{2,m}(\mathbf{p}), \ldots, a_{L,m}(\mathbf{p})\right]^T \in \mathbb{R}^L\,. \tag{5.16}$$

Taking advantage of the series expansions (5.15), it is possible to rewrite (5.6) in vector terms as

$$\mathbf{r}^{(m)} = \mathbf{W}_{(m)}(\mathbf{p})\, \mathbf{a}^{(m)} + \mathbf{n}^{(m)} \tag{5.17}$$

where $\mathbf{W}_{(m)}(\mathbf{p}) \in \mathbb{R}^{N \times L}$ has the form[6]

$$\mathbf{W}_{(m)}(\mathbf{p}) = \left[\mathbf{w}_{D_{1,m}(\mathbf{p})}^{(m)}, \mathbf{w}_{D_{2,m}(\mathbf{p})}^{(m)}, \ldots, \mathbf{w}_{D_{L,m}(\mathbf{p})}^{(m)}\right] \tag{5.18}$$

and

$$\mathbf{w}_{D_{l,m}(\mathbf{p})}^{(m)} = \left[\mathbf{0}_{D_{l,m}(\mathbf{p})}, \mathbf{g_l}^{(m)}, \mathbf{0}_{N-M^{(l,m)}-D_{l,m}(\mathbf{p})}\right]^T \in \mathbb{R}^N \tag{5.19}$$

having indicated with $D_{l,m}(\mathbf{p})$ the discrete version of delay $\tau_{l,m}(\mathbf{p}, t_0)$, that is, $D_{l,m}(\mathbf{p}) \triangleq \lceil \tau_{l,m}(\mathbf{p}, t_0)/\delta t \rceil$.

Considering the vector $\mathbf{a}^{(m)}$ unknown but deterministic, the estimation of the position can be realized substituting in (5.10) a ML estimate $\hat{\mathbf{a}}^{(m)}$ of $\mathbf{a}^{(m)}$ for each anchor, that is,

$$\hat{\mathbf{p}} = \underset{(\mathbf{p}, t_0)}{\operatorname{argmax}}\; l\left(\mathbf{p}, t_0; \{\mathbf{a}^{(m)}\} = \{\hat{\mathbf{a}}^{(m)}\}\right)\,. \tag{5.20}$$

[6]Actually $\mathbf{W}_{(m)}(\mathbf{p})$ is a function also of t_0. However, for notation simplicity, this dependence will be omitted in the rest of the chapter.

The previous expression can be further detailed as

$$\hat{\mathbf{p}} = \underset{(\mathbf{p},t_0)}{\operatorname{argmax}} \left\{ -\sum_{m=1}^{N_\mathrm{a}} \frac{1}{2\sigma_m^2} \left\| \mathbf{r}^{(m)} - \mathbf{W}_{(m)}(\mathbf{p})\, \hat{\mathbf{a}}^{(m)} \right\|^2 \right\} \tag{5.21}$$

where $\sigma_m^2 = N_m W$ is the noise power.

According to the derivation presented in Appendix 5.A, the ML estimator is

$$\hat{\mathbf{p}} = \underset{(\mathbf{p},t_0)}{\operatorname{argmax}} \left\{ \sum_{m=1}^{N_\mathrm{a}} \frac{1}{2\sigma_m} \tilde{\boldsymbol{\chi}}_{(m)}{}^T(\mathbf{p})\, \tilde{\mathbf{R}}_{(m)}{}^{-1}(\mathbf{p})\, \tilde{\boldsymbol{\chi}}_{(m)}(\mathbf{p}) \right\} \tag{5.22}$$

where the vector $\tilde{\boldsymbol{\chi}}_{(m)}(\mathbf{p})$ and the matrix $\tilde{\mathbf{R}}_{(m)}(\mathbf{p})$, defined respectively in (5.51) and (5.52), have the following continuous-time equivalents

$$\boldsymbol{\chi}_{(m)}(\mathbf{p}) = \int_0^{T_\mathrm{ob}} r_m(t) \begin{bmatrix} g_{0,m}(t - \tau_{1,m}(\mathbf{p}, t_0)) \\ g_{1,m}(t - \tau_{2,m}(\mathbf{p}, t_0)) \\ \vdots \\ g_{N_\mathrm{r},m}(t - \tau_{L,m}(\mathbf{p}, t_0)) \end{bmatrix} dt \tag{5.23}$$

and $\mathbf{R}_{(m)}(\mathbf{p}) = \left\{ R_{i,j}^{(m)} \right\}$, where each entry $R_{i,j}^{(m)}$ takes the form

$$R_{i,j}^{(m)} = \int_0^{T_\mathrm{ob}} g_{i-1,m}(t - \tau_{i,m}(\mathbf{p}, t_0))\, g_{j-1,m}(t - \tau_{j,m}(\mathbf{p}, t_0))\, dt\,. \tag{5.24}$$

The implementation of estimator (5.22) can be complex since it requires the evaluation of $\tilde{\boldsymbol{\chi}}_{(m)}(\mathbf{p})$ and $\tilde{\mathbf{R}}_{(m)}(\mathbf{p})$ for each hypothesis $\mathbf{p}$, as well as potentially complex matrix inversions. However, if the duration $T_\mathrm{p}^{(l,m)}$ of signals $g_{l,m}(t)$ is such that the replicas at each anchor are not overlapped, all the cross-correlations $R_{i,j}^{(m)}$, with $i \neq j$, are zero and $\mathbf{R}_{(m)}(\mathbf{p})$ becomes a diagonal energy matrix, independent on $\mathbf{p}$, where each non-zero element in the main diagonal $E_k^{(m)} = R_{k,k}^{(m)}$, $k = 1, \ldots, L$ is

$$E_k^{(m)} = \int_0^{T_\mathrm{ob}} g_{k-1,m}^2(t)\, dt\,. \tag{5.25}$$

In this case it is possible to simplify (5.22) as

$$\hat{\mathbf{p}} = \underset{(\mathbf{p},t_0)}{\operatorname{argmax}} \left\{ \sum_{m=1}^{N_\mathrm{a}} \frac{1}{N_m} \sum_{l=1}^{L} \frac{1}{E_l^{(m)}} \chi_{l,m}^2\left(\tau_{l,m}(\mathbf{p}, t_0)\right) \right\} \tag{5.26}$$

where $\chi_{i,j}(\cdot)$ have been defined in (5.12). The position estimator (5.26) relies on the TOA only since the signal amplitudes $a_{l,m}$, supposed unknown, are not present in the expression.

Notice that (5.26) requires the sum of the correlation terms related to all the L replicas at each anchor while, as explained in 5.2.2, only a subset of the relays and anchors will be, in general, in visibility of a tag in position $\mathbf{p}$, and this is accounted by the fact that some of the coefficients $w(\cdot,\cdot)$ are zero. Therefore, if this a priori information on blocked signal replicas, obtained for example from environment map, is available, it can be exploited by setting to zero the corresponding coefficients in (5.16). In this case, defining a vector $\boldsymbol{\lambda}(\mathbf{p}) \in \mathbb{R}^L$ with elements

$$\lambda_l(\mathbf{p}) = \begin{cases} 0, & \text{if } a_l = 0\,, \\ 1, & \text{if } a_l \neq 0 \end{cases} \tag{5.27}$$

(5.26) has to be modified leading to

$$\hat{\mathbf{p}} = \underset{(\mathbf{p},t_0)}{\mathrm{argmax}} \left\{ \sum_{m=1}^{N_\mathrm{a}} \frac{1}{N_m} \sum_{l:\lambda_l(\mathbf{p})\neq 0} \frac{1}{E_l^{(m)}} \chi_{l,m}^2\left(\tau_{l,m}(\mathbf{p},t_0)\right) \right\} . \tag{5.28}$$

It is important to remark that both estimators (5.10)-(5.11) and (5.28) require, in general, the knowledge of the complete CRs $g_{i,m}(t)$. This is analogue of considering an ideal all-rake receiver at each anchor able to estimate all the signal replicas. Obviously these estimators can be implemented in sub-optimal manner considering, instead of the complete CR, the first-path only, with a substantial reduction of the complexity.

Unknown Signal, Joint TOA- and RSSI-based ML Position Estimation (Estimator B2)

The purpose of the following estimator is to avoid the need for performing the correlation in (5.12) that implies, in general, an implementation at Nyquist rate. The resulting estimator provides a combination of the information available via both RSSI and TOA for position estimation without a priori knowledge of CRs.

We start from the assumption that all the replicas $g_{l,m}(t)$ have the same shape $g(t)$. This assumption is obviously far from the reality considering, as $g_{l,m}(t)$, the complete CR, but can be verified with better approximation in the case we consider only the first-path of each replica (now assumed of duration T_p), that is equivalent of exploiting the received energy related uniquely to this part of the signal, without taking advantage of the following multipath components.[7]

Denote the transmitted energy $E_T = \int_0^{T_p} g(t)\, dt$. Defining $\mathbf{g} \in \mathbb{R}^M$, with $M = \lceil T_p/\delta t \rceil$, the corresponding sampled version of $g(t)$, we have $\|\mathbf{g}\|^2 = \breve{E}_T$, where $\breve{E}_T = E_T/\delta t$ according to (5.14). Adopting this representation it is possible to rewrite (5.17) in the form:

$$\mathbf{r}^{(m)} = \mathbf{H}_{(m)}(\mathbf{p})\, \mathbf{g} + \mathbf{n}^{(m)} \tag{5.29}$$

where the matrix $\mathbf{H}_{(m)}(\mathbf{p}) \in \mathbb{R}^{N \times M}$ accounts for the delays and the channel coefficients and can be written as

$$\mathbf{H}_{(m)}(\mathbf{p}) = \sum_{l=1}^{L} a_{l,m}(\mathbf{p}) (\mathbf{P}_N)^{D_{l,m}(\mathbf{p})} \mathbf{G} \tag{5.30}$$

where $\mathbf{P}_N$ is the N-order basic circulant permutation matrix [265, pag. 26], and $\mathbf{G} \in \mathbb{R}^{N \times M}$ is

$$\mathbf{G} = \begin{bmatrix} \mathbf{I}_M \\ \mathbf{0}_{N-M,M} \end{bmatrix} \tag{5.31}$$

having denoted with $\mathbf{I}_M$ the M-order identity matrix and with $\mathbf{0}_{N-M,M}$ the $N-M \times M$ null matrix. Since we want to derive a non-coherent estimator which does not require the knowledge of the CRs (i.e., the shape of $\mathbf{g}$) we perform the estimation substituting the ML estimate $\hat{\mathbf{g}}$ of $\mathbf{g}$, that is,

$$\hat{\mathbf{p}} = \underset{(\mathbf{p},t_0)}{\operatorname{argmax}}\, l\left(\mathbf{p}, t_0; \{\mathbf{g}\} = \{\hat{\mathbf{g}}\}\right) \tag{5.32}$$

obtaining

$$\hat{\mathbf{p}} = \underset{(\mathbf{p},t_0)}{\operatorname{argmax}} \left\{ -\sum_{m=1}^{N_a} \frac{1}{2\sigma_m} \left\| \mathbf{r}^{(m)} - \mathbf{H}_{(m)}(\mathbf{p})\, \hat{\mathbf{g}} \right\|^2 \right\}. \tag{5.33}$$

According to the derivation presented in Appendix 5.B, the ML estimator is

$$\hat{\mathbf{p}} = \underset{(\mathbf{p},t_0)}{\operatorname{argmax}} \left\{ \sum_{m=1}^{N_a} \frac{1}{2\sigma_m} \frac{\sqrt{\breve{E}_T}}{\|\mathbf{H}_{(m)}{}^{+}(\mathbf{p})\mathbf{r}^{(m)}\|} \mathcal{E}^{(m)}(\mathbf{p}) \left(2 - \frac{\sqrt{\breve{E}_T}}{\|\mathbf{H}_{(m)}{}^{+}(\mathbf{p})\mathbf{r}^{(m)}\|} \right) \right\} \tag{5.34}$$

where

$$\mathcal{E}^{(m)}(\mathbf{p}) = \mathbf{r}^{(m)^T} \mathbf{H}_{(m)}(\mathbf{p}) \mathbf{H}_{(m)}{}^{+}(\mathbf{p}) \mathbf{r}^{(m)}. \tag{5.35}$$

[7] Moreover, when the first-path is resolvable, the following multipath components do not carry any addition information on ranging [51, 136].

Although estimator (5.34) is in closed form, its implementation complexity can be still high as sampling at Nyquist rate and matrix inversion are required. However further simplifications are possible in the case the signal replicas are not overlapped, as shown in Appendix 5.C, obtaining

$$\hat{\mathbf{p}} = \underset{(\mathbf{p},t_0)}{\operatorname{argmax}} \left\{ \sum_{m=1}^{N_\mathrm{a}} \frac{1}{N_m} \left(2\sqrt{E^{(m)}(\mathbf{p}) \int_{\mathcal{D}^{(m)}(\mathbf{p})} r_m^2(t)\, dt} - E^{(m)}(\mathbf{p}) \right) \right\} \tag{5.36}$$

where

$$\mathcal{D}^{(m)}(\mathbf{p}) = \bigcup_{l:\lambda_l(\mathbf{p})\neq 0} \left\{ (\tau_{l,m}(\mathbf{p}, t_0), \tau_{l,m}(\mathbf{p}, t_0) + T_\mathrm{p}) \right\}. \tag{5.37}$$

The obtained estimator leads to very simple implementation since it requires energy measurements in particular windows of the received signal where, for each hypothesis on $\mathbf{p}$, we suppose to receive a useful contribution. These energy measurements are weighted by the expected received energies (the expected RSSI).

Completely Unknown Signal, TOA-based ML Position Estimation (Estimator B3)

If the signal is completely unknown and it is not possible to exploit the amplitude-distance dependence (i.e., the RSSI), localization can be based only on the expected TOA information coming from geometrical considerations.

Equations (5.17) or (5.29) can be now written as

$$\mathbf{r}^{(m)} = \mathbf{s}^{(m)} + \mathbf{n}^{(m)} \tag{5.38}$$

where $\mathbf{s}^{(m)}$ is treated as an unknown vector. Again, the ML position estimation can be derived as

$$\hat{\mathbf{p}} = \underset{(\mathbf{p},t_0)}{\operatorname{argmax}}\, l\left(\mathbf{p}, t_0; \{\mathbf{s}^{(m)}\} = \{\hat{\mathbf{s}}^{(m)}\}\right) \tag{5.39}$$

where the ML estimate of $\mathbf{s}^{(m)}$ is considered, thus obtaining

$$\hat{\mathbf{p}} = \underset{(\mathbf{p},t_0)}{\operatorname{argmax}} \left\{ -\sum_{m=1}^{N_\mathrm{a}} \frac{1}{2\sigma_m^2} \left\| \mathbf{r}^{(m)} - \hat{\mathbf{s}}^{(m)} \right\|^2 \right\}. \tag{5.40}$$

Specifically, according to the only available a priori information on the expected TOA, the estimates of $\mathbf{s}^{(m)}$ are those exploiting the knowledge about the CRs arrival time, that is,

$$\hat{\mathbf{s}}^{(m)} = \mathbf{r}^{(m)} \ \text{ for } \ n \in \tilde{\mathcal{D}}^{(m)}(\mathbf{p}), \tag{5.41}$$

where we have defined $\tilde{\mathcal{D}}^{(m)}(\mathbf{p})$ the set of indexes n for which we expect to received signal, given an hypothesis $\mathbf{p}$ for the position according to

$$\tilde{\mathcal{D}}^{(m)}(\mathbf{p}) = \bigcup_{l:\lambda_l(\mathbf{p})\neq 0} \left\{ D_{l,m}(\mathbf{p}), D_{l,m}(\mathbf{p})+1, \ldots, D_{l,m}(\mathbf{p})+M-1 \right\}. \quad (5.42)$$

Substituting (5.41) in (5.40) and neglecting the terms not dependent on $\mathbf{p}$ we obtain

$$\hat{\mathbf{p}} = \underset{(\mathbf{p},t_0)}{\mathrm{argmax}} \left\{ \sum_{m=1}^{N_\mathrm{a}} \frac{1}{2\sigma_m^2} \sum_{n\in\tilde{\mathcal{D}}^{(m)}(\mathbf{p})} \left(r_n^{(m)}\right)^2 \right\}. \quad (5.43)$$

The corresponding continuous-time estimator is simply

$$\hat{\mathbf{p}} = \underset{(\mathbf{p},t_0)}{\mathrm{argmax}} \left\{ \sum_{m=1}^{N_\mathrm{a}} \frac{1}{N_m} \int_{\mathcal{D}^{(m)}(\mathbf{p})} r_m^2(t)\, dt \right\}. \quad (5.44)$$

The structure of estimator (5.44) is very simple as it consists in collecting the energy in those time intervals in which, according to the hypothesis on $\mathbf{p}$ and t_0, we expect the presence of signal replica.

5.4 Case Study

We now evaluate the performance of the proposed relay-based localization scheme, adopting the derived position estimators. The purpose is, with the presented case study, to demonstrate the feasibility of the relaying approach for network localization. The considered scenario is described in Sec. 5.4.1, the adopted performance metrics are reported in Sec. 5.4.2, and simulation results are presented in Sec. 5.4.3.

5.4.1 Scenario

Figure 5.4 presents the scenario considered for simulations. It is a square cell of 20×20 meters with four obstacles of one meter width. As worst-case assumption, obstacles are intended to be completely blocking the signal propagation. Anchors are placed at the four corners of the square cell. Four non-regenerative relays are present in the environment, placed at the corners of the four blocking obstacles (i.e., at the corners of the area partially shadowed). Each relay is placed in such a way its directional antenna (antenna B) is oriented towards an anchor node, and its weak directional antenna (antenna A) is oriented toward the shadowed area. In Fig. 5.4 the antennas'

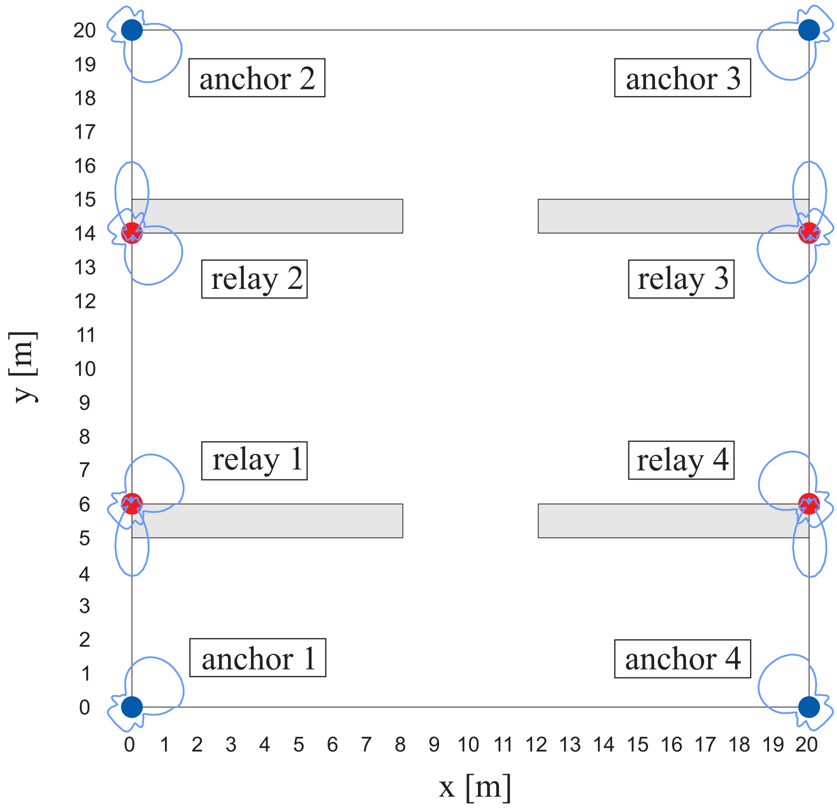

Figure 5.4: Scenario considered in the simulation results. Blue points refer to anchors. Red points refer to relays. Antennas' radiation patterns and orientation are reported. Obstacles are depicted in grey.

radiation patterns and orientations adopted, respectively, for anchors and relays are also depicted.

An IEEE 802.15.4a compliant UWB transmitted signal is considered [113], with RRC pulses[8] centered at frequency $f_c = 4\,\text{GHz}$, roll-off factor $\nu = 0.6$, and a pulse width parameter $T_w = 1\,\text{ns}$. Tags are supposed to be equipped with an omnidirectional antenna with gain $G_T = 0\,\text{dBi}$, and with transmitting power compliant to the Federal Communications Commission (FCC) $-41.3\,\text{dBm/MHz}$ emission limit in the $3-5\,\text{GHz}$ band. Real UWB antennas are considered, with radiation patterns characterized in anechoic chamber. Antennas have been measured in a range of frequencies between 2.5 and 10.5 GHz.[9] Furthermore, antennas have been measured on one plane by steps of 5 degrees. A Vivaldi UWB antenna presenting a peak gain

[8]See (3.63) for the definition.

[9]Frequency selectivity is here neglected considering the radiation pattern at 4 GHz only.

$G_\mathrm{A} = 5\,\mathrm{dBi}$ and a half power beam width (HPBW) of 101 degrees is adopted for anchors and relay's antenna A (tag-relay links) [266]. A four-patch array antenna presenting a peak gain $G_\mathrm{A} = 12\,\mathrm{dBi}$ and a HPBW of 45 degrees is considered as the relay's antenna B (relay-anchor links) [267]. Antennas measurements have stressed out how some antennas features, such as the radiation pattern, could drive the choice of adopting an antenna instead of another in a localization context.

Anchors have a noise figure $F = 5$ dB. Additive noise at relays should in principle be taken into account. The extra noise power radiated by the relay scales with $GF_\mathrm{R} - 1$, where G and F_R have been defined in Sec. 5.2.1. However, when received by an anchor, this power is attenuated by the path-loss between the anchor and the relay. When putting realistic figures, it turns out that in most practical cases the relay noise power received by an anchor is well below the anchor additive noise and is therefore negligible. Consequently, it is $N_{i,m} \ll N_0$, and hence $N_{i,m}$, for $i \neq 0$, are neglected in the following simulation results.

In order to show the performance of the relay-based localization in different propagation conditions, two dense multipath models [102, 56] are adopted for the tag-anchor and tag-relay channels, considering a rms channel delay spread of 1.5 ns (*softer* multipath) and of 5 ns (*stronger* multipath), respectively. In both cases we consider an exponential PDP with paths separated of 1.5 ns apart, a probability $b = 0.7$ of having a path, each path with Nakagami fading (severity factor $m = 3$) except for the first-path taken as deterministic according to the free-space path loss model ($\beta = 2$).[10] Due to the high directivity of the relay antenna oriented in the anchor direction, an AWGN relay-anchor channel is considered.

Unless differently reported, a total of $N_\mathrm{s} = 256$ pulses is considered in the ranging packet with a PRP $T_\mathrm{f} = 100\,\mathrm{ns}$. Ideal knowledge of the delay t_0 is assumed.

[10] This is, obviously, a best-case assumption since also the first-path (i.e., the direct one) expresses a variance with respect to the deterministic free-space propagation model. However, recently it has been shown how the RSSI measurements performed on UWB signals can lead to an accurate distance estimation, thanks to the capability of mitigating fading effects [268, 269]. This estimation capability is a consequence of the small variance experienced by the first path with respect to an ideal propagation condition, motivation of our choice of this deterministic value (furthermore the obtained performance can be intended as a performance limit).

5.4.2 Performance Metrics

Results have been obtained with Monte Carlo simulations considering the tags uniformly and equally-spaced distributed in the monitored area. In particular a 50 cm grid, resulting in the set of positions $\mathbf{p}_n$, $n = 1, \ldots, N$, has been defined in the environment, which points are adopted as potential tag locations and test locations for position estimation.

As performance indicator we adopt the localization error outage (LEO), defined as the rate at which the localization error is greater than a given target error e_{th} [138, 28] (i.e., the fraction of spatial test locations that do not fulfill a target error requirement), that is

$$\text{LEO} = \frac{1}{N} \sum_{n=1}^{N} \mathbf{1}_{\mathbb{R}^+}(e(\mathbf{p}) - e_{\text{th}}) \tag{5.45}$$

where we have defined the indicator function $\mathbf{1}_{\mathcal{A}}(x) = 1$ if $x \in \mathcal{A}$, 0 otherwise, and $e(\mathbf{p})$ is the localization error in the nth test position of the grid. The RMSE is adopted as error metric $e(\mathbf{p})$ output of the Monte Carlo simulation, that is

$$e(\mathbf{p}) = \sqrt{\frac{1}{M} \sum_{m=1}^{M} e_m^2(\mathbf{p})} \tag{5.46}$$

where the localization error related to the mth iteration $e_m(\mathbf{p})$ is the Euclidean distance between the estimated position $\hat{\mathbf{p}}_m$ and the true position, that is $e_m(\mathbf{p}) = ||\hat{\mathbf{p}}_m - \mathbf{p}||$, and M is the number of simulation iterations. LEO is presented as function of the relay gain G, assumed the same for all the relays present in the environment (i.e., $G_i = G \; \forall i = 1, \ldots, N_{\text{r}}$). Results are provided considering a target error $e_{\text{th}} = 50$ cm.

The c.d.f.s of the RMSE, and the RMSE itself in the two-dimensional (2D) environment are also reported for selected configurations. Each c.d.f. represents the ratio between the number of test locations for which the RMSE is lower or equal than a specific value and the total amount of test locations in the grid.

5.4.3 Simulation Results

Figure 5.5 reports the LEO for the *softer* multipath channel. In particular the violet curve (□) refers to the estimator A (5.10). Blue curve (○) refers to the estimator B1 (5.28), yellow curve (△) refers to the estimator B2 (5.36), while the red curve (◇) refers to the estimator B3 (5.44). Estimator A and estimator B1 have been implemented according to a sub-optimal, and more

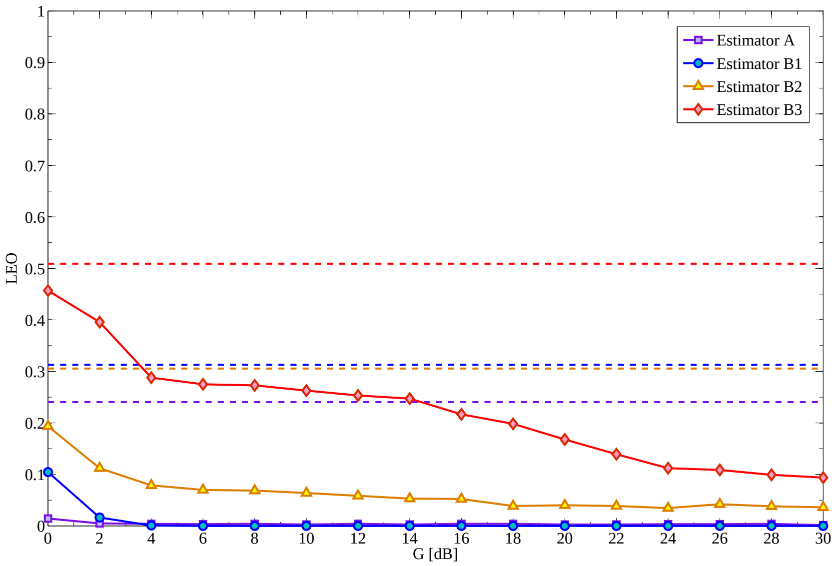

Figure 5.5: LEO as function of the relay gain for a *softer* multipath channel. Constant dashed lines (--) refer to the absence of relays.

practical, realization which considers a template waveform at the receiver equal to the transmitted pulse, without assuming any multipath knowledge or estimation.[11] Non-coherent estimators B2 and B3, based on energy detection, have been implemented considering $T = 1.6$ ns, that is the time window corresponding, approximately, to the main lobe of the pulse envelope.[12] For comparison, the LEO in absence of relay is reported with a constant dashed line,[13] considering the equivalent estimator specified in the case of absence of relays (i.e., $N_{\mathrm{r}} = 0$). JF relays corresponds to the first point along the abscissa $G = 0$, while the performance for AF relays is related to the following points on the x axis. As expected, the ML estimator A guarantees the best performance. In particular, for every considered estimator, the LEO decreases by increasing the relay gain G, thanks to the additional information carried out from the relayed signals. It is possible to notice how, in this configuration, the adoption of JF relays increase the localization capability of the system. Considering the coherent estimators, JF relays assures a LEO with a 50 cm RMSE threshold close to zero, in case of perfect CSI and around

[11] This is equivalent on assuming a filter matched to the first-path only, without taking advantage of the multipath energy.

[12] This is not the optimum value in case of multipath propagation. Performance can be improved with integration time optimization or weighting techniques for collecting energy from multipath, see, e.g., [94, 25].

[13] This would be a single point since the relay gain in the x axis does not make sense, the line is plotted for sake of comparison.

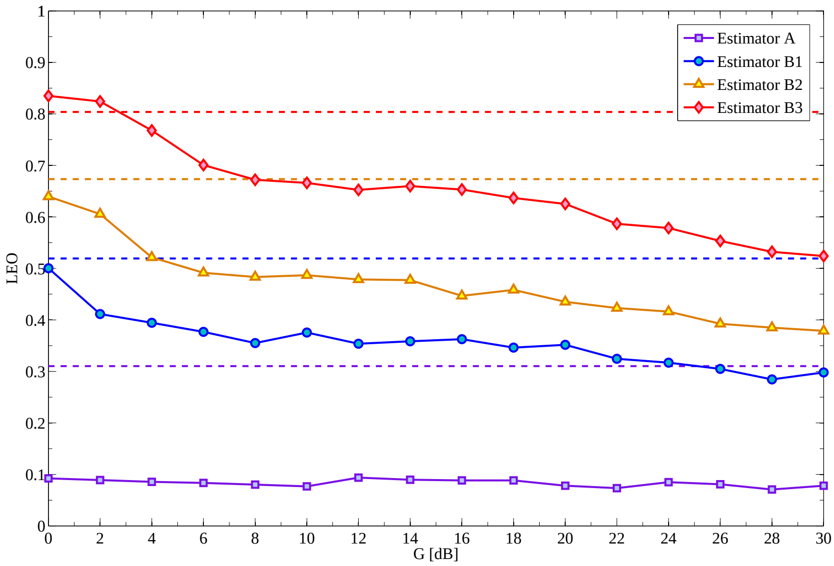

Figure 5.6: LEO as function of the relay gain for a *stronger* multipath channel. Constant dashed lines (- -) refer to the absence of relays.

the 10% in case of partial CSI, while outage values around the 25−30% are present in absence of relays due to the ambiguities that arise in the shadowed areas. Moreover, employing AF relays, the LEO substantially decreases by increasing the relay gain. In particular, each of the proposed estimators outperforms the corresponding one in absence of relays. As expected the ML coherent estimator A (with perfect CSI) offers the best performance in terms of outage, while the TOA-based non-coherent (estimator B3) requires higher values of gain in order to give an important performance enhancement.

For comparison in Fig. 5.6 the LEO in a *stronger* multipath environment is reported. Also in this case the adoption of the non-regenerative relaying technique allows a substantial performance improvement with respect to the absence of relays. As it is possible to notice, the performance of the system is strongly related to the propagation environment, so the proposed relaying technique can result suitable or not depending on the application context. In particular, coherent estimators are necessary in harsh propagation environments in order to obtain outages below the 10%.

In order to show how the relaying technique helps the localization process, we report a contour map plot of the localization RMSE in the 2D scenario considering absence of relays (Fig. 5.7a) and presence of JF relays (Fig. 5.7b), the TOA-based coherent estimator (5.28) and the *softer* multipath channel. It is possible to notice how, in absence of relays, the localization capabilities in the central area shadowed by the obstacles result very poor, and errors of

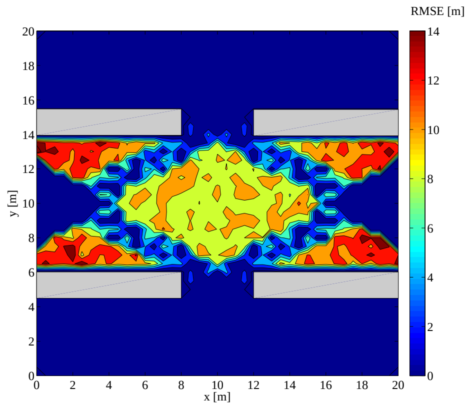

(a) Without relays

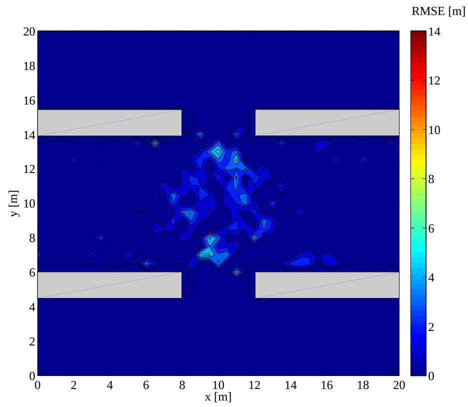

(b) JF relays

Figure 5.7: RMSE contour map in the 2D environment.

several meters can occur due to the lack of anchors visibility. Differently, the adoption of non-regenerative AF relays allows extending the system coverage in the shadowed areas, ensuring enhanced localization performance.

The performance improvement can be shown also in terms of c.d.f. of the localization error. Figure 5.8 shows the results considering absence of relays (in dashed lines) as well as presence of JF relays (in continuous lines), and AF relays with $G = 10\,\text{dB}$ (in dot-dashed lines) for the *softer* multipath channel. Again, the adoption of relaying assures a benefit in terms of the number of spatial points that can be localized with a target location accuracy without ambiguity.

The presented results proved the effectiveness of the relaying technique for network localization. In the proposed configuration the adoption of both JF and AF produce important benefits.

5.5 Conclusion

The idea of UWB non-regenerative relays for network localization has been introduced as a low complexity solution to increase the service coverage in high-definition RTLS based on UWB technique when operating in severe NLOS propagation conditions. The adoption of JF or AF relays increases the number of received signal components that, thanks to the a priori knowledge of relay positions, contribute in decreasing the possibility of ambiguities in ML estimators. Thus the relays act as additional virtual anchors. Numerical results show that significant performance improvement can be achieved, even using simple passive JF relays, with respect to the absence of relays. UWB

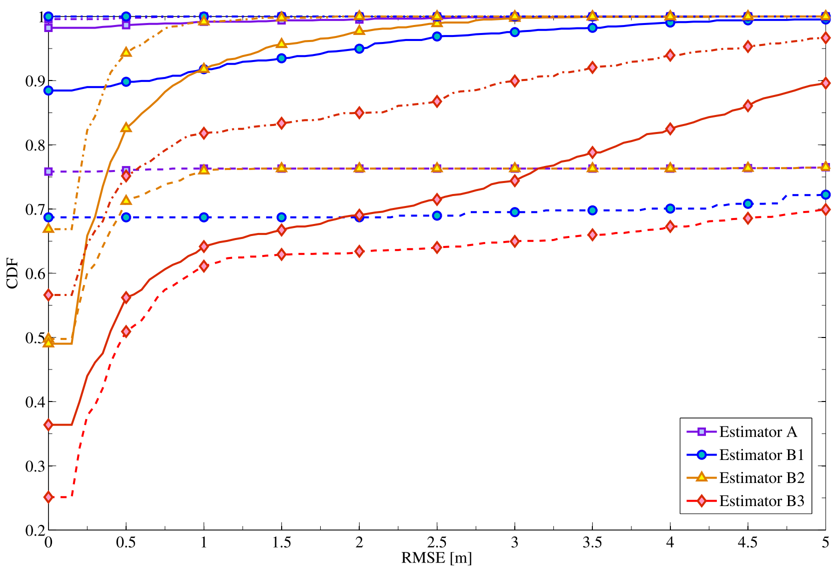

Figure 5.8: c.d.f.s of the RMSE. Dashed lines (- -) refer to the absence of relays, continuous lines (–) refer to the presence of JF relays, dot-dashed lines (·-) refer to the presence of AF relays.

non-regenerative relays can also be adopted to reduce the number of anchors with consequent reduction of the network infrastructure cost and complexity.

5.A Derivation of the ML estimator

The ML estimate $\hat{\mathbf{a}}^{(m)}$ of $\mathbf{a}^{(m)}$ can be easily obtained via LS [161, ch. 8] as

$$\hat{\mathbf{a}}^{(m)} = \mathbf{W}_{(m)}{}^{+}(\mathbf{p})\mathbf{r}^{(m)} \tag{5.47}$$

where $\mathbf{W}_{(m)}{}^{+}(\mathbf{p}) = \left(\mathbf{W}_{(m)}{}^{T}(\mathbf{p})\mathbf{W}_{(m)}(\mathbf{p})\right)^{-1}\mathbf{W}_{(m)}{}^{T}(\mathbf{p})$ is the Moore-Penrose pseudo-inverse matrix [265, p. 421]. Sobstituting (5.47) in (5.21) and neglecting the term not function of $\mathbf{p}$ we obtain

$$\begin{aligned}\hat{\mathbf{p}} = & \underset{(\mathbf{p},t_0)}{\mathrm{argmax}} \left\{ \sum_{m=1}^{N_\mathrm{a}} \frac{1}{2\sigma_m^2} \left(2\, \mathbf{r}^{(m)T} \mathbf{W}_{(m)}(\mathbf{p}) \mathbf{W}_{(m)}{}^{+}(\mathbf{p}) \mathbf{r}^{(m)} \right.\right. \\ & \left.\left. - \left\| \mathbf{W}_{(m)}(\mathbf{p}) \mathbf{W}_{(m)}{}^{+}(\mathbf{p}) \mathbf{r}^{(m)} \right\|^2 \right) \right\}. \end{aligned} \tag{5.48}$$

Considering that[14]

$$\left\|\mathbf{W}_{(m)}(\mathbf{p})\mathbf{W}_{(m)}{}^{+}(\mathbf{p})\mathbf{r}^{(m)}\right\|^2 = \mathbf{r}^{(m)T}\mathbf{W}_{(m)}(\mathbf{p})\mathbf{W}_{(m)}{}^{+}(\mathbf{p})\mathbf{r}^{(m)} \tag{5.49}$$

the final form of (5.48) is

$$\hat{\mathbf{p}} = \underset{(\mathbf{p},t_0)}{\operatorname{argmax}} \left\{ \sum_{m=1}^{N_\mathrm{a}} \frac{1}{2\sigma_m^2} \tilde{\boldsymbol{\chi}}_{(m)}{}^{T}(\mathbf{p})\, \tilde{\mathbf{R}}_{(m)}{}^{-1}(\mathbf{p})\, \tilde{\boldsymbol{\chi}}_{(m)}(\mathbf{p}) \right\} \tag{5.50}$$

where

$$\begin{aligned}\tilde{\boldsymbol{\chi}}_{(m)}(\mathbf{p}) &= \mathbf{W}_{(m)}{}^{T}(\mathbf{p})\, \mathbf{r}^{(m)} \\ &= \left[\mathbf{w}^{(m)T}_{D_{1,m}(\mathbf{p})}\mathbf{r}^{(m)}, \mathbf{w}^{(m)T}_{D_{2,m}(\mathbf{p})}\mathbf{r}^{(m)}, \ldots, \mathbf{w}^{(m)T}_{D_{L,m}(\mathbf{p})}\mathbf{r}^{(m)}\right] \in \mathbb{R}^L\end{aligned} \tag{5.51}$$

is the vector of correlation between the received signal and the delayed versions of the template pulses $\mathbf{g_l}^{(m)}$, and

$$\begin{aligned}\tilde{\mathbf{R}}_{(m)}(\mathbf{p}) &= \mathbf{W}_{(m)}{}^{T}(\mathbf{p})\, \mathbf{W}_{(m)}(\mathbf{p}) \\ &= \begin{bmatrix} \mathbf{w}^{(m)T}_{D_{1,m}(\mathbf{p})}\mathbf{w}^{(m)}_{D_{1,m}(\mathbf{p})} & \mathbf{w}^{(m)T}_{D_{1,m}(\mathbf{p})}\mathbf{w}^{(m)}_{D_{2,m}(\mathbf{p})} & \cdots & \mathbf{w}^{(m)T}_{D_{1,m}(\mathbf{p})}\mathbf{w}^{(m)}_{D_{L,m}(\mathbf{p})} \\ \mathbf{w}^{(m)T}_{D_{2,m}(\mathbf{p})}\mathbf{w}^{(m)}_{D_{1,m}(\mathbf{p})} & \mathbf{w}^{(m)T}_{D_{2,m}(\mathbf{p})}\mathbf{w}^{(m)}_{D_{2,m}(\mathbf{p})} & \cdots & \mathbf{w}^{(m)T}_{D_{2,m}(\mathbf{p})}\mathbf{w}^{(m)}_{D_{L,m}(\mathbf{p})} \\ \vdots & \vdots & \ddots & \vdots \\ \mathbf{w}^{(m)T}_{D_{L,m}(\mathbf{p})}\mathbf{w}^{(m)}_{D_{1,m}(\mathbf{p})} & \mathbf{w}^{(m)T}_{D_{L,m}(\mathbf{p})}\mathbf{w}^{(m)}_{D_{2,m}(\mathbf{p})} & \cdots & \mathbf{w}^{(m)T}_{D_{L,m}(\mathbf{p})}\mathbf{w}^{(m)}_{D_{L,m}(\mathbf{p})} \end{bmatrix}\end{aligned} \tag{5.52}$$

is the cross-correlation matrix of the template pulses.

5.B Derivation of the ML estimator

The ML estimate $\hat{\mathbf{g}}$ of $\mathbf{g}$ can be obtained adopting the LS technique [161, ch. 8] as

$$\hat{\mathbf{g}} = \sqrt{\breve{E}_T}\frac{\mathbf{H}_{(m)}{}^{+}(\mathbf{p})\mathbf{r}^{(m)}}{\|\mathbf{H}_{(m)}{}^{+}(\mathbf{p})\mathbf{r}^{(m)}\|} \tag{5.53}$$

where $\mathbf{H}_{(m)}{}^{+}(\mathbf{p}) = \left(\mathbf{H}_{(m)}{}^{T}(\mathbf{p})\mathbf{H}_{(m)}(\mathbf{p})\right)^{-1}\mathbf{H}_{(m)}{}^{T}(\mathbf{p})$ is the Moore-Penrose pseudo-inverse matrix [265, p. 421], and the normalization is imposed in such a way

[14] *Proof of* (5.49)
Considering that $\|\mathbf{x}\|^2 = \mathbf{x}^T\mathbf{x}$, and posing $\boldsymbol{\Xi} = \mathbf{W}_{(m)}(\mathbf{p})\mathbf{W}_{(m)}{}^{+}(\mathbf{p})$, we have $\|\boldsymbol{\Xi}\mathbf{r}^{(m)}\|^2 = \mathbf{r}^{(m)T}\boldsymbol{\Xi}^T\boldsymbol{\Xi}\,\mathbf{r}^{(m)}$. Since $\boldsymbol{\Xi}$ is an orthogonal projection matrix [161, pag. 231], that is, a symmetric ($\boldsymbol{\Xi}^T = \boldsymbol{\Xi}$) and idempotent ($\boldsymbol{\Xi}^2 = \boldsymbol{\Xi}$) matrix, we obtain directly (5.49).

the estimate is consistent according to the transmitted energy assumption $\|\mathbf{g}\|^2 = \breve{E}_T$. Substituting (5.53) in (5.33) and neglecting the terms not dependent on $\mathbf{p}$ we obtain

$$\hat{\mathbf{p}} = \underset{(\mathbf{p},t_0)}{\operatorname{argmax}} \left\{ \sum_{m=1}^{N_a} \frac{1}{2\sigma_m} \left(2\sqrt{\breve{E}_T} \frac{\mathbf{r}^{(m)^T} \mathbf{H}_{(m)}(\mathbf{p}) \mathbf{H}_{(m)}^{+}(\mathbf{p}) \mathbf{r}^{(m)}}{\left\| \mathbf{H}_{(m)}^{+}(\mathbf{p}) \mathbf{r}^{(m)} \right\|} \right. \right. \\ \left. \left. - \breve{E}_T \frac{\left\| \mathbf{H}_{(m)}(\mathbf{p}) \mathbf{H}_{(m)}^{+}(\mathbf{p}) \mathbf{r}^{(m)} \right\|^2}{\left\| \mathbf{H}_{(m)}^{+}(\mathbf{p}) \mathbf{r}^{(m)} \right\|^2} \right) \right\}. \tag{5.54}$$

Considering that (same proof of 5.A-(5.49) considering $\mathbf{H}_{(m)}(\mathbf{p})$ instead of $\mathbf{W}_{(m)}(\mathbf{p})$)

$$\left\| \mathbf{H}_{(m)}(\mathbf{p}) \mathbf{H}_{(m)}^{+}(\mathbf{p}) \mathbf{r}^{(m)} \right\|^2 = \mathbf{r}^{(m)^T} \mathbf{H}_{(m)}(\mathbf{p}) \mathbf{H}_{(m)}^{+}(\mathbf{p}) \mathbf{r}^{(m)} \tag{5.55}$$

we get the expression (5.34).

5.C Derivation of the ML estimator

In the case of not overlapped replicas matrix $\mathbf{H}_{(m)}(\mathbf{p})$ takes the form of a block matrix

$$\mathbf{H}_{(m)}(\mathbf{p}) = \begin{bmatrix} \mathbf{0}_{D_{1,m}(\mathbf{p}),M} \\ \mathbf{H}_1^{(m)}(\mathbf{p}) \\ \mathbf{0}_{D_{2,m}(\mathbf{p})-D_{1,m}(\mathbf{p})-M,M} \\ \mathbf{H}_2^{(m)}(\mathbf{p}) \\ \vdots \\ \mathbf{H}_L^{(m)}(\mathbf{p}) \end{bmatrix} \tag{5.56}$$

where $\mathbf{H}_i^{(m)}(\mathbf{p}) = a_{i,m}(\mathbf{p}) \mathbf{I}_M$, $i = 1, \ldots, L$, are $M \times M$ scalar matrices. Exploiting the property of block matrix product, the block $\mathbf{H}_{(m)}^T(\mathbf{p}) \mathbf{H}_{(m)}(\mathbf{p})$ in (5.34) takes the form

$$\mathbf{H}_{(m)}^T(\mathbf{p}) \mathbf{H}_{(m)}(\mathbf{p}) = \sum_{l=1}^{L} \mathbf{H}_l^{(m)^2}(\mathbf{p}) = \sum_{l=1}^{L} a_{l,m}^2(\mathbf{p})\, \mathbf{I}_M\,. \tag{5.57}$$

Consequently we can define the scalar matrix $\mathbf{D} = \left(\mathbf{H}_{(m)}^T(\mathbf{p}) \mathbf{H}_{(m)}(\mathbf{p}) \right)^{-1}$ with non zero elements on the main diagonal equals to $\left(\sum_{l=1}^{L} a_{l,m}^2(\mathbf{p}) \right)^{-1}$. It is so possible to rewrite (5.35) as

$$\begin{aligned}\mathcal{E}^{(m)}(\mathbf{p}) &= \mathbf{r}^{(m)^T}\mathbf{H}_{(m)}(\mathbf{p})\,\mathbf{D}\,\mathbf{H}_{(m)}{}^T(\mathbf{p})\mathbf{r}^{(m)} \\ &= \frac{1}{\sum_{l=1}^{L} a_{l,m}^2(\mathbf{p})}\mathbf{r}^{(m)^T}\mathbf{H}_{(m)}(\mathbf{p})\mathbf{H}_{(m)}{}^T(\mathbf{p})\mathbf{r}^{(m)} \\ &= \frac{1}{\sum_{l=1}^{L} a_{l,m}^2(\mathbf{p})}\left\|\mathbf{r}^{(m)^T}\mathbf{H}_{(m)}(\mathbf{p})\right\|^2 . \end{aligned} \tag{5.58}$$

It is now easy to show that

$$\left\|\mathbf{r}^{(m)^T}\mathbf{H}_{(m)}(\mathbf{p})\right\|^2 = \sum_{i=1}^{L}\sum_{j=1}^{L} a_{i,m}(\mathbf{p})\, a_{j,m}(\mathbf{p}) \sum_{n=0}^{M-1} r_{D_{i,m}(\mathbf{p})+n}^{(m)}\, r_{D_{j,m}(\mathbf{p})+n}^{(m)} \tag{5.59}$$

and consequently

$$\mathcal{E}^{(m)}(\mathbf{p}) = \frac{1}{\sum_{l=1}^{L} a_{l,m}^2(\mathbf{p})} \sum_{i=1}^{L}\sum_{j=1}^{L} a_{i,m}(\mathbf{p})\, a_{j,m}(\mathbf{p}) \sum_{n=0}^{M-1} r_{D_{i,m}(\mathbf{p})+n}^{(m)}\, r_{D_{j,m}(\mathbf{p})+n}^{(m)} . \tag{5.60}$$

With similar considerations and operations on block matrices, it is possible to show that $\|\mathbf{H}_{(m)}{}^+(\mathbf{p})\mathbf{r}^{(m)}\|^2$ in (5.54) takes the form

$$\begin{aligned}\|\mathbf{H}_{(m)}{}^+(\mathbf{p})\mathbf{r}^{(m)}\|^2 =& \frac{1}{\left(\sum_{l=1}^{L} a_{l,m}^2(\mathbf{p})\right)^2} \sum_{i=1}^{L}\sum_{j=1}^{L} a_{i,m}(\mathbf{p})\, a_{j,m}(\mathbf{p}) \\ &\times \sum_{n=0}^{M-1} r_{D_{i,m}(\mathbf{p})+n}^{(m)}\, r_{D_{j,m}(\mathbf{p})+n}^{(m)} . \end{aligned} \tag{5.61}$$

By substituting (5.60) and (5.61) in (5.34) the following formulation of the estimator is obtained

$$\begin{aligned}\hat{\mathbf{p}} =& \underset{(\mathbf{p},t_0)}{\operatorname{argmax}}\left\{ \sum_{m=1}^{N_\mathrm{a}} \frac{1}{2\sigma_m^2}\left[2\left(\breve{E}_T \sum_{i=1}^{L}\sum_{j=1}^{L} a_{i,m}(\mathbf{p})\, a_{j,m}(\mathbf{p}) \sum_{n=0}^{M-1} r_{D_{i,m}(\mathbf{p})+n}^{(m)}\, r_{D_{j,m}(\mathbf{p})+n}^{(m)}\right)^{1/2} \right.\right. \\ &\left.\left. - \breve{E}_T \sum_{l=1}^{L} a_{l,m}^2(\mathbf{p})\right]\right\} . \end{aligned} \tag{5.62}$$

This estimator has an immediate continuous-time equivalent as

$$\begin{aligned}\hat{\mathbf{p}} =& \underset{(\mathbf{p},t_0)}{\operatorname{argmax}}\left\{ \sum_{m=1}^{N_\mathrm{a}} \frac{1}{N_m}\left[2\left(E_T \sum_{l=1}^{L} a_{l,m}^2(\mathbf{p}) \int_{\tau_{l,m}(\mathbf{p})}^{\tau_{l,m}(\mathbf{p})+T_\mathrm{p}} r_m^2(t)\,dt \right.\right.\right.\\ &+ \left. \sum_{i=1}^{L}\sum_{j=1,j\neq i}^{L} a_{i,m}(\mathbf{p})\, a_{j,m}(\mathbf{p}) \int_0^{T_\mathrm{p}} r_m(t-\tau_{i,m}(\mathbf{p}))\, r_m(t-\tau_{j,m}(\mathbf{p}))\,dt\right)^{1/2}\\ &\left.\left. - E_T \sum_{l=1}^{L} a_{l,m}^2(\mathbf{p})\right]\right\}. \end{aligned} \tag{5.63}$$

If now we make the assumption[15]

$$r_m(t-\tau_{i,m}(\mathbf{p})) \simeq \frac{a_{i,m}(\mathbf{p})}{a_{j,m}(\mathbf{p})}\, r(t-\tau_{j,m}(\mathbf{p})) \ \text{ for } \ t \in (0, T_\mathrm{p}) \tag{5.64}$$

we have that (5.63) simplifies to

$$\begin{aligned}\hat{\mathbf{p}} =& \underset{(\mathbf{p},t_0)}{\operatorname{argmax}}\left\{ \sum_{m=1}^{N_\mathrm{a}} \frac{1}{N_m}\left(2\sqrt{E_T \sum_{l=1}^{L} a_{l,m}^2(\mathbf{p}) \sum_{k=1}^{L} \int_{\tau_{k,m}(\mathbf{p})}^{\tau_{k,m}(\mathbf{p})+T_\mathrm{p}} r_m^2(t)\,dt} \right.\right.\\ &\left.\left. - E_T \sum_{l=1}^{L} a_{l,m}^2(\mathbf{p})\right)\right\}. \end{aligned} \tag{5.65}$$

By considering that $E_T \sum_{l=1}^{L} a_{l,m}^2(\mathbf{p})$ is the overall received energy $E^{(m)}(\mathbf{p})$ from a tag in position $\mathbf{p}$ at the anchor m, collected considering the L replicas, we get the final estimator form

$$\hat{\mathbf{p}} = \underset{(\mathbf{p},t_0)}{\operatorname{argmax}}\left\{ \sum_{m=1}^{N_\mathrm{a}} \frac{1}{N_m}\left(2\sqrt{E^{(m)}(\mathbf{p}) \int_{\bar{\mathcal{D}}^{(m)}(\mathbf{p})} r_m^2(t)\,dt} - E^{(m)}(\mathbf{p})\right)\right\} \tag{5.66}$$

where we have indicated with

$$\begin{aligned}\bar{\mathcal{D}}^{(m)}(\mathbf{p}) =& \Big\{ (\tau_{1,m}(\mathbf{p},t_0), \tau_{1,m}(\mathbf{p},t_0)+T_\mathrm{p}) \ \cup \ (\tau_{2,m}(\mathbf{p},t_0), \tau_{2,m}(\mathbf{p},t_0)+T_\mathrm{p}) \cup \ldots \\ & \cup \ (\tau_{L,m}(\mathbf{p},t_0), \tau_{L,m}(\mathbf{p},t_0)+T_\mathrm{p}) \Big\} \end{aligned} \tag{5.67}$$

the set of time intervals in which replica contributions are expected when tag's position $\mathbf{p}$ is under hypothesis.

Notice that in this case the estimator takes advantage of the knowledge of the expected received energy for each replica, through the vector (5.16), so

[15] This assumption is verified with increasing confidence while increasing the SNR.

in the formulation (5.66) it would be expected that the energy measurements related to replicas corresponding to $w(\cdot, \cdot) = 0$ were discarded. Conversely in (5.66) the energy measurement is performed on the overall set of L replicas, also if some of these do not carry useful signal contribution. The problem arises due to the approximation (5.64): in fact, in the exact formulation of the estimator in (5.63) each correlation and energy measurement is properly weighted and discarded if related to replicas with $w(\cdot, \cdot) = 0$ (i.e., replicas not effectively present at the receiver.). Therefore, in order to maximize the performance for the simplified implementation (5.66) it is important to restrict the integral extremes at only the windows where, for each hypothesis, we effectively expect useful signal, in order to not add noise or interference contributions. This can be accounted for by adopting $\mathcal{D}^{(m)}(\mathbf{p})$, defined in (5.37), instead of $\bar{\mathcal{D}}^{(m)}(\mathbf{p})$ in (5.66), leading to (5.36).

Part IV

A Case-Study: The UWB-RFID System

Introduction

One of the more interesting applications of context-aware networks is related to the possibility of monitoring environments, such as security areas or factories, in this second case mainly in order to increase the efficiency of the logistic process. In fact, in recent years, a significant number of industrial realities have moved towards the so-called supply chain management (SCM) approach [270], relying on the administration of the various logistics aspects of the company. One of the main requirements of the SCM approach is the *visibility* of the goods along the chain. More precisely, it is necessary to know what a given object is (the *who* question), and where it can be found (the *where* question) at a given instant in time (the *when* question). Existing automatic identification (AI) technologies (e.g., bar codes or RFID) and the RTLS are not able to provide a complete solution. In fact, both of them suffer from significant limitations. On the one hand AI systems are able to answer to the "who" question, but they are weak on the "where" question. To obtain the complete item visibility, items have to be scanned and a position information must be manually inserted or read from a separate source (e.g., another tag). These aspects severely reduce the efficiency of SCM and introduce uncertainty because of manual operations. On the other hand, RTLS satisfy mainly the location requirement, but fail to manage the identification requirement when the item is out of the RTLS working area. Moreover, the current generation of RTLS is based on active tags. This leads to two deficiencies: a limited battery lifetime and a high cost of the tag. As a consequence, the wide spreading of RTLS systems is still not fully exploited.

Recently it has been shown that IR-UWB is a very promising technique, which could meet the stringent requirements of passive tag localization in terms of accuracy [50]. In [271] a passive UWB-RFID scheme has been proposed, showing its potential operating range/data rate trade-off. The advantage of such a technology is to provide the typical accuracy of UWB-RTLS by employing a very simple tag, which adopts backscattering modulation instead of using a complete UWB active transmitter. However one of the most important issues in these systems is the energy supply. Combining UWB (semi-)passive RFID with already existing UHF technologies can be a possible solution to exploit energy harvesting [272] or to implement wake-up strategies in order to increase the battery life of semi-passive tags. Moreover the UHF module can be employed to ensure compatibility with already existing RFID systems working in the UHF band.

In this last part of the thesis the study of a UHF-UWB semi-passive RFID system is presented as example of possible context-aware network solution which enables localization and tracking features. Chapter 6 introduces the system concept providing an overview of the main features and issues related to the realization of such a network. Chapter 7 investigates the feasibility of the system from the signal demodulation point of view, highlighting particular characteristics and signal processing techniques for dealing with impairments such as the clutter. Chapter 8 analyzes the problem of multi tag interference providing design guides of solution able to counteract these effects, also in presence of hardware non idealities. Finally, Chapter 9 focuses on the localization aspect deriving the fundamental limits on the achievable accuracy adopting this kind of system. The work has been carried out in the context of the European project SELECT.[16] The scopes of the project are related to the investigation of this new technology able of combining functionalities of detection, identification and localization by fusing the concept RFID based on backscatter modulation, and adopting semi-passive tags, and RTLS. In additions sensing capabilities are supposed to be provided by the networks thanks to the adoption of WSR techniques [273, 274, 275, 276, 277, 278, 279, 280, 281] for detection and tracking of untagged objects.

[16] www.selectwireless.eu

Chapter 6

System Overview

6.1 Introduction

We consider here a UWB-RFID system composed of a network of readers monitoring an area where tags are present. In particular tags are semi-passive and based on backscatter modulation, where the low energy available from harvesting or batteries is used only for memory access or modulation operation without powering an active transmitter. The high accuracy estimation of the TOA from the backscatter signals enables accurate localization of tags in addition to their detection [50, 136, 51]. The joint use of the RFID and UWB technology is an appealing solution, as UWB leads to advantages in terms of communication robustness, localization accuracy, multi-tag capability, even in harsh propagation environments [53, 48].

Figure 6.1 shows an example of such an architecture. In particular the network of readers cover a scenario where several tagged objects are present. Readers act as reference nodes and are placed in known positions. They are the only active entity capable of transmitting, receiving and processing signals. The goal of the network is detect the presence of tagged objects by the analysis of the response (i.e., the backscatter) of the tags. Moreover, in addition to the detection, high-accuracy localization, enabled by TOA estimation, is performed by the readers' network to locate tagged objects. The passive link between the tag and the reader can be also exploited to transmit information between these two entities, for example the tag ID or data collected by sensors attached to tags. In addition, the same readers infrastructure is exploited as a radar sensor network (RSN) to detect and locate untagged entities (i.e., passive scatters) not equipped with tags [50, 274, 282]. This is possible adopting radar techniques able to track the changes in the environment response caused by the movement of untagged objects.

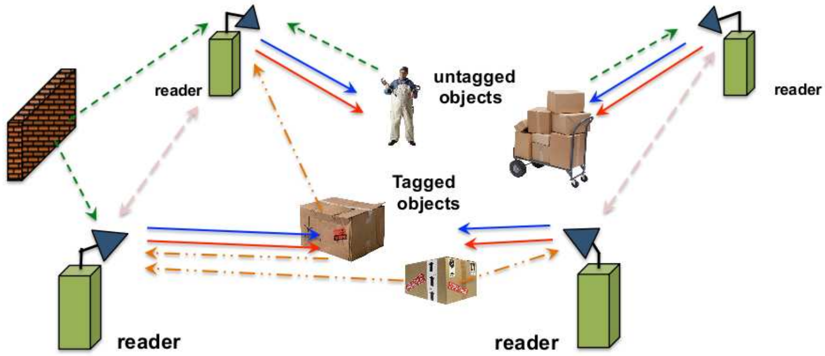

Figure 6.1: Application scenario.

The standard application scenario, composed a square cell monitored by four readers is depicted in Fig. 6.2.

6.2 UWB Backscattering Principle

Backscatter communication is based on the modulation of the interrogation signal emitted by a reader. This modulation, operated by a tag, is realized by changing the load connected to the tag antenna [4].

An example of the received signal at reader side, when backscatter modulation at tag side is adopted, is shown on Fig. 6.3, where the received backscatter signal for three states of the load impedance Z_L connected to the tag antenna is presented. In one of them (black), the load is 50 Ohms, which equals the antenna internal impedance. In this case, the backscatter signal is called *structural mode* and is dominated by the physical structure of the antenna and its various parts. In the two other cases, we distinctly see that a portion of the signal depends on the load impedance. This part of the backscatter signal is named *antenna mode* and it is the one that allows differential detection through the tag load impedance state.

The round trip backscatter CIR is the result of the convolution between the reader-tag propagation CIR convoluted by itself and the backscatter antenna mode response of the tag. The contours of a complete backscatter channel model encompassing all these contributions have been described in [283]. The UWB round trip backscattering channel is strongly unfavorable from the energetic point of view, since the received backscattered signal experiences pathloss between the reader and the tag twice. Basically, similarly to the radar equation, the distance-dependence of the received signal power scales, in free space, with the 4th power of the reader-tag distance, which means a detection distance much smaller than for an ordinary communica-

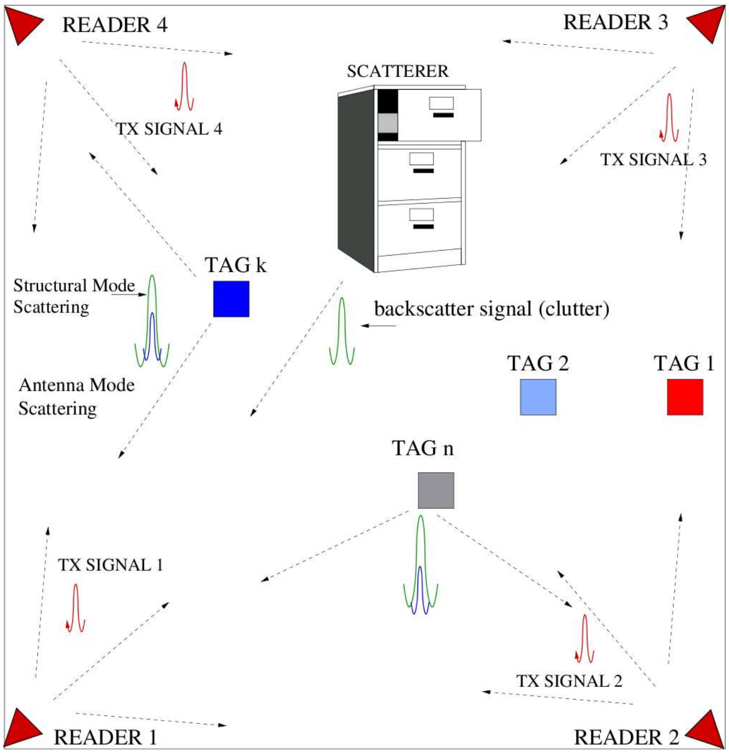

Figure 6.2: Example of a square cell monitored by four readers.

tion link. It is important to underline that the tag backscattering behavior is strongly impacted by the presence of the object on which it is attached [284]. Together with the tag response the reader receives the signal reflected by the surrounding environment, that is the clutter component. A scheme of these propagation effects is reported in Fig. 6.4.

6.3 System Architecture and Main Functionalities

The overall RFID network architecture is depicted in Fig. 6.5. It comprises a central unit, readers and tags. Moreover, relay nodes, that are devices unconnected to the wired core network, can be incorporated herein [30].[1] Each reader communicates with the central unit mostly for transferring the signal processing data (e.g., the TOA estimate allowing the tag positioning). In addition these wired connections can be exploited in order to ensure a general coarse synchronization between the readers, as well as for network

[1]These are, for example, the relays described in Chapter 5.

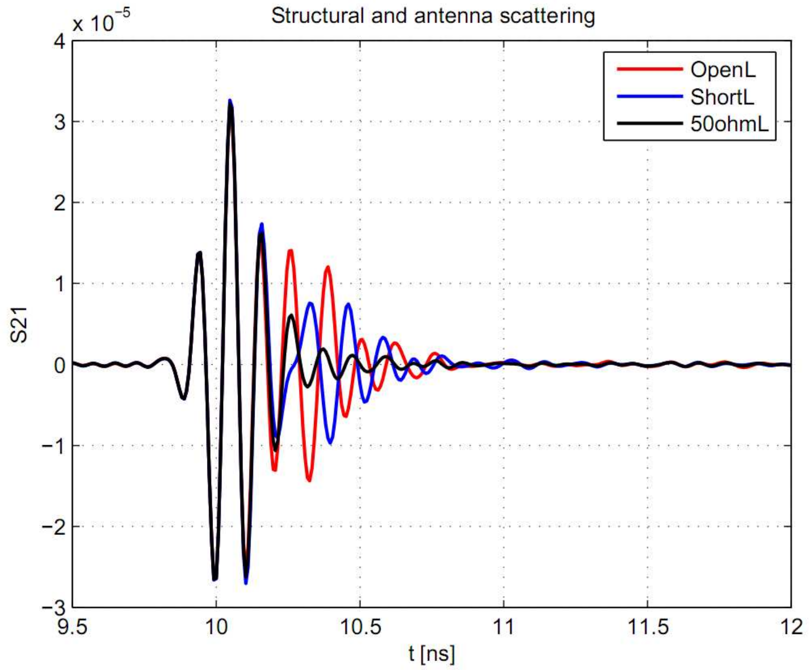

Figure 6.3: Example of backscattered signal, for three tag load impedance values (free space).

maintenance. Reader synchronization will be further detailed in Sec. 6.3.2.

In Fig. 6.6 and Fig. 6.7, the architecture proposed in [271] and analyzed in [285] for UWB readers and tags adopting backscatter modulation is reported. This architecture represents the UWB core enabling the backscattering scheme for localization and tracking.

In particular, the reader is composed of a transmitter and a receiver section. During the interrogation cycle, the reader transmits a sequence of UWB pulses modulated by a periodic binary spreading sequence $\{d_n\}$ of period $N_{\rm c}$ with $d_n \in \{-1, 1\}$, specific of that particular reader (reader's code). In general, $N_{\rm pc}$ pulses are associated to each code symbol (chip) of duration $T_{\rm c}$ seconds. To accommodate the signals backscattered by tags corresponding to an entire packet of $N_{\rm r}$ bits, the UWB interrogation contains $N_{\rm t} = N_{\rm r} N_{\rm s}$ pulses, where $N_{\rm s} = N_{\rm c}\, N_{\rm pc}$ is the number of pulses associated to each bit. Pulses are separated by $T_{\rm p}$ seconds, thus the chip time is $T_{\rm c} = N_{\rm pc}\, T_{\rm p}$. Each transmitted pulse is backscattered by the tag's antenna as well as by all the surrounding scatterers present in the environment which form the clutter component.

In Fig. 6.6, an example of UWB tag architecture employing a binary backscatter modulator composed of an UWB switch is shown. The switch

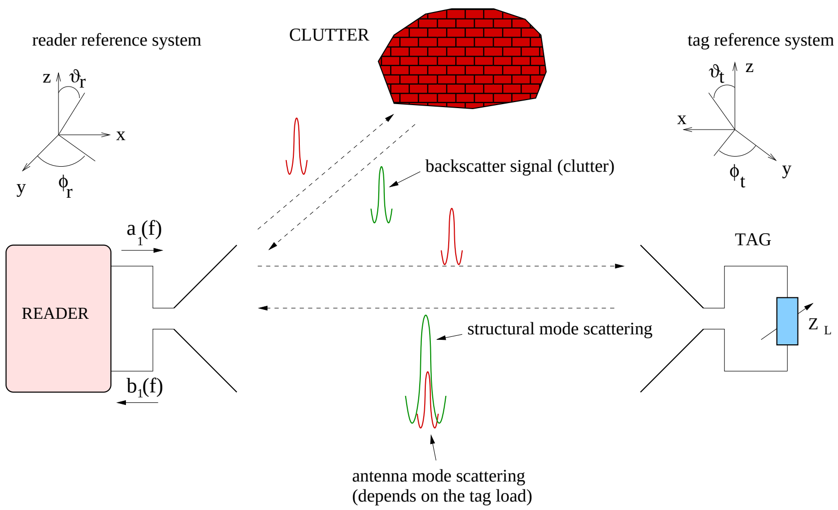

Figure 6.4: Signal contributions at the reader port [285].

is controlled by a micro-controller whose purpose is to change the switch status (short or open circuit) at each chip time T_{c} according to the data to be transmitted and a zero mean (balanced) periodic tag's code $\{c_n\}$, with $c_n \in \{-1, +1\}$, of period N_{c}. The adoption of balanced codes ensures the removal of the clutter as will be demonstrated in Chapter 7 and Chapter 8. Specifically, each tag information bit $b_k \in \{-1, +1\}$ is associated to N_{s} pulses, thus the symbol time becomes $T_{\text{s}} = T_{\text{c}}\, N_{\text{c}} = T_{\text{p}}\, N_{\text{s}}$. In this way the polarity of the reflected signal changes according to the tag's code during a symbol time, whereas the information symbol (bit) affects the polarity of all pulses composing the sequence each symbol time.

By analyzing the received signal components shown in Fig. 6.8, it can be noted that the antenna mode scattered component only is modulated by the combination of the tag's and reader's codes $\{c_n\}$ and $\{d_n\}$, whereas all clutter signals components (included the antenna structural mode scattering) are received modulated by the reader's code $\{d_n\}$ only. This property is exploited at the reader receiver section to remove the clutter component through a proper processing, therefore isolating the useful component coming from the intended tag. The presented MAC scheme is fundamentally a direct-sequence code division multiple access (CDMA) approach, according to which a de-spreading phase at reader side can be exploited to detect and demodulate a specific tag signal. However, several issues arise due to tag multi-user interference (MUI) and near-far effects, as will be presented in Chapter 8.

An example of possible receiver scheme is that reported in Fig. 6.6 where a correlator-based demodulator is considered. This scheme performs a de-spreading operation (i.e., the accumulation of the N_{s} pulses composing a

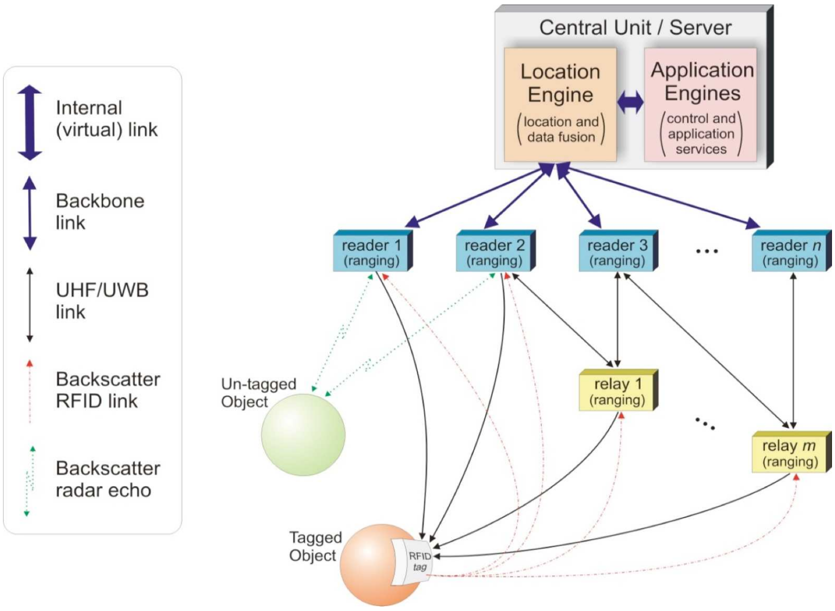

Figure 6.5: SELECT general system architecture.

symbol) using the combined code $\{c_n \cdot d_n\}$, which identifies both the reader and the desired tag.

Several signal processing tasks have to be accomplished by the readers in order to provide to the RFID network detection and localization capabilities. In particular the first task consists of tag detection, that is the process thanks to which the network knows that a certain tag is present in the monitored area. When tags multiple access is performed with CDMA and a certain spreading code is uniquely assigned to a tag, a decision at the output to the de-spreading phase is sufficient to accomplish the identification purpose. If the network aim is only confined to detection and localization, the second task to be accounted is related to TOA estimation, thanks to which localization capabilities are provided. If the tag itself has data to transmit to the reader (e.g., because it has an embedded sensor, or data related to the object to which it is attached, or because the spreading code associated to it is not unique), the reader must perform signal demodulation in addition to detection.

As already mentioned, TOA estimation enables localization capabilities, thanks to the location estimation process realized at central unit by fusing the data provided by at least three readers. For this kind of system, due to the low complexity of the tag and to the fact that tags cannot directly communicate, no cooperative techniques can be exploited for performance improvement and coverage extension, so that every point of the monitored

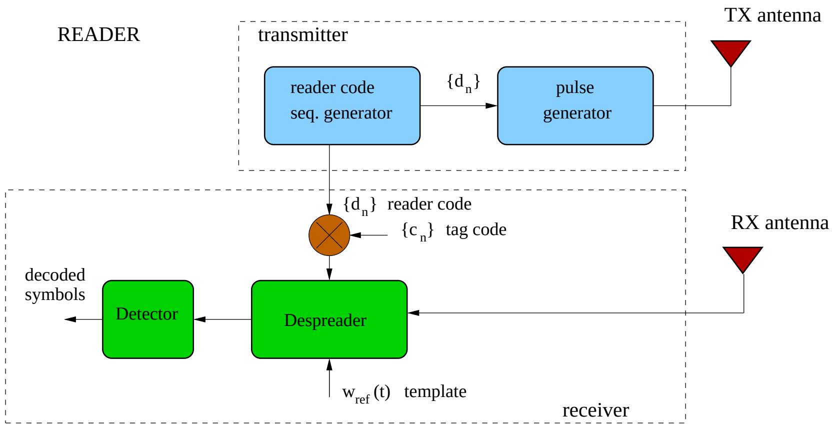

Figure 6.6: UWB reader architecture in backscattering schemes [271].

area must be directly covered by a sufficient number of readers.[2]

The most interesting unique feature of the UWB-RFID network is related to the possibility of performing all these functionalities, tag detection, signal demodulation, TOA estimation and location determination, not only reader by reader as independent entities, but at network level, providing an inherent diversity. Some examples will be provided in the following sections.

6.3.1 Tags Synchronization

Tags synchronization is a fundamental task allowing several benefices in the UWB-RFID system. In fact, if tags code generators are completely free-running, the reader must perform an exhaustive code acquisition search in order to synchronize its code generator used for de-spreading with the incoming tag signal. A (partial) synchronization of the system allows exploiting particular codes families able to better mitigate the multi-user interference (see Chapter 8). To accomplish this task, the UHF link[3] can be used to derive the synchronization signal necessary to reset the tags' spreading code generators.

Specifically, according to Fig. 6.9 the reset of the tag code generator is performed on the falling edge of a wake up UHF carrier received by the tags. This signal enables powering up a UHF circuit by charging a capacitor via the antenna and a rectifier circuit. The resulting voltage is used to power a control circuit that, at the time the transmission of the continuous wave (CW) signal has ended, activates the switch via powering its control logic from the

[2] Also relaying techniques can be adopted as presented in Chapter 5.

[3] We consider a hybrid solution including both UWB and standard UHF readers and tags.

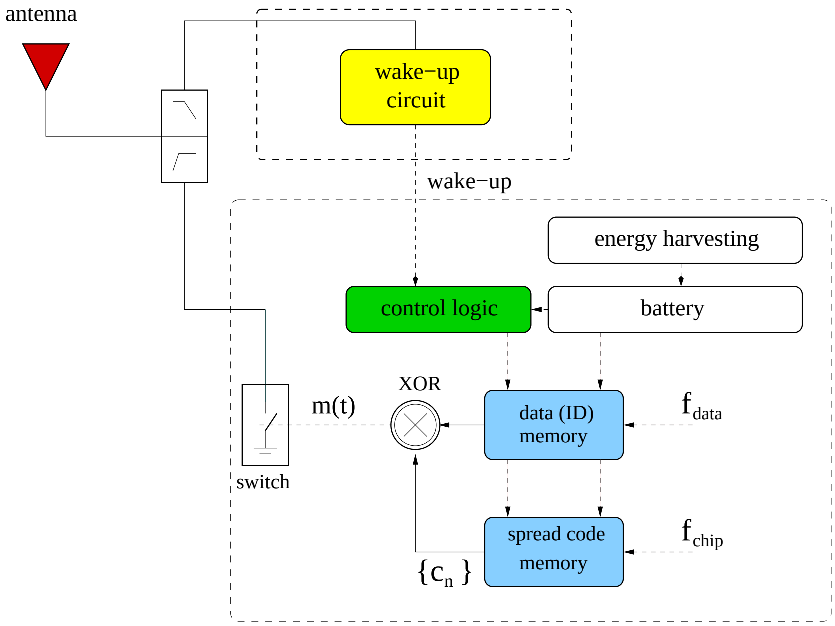

Figure 6.7: UWB tag architecture in backscattering schemes [271].

battery, thus, initiating the backscatter modulation of the UWB signals. In this way the propagation-dependent capacitor charge time[4] does not play a significant role in the synchronization jitter, since the discharge starting event is not affected by the pathloss and depends only on the tags' positions and orientations. This wake-up synchronization process is depicted in Fig. 6.10.

6.3.2 Readers Synchronization

Readers must be kept synchronized in order to ensure satisfactory MAC performance (presented in Sec. 8.6.2) and to allow multistatic functionalities that will be described in the following sections. Readers coarse synchronization can be provided with the wired readers-central unit links (realized, e.g., with a standard Ethernet protocol). Readers fine synchronization can be based on UWB signals by re-using the same hardware developed for tag detection. In fact the direct reader-to-reader link, associated with the de-spreading performed accumulating a number of pulses N_s, ensures a very high SNR for the demodulation of the interfering reader signal, allowing very accurate (sub-nanosecond), TOA estimation. In this case the de-spreading is operated according to the incoming reader's code. Since the reader-reader distance is

[4]This is due to the narrowband UHF signals that may experience selectively channels, and to different reader-tag distances.

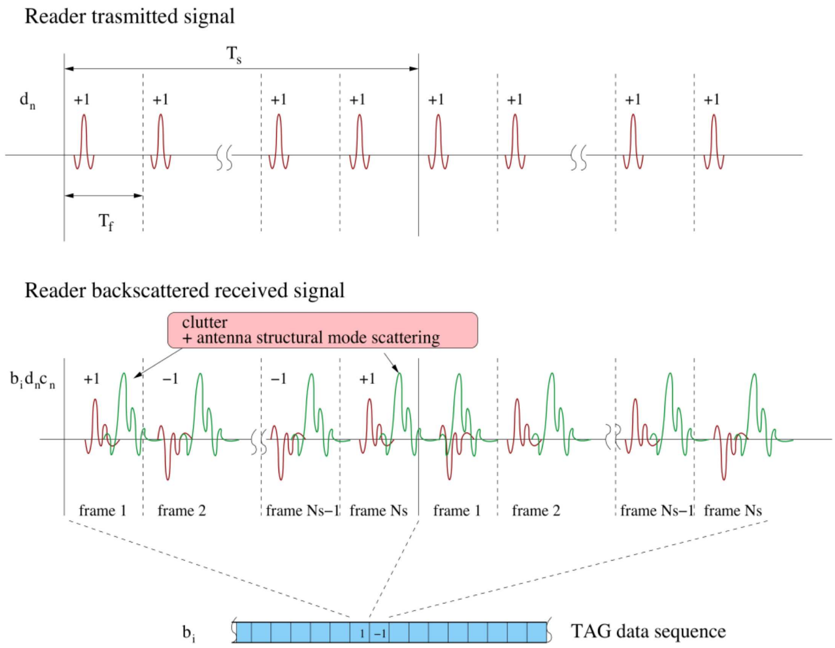

Figure 6.8: Backscatter modulation.

fixed, TOA estimation can be compared with the expected propagation time between the two readers' antennas, adjusting consequently the reader's clock according to the difference between the estimated and expected range. The process can be further iterated until the difference in the clock adjustment falls below a threshold, indicating the reached synchronism.

6.3.3 Tag Detection

Generically, tag detection can be realized at each reader if the de-spread signal level related to a specific tag code is above a certain threshold. Since more than one reader is supposed to perform this de-spreading, the decision on the tag presence can be taken, instead reader by reader, from the central unit, by properly combining the different observations.

Moreover, especially in conjunction with time division multiple access (TDMA) readers MAC, each reader can perform the de-spreading also when an other reader is interrogating the tag, adopting, as de-spreading code, the other reader one combined with the tag code.[5] In this manner, if a network of N_R readers is monitoring a certain area (e.g., $N_R = 4$ in our square reference scenario), up to N_R^2 observations can be combined for robust tag detection.

[5]This requires a synchronous readers network.

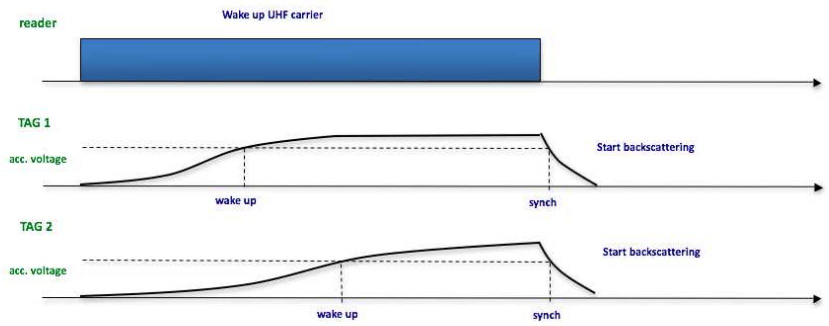

Figure 6.9: Wake-up scheme.

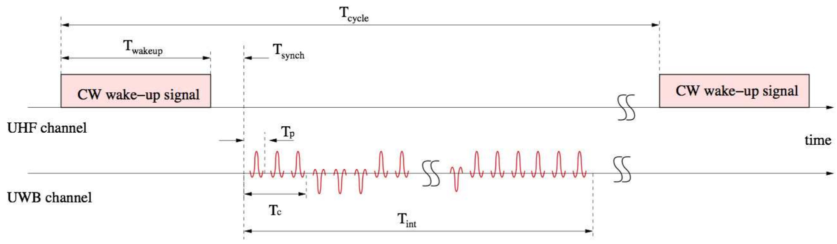

Figure 6.10: UHF-UWB interrogation cycle.

The analysis of tag detection strategies and performance analysis, considering a single reader, will be presented in Chapter 8.

6.3.4 Signal Demodulation

Signal demodulation allows data communication between tags and readers. In this manner the tag ID can be transfered to the network or, if the tag has embedded sensors, the network can receive these data.

As for the tag detection, also signal demodulation can benefit of the inherent diversity provided by the multi-reader architecture. As example, suppose that each reader demodulates the signal of a specific tag. The demodulation result, with soft or hard decisions, can be then forwarded to the central unit for a proper combining and to take a final decision on the received message, enabling improved performance also whitout high rate channel coding strategies.

The analysis of signal demodulation performance, considering a single reader, will be presented in Chapter 7.

6.3.5 Time of Arrival Estimation

TOA estimation enables the ranging and localization, and it can be operated with high precision thanks to the adoption of UWB signals [51]. Diversity in TOA estimation is ensured by the fact that each reader can perform the estimate not only when it is transmitting, but also when other readers are sending their signals. In this manner we are in the presence of a multistatic network similar to that generally adopted in WSR systems, as explained in the following section.

6.3.6 Localization

The availability of TOA estimates between the different readers allow the central unit to properly fuse the data obtaining the position estimate as intersection, as example, of circles and ovals. The fundamental limits for the accuracy of this technique will be analyzed in Chapter 9.

Moreover, filtering techniques can be adopted for improving the position estimation when tags are moving.

6.3.7 Untagged Object Detection and Tracking

There is growing on interest in new radar applications, especially for indoor and outdoor monitoring of high-security areas to prevent intruders [282, 286, 274, 275, 276, 277, 278]. One of the key features of the UWB-RFID network is the possibility of providing, with the same readers infrastructure, radar capabilities, basically detection and tracking of untagged objects in addition to detection, demodulation and localization of tags.

Tracking of moving untagged objects can be realized by analyzing the changes in the clutter components caused by object movement. To this purpose the reader has to isolate the clutter component generated by its own interrogation signal by de-spreading the received signal using only the reader code. Static clutter is usually removed through differential operations [287, 288, 289, 290, 291].

Chapter 7

Performance Analysis in Ideal Conditions

7.1 Motivations

Chapter 6 introduced the general concept of UWB-RFID system, presenting an overview and some design and implementation challenges. Here in this chapter the mathematical system description and the performance analysis in realistic conditions but in absence of hardware constraints are presented. In particular the signal structure proposed in [50, 292, 271] for semi-passive UWB-RFID with clutter suppression is extended to a multi-tag scenario. The potential performance of backscatter RFID communication using UWB signals is investigated in terms clutter suppression and multiple access capability using both simulated and experimental data obtained in realistic environments. A generic correlation-based receiver is here considered, while performance analysis in presence of simplified low-complexity non-coherent schemes and hardware impairments will be addressed in Chapter 8.

7.2 Backscatter Communication using UWB Signals

Consider a scenario where a reader interrogates N_{tag} tags located in the same area. In Fig. 7.1 the architectures for tag and reader are shown. The reader is composed of a transmitter and a receiver section both connected to the same UWB antenna through a TX/RX switch. During the interrogation phase, the reader transmits a sequence of UWB pulses, each having energy E_{p}. An

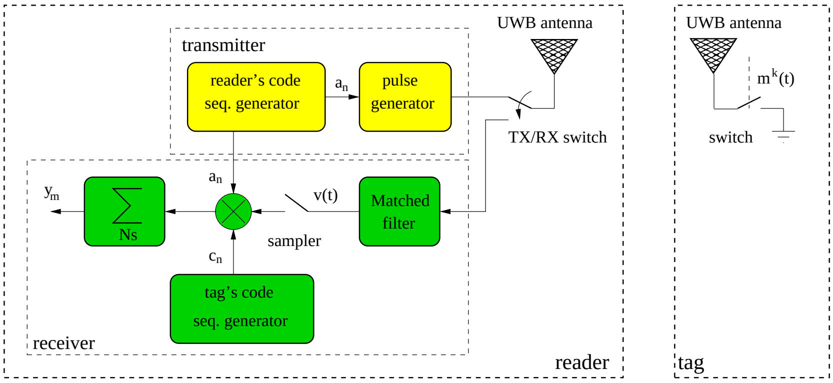

Figure 7.1: The considered scheme of the tag and the reader composed of a transmitter and a receiver section.

interrogation sequence or N_r symbols is here considered, that is,

$$s_\mathrm{reader}(t) = \sum_{m=0}^{N_\mathrm{r}} s(t - mN_\mathrm{c}T_\mathrm{c}) \tag{7.1}$$

with

$$s(t) = \sum_{n=0}^{N_\mathrm{c}} d_n g(t - nT_\mathrm{c}) \tag{7.2}$$

and

$$g(t) = \sum_{k=0}^{N_\mathrm{pc}-1} p(t - kT_\mathrm{p}) \tag{7.3}$$

indicating the composite waveform associated to each code symbol (chip) d_n composed of N_pc elementary UWB pulses $p(t)$, centered at frequency f_c and with bandwidth W, each of energy $E_\mathrm{p} = \int_0^{T_\mathrm{p}} p^2(t)\, dt$. Moreover, the pulse energy E_p and the PRP T_p are set to guarantee a radiated spectrum emission compliant with the regulation mask (in terms of effective radiated isotropic power (EIRP)) [293]. The PRP T_p is chosen so that all backscattered signals are received by the reader before the transmission of the successive pulse, thus avoiding inter-frame interference. In indoor scenario $T_\mathrm{p} = 50 - 100\,\mathrm{ns}$ is usually sufficient for this purpose [92]. In the following of this chapter we consider for convenience d_n as an infinite periodic sequence.

During the transmission of each pulse the antenna is connected to the transmitter section. It is then kept connected to the receiver section during the remaining time until the successive pulse is transmitted. Each pulse in (7.1) is backscattered by all tags as well as by all the surrounding scatterers present in the environment that form the clutter component. As shown in Fig. 7.1, the tag changes its scattering properties by varying the antenna load between open and short circuit conditions. In [271] it is shown that this affects the polarity of the backscattered antenna mode component. To make the uplink communication between the kth tag and the reader robust to the presence of clutter, interference, and to allow multiple access, each tag is designed to change its status (short or open circuit) at each chip time T_{c}, with $T_{\mathrm{c}} = N_{\mathrm{pc}}\,T_{\mathrm{p}}$, according to the data to be transmitted and a periodic tag's code $\left\{c_n^{(k)}\right\}$, with $c_n^{(k)} \in \{-1,+1\}$, of length N_{c} chips. Specifically, each tag information symbol $b_n^{(k)} \in \{-1,+1\}$ is associated to $N_{\mathrm{s}} = N_{\mathrm{c}}\,N_{\mathrm{pc}}$ pulses, resulting in a symbol time $T_{\mathrm{s}} = T_{\mathrm{p}} N_{\mathrm{s}}$. In this way the polarity of the reflected signal changes according to the tag's code sequence during a symbol time, whereas the information symbol affects the entire sequence pulse's polarity at each symbol time. The reader and the tags have their own clock sources and hence they have to be treated as asynchronous. We denote with $\Delta^{(k)} = \delta^{(k)} + T_{\mathrm{c}}\,u^{(k)}$, with u_k integer and $0 \leq \delta^{(k)} < T_{\mathrm{c}}$, the clock offset of the kth tag with respect to the reader clock. Therefore, the backscatter modulator signal, commanding the tag's switch, can be expressed as

$$\begin{aligned} m^{(k)}(t) =& \sum_{n=-\infty}^{\infty} \sum_{i=0}^{N_{\mathrm{c}}-1} c_i^{(k)} b_n^{(k)} \Pi \left(\frac{1}{T_{\mathrm{c}}} \left[t - nT_{\mathrm{s}} - iT_{\mathrm{c}} - \Delta^{(k)} \right] \right) \\ =& \sum_{n=-\infty}^{\infty} c_n^{(k)} b_{f(n)}^{(k)} \Pi \left(\frac{1}{T_{\mathrm{c}}} \left[t - (n + u^{(k)}) T_{\mathrm{c}} - \delta^{(k)} \right] \right) \end{aligned} \tag{7.4}$$

having defined $f\,(n) \triangleq \lceil n/N_{\mathrm{s}} \rceil$ and $\Pi(t) \triangleq 1$ for $t \in [0,1]$ and zero otherwise. In the following analysis the tag response due to the antenna mode (depending on the data) is examined whereas the antenna structural mode will be treated as a part of clutter since it does not depend on data symbols. The signal received by the kth tag is

$$r_{\mathrm{tag}}^{(k)}(t) = \sum_{n=-\infty}^{\infty} d_n \cdot p^{(k)}(t - nT_{\mathrm{c}}) \tag{7.5}$$

where $p^{(k)}(t)$ is the down-link (reader-tag) channel response to $g(t)$ which includes also the propagation delay.

According to (7.5) and (7.4), and considering perfect pulse symmetry in the two antenna load conditions, the signal scattered by the kth tag can be written as (see also the example in Fig. 7.2 where $N_{\mathrm{pc}} = 1$ is considered for simplicity)

$$\begin{aligned}
s_{\text{tag}}^{(k)}(t) &= r_{\text{tag}}^{(k)}(t) \cdot m^{(k)}(t) \\
&= \sum_{n=-\infty}^{\infty} d_n \left[c_{n-u^{(k)}}^{(k)} b_{f\left(n-u^{(k)}\right)}^{(k)} p_{\text{I}}^{(k)}(t - nT_{\text{c}}) \right. \\
&\left. + c_{n-u^{(k)}-1}^{(k)} b_{f\left(n-u^{(k)}-1\right)}^{(k)} p_{\text{II}}^{(k)}(t - nT_{\text{c}}) \right] \qquad (7.6)
\end{aligned}$$

where we define

$$p_{\text{I}}^{(k)}(t) \triangleq p^{(k)}(t) \cdot \Pi\left(\frac{t - \delta^{(k)}}{T_{\text{c}} - \delta^{(k)}}\right), \qquad (7.7)$$

$$p_{\text{II}}^{(k)}(t) \triangleq p^{(k)}(t) \cdot \Pi\left(\frac{t}{\delta^{(k)}}\right). \qquad (7.8)$$

The main task of the receiver section of the reader is to detect the useful backscattered signal component (i.e., the antenna mode scattering dependent on antenna load changes) from those backscattered by the antenna structural mode and other scatterers (clutter) that are, in general, dominant [271]. The received signal at the reader is

$$r_{\text{reader}}(t) = \sum_{k=1}^{N_{\text{tag}}} r_{\text{reader}}^{(k)}(t) + \sum_{n=-\infty}^{\infty} d_n w^{(\text{C})}(t - nT_{\text{c}}) + n(t), \qquad (7.9)$$

where $n(t)$ is the AWGN with two-sided power spectral density $N_0/2$ and $w^{(\text{C})}(t)$ is the backscattered version of the waveform $g(t)$ due to the clutter component which also accounts for pulse distortion, multipath propagation, and tag's antenna structural mode. The signal $r_{\text{reader}}^{(k)}(t)$ represents the received useful component due to the kth tag, that is,

$$\begin{aligned}
r_{\text{reader}}^{(k)}(t) = \sum_{n=-\infty}^{\infty} d_n & \left[c_{n-u^{(k)}}^{(k)} b_{f\left(n-u^{(k)}\right)}^{(k)} w_{\text{I}}^{(k)}(t - nT_{\text{c}}) \right. \\
& \left. + c_{n-u^{(k)}-1}^{(k)} b_{f\left(n-u^{(k)}-1\right)}^{(k)} w_{\text{II}}^{(k)}(t - nT_{\text{c}}) \right] \qquad (7.10)
\end{aligned}$$

having denoted $w_{\text{I}}^{(k)}(t)$ and $w_{\text{II}}^{(k)}(t)$, respectively, the uplink channel response to $p_{\text{I}}^{(k)}(t)$ and $p_{\text{II}}^{(k)}(t)$ (see Fig. 7.2). Note that $w^{(k)}(t) = w_{\text{I}}^{(k)}(t) + w_{\text{II}}^{(k)}(t)$ is the round-trip response to $g(t)$ of the backscatter link.

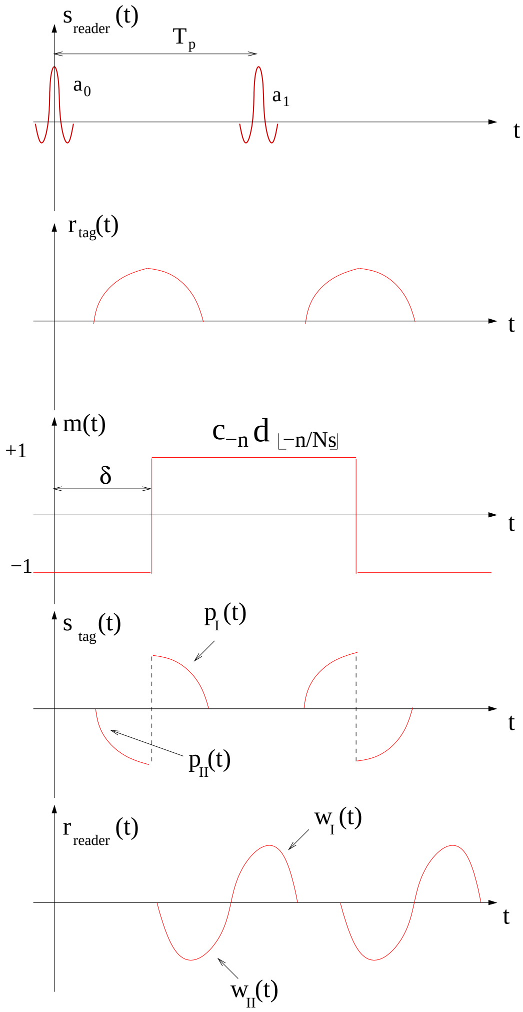

Figure 7.2: The behavior of the signals described in section 7.2.

7.3 Multiple Users Interference and Clutter

Consider the reader's receiver scheme reported in Fig. 7.1 where the received signal is correlated with a local composite waveform template $h(t)$ with unitary energy. The output is then sampled at sampling intervals $t_{i,m} = i\,T_c + m\,T_s + \tau_0$, with $i = 0, 1, ..., N_s - 1$ and where τ_0 accounts for the propagation delay, thus obtaining the samples

$$v_{i,m} = \int_0^{T_\mathrm{c}} h(t)\, r_{\mathrm{reader}}(t - t_{i,m})\, dt = r_{\mathrm{reader}}(t_{i,m}) \otimes h(-t_{i,m})$$
$$= \sum_{k=1}^{N_{\mathrm{tag}}} v_{i,m}^{(k)} + v_{i,m}^{(C)} + z_{i,m} \qquad (7.11)$$

where

$$v_{i,m}^{(k)} = \sum_{n=-\infty}^{\infty} d_n \left[c^{(k)}_{n-u^{(k)}} b^{(k)}_{f\left(n-u^{(k)}\right)} \gamma_{\mathrm{I}}^{(k)}(iT_\mathrm{c} + mT_\mathrm{s} + \tau_0 - nT_\mathrm{c}) \right.$$
$$\left. + c^{(k)}_{n-u^{(k)}-1} b^{(k)}_{f\left(n-u^{(k)}-1\right)} \gamma_{\mathrm{II}}^{(k)}(iT_\mathrm{c} + mT_\mathrm{s} + \tau_0 - nT_\mathrm{c}) \right] \qquad (7.12)$$

and

$$v_{i,m}^{(C)} = \sum_{n=-\infty}^{\infty} d_n \gamma^{(C)}(iT_\mathrm{c} + mT_\mathrm{s} + \tau_0 - nT_\mathrm{c})\,. \qquad (7.13)$$

In (7.11) and (7.12) we have defined $\gamma_{\mathrm{I}}^{(k)}(t) \triangleq w_{\mathrm{I}}^{(k)}(t) \otimes h(-t)$, $\gamma_{\mathrm{II}}^{(k)}(t) \triangleq w_{\mathrm{II}}^{(k)}(-t) \otimes h(-t)$,$\gamma^{(\mathrm{C})}(t) \triangleq w^{(\mathrm{C})}(t) \otimes h(-t)$, $z(t) \triangleq n(t) \otimes h(-t)$, and $z_{i,m} \triangleq z(iT_\mathrm{c} + mT_\mathrm{s} + \tau_0)$. Without loss of generality, we consider the problem of detecting the data bit $b_m^{(1)}$ of tag $k = 1$ (useful tag). As shown in [50], to remove the clutter component at the receiver, the sampled signal $v_{i,m}$ is multiplied by the composite sequence $\{c_n^{(1)} d_n\}$, which identifies both the reader and the desired tag. In particular, all N_c resulting samples at the output of the correlator composing a data symbol are summed up to form the mth decision variable at the detector input. Considering that $c^{(k)}_{i+mN_\mathrm{s}} = c_i^{(k)}$, $d^{(k)}_{f(m+i)} = d_m^{(k)}$ and $b_{i+mN_\mathrm{s}} = b_i \ \forall i$, the decision variable for the mth symbol $b_m^{(1)}$ becomes

$$y_m = \sum_{i=0}^{N_\mathrm{c}-1} c_i^{(1)}\, d_i\, v_{i,m}$$
$$= \gamma_{\mathrm{I}}^{(1)}(\tau_0) \sum_{i=0}^{N_\mathrm{c}-1} \left[d_i^2\, c_i^{(1)}\, c^{(1)}_{i-u^{(1)}}\, b^{(1)}_{f\left(m-u^{(1)}\right)} \right]$$
$$+ \gamma_{\mathrm{II}}^{(1)}(\tau_0)\, a_0^2\, c_0^{(1)} c^{(1)}_{-u^{(1)}-1} b^{(1)}_{f\left(m-u^{(1)}-1\right)}$$
$$+ \gamma_{\mathrm{II}}^{(1)}(\tau_0) \sum_{i=1}^{N_\mathrm{c}-1} \left[d_i^2 c_i^{(1)} c^{(1)}_{i-u^{(1)}-1}\, b^{(1)}_{f\left(m-u^{(1)}-1\right)} \right]$$
$$+ \xi_m + y_m^{(C)} + z_m \qquad (7.14)$$

where

$$y_m^{(C)} = \sum_{i=0}^{N_\mathrm{c}-1} c_i^{(1)}\, d_i \sum_{n=-\infty}^{\infty} d_n \gamma^{(C)}(iT_\mathrm{c} + mT_\mathrm{s} + \tau_0 - nT_\mathrm{c}) = \gamma^{(C)}(\tau_0) \sum_{i=0}^{N_\mathrm{c}-1} c_i^{(1)} \tag{7.15}$$

and $z_m \triangleq \sum_{i=0}^{N_\mathrm{c}-1} d_i\, c_i\, z_{i,m}$ is a Gaussian distributed r.v. with zero mean and variance $\sigma_z^2 = N_\mathrm{c}\, N_0/2$. The component ξ_m accounts for the MUI and can be expressed as follows

$$\begin{aligned} \xi_m &= \sum_{k=2}^{N_\mathrm{tag}} \sum_{i=0}^{N_\mathrm{c}-1} c_i^{(1)}\, d_i\, v_{i,m}^{(k)} \\ &= \sum_{k=2}^{N_\mathrm{tag}} \Bigg\{ \gamma_\mathrm{I}^{(k)}(\tau_0) \sum_{i=0}^{N_\mathrm{c}-1} \left[d_i^2\, c_i^{(1)}\, c_{i-u^{(k)}}^{(k)}\, b_{f\left(m-u^{(k)}\right)}^{(k)} \right] \\ &\quad + \gamma_\mathrm{II}^{(k)}(\tau_0)\, a_0^2\, c_0^{(1)} c_{-u^{(k)}-1}^{(k)} b_{f\left(m-u^{(k)}-1\right)}^{(k)} \\ &\quad + \gamma_\mathrm{II}^{(k)}(\tau_0) \sum_{i=1}^{N_\mathrm{c}-1} \left[d_i^2\, c_i^{(1)} c_{i-u^{(k)}-1}^{(k)}\, b_{f\left(m-u^{(k)}-1\right)}^{(k)} \right] \Bigg\} \end{aligned} \tag{7.16}$$

which effect on the decision variable strictly depends on the cross-correlation property between codes $\left\{c_i^{(1)}\right\}$ and $\left\{c_i^{(k)}\right\}$.

7.3.1 Perfect Timing Acquisition

In the following we assume that a perfect code synchronization is achieved after an initial acquisition phase, that is, $u^{(1)} = 0$. From (7.14) we have

$$\begin{aligned} y_m = b_m^{(1)} &\left[\gamma_\mathrm{I}^{(1)}(\tau_0) N_\mathrm{c} + \gamma_\mathrm{II}^{(1)}(\tau_0) \sum_{i=1}^{N_\mathrm{c}-1} c_{i-1}^{(1)}\, c_i^{(1)} \right] \\ &+ \gamma_\mathrm{II}^{(1)}(\tau_0) c_{-1}^{(1)}\, c_0^{(1)} d_{m-1}^{(1)} + \xi_m + y_m^{(C)} + z_m\,. \end{aligned} \tag{7.17}$$

Looking at (7.17) it can be noted that the useful term depends on the auto-correlation properties of code $\left\{c_i^{(1)}\right\}$. In addition, we assume that a perfect TOA estimate is available. The TOA estimator robust to clutter proposed in [294] can be adopted to this purpose. Once the TOA is known, the reader can adjust its internal clock so that it becomes synchronous to that of the intended tag, that is, $\delta^{(1)} = 0$, and the optimal choice for τ_0 can be derived. In such a case

$$\gamma_\mathrm{I}^{(1)}(\tau_0) = E_\mathrm{w} = \int_{-\infty}^{\infty} \left| w^{(1)}(t) \right|^2 dt \tag{7.18}$$

and (7.17) can be further simplified leading to

$$\begin{aligned} y_m &= b_m^{(1)} N_c \gamma_I^{(1)}(\tau_0) + \xi_m + y_m^{(C)} + z_m \\ &= b_m^{(1)} \rho E_s + y_m^{(C)} + \xi_m + z_m , \end{aligned} \tag{7.19}$$

where $E_s = N_c E_w$, and ρ is the normalized cross-correlation between pulses $w_I^{(1)}(t)$ and $h(t)$, which accounts for the mismatch due to pulse distortion.[1] Parameters E_w and E_s represent the average received energy per chip and symbol, respectively.

7.4 Code Choice for Clutter Removal and Multiple Access

Looking at (7.14) and (7.15), it can be noted that only the antenna mode scattered signals result to be modulated by the combination of the tag's and reader's codes $\left\{c_i^{(k)}\right\}$ and $\{d_i\}$, whereas all clutter signals components (including the antenna structural mode scattering) are received modulated only by the reader's code $\{d_i\}$. This suggests, as can be deduced from (7.15), that to completely remove the clutter component it is sufficient that the tag's code $\left\{c_i^{(1)}\right\}$ has zero mean, that is, $\sum_{n=0}^{N_c-1} c_n^{(1)} = 0$, leading to $y_m^{(C)} = 0$, if a quasi-stationary scenario within the symbol time T_s is assumed. Regarding the MUI, the situation is similar to what happens in conventional CDMA systems where the performance is strictly related to the partial cross-correlation properties of codes $\left\{c_i^{(1)}\right\}$ and $\left\{c_i^{(k)}\right\}$. Classical codes such as Gold codes or m-sequences offer good performance. However they are composed of an odd number of symbols and hence there is no way to obtain a zero mean code to completely remove the clutter. However, considering that m-sequences have a quasi-balanced number of $'+1'$ and $'-1'$, that is, their number differs no more than 1, one option to deal with clutter removal is to lengthen the code by one symbol in such a way the resulting code has zero mean by accepting a certain degradation in terms of multiple access performance. In the numerical results this aspect will be investigated.

When the scenario is quasi-synchronous, that is, $u^{(k)} = 0\ \forall k$ and $\delta^{(k)} \neq 0$, orthogonal codes, such as Hadamard codes, represent a good choice and $\xi_m = 0$. This could be the situation where a downlink communication channel is available (either UWB or UHF) and coarse code synchronization between the reader and tags is then feasible. Further details on code assignment strategies will be provided in the next chapter.

[1] Note that under perfect timing condition $w_I^{(1)}(t) = w^{(1)}(t)$ and $w_{II}^{(1)}(t) = 0$.

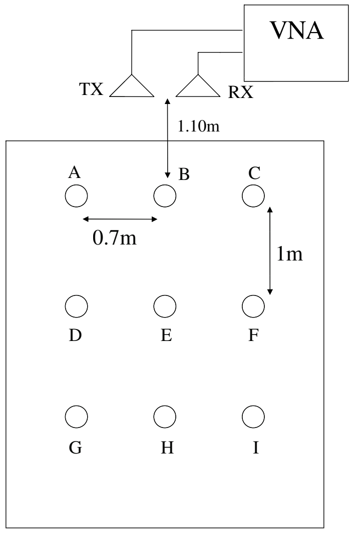

Figure 7.3: Indoor scenario considered for the measurement campaign at ENSTA-ParisTech.

7.5 Numerical Results

In order to evaluate the performance of the proposed passive UWB-RFID communication system, a RRC signal[2], compliant to the EU-UWB mask in the bandwidth $3.1 - 4.8\,\text{GHz}$ is used as transmitted signal. At the receiver side, a receiver noise figure $F = 4\,\text{dB}$ and a single-path matched filter (SPMF) are considered. The SPMF is adapted to the received pulse at the reference distance in free-space propagation and at the orientation of tag's maximum radiation.

7.5.1 BER Analysis with Measured Signals

Measurements were performed in typical indoor environment such as a laboratory, as described in [292]. In particular, a rectangular grid of nine points, spaced out of about 1m in depth and 70 cm in width, was defined in a room with furniture and having dimensions $(5.13 \times 4.49)\,\text{m}^2$ (see Fig. 7.3). In Fig. 7.4 the bit error rate (BER) as a function of the number of pulses per symbol N_s when $N_\text{tag} = 6$ tags are present is reported. Curves are obtained for $T_\text{p} = 64\,\text{ns}$. The signal measured from the location D of the grid is considered as the signal backscattered by the useful tag, and the backscattered signals coming from locations A,B, C, E, F are considered as MUI. In the

[2]See (3.63) for the definition.

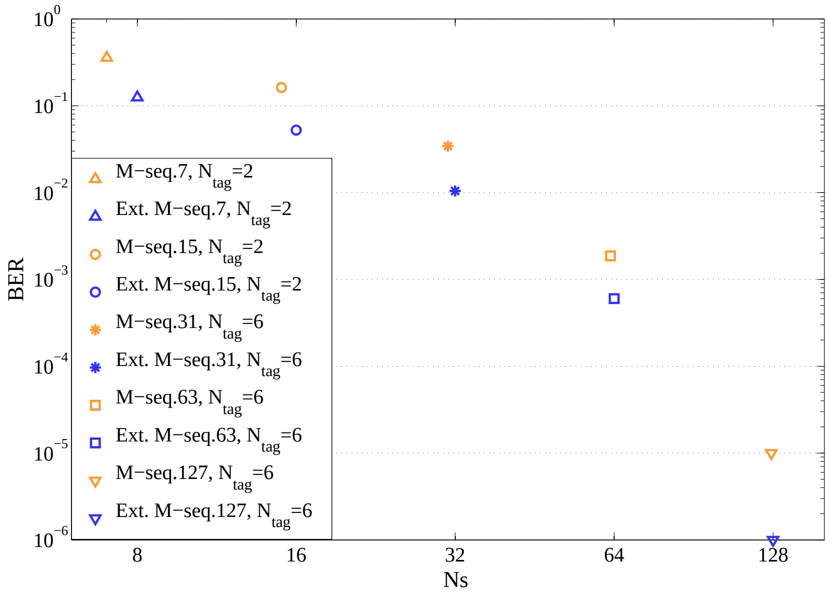

Figure 7.4: BER vs N_s in multi-tag laboratory environment and asynchronous scenario.

asynchronous scenario, where reader and tag code generators are not synchronized, it is possible to observe how considering extended m-sequences at length 31, 63, 127 is beneficial. In the same plot we show the performance obtained when only one interfering tag located in F is present. Again, the use of an extended m-sequence leads to an improved performance. This confirms that extend m-sequences are a good solution for clutter and MUI mitigation in asynchronous scenario.

7.5.2 BER Analysis in the 802.15.4a Channel

We analyze now the BER in a more complex scenario in which 59 interfering tags are present, as a function of the total number of pulses per symbol N_s, with $T_p = 128$ ns and $N_c = 1024$. Results has been obtained by Monte Carlo simulations, starting from channel responses obtained considering the 802.15.4a CM1 channel model [92]: a double convolution of the transmitting pulse with a channel impulse response has been performed in order to take into account the two-way link of the backscattered signal. The useful tag have been placed at 7 m distance from the reader having an antenna with 5 dBi gain, while the 59 interfering tags have been considered uniformly distributed in one meter around the useful one. For what the clutter is concerned, a uniform power delay profile in the overall interval T_p has been considered, with paths spaced apart of 0.95ns, each path with Nakagami-m fading, with $m = 3$ and a root-mean-squared value of 0.5 mV at the receiver.

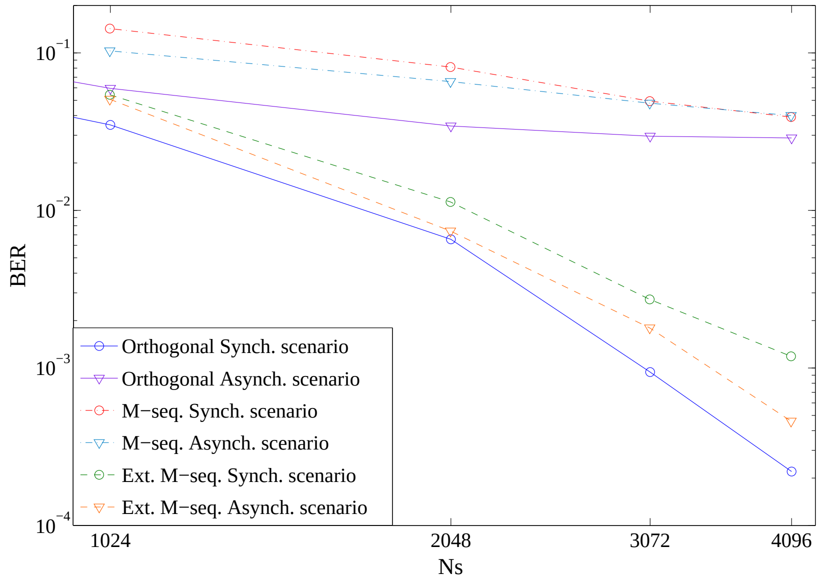

Figure 7.5: BER vs N_s in multipath 802.15.4a CM1 channel.

In Fig. 7.5 results related to different spreading codes are compared. In a quasi-synchronous scenario, where tags and reader code generators are synchronized and the time of arrival of interference depends on the tag's position, the performance of zero-mean orthogonal Hadamard codes is not sensitive to both the MUI and clutter. On the contrary, orthogonal codes do not allow good performance when reader and tags code generators are asynchronous, due to the interference caused by the presence of multipath and the poor cross-correlation properties of the shifted sequences. For what m-sequences are concerned, significant performance degradation is obtained in the presence of strong clutter since sequences are not balanced. On the other hand, the choice of zero mean codes still seems a promising solution to avoid clutter effects at the expense of a slight performance loss due to degraded cross-correlation properties, as can be noticed in Fig. 7.5.

7.6 Conclusion

In this chapter we have addressed UWB-RFID systems adopting backscatter modulation by proposing a reader and tag architecture able to work in the presence of strong clutter and interference. The performance has been investigated using simulated and measured data collected in realistic environments. It has been shown that clutter is one of the main limiting factor and that it can be mitigated or suppressed through the architecture here proposed and the adoption of zero mean spreading codes without compromising the performance in multi-tag scenario. A more detailed analysis in the presence of strong multi-tag interference and with hardware constraints, as well as without assuming perfect timing at receiver side will be provided in the following chapter.

Chapter 8

System Design and Tag Detection in Presence of Hardware Constraints

8.1 Motivations

In the UWB-RFID system several issues arise due to the presence of clutter (the signal backscattered by the environment), multi-tag interference, tag clock drift (due to typical poor local oscillator performance), and the poor link budget intrinsic of the backscattering mechanism [285, 33, 283]. In particular, the near-far interference effect could be detrimental for the reader-tag communication, as classic power control approaches cannot be adopted contrary to what happens in active CDMA systems. These issues have been only partially and separately investigated in the literature [271, 33, 295, 294, 285].

In this chapter the design of a system architecture capable of tag detection even in presence of multi-tag interference and of strong drift is presented. A low complexity non-coherent detection scheme is proposed and analyzed. Spreading code design strategies are investigated. Specifically, the near-far interference problem which derives from the semi-passive nature of the system is addressed, and a solution to counteract this issue is proposed in order to guarantee good tag detection performance. Finally, simulation results assess the performance in terms of tags detection capabilities.

The key contributions of this chapter can be summarized as follows:

- Presentation of an analysis of the UWB-RFID system based on backscatter modulation in presence of multi-tag interference and non-idealities such as clock drift;

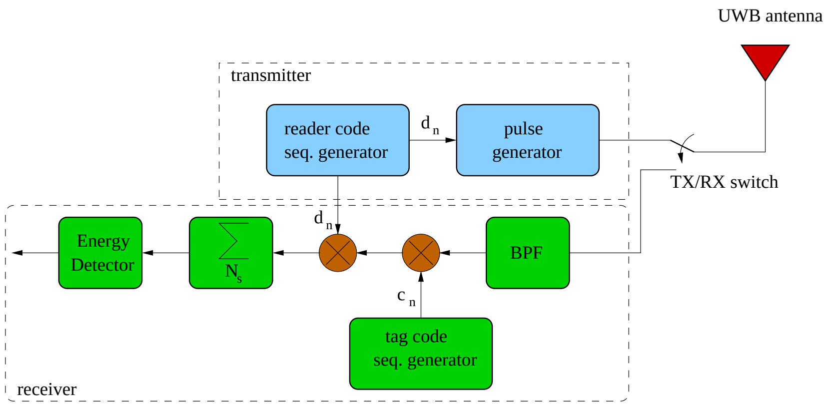

Figure 8.1: Reader internal structure.

- Introduction of a low-complexity non-coherent tag-detection scheme able to counteract near-far interference effects characteristic of the semi-passive nature of the system;
- Investigation on how the system parameters such as code length, interference level, and clock drift entity affect the system performance and hence system design guidelines;
- Description of practical implementation issues and introduction of strategies to deal with that.

The remainder of the chapter is organized as follows. The considered backscatter communication mechanism is described in Sec. 8.2. In Sec. 8.3 an analysis on the design of the tag codes which takes into account all the non-idealities present in the considered system is reported. In Sec. 8.4 a low-complexity tag detection scheme both in single-tag and multi-tags scenario is introduced. Numerical results assessing the system performance are then shown in Sec. 8.5. Various implementation issues are finally described in Sec. 8.6.

8.2 Backscatter Communication

For the reader's convenience we report, in part, the transmitting signal format described in Chapter 7 including details due to non idealities such as clock drift effects.

8.2.1 Transmitted Signal Format

Initially, tags are assumed to be in sleeping mode, with the backscattering section turned off in order to save energy. We consider here the adoption of a wake-up signal (e.g., in the UHF band) exploited for waking up all the N_{tag} tags present in the environment monitored by the reader. After the transmission of the wake-up signal, the reader starts sending the UWB interrogation signal described in (7.1).

After the transmission of each pulse, the reader's receiving section (see Fig. 8.1) collects the backscatter response from the tags located in the environment, as well as the environment response (i.e., the clutter) in order to detect the intended tag as will be detailed in the next section.

8.2.2 Tag-to-Reader Communication

When tags are woken up thanks to the wake-up signal, they activate their backscatter modulator that starts switching the antenna load according to the tags' codes $\left\{c_n^{(k)}\right\}$. The reader and the tags have independent clock sources, thus they have to be considered asynchronous. However, the wake-up signal can also be exploited to reset the tag spreading code generator. This allows considering the system as quasi-synchronous, thus drastically reducing the code acquisition time as will be clarified afterward.

The presence of a low cost oscillator in the tag and the typical long duration of the symbol[1] make clock drift effects not negligible after the reception of a few symbols. We consider here a simplified model where the clock drift mainly derives from the presence of a tag oscillator with frequency slightly different from the nominal one.[2] According to this assumption, the clock skew between the kth tag and the reader can be modeled as $\delta^{(k)}(t) = T_{\mathrm{o}}^{(k)} + D^{(k)}t$, where $T_{\mathrm{o}}^{(k)}$ is the residual initial offset after the wake-up, and $D^{(k)}$ is the clock drift entity. Therefore, the backscatter modulator signal commanding the switch of the kth tag, already introduced in (7.4), can be written as

$$m^{(k)}(t) = \sum_{m=0}^{N_{\mathrm{r}}-1} \sum_{n=0}^{N_{\mathrm{c}}-1} c_n^{(k)} \cdot \Pi\left(\frac{1}{\widetilde{T}_{\mathrm{c}}}\left[t - mN_{\mathrm{c}}\widetilde{T}_{\mathrm{c}}^{(k)} - n\widetilde{T}_{\mathrm{c}}^{(k)} - T_{\mathrm{o}}^{(k)}\right]\right) \tag{8.1}$$

with $\widetilde{T}_{\mathrm{c}}^{(k)} = T_{\mathrm{c}}\left(1 + D^{(k)}\right)$ and $\Pi(t)$ denoting the rectangular function of unitary

[1] The duration is higher with respect to conventional active UWB transmission schemes due to the need to counteract the poor link budget typical of two-hop links through the collection of a higher number of UWB pulses per symbol [283].

[2] This is equivalent to consider, as first approximation, the effects of the phase noise constant on a symbol time T_{s}, (i.e., neglecting the presence of a fast jitter).

duration for $t \in [0, 1]$. In this way the polarity of the reflected signal changes each chip time (i.e., every N_{pc} pulses) according to the kth tag's code value $c_n^{(k)}$.

Due to the reciprocity principle, the signal backscattered by the tag propagates to the reader antenna on the same wireless channel related to the reader-tag transmission. The received signal at reader side can be written as

$$\begin{aligned} r_{\mathrm{reader}}(t) = & \sum_{k=1}^{N_{\mathrm{tag}}} \left[\left(s_{\mathrm{reader}}(t) \otimes h^{(k)}(t) \right) \cdot m^{(k)}(t) \right] \otimes h^{(k)}(t) \\ & + s_{\mathrm{reader}}(t) \otimes h^{(\mathrm{C})}(t) + n(t) = w(t) + n(t) \end{aligned} \tag{8.2}$$

where $h^{(k)}(t)$ is the one-way CIR related to the reader-kth tag link, $h^{(\mathrm{C})}(t)$ is the CIR of the environment comprehensive of tags' structural scatterings (that is, the unmodulated response), and $n(t)$ is AWGN with two-sided power spectral density $N_0/2$. We consider the CIRs $h^{(k)}(t)$ and $h^{(\mathrm{C})}(t)$ static over the N_{r} interrogation symbols.[3] The tag antenna structural mode is treated as part of clutter since it is not affected by data modulation. Note that the received signals are obtained through the double convolution of the transmitted signal with the one-way CIR [296, 283].

It is interesting to remark that the clock drift in conventional active UWB communication systems affects the instant in which UWB pulses are transmitted by tags: thus the TOA and the PRP, as seen at the receiver, result different from that expected, and proper synchronization schemes have to be implemented if T_{s} is not small. On the contrary, the TOA (hence the PRP) of the backscattered pulses in backscattering communication are not affected by the clock drift (because generated by the reader itself), since clock drift modifies only how signals are modulated at the tag side. As direct consequence tag's code as seen by the reader (which is tuned on the expected symbol duration T_{s}) start exhibiting an increasing offset after the transmission of a certain number of data symbols, in addition to the initial residual offset of the wake-up phase.

8.2.3 Signal De-Spreading

As a result of the spreading process at the transmitter, and the backscatter modulation in the tag, the signal backscattered by the generic intended tag $\hat{k}$ results to be spread by the composed code $\left\{ d_n \cdot c_n^{(\hat{k})} \right\}$, whereas the clutter

[3] For the validity of the following discussions and schemes it is sufficient the CIRs static on the symbol time T_{s}.

results to be spread by the reader code $\{d_n\}$ only. Therefore, through the de-spreading process shown in Fig. 8.1 it is possible to discriminate an intended tag signal from the other tags' signals (that act as interference) and from the clutter and the noise. Specifically, the tag backscattered signal de-spreading is operated coherently accumulating the N_s CRs composing a symbol, using the combined code $\left\{d_n \cdot c_n^{(\hat{k})}\right\}$ related to the intended useful tag of index $\hat{k}$.[4] This allows discriminating the backscatter signal associated to a specific reader-tag couple. We define the periodically repeated sequences (with period N_s) $\left\{\tilde{c}_l^{(k)}\right\} \triangleq \left\{c_{\lfloor l/N_\mathrm{pc}\rfloor}^{(k)}\right\}$ and $\left\{\tilde{d}_l\right\} \triangleq \left\{d_{\lfloor l/N_\mathrm{pc}\rfloor}\right\}$, for $l = 0, 1, \ldots N_\mathrm{s}-1$, with $\tilde{c}_{l+N_\mathrm{s}}^{(k)} = \tilde{c}_l^{(k)}$ and $\tilde{d}_{l+N_\mathrm{s}} = \tilde{d}_l$.

The wake-up offset $T_\mathrm{o}^{(k)}$ and the clock drift $D^{(k)}$ generate an uncertainty on the offset (phase) of the tag spreading code with respect to the reader's local clock. To overcome tag clock drift effects, the simplest solution is to adopt codes with $N_\mathrm{pc} \gg 1$ (i.e., with higher chip time T_c), more robust to the presence of drift, as will be detailed in Sec. 8.3. Alternatively, tag detection can be performed jointly with code acquisition, requiring the availability of de-spreading outputs for different code shifts within the expected maximum acquisition range. This is achieved by correlating the backscatter response with differently shifted versions of $\left\{\tilde{c}_l^{(\hat{k})}\right\}$ and in-phase version of $\left\{\tilde{d}_l\right\}$. We consider N_span shifts with span step Δ for code acquisition, determining an overall acquisition range of $\Delta(N_\mathrm{span} - 1)$. The values of N_span and Δ have to be determined according to the robustness of codes to shifts and to the expected clock drift and initial offset due to the non ideal wake-up procedure. In addition N_span should be chosen not too large in order to keep the system complexity affordable.

Without loss of generality, we consider the detection of tag $\hat{k} = 1$ by observing the first symbol (i.e., acquiring N_s pulses). The received signal $r_\mathrm{reader}(t)$ is first passed through an ideal bandpass filter of bandwidth W with center frequency f_c to eliminate out-of-band noise.[5] The filtered signal is denoted by

$$\tilde{r}(t) = \tilde{w}_\mathrm{u}(t) + \tilde{n}(t) \tag{8.3}$$

where $\tilde{w}_\mathrm{u}(t) = w(t) \otimes h_\mathrm{F}(t)$, $h_\mathrm{F}(t)$ is the impulse response of the filter, and the term $\tilde{n}(t) = n(t) \otimes h_\mathrm{F}(t)$ is a zero-mean Gaussian random process with autocorrelation function $R_{\tilde{n}}(\tau) = W N_0 \,\mathrm{sinc}(W\tau)\cos(2\pi f_\mathrm{c}\tau)$. De-spreading

[4] This is equivalent to a process gain, (i.e., an enhancement of the SNR), of a factor N_s.

[5] This operation is necessary since the receiver we will consider is energy-based.

is operated by coherently accumulating N_s CRs. Specifically we have

$$y_n(t) = \sum_{l=0}^{N_\mathrm{s}-1} \tilde{d}_l \, \tilde{c}^{(1)}_{l+(n+\nu)\Delta} \, \tilde{r}(t-lT_\mathrm{p}) \tag{8.4}$$

with $\nu = -(N_\mathrm{span}+1)/2$, $n=1,2,\ldots,N_\mathrm{span}$. In case a code acquisition scheme is not adopted, because the code is sufficiently robust to the expected offset (i.e., if $N_\mathrm{pc} \gg 1$ as will be clarified in Sec. 8.3), we have $N_\mathrm{span} = 1$ and thus $(n+\nu)\Delta = 0$.

In particular it is possible to decompose (8.4) as $y_n(t) = x_n(t) + z_n(t)$, with the noise term $z_n(t)$ given by

$$z_n(t) = \sum_{l=0}^{N_\mathrm{s}-1} \tilde{d}_l \, \tilde{c}^{(1)}_{l+(n+\nu)\Delta} \, \tilde{n}(t-lT_\mathrm{p}) \tag{8.5}$$

which is a zero-mean, Gaussian random process with autocorrelation function $N_\mathrm{s} \, R_{\tilde{n}}(\tau)$. The term $x_n(t)$ can be instead expressed as

$$x_n(t) = \sum_{l=0}^{N_\mathrm{s}-1} \tilde{d}_l \, \tilde{c}^{(1)}_{l+(n+\nu)\Delta} \, \tilde{r}_\mathrm{u}(t-lT_\mathrm{p}) + \sum_{l=0}^{N_\mathrm{s}-1} \tilde{d}_l \, \tilde{c}^{(1)}_{l+(n+\nu)\Delta} \, \tilde{r}_\mathrm{c}(t-lT_\mathrm{p}) \tag{8.6}$$

where the received useful signal component $\tilde{r}_\mathrm{u}(t)$ is given by

$$\tilde{r}_\mathrm{u}(t) = \sum_{k=1}^{N_\mathrm{tag}} \left[\left(s_\mathrm{reader}(t) \otimes h^{(k)}(t) \right) \cdot m^{(k)}(t) \right] \otimes h^{(k)}(t) \otimes h_\mathrm{F}(t). \tag{8.7}$$

Note that here we comprise in $\tilde{r}_\mathrm{u}(t)$ both the useful and the interferer tags' responses. Signal $\tilde{r}_\mathrm{c}(t)$ denotes the clutter component $\tilde{r}_\mathrm{c}(t) = s_\mathrm{reader}(t) \otimes h^{(\mathrm{C})}(t) \otimes h_\mathrm{F}(t)$. With the assumption on the clutter CIR $h^{(\mathrm{C})}(t)$ stationary over a symbol time T_s, we have that the clutter channel response is given by $\tilde{r}_\mathrm{c}(t-lT_\mathrm{p}) = \tilde{d}_l \, \zeta(t)$, for $t \in [0, T_\mathrm{p}]$, $\forall l$, with $\zeta(t) = p(t) \otimes h^{(\mathrm{C})}(t) \otimes h_\mathrm{F}(t)$. In this manner, the clutter component at the output of the de-spreading process yelds

$$\sum_{l=0}^{N_\mathrm{s}-1} \tilde{d}_l \, \tilde{c}^{(1)}_{l+(n+\nu)\Delta} \, \tilde{r}_\mathrm{c}(t-lT_\mathrm{p}) = \zeta(t) \sum_{l=0}^{N_\mathrm{s}-1} \tilde{c}^{(1)}_{l+(n+\nu)\Delta}, \quad t \in [0, T_\mathrm{p}] \, . \tag{8.8}$$

Equation (8.8) shows that the clutter component at the output of the de-spreading process is canceled provided that the tag code $\left\{ \tilde{c}^{(1)}_l \right\}$ (i.e., $\left\{ c^{(1)}_l \right\}$) is exactly balanced (i.e., with the same number of $'+1'$ and $'-1'$). This and other properties that tags' codes have to fulfill are presented in the following section.

8.3 Tags Code Assignment Strategies

The backscatter communication scheme hides several potential issues that have to be addressed during the design of spreading codes used by the N_{tag} tags in the monitored area. In fact, it is necessary to fulfill various requirements, such as the suppression or mitigation of the multi-tag interference, provide a sufficient available number of codewords for a specific code length N_{c}, and counteract other effects such as clutter and clock drift. Here below we detail these aspects, and their impact on code design.

Number of available codewords A system with N_{tag} tags in the same environment requires the adoption of N_{tag} different codewords, apart from special cases where the same codeword is assigned to different users.[6] Considering that longer codewords imply higher complexity and a longer symbol time, it is necessary to adopt the shortest code length available which leads the fulfillment of the other requirements here reported.

Link-budget constraints The de-spreading process at receiver side must guarantee an accumulation of at least $\hat{N}_{\text{s}}$ pulses per symbol to reach the target SNR after the de-spreading which lets to achieve a reliable communication between reader and tags, as described in Sec. 8.5.2. There are several ways to fulfill such a requirement. The simplest option is to assign codes of length $N_{\text{c}} = N_{\text{s}} \geq \hat{N}_{\text{s}}$ (i.e., with $N_{\text{pc}} = 1$). An alternative solution is represented by the use of a shorter code of length $N_{\text{c}} < N_{\text{s}}$ with $N_{\text{pc}} > 1$ pulses per chip, with $N_{\text{s}} = N_{\text{c}} N_{\text{pc}} \geq \hat{N}_{\text{s}}$. The first option lets to manage a greater number of users in the environment, as the number of available codewords, is greater than adopting $N_{\text{c}} < N_{\text{s}}$. On the contrary, the second solution reduces the tag complexity and power consumption since the UWB switch works at lower frequency, but at the expense of less codewords available given a specific N_{s}.

Clutter removal constraints For what clutter removal is concerned, in Sec. 8.2.3 we have seen that if the tag code is exactly balanced, the clutter is completely removed at the output of the de-spreading process, regardless the reader's code $\{d_n\}$. Differently, if the code is not exactly balanced a clutter residual might be present. Specifically, according to (8.8), if the number of $'+1'$ and $'-1'$ differs for one chip, as happen for example for m-sequences (odd codes), we have N_{pc} clutter responses $\tilde{r}_{\text{c}}(t)$ summed up to the useful

[6] This is possible adopting proper code families and assigning the some sequence with a different initial phase (shift) to different users. Here we consider each tag with a unique sequence.

Table 8.1: Clutter rejection and process gain properties of odd codes.

Code type $N_{\mathrm{pc}} \times N_{\mathrm{c}}$	N_{s}	Clutter residual	Clutter rejection [dB]
1×8191	8191	1:8191	78
2×4095	8190	2:8190	72
4×2047	8188	4:8188	66
8×1023	8184	8:8184	60
16×511	8176	16:8176	54
32×255	8160	32:8160	48
64×127	8128	64:8128	42
128×63	8064	128:8064	36

de-spreaded signal in (8.4). Table 8.1 summarizes this effect considering odd codes starting from a code with $N_{\mathrm{pc}} = 1$ and increasing N_{pc} till 128, under the constraints $N_{\mathrm{s}} > \hat{N}_{\mathrm{s}} = 8000$.[7] In particular, the second column shows the reduction of the process gain N_{s} while increasing N_{pc} since original codewords are odd. The third and fourth columns put in evidence the decreasing in clutter rejection capability, which decreases as N_{pc} increases.

When strong clutter is present in the environment the adoption of an odd code with $N_{\mathrm{pc}} > 1$ may compromise the functionality of the system. Coherently with [33], the adoption of an exactly balanced even code, able to cancel out the clutter component, is mandatory to avoid clutter effects in harsh environments.

Interference mitigation constraints The tag code must guarantee a reliable reader-tag communication depending on the scenario considered in terms of reader-tag synchronization capability and multi-tag interference. Specifically, the code behavior in presence of these effects (lack of synchronization and presence of interference) must be separately analyzed for $N_{\mathrm{pc}} = 1$ and $N_{\mathrm{pc}} > 1$.

In case we considered an ideal synchronous scenario, with all tags' codes synchronous at PRP level, orthogonal codes would result the best option, since the interference would be always canceled out and clutter perfectly removed as they are perfectly balanced [285]. In this ideal case, there is no difference between the two approaches in terms of interference rejection. Unfortunately a perfect synchronization for all the tags is difficult to achieve

[7] This value is taken from the link budget analysis carried out in Sec. 8.5.2.

Table 8.2: Interference mitigation properties of PN codes.

Code type $N_{\mathrm{pc}} \times N_{\mathrm{c}}$	N_{s}	$\theta^{(\mathrm{peak})}$	$\hat{\theta}^{(\mathrm{peak})}$	Min. interf. residual	Min. interf. mitigation [dB]
1×8191	8191	129	129	129:8191	36
2×4095	8190	129	258	258:8190	30
4×2047	8188	65	260	260:8188	30
8×1023	8184	65	520	520:8184	24
16×511	8176	33	528	528:8176	24
32×255	8160	33	1056	1056:8160	18
64×127	8128	17	1088	1088:8128	17
128×63	8064	17	2176	2176:8064	11

as well as to maintain due to the clock drift effect $D^{(k)}$ and the residual wake-up offset $T_{\mathrm{o}}^{(k)}$ described in Sec. 8.2.2.

Considering, instead, a completely asynchronous scenario where tags' codes are not kept synchronized and each backscatter modulator is completely free-running, it is well known that pseudo-noise (PN) codes represent, in general, a good solution which allows to control the interference [297]. As PN codes are composed of odd sequences, extended PN codes are a potential solution to completely remove clutter without a significant performance loss, as proposed in [285]. On the contrary, orthogonal codes offer in this scenario poor performance due to the not optimal cross-correlation properties when not aligned. In case (extended) PN codes are adopted, the two considered approaches, that is, $N_{\mathrm{pc}} = 1$ and $N_{\mathrm{pc}} > 1$, are not equivalent. In fact, suppose of having a set of codewords of length N_{c}. Define the periodic crosscorrelation function (CcF) between a pair of different code sequences x and y of length N_{c} as $\theta_{x,y}(m)$, for $m = 0, 1, \ldots, N_{\mathrm{c}} - 1$, where $\theta_{x,y}(m) = \langle x, T^m y \rangle$, with $\langle a, b \rangle$ denoting the inner product between sequences a and b, and T^m denoting the operator which shifts vectors cyclically to the left by m places.[8] The behavior of the CcF determines the interference level at the output of the de-spreading process [285]. Let us now indicate with $\hat{x}$ and $\hat{y}$ the code sequences obtained as chip repetition of a factor N_{pc} of x and y. We have that $\hat{\theta}_{\hat{x},\hat{y}}(l)$, for $l = 0, 1, \ldots, N_{\mathrm{s}} - 1$, is the CcF between the pair of code sequences $\hat{x}$ and $\hat{y}$ of length N_{s}. When $N_{\mathrm{pc}} = 1$, $N_{\mathrm{s}} = N_{\mathrm{c}}$ and obviously

[8]Sequences x and y denote, respectively, the intended useful tag code $\left\{c_l^{(\hat{k})}\right\}$ and the k-th tag code $\left\{c_l^{(k)}\right\}$ assigned to another user, with $k \neq \hat{k}$.

$\hat{\theta}_{\hat{x},\hat{y}}(l) = \theta_{x,y}(m)$, since $\hat{x} = x$ and $\hat{y} = y$. Differently, if $N_{\text{pc}} > 1$ is adopted, the resulting code of length N_{s} exhibits a CcF $\hat{\theta}_{\hat{x},\hat{y}}(l)$ which can be expressed as a function of the original $\theta_{x,y}(m)$ as[9]

$$\hat{\theta}_{\hat{x},\hat{y}}(l) = N_{\text{pc}}\, \theta_{x,y}(\lfloor l/N_{\text{pc}} \rfloor) + (l \mod N_{\text{pc}}) \left[\theta_{x,y}(\lfloor l/N_{\text{pc}} \rfloor + 1) - \theta_{x,y}(\lfloor l/N_{\text{pc}} \rfloor)\right] . \tag{8.9}$$

As it is possible to observe from (8.9), when adopting $N_{\text{pc}} > 1$, the CcF peak $\hat{\theta}^{(\text{peak})} = \max\limits_{l} \left\{ \left| \hat{\theta}_{\hat{x},\hat{y}}(l) \right| \right\}$, given by $\hat{\theta}^{(\text{peak})} = N_{\text{pc}} \max\limits_{l} \left\{ \left| \theta_{x,y}(\lfloor l/N_{\text{pc}} \rfloor) \right| \right\}$, is worsen of a factor N_{pc} with respect to the original code, that is $\hat{\theta}^{(\text{peak})} = N_{\text{pc}} \max\limits_{m} \left\{ \left| \theta_{x,y}(m) \right| \right\} = N_{\text{pc}} \theta^{(\text{peak})}$. Thus, the adoption of a code with $N_{\text{pc}} > 1$ results in an increasing of the peak (and average) value of the CcF $\hat{\theta}(l)$, that is a decreasing of the code interference mitigation capability. However, it is well known that a shorter sequence presents a lower peak for its CcF $\theta_{x,y}(m)$, which is directly related to the sequence length [297]. Thus, we have two conflicting factors: on one side, the interference level is increased by the fact that $N_{\text{pc}} > 1$, but on the other side it is decreased thanks to the adoption of a shorter code $N_{\text{c}} < N_{\text{s}}$.

Table 8.2 shows the values of the peak CcFs $\theta^{(\text{peak})}$ and $\hat{\theta}^{(\text{peak})}$ for different N_{pc}, as well as the resulting minimum interference mitigation level for classical PN codes, in particular codes derived from maximal connected sets of m-sequences presenting the optimal three-valued cross correlation spectrum[10] $\left\{-1, -\theta^{(\text{peak})}, \theta^{(\text{peak})} - 2\right\}$ (e.g., Gold sequences) [297].[11] Looking at the last column on the right of Table 8.2 it is evident how the gain in interference mitigation capability presented by the adoption of a code with shorter N_{c} is not sufficient to counteract the decreasing in interference mitigation capability due to the increased N_{pc} necessary for guaranteeing the target $\hat{N}_{\text{s}}$. Due to this effect, considering an asynchronous scenario, we have that the best performance in terms of interference mitigation is achieved by adopting the strategy with $N_{\text{pc}} = 1$.

Wake-up offset and clock drift constraints Due to the non-idealities of the wake-up process described in Sec. 8.2.2, small residual offsets with respect to the reader timing of tag codes are present (quasi-synchronous scenario). In this case it is important to exploit this peculiarity, by assigning (to tags)

[9] The expression is derived from [297, eq. 1.11].

[10] For $N_{\text{c}} = 4095$ and $N_{\text{c}} = 255$ there are no preferred pairs of m-sequences so the corresponding CcFs do not exhibit the optimal three-valued spectrum.

[11] Similar considerations can be formulated for extended PN codes considering a less favorable interference mitigation capability.

codes able to guarantee the orthogonality (or very small cross-correlation values) even in the presence of these small offsets [298]. In the presence of significant clock drift, the scenario from quasi-synchronous can become asynchronous, so that codes are also required to preserve good correlation properties also in asynchronous conditions.

Moreover a code presenting $N_{\text{pc}} > 1$ is intrinsically more robust to synchronization errors and the presence of clock drift. As an example, consider the useful tag code is shifted of q PRPs with respect to the code generator at reader side due to the presence of offsets. Thus, the process gain, instead of being N_{s}, as expected, is equal to the code autocorrelation function (AcF) evaluated in q, that is $\hat{\theta}_{\hat{x},\hat{x}}(q)$, where $\hat{x}$ is the tag code $\left\{\tilde{c}_l^{(\hat{k})}\right\}$ [285]. According to (8.9), as N_{pc} increases, the AcF function presents smoother transitions making the de-spreading more robust to synchronization errors.

To counteract the effects of the wake-up offset and of clock drift we may operate in two directions. The first and simplest solution is to adopt $N_{\text{pc}} \gg 1$, which guarantees a lower receiver complexity at the expense of a reduced number of available codewords and lower interference mitigation. This corresponds to set $n = N_{\text{span}} = 1$ and thus $(n+\nu)\Delta = 0$ in (8.4). The second and more complex approach, which uses smaller values of N_{pc} (ideally $N_{\text{pc}} = 1$ for the best interference mitigation), requires the adoption of tag code acquisition schemes at the receiver to deal with the non ideal wake-up offset, as well as code tracking schemes to compensate the clock drift. In this case the adoption of a code with good AcF (ideally, m-sequence) is beneficial for acquisition and tracking. It has to be remarked that with small N_{pc} it becomes important to adopt a small span step Δ (e.g., $\Delta = 1$ if $N_{\text{pc}} = 1$) to have a refined code acquisition search which can increase the complexity in case of high wake-up offset $T_{\text{o}}^{(k)}$. As will be investigated in the numerical results, a trade-off between N_{pc}, hence the required Δ, and the corresponding system complexity has to be found.

8.4 Tag Detection

8.4.1 Tag Detection Scheme

The first task to be accomplished by the reader is the tag detection, that is the process to detect the presence of a specific tag in the monitored area. The detection in parallel of N tags requires that N detection circuits are employed at receiver section, with a consequent increase of complexity. For this reason, the tag detection scheme we propose is a partially non-coherent approach based on energy detection, which helps to keep the system complexity affordable, thanks to the possibility of adopting sub-Nyquist sampling rates [60].

According to the considerations made in Sec. 8.3, we assume to adopt balanced codes, so that (8.6) reduces to

$$x_n(t) = \sum_{l=0}^{N_s-1} \tilde{d}_l \, \tilde{c}^{(1)}_{l+(n+\nu)\Delta} \, \tilde{r}_u(t - lT_p) \, . \tag{8.10}$$

The term $x_n(t)$ can be further detailed considering that $\tilde{r}_u(t)$ is the combination of N_{tag} tags CRs (backscatter), that is

$$x_n(t) = \sum_{l=0}^{N_s-1} \tilde{d}_l \, \tilde{c}^{(1)}_{l+(n+\nu)\Delta} \sum_{k=1}^{N_{\mathrm{tag}}} \omega^{(k)}(t - lT_p) \tag{8.11}$$

where the single-tag channel response is

$$\omega^{(k)}(t) = \left[\left(s_{\mathrm{reader}}(t) \otimes h^{(k)}(t) \right) \cdot m^{(k)}(t) \right] \otimes h^{(k)}(t) \otimes h_{\mathrm{ZF}}(t) \, . \tag{8.12}$$

The de-spreading process is then followed by energy evaluations performed over the PRP T_p, that is

$$e_{n,m} = \int_{(m-1)\,T_{\mathrm{ED}}}^{m\,T_{\mathrm{ED}}} y_n^2(t) \, dt \quad n = 1, 2, \ldots, N_{\mathrm{span}}, \; m = 1, 2, \ldots, N_{\mathrm{bin}} \tag{8.13}$$

with $N_{\mathrm{bin}} = \lfloor T_p / T_{\mathrm{ED}} \rfloor$ representing the number of integration bins each PRP is divided into, and with T_{ED} the integration time. The detection strategy consists of comparing each element $e_{n,m}$ with a threshold $\xi_{n,m}$. If the energy value of at least one bin is above the threshold, then the tag is considered detected. Obviously, the challenging issues is the evaluation of the threshold $\xi_{n,m}$.

To this purpose, we define the global probability of false alarm (PFA) as the probability of deciding that the tag is present when it is not present in the considered environment, and the global probability of detection (PD) the probability of taking the correct decision when the tag is present. We then define $\mathcal{H}_1$ and $\mathcal{H}_0$ the hypotheses related to the presence and absence of the tag, respectively. The choice of the threshold affects the performance of the detection scheme in terms of PD and PFA. Low values for the threshold lead to higher PFA and higher PD. The vice versa holds for high values of $\xi_{n,m}$. For further convenience we define the single-bin PFA as the probability that the single bin energy exceeds the threshold when the tag is not present, and the single-bin PD as the probability that the single bin exceeds the threshold when the tag is effectively present. Global PFA and PD are indicated

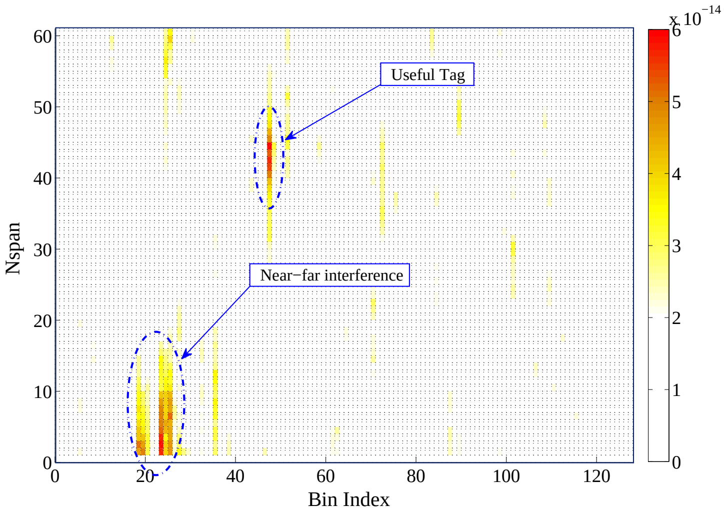

Figure 8.2: Example of energy matrix $\mathbf{E}$ in presence of wake-up offset, clock drift and near-far interference effect.

in the following with capital letters, specifically P_{FA} and P_D, respectively, the single-bin PFA and PD, for the bin of coordinate (n, m), are indicated with lower cases, specifically $p_{FA}^{(n,m)}$ and $p_D^{(n,m)}$, respectively. If the threshold is exceeded, the coordinates $(\widehat{n}, \widehat{m})$ associated to the maximum provide an estimate of the tag clock offset and a coarse estimate of the signal TOA, respectively, thanks to the adoption of UWB signals. The maximum resolution in TOA estimation (and hence ranging) is determined by T_{ED} [51]. TOA estimates can be further improved by adopting ranging strategies as described in [51].

8.4.2 Threshold Evaluation Criteria

The usual strategy for signal detection is defining a fixed threshold, that is a threshold $\xi_{n,m} = \xi$ [111]. However, this approach is not suitable in UWB-RFID systems based on backscatter modulation in presence of multi-tag interference. In fact, the useful tag can be hidden by interference peaks coming from tags closer to the reader than the intended useful one (i.e., a near-far effect). This fact is clearly depicted in Fig. 8.2, which shows an example of energy matrix $\mathbf{E} = \{e_{n,m}\}$ where the near-far effect is evident. If a constant threshold over all bins were adopted, the PFA would increase significantly due to the presence of interferers close to the reader. The effect is very pronounced in this kind of system due to the two-hop propagation channel, as the received power, in free-space propagation, is proportional to d^4, where d is the reader-tag distance [50, 283]. Assuming a useful and an interferer tag at distance, respectively, d_{U} and d_{I} from the reader, the difference in the receiving power at reader side from the two tags is $40[\log_{10}(d_{\mathrm{U}}) - \log_{10}(d_{\mathrm{I}})]$ dB. For example, considering a useful and an interferer tag placed, respectively, at $d_{\mathrm{U}} = 10\,\mathrm{m}$ and $d_{\mathrm{I}} = 2\,\mathrm{m}$ from the reader, we find a difference of approximately 27 dB in the signals amplitude. If this difference is not properly managed by the interference mitigation capability provided by the tag codes, a high PFA due to near-far effects is expected.[12] Unfortunately classical power control approaches, as usually adopted in CDMA systems, cannot be used due to the passive nature of the communication here considered. Therefore we propose a bin-dependent threshold strategy able to counteract near-far effects. In the following the threshold will be analytically computed considering a constant target PFA P^*_{FA}, under the hypothesis of absence and presence of multi-tag interference.

Consider now the elements $e_{n,m}$ of the energy matrix. The presented decision rule consist in

$$\text{Decide} : \begin{cases} \widehat{\mathcal{H}}_0\ , & \text{if } e_{n,m} < \xi_{n,m}\, \forall\, n, m\ , \\ \widehat{\mathcal{H}}_1\ , & \text{if } \exists\, \{n, m\} \text{ s.t. } e_{n,m} \geq \xi_{n,m}\ . \end{cases} \tag{8.14}$$

Define now the normalized test

$$\Lambda^{(n,m)} = \frac{2}{N_{\mathrm{s}} N_0} e_{n,m} \underset{\widehat{\mathcal{H}}_0}{\overset{\widehat{\mathcal{H}}_1}{\gtrless}} \tilde{\xi}_{n,m} \tag{8.15}$$

where $\tilde{\xi}_{n,m} = \frac{2}{N_{\mathrm{s}} N_0} \xi_{n,m}$. According to the approach proposed in [86] we have

$$\Lambda^{(n,m)} = \frac{2}{N_{\mathrm{s}} N_0} \int_{(m-1)\,T_{\mathrm{ED}}}^{m\,T_{\mathrm{ED}}} y_n^2(t)\, dt \simeq \frac{1}{\sigma^2} \sum_{i=(m-1)N}^{mN} y_{n,i}^2(t) \tag{8.16}$$

where $N = 2WT_{\mathrm{ED}}$, $\sigma^2 = N_{\mathrm{s}} N_0 W$ is the noise variance, and $y_{n,i}$ are for odd i (even i) the samples of the real (imaginary) part of the ELP $\hat{y}_n(t)$ of $y_n(t)$, with $y_n(t) = \Re\left\{\hat{y}_n(t) e^{j2\pi f_{\mathrm{c}} t}\right\}$, taken at Nyquist rate $W/2$ in each interval T_{ED}.[13]

It is well known that the output of the energy detector is distributed according to a central Chi-square distribution, with p.d.f. $f_{\mathrm{C}}(y, \nu)$, under $\mathcal{H}_0$, and according to a non-central Chi-square distribution, with p.d.f. $f_{\mathrm{NC}}(y, \lambda, \nu)$, under $\mathcal{H}_1$ [86]. For further convenience we report the p.d.f.s of these r.v.s,

[12] The effects are obviously even more pronounced in presence of multiple interfering tags and multipath propagation.

[13] We consider $WT_{\mathrm{ED}} \in \mathbb{N}$.

having indicated with $\tilde{\nu}$ the number of degrees of freedom, and with λ the non-centrality parameter, that is

$$f_{\mathrm{NC}}(y,\lambda,\tilde{\nu}) = \frac{1}{2}e^{-\frac{y+\lambda}{2}}\left(\frac{y}{\lambda}\right)^{\frac{\tilde{\nu}-2}{4}} I_{\frac{\tilde{\nu}}{2}-1}(\sqrt{y\lambda})\,, \quad y \geq 0, \tag{8.17}$$

$$f_{\mathrm{C}}(y,\tilde{\nu}) = \frac{y^{(\frac{\tilde{\nu}}{2}-1)}}{2^{\frac{\tilde{\nu}}{2}}\Gamma\left(\frac{\tilde{\nu}}{2}\right)}\, e^{-\frac{y}{2}}\,, \quad y \geq 0 \tag{8.18}$$

where $I_\kappa(\cdot)$ denotes the κth order modified Bessel function of the first kind [106, p. 374] and $\Gamma(\cdot)$ is the gamma function [106, p. 255].

In the following we propose two different threshold criteria according to the presence or not of multiple tags in the environment.

Single-Tag Scenario

In the absence of interference (i.e., $N_{\mathrm{tag}} = 1$) the only component at the de-spreader output under hypothesis $\mathcal{H}_0$ is the noise $z_n(t)$ (i.e., $x_n(t) = 0$). A threshold-crossing event in absence of the useful tag, causing a false alarm, happens when the r.v. $\Lambda^{(n,m)}|_{\mathcal{H}_0}$ is above the threshold $\tilde{\xi}_{n,m}$, where we have indicated with $\Lambda^{(n,m)}|_{\mathcal{H}_0}$ the test (8.15) under the hypothesis $\mathcal{H}_0$, that is

$$\Lambda^{(n,m)}|_{\mathcal{H}_0} = \frac{2}{N_{\mathrm{s}}N_0}\int_{(m-1)\,T_{\mathrm{ED}}}^{m\,T_{\mathrm{ED}}} z_n^2(t)\,dt \simeq \frac{1}{\sigma^2}\sum_{i=(m-1)N}^{mN} z_{n,i}^2 \tag{8.19}$$

where $z_{n,i}$ are the sampling expansion coefficients of the ELP $\hat{z}_n(t)$ of $z_n(t)$. Since $z_{n,i}$ are statistically independent Gaussian r.v.s with zero mean and unit variance, the r.v. $\Lambda^{(n,m)}|_{\mathcal{H}_0}$ is central Chi-square distributed, with N degrees of freedom. This results in a single-bin PFA $p_{FA}^{(n,m)}$ given by

$$p_{FA}^{(n,m)} = \int_{\tilde{\xi}_{n,m}}^{\infty} f_{\mathrm{C}}(y,N)\,dy = \frac{\Gamma\left(\frac{N}{2},\frac{\tilde{\xi}_{n,m}}{2}\right)}{\Gamma\left(\frac{N}{2}\right)} = \tilde{\Gamma}\left(\frac{N}{2},\frac{\tilde{\xi}_{n,m}}{2}\right) \tag{8.20}$$

where we used [111, 62] to solve the integral, and with $\Gamma(a,x) = \int_x^\infty x^{\alpha-1}e^{-x}dx$ the upper incomplete gamma function and $\tilde{\Gamma}(\cdot,\cdot)$ the gamma regularized function. Since the only component at the de-spreader output is the noise $z_n(t)$, the single-bin PFA results to be the same in each bin, that is $p_{FA}^{(n,m)} = p_{FA}$, $\forall\, n,m$. This leads to a constant threshold $\tilde{\xi}_{n,m} = \tilde{\xi}$, $\forall\, n,m$. Under the assumption of independent energy bins in n and m we have that the global

PFA is[14]

$$P_{FA} = 1 - (1 - p_{FA})^M \simeq M p_{FA} \tag{8.21}$$

where $M = N_{\text{bin}} \times N_{\text{span}}$. The threshold ξ, corresponding to the global PFA P_{FA}^*, can be then calculated by inverting (8.21) and (8.20) obtaining

$$\xi = \frac{N_{\text{s}} N_0}{2} \cdot 2\, \tilde{\Gamma}^{-1} \left(\frac{P_{FA}^*}{M}, \frac{N}{2} \right) \tag{8.22}$$

which now depends on the target PFA P_{FA}^*.

Once the threshold is set to guarantee a certain PFA, we can determine the correspondent single-bin PD. Under the hypothesis $\mathcal{H}_1$, the ED statistics $\Lambda^{(n,m)}|_{\mathcal{H}_1}$ is given by

$$\Lambda^{(n,m)}|_{\mathcal{H}_1} = \frac{2}{N_{\text{s}} N_0} \int_{(m-1)\,T_{\text{ED}}}^{m\,T_{\text{ED}}} \left(x_n(t) + z_n(t)\right)^2 \, dt \simeq \frac{1}{\sigma^2} \sum_{i=(m-1)N}^{mN} \left(x_{n,i} + z_{n,i}\right)^2 \tag{8.23}$$

where $x_{n,i}$ are the sampling expansion coefficients of the ELP $\hat{x}_n(t)$ of $x(t)$. Since $z_{n,i}$ are statistically independent Gaussian r.v.s with zero mean and unit variance, the r.v. $\Lambda^{(n,m)}|_{\mathcal{H}_1}$ is non-central Chi-square distributed, with N degrees of freedom, and non-centrality parameter $\lambda_{n,m} = 2\gamma_{n,m}$, where the SNR per bin is denoted by

$$\gamma_{n,m} = \frac{1}{N_{\text{s}} N_0} \int_{(m-1)\,T_{\text{ED}}}^{m\,T_{\text{ED}}} x_n(t)^2 \, dt \simeq \frac{1}{2\sigma^2} \sum_{i=(m-1)N}^{mN} x_{n,i}^2 \,. \tag{8.24}$$

The single-bin PD $p_D^{(n,m)}$ is then given by [111, 62]

$$p_D^{(n,m)} = Q_k \left(\sqrt{\lambda_{n,m}}, \sqrt{\tilde{\xi}} \right) \tag{8.25}$$

where $k = N/2$ and $Q_k(\alpha, \beta) = \int_\beta^\infty x \left(\frac{x}{\alpha}\right)^{k-1} \exp\left\{-\frac{x^2+\alpha^2}{2}\right\} I_{k-1}(\alpha x)\, dx$ is the generalized Marcum's Q function of order k. The global PD P_D can be finally computed as

$$P_D = 1 - \prod_{n=1}^{N_{\text{span}}} \prod_{m=1}^{N_{\text{bin}}} \left(1 - p_D^{(n,m)}\right) \tag{8.26}$$

under the assumption of having independent energy bins.

[14]This assumption is exact in case of $N_{\text{span}} = 1$, since the energy bins are independent, while results an approximation when $N_{\text{span}} > 1$ as the energy matrix elements are correlated for different code shifts. Consequently, (8.22) leads to a threshold more conservative than the necessary and, consequently, a PD lower than expected.

Multi-Tags Scenario

We now extend the derivation 8.4.2 to include the multi-tag interference effect in the threshold evaluation process. As previously discussed, a proper threshold design is fundamental to avoid the detrimental effects of near-far interference.

We consider now N_{tag} tags placed in the environment. Without loss of generality we consider tag $\hat{k} = 1$ as the intended one to be detected, while tags for $k = 2, 3, \ldots, N_{\text{tag}}$ are considered as interferers. In this case, also in absence of the useful tag, $x_n(t) \neq 0$ due to the presence of the residual interference term after the de-spreading [285]. For further convenience, we distinguish the case whether the desired tag is present or absent, by defining

$$\begin{cases} x_n^{(\mathcal{H}_0)}(t) = \sum_{l=0}^{N_\text{s}-1} \tilde{d}_l \, \tilde{c}^{(1)}_{l+(n+\nu)\Delta} \sum_{k=2}^{N_\text{tag}} \omega_k(t) \, , \\ x_n^{(\mathcal{H}_1)}(t) = \sum_{l=0}^{N_\text{s}-1} \tilde{d}_l \, \tilde{c}^{(1)}_{l+(n+\nu)\Delta} \sum_{k=1}^{N_\text{tag}} \omega_k(t) \, . \end{cases} \tag{8.27}$$

Since $z_{n,i}$ are statistically independent Gaussian r.v.s with zero mean and unit variance, under both hypotheses $\mathcal{H}_0$ and $\mathcal{H}_1$ the r.v. Λ, that is, the ED output, is non-central Chi-square distributed with N degrees of freedom, and with a non-centrality parameter depending on $\mathcal{H}_0$ and $\mathcal{H}_1$. Under the hypothesis $\mathcal{H}_0$ (no useful tag), the ED output results in

$$\Lambda^{(n,m)}|_{\mathcal{H}_0} = \frac{2}{N_\text{s} N_0} \int_{(m-1)T_\text{ED}}^{mT_\text{ED}} \left(x_n^{(\mathcal{H}_0)}(t) + z_n(t)\right)^2 dt \simeq \frac{1}{\sigma^2} \sum_{i=(m-1)N}^{mN} \left(x_{n,i}^{(\mathcal{H}_0)} + z_{n,i}\right)^2 \tag{8.28}$$

where $x_{n,i}^{(\mathcal{H}_0)}$ are the sampling expansion coefficients of the ELP $\hat{x}_n^{(\mathcal{H}_0)}(t)$ of $x_n^{(\mathcal{H}_0)}(t)$, leading to the non-centrality parameter $\lambda_{n,m}^{(\mathcal{H}_0)} = 2\gamma_{n,m}^{(\mathcal{H}_0)}$ where the interference-to-noise ratio (INR) per bin is defined as

$$\gamma_{n,m}^{(\mathcal{H}_0)} = \frac{1}{N_\text{s} N_0} \int_{(m-1)\,T_\text{ED}}^{m\,T_\text{ED}} x_n^{(\mathcal{H}_0)}(t)^2 \, dt \simeq \frac{1}{2\sigma^2} \sum_{i=(m-1)N}^{mN} \left(x_{n,i}^{(\mathcal{H}_0)}\right)^2 . \tag{8.29}$$

A threshold-crossing event in absence of the useful tag, causing the false alarm event, happens when the r.v. $\Lambda^{(n,m)}|_{\mathcal{H}_0}$ is above the threshold $\tilde{\xi}_{n,m}$. This results in a single-bin PFA $p_{FA}^{(n,m)}$ given by

$$p_{FA}^{(n,m)} = \int_{\tilde{\xi}_{n,m}}^{\infty} f_\text{NC}(y, \lambda_{n,m}^{(\mathcal{H}_0)}, N) \, dy = Q_k\left(\sqrt{\lambda_{n,m}^{(\mathcal{H}_0)}}, \sqrt{\tilde{\xi}_{n,m}}\right) \tag{8.30}$$

where we used [111, 62] to solve the integral. The non-centrality parameters are strictly related to the interference level at each bin $e_{n,m}$, then a constant

PFA in each bin, that is $p_{FA}^{(n,m)} = p_{FA}$, $\forall\, n, m$, is obtained if a bin-dependent threshold $\xi_{n,m}$ is adopted according to (8.30). In particular, under the assumption of independent energy bins in n and m as in (8.21), the threshold $\xi_{n,m}$ can be calculated from (8.21) and (8.30) as

$$\xi_{n,m} = \frac{N_{\mathrm{s}} N_0}{2} \cdot \left[Q_k^{-1}\left(\sqrt{\lambda(\mathcal{H}_0)_{n,m}}\, , \frac{P_{FA}^*}{M} \right) \right]^2 \tag{8.31}$$

with $Q_k^{-1}(\cdot,\cdot)$ denoting the inverse generalized Marcum Q function. Again, once the bin-dependent threshold is set to guarantee a certain PFA, we can determine the corresponding single-bin PD. Under the hypothesis $\mathcal{H}_1$, the ED output is described by

$$\Lambda^{(n,m)}|_{\mathcal{H}_1} = \frac{2}{N_{\mathrm{s}} N_0} \int_{(m-1)T_{\mathrm{ED}}}^{mT_{\mathrm{ED}}} \left(x_n^{(\mathcal{H}_1)}(t) + z_n(t) \right)^2 dt \simeq \frac{1}{\sigma^2} \sum_{i=(m-1)N}^{mN} \left(x_{n,i}^{(\mathcal{H}_1)} + z_{n,i} \right)^2 \tag{8.32}$$

where $x_{n,i}^{(\mathcal{H}_1)}$ are the sampling expansion coefficients of the ELP $\hat{x}_n^{(\mathcal{H}_1)}(t)$ of $x_n^{(\mathcal{H}_1)}(t)$, leading to the non-centrality parameter $\lambda_{n,m}^{(\mathcal{H}_1)} = 2\gamma_{n,m}^{(\mathcal{H}_1)}$, where the interference-plus-signal-to-noise-ratio (ISNR) per bin is defined as

$$\gamma_{n,m}^{(\mathcal{H}_1)} = \frac{1}{N_{\mathrm{s}} N_0} \int_{(m-1)\, T_{\mathrm{ED}}}^{m\, T_{\mathrm{ED}}} x_n^{(\mathcal{H}_1)}(t)^2\, dt \simeq \frac{1}{2\sigma^2} \sum_{i=(m-1)N}^{mN} \left(x_{n,i}^{(\mathcal{H}_1)} \right)^2 . \tag{8.33}$$

The single-bin PD $p_D^{(n,m)}$ is then given by [111, 62]

$$p_D^{(n,m)} = Q_k\left(\sqrt{\lambda_{n,m}^{(\mathcal{H}_1)}}, \sqrt{\tilde{\xi}_{n,m}} \right) \tag{8.34}$$

and the global PD P_D can be computed according to (8.26).

The presented tag detection scheme in the presence of interference requires the knowledge of the INR per bin in order to define the proper bin-dependent threshold $\xi_{n,m}$ according to (8.31) necessary to keep $P_{FA} < P_{FA}^*$. In Sec. 8.5 practical approaches for defining the threshold without exact a-priori knowledge of the interference level will be detailed.

Note that the detection performance in terms of PD in (8.25) and (8.34) is related to N_{s}. Since the transmitting power of the UWB transmitter is constrained by maximum spectrum emission masks, N_{s} results the design parameter to be determined to guarantee a target PD P_D^* given a certain reader-tag distance. Numerical results in Sec. 8.5 will provide an example of system design.

8.5 Numerical Results

In this section we present an example of system design, and performance evaluated in realistic conditions. Specifically we analyze the tag detection rate as a function of the false alarm rate considering the low complexity non-coherent scheme based on energy detection proposed in Sec. 8.4.

8.5.1 Simulation Parameters

We assume to perform the tag detection in a preamble consisting of data symbols $\left\{b_m^{(k)}\right\}$ of all '+1'. We considered a scenario with a system composed of one reader, and one or more tags placed in the direction of reader's antenna maximum radiation. In addition, we considered the signal backscattered by any untagged object as part of the clutter.

We adopt $T_\mathrm{p} = 128\,\mathrm{ns}$.[15] A reader with $G_\mathrm{r} = 5\,\mathrm{dBi}$ antenna gain, tags equipped with an $G_\mathrm{r} = 1\,\mathrm{dBi}$ antenna and $L_\mathrm{t} = 2\,\mathrm{dB}$ switch losses have been considered. Results have been obtained starting from multipath channel responses with exponential power delay profile and Nakagami-m fading (severity factor $m=3$), a rms channel delay-spread of $10\,\mathrm{ns}$[16] and paths separated of $2\,\mathrm{ns}$ apart. A transmitted signal compliant with the IEEE 802.15.4a emission mask in the $3-5\,\mathrm{GHz}$ is considered, adopting RRC pulses[17] with pulse width parameter $T_\mathrm{w} = 1\,\mathrm{ns}$, roll-off factor $\nu = 0.6$ and center frequency $f_\mathrm{c} = 4\,\mathrm{GHz}$. For what concerns the clutter, a worst-case of uniform power delay profile in the overall interval T_p is considered, with paths spaced $0.95\,\mathrm{ns}$ apart, each path with amplitude characterized by Nakagami-m fading, with $m = 3$, and a rms value of $0.5\,\mathrm{mV}$ at the receiver. In addition, at receiver side a figure noise $F = 4\,\mathrm{dB}$ is considered and an ideal bandpass filter bandwidth $W = 2\,\mathrm{GHz}$ and center frequency $f_\mathrm{c} = 4\,\mathrm{GHz}$. Energy evaluations are performed with a bin of width $T_\mathrm{ED} = 1\,\mathrm{ns}$.

8.5.2 System Design

Link budget and system parameter choice

The principal parameter to be accounted in the system design is the number of pulses per symbol N_s, in order to guarantee a target PD P_D^* at a certain

[15] This and the next system specifications are driven by the outcome of the European project SELECT, http://www.selectwireless.eu

[16] This value is comprehensive of the two-way link of the backscatter signal [283].

[17] See (3.63) for the definition.

maximum reader-tag distance, which poses a constraint on a minimum $\hat{N}_\mathrm{s}$. Thus, the relation $N_\mathrm{s} \geq \hat{N}_\mathrm{s}$ has to be satisfied.

This parameter can be easily derived under some approximations. In particular we assume i) AWGN conditions, ii) that the received pulse always falls entirely in one bin, iii) absence of interference and ideal tag code phase retrieving with $N_\mathrm{span} = 1$. In this case the single-bin detection probability $p_D^{(n,m)}$ equals the system detection probability P_D, which will be imposed equal to the target P_D^*. Specifically, according to (8.25), we have

$$P_D^* = Q_k\left(\sqrt{\lambda(d)}, \sqrt{\tilde{\xi}}\right) \tag{8.35}$$

with $\lambda(d) = 2\,\mathsf{SNR}_\mathrm{p}(d)$, having indicated with $\mathsf{SNR}_\mathrm{p}(d)$ the SNR obtained in AWGN and free-space conditions after the de-spreading process for a reader-tag distance d, that is

$$\mathsf{SNR}_\mathrm{p}(d) = \frac{N_\mathrm{s}}{N_0}\frac{E_\mathrm{p}}{P_L(d)}\,. \tag{8.36}$$

The factor $P_L(d)$ indicates the free-space pathloss, that is[18]

$$P_L(d) = \left(\frac{4\pi\, d\, f_c}{c}\right)^4 \frac{L_\mathrm{t}}{G_\mathrm{r}^2\, G_\mathrm{t}^2} \tag{8.37}$$

with c denoting the speed of light. Noticing that $\tilde{\xi}$, given by

$$\tilde{\xi} = 2\,\tilde{\Gamma}^{-1}\left(\frac{P_{FA}^*}{N_\mathrm{bin}}, WT_\mathrm{ED}\right) \tag{8.38}$$

is not function of N_s, it is possible to obtain the number of pulses per symbol inverting (8.35) as

$$N_\mathrm{s} \geq \left\lceil \frac{N_0 P_L(d)}{2E_\mathrm{p}}\left[Q_k^{-1}\left(P_D^*, \sqrt{\tilde{\xi}}\right)\right]^2 \right\rceil \tag{8.39}$$

with $Q_K^{-1}(\cdot,\cdot)$ denoting the inverse generalized Marcum Q function, $N_0 = k_B\, F\, T_\mathrm{o}$, $T_\mathrm{o} = 290\,K$ the reference temperature, and k_B the Boltzmann constant. Substituting the simulation parameters indicated in Sec. 8.5.1, and considering $P_{FA}^* = 10^{-3}$ and $P_D^* = 0.9$, we obtain the curve providing N_s as function of the distance depicted in Fig. 8.3. For comparison, in the same figure, results obtained considering a transmitting power exceeding the FCC

[18]Here we adopt a central-frequency approximation. The reader gain G_r is only accounted once since the transmitted energy E_p already accounts for it at transmitting side.

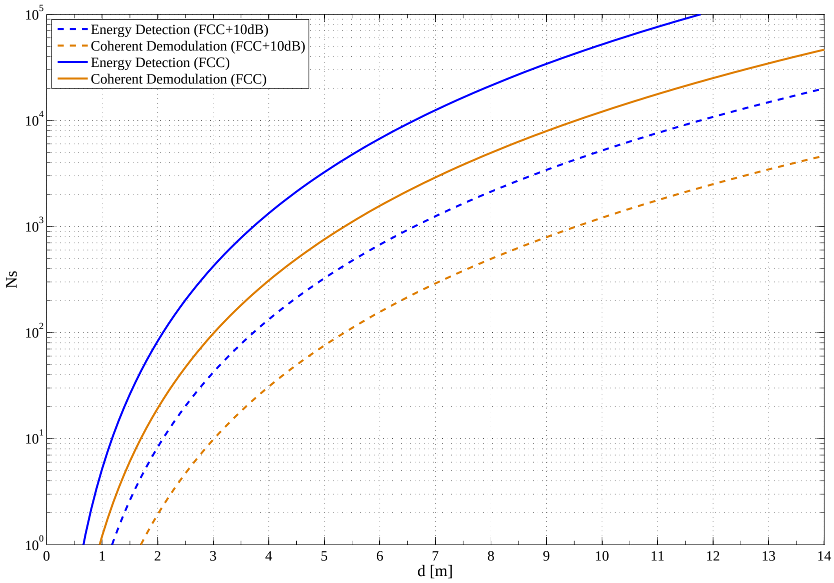

Figure 8.3: Minimum number of pulses per symbol as function of the reader-tag distance.

mask of 10 dB is also reported, as well as the resulting N_{s} coming from a different analysis, specifically from the fulfillment of a requirement of BEP P_{eb} higher of a target $P^*_{\mathrm{eb}} = 10^{-3}$. Considering an ideal MF and AWGN conditions this can be derived from[19]

$$N_{\mathrm{s}} \geq \frac{N_0 P_L(d)}{E_{\mathrm{p}}} \operatorname{erfc}^{-1}\left(2P^*_{\mathrm{eb}}\right)^2 . \tag{8.40}$$

It is possible to notice how the number of minimum pulses per symbol is significantly higher for the receiver here considered. This is mainly due to the fact that the detection process is non-coherent. Moreover, considering that it is important to keep the symbol time not too high in order to ensure a channel static (for clutter removal) and the phase noise constant on a symbol (for clock drift problems), practical values of N_{s} are around 10000. This corresponds to a detection range between 6 and 7 so not satisfactory fore some applications. In this case it can be noticed how an increasing of the transmitting power is high effective for reducing the number of pulses needed.[20] Differently, it is necessary to adopts more sophisticated receivers,

[19]Note that the presented architecture does not allow coherent bit demodulation since it is energy-based. However, sub-optimal hybrid solutions, as for example presented in [299], allow taking advantage of the low-complexity receiver structure here described also allowing bit demodulation provided that symbols are differentially encoded (i.e., with differential binary phase shift keying (DBPSK) modulation at tag side).

[20]Moreover it is possible to adopt antennas with higher gain, but in this case the effective

able to collect the energy from the environmental multipath, and combine it for detection and demodulation purposes. In the following performance analysis we adopt $N_s = 8192$, corresponding to a symbol time $T_s \approx 1\,\text{ms}$.

Tag Code Assignment

For what concerns the code family choice, an interesting possibility for the UWB-RFID system is to adopt *Orthogonal Gold codes* [300]. These codes are exactly orthogonal in the synchronous scenario ($l = 0$) and maintain the properties of extended Gold Codes (low cross-correlation) in the asynchronous scenario. They are constructed by lengthening of one chip the *Preferentially-Phased* Gold codes [301], that present the optimum value -1 of cross-correlation between all the pairs of codewords when aligned. In this manner an even code is obtained enabling the complete clutter cancellation. By using these codewords, the detection procedure is performed in a quasi-orthogonal environment without suffer of interference. The possibility of adopting such a family of codes is very interesting in presence of wake-up offset and possibility of avoiding code acquisition by increasing N_{pc}: since the codes present an orthogonal behavior when aligned, increasing N_{pc} does not causes excessive interference degradation during the detection phase.

8.5.3 Results in Multi-Tags Scenario

In Fig. 8.4, we report the receiver operating characteristic (ROC) corresponding to perfectly synchronous and asynchronous scenarios with ideal code phase retrieving, related to a useful tag placed at 7 m from the reader. We consider 59 interfering tags uniformly distributed in two meters around the useful tag, to reproduce interference effects. In particular, orthogonal Walsh codes in synchronous scenario represent the benchmark, since the interference is completely removed. On the contrary, their performance drastically degrades when the scenario becomes asynchronous. For what extended Gold codes are concerned, obtained by lengthening of one chip the Gold codes without any kind of phase optimization when aligned, they evidence a loss while the scenario is synchronous, but they allow satisfactory detection capabilities also in asynchronous conditions. Orthogonal Gold codes represent instead the best trade-off for both scenarios since they achieve a detection rate higher than 0.8 with a false alarm of 10^{-3} also in the asynchronous scenario, while maintaining the optimal behavior of Walsh codes in perfectly

improvement is given by the antenna gain at receiver side only, since the regulations are imposed on the EIRP. This means that the adoption of a higher gain at transmitting side requires a decrease of the transmitting power of the same amount.

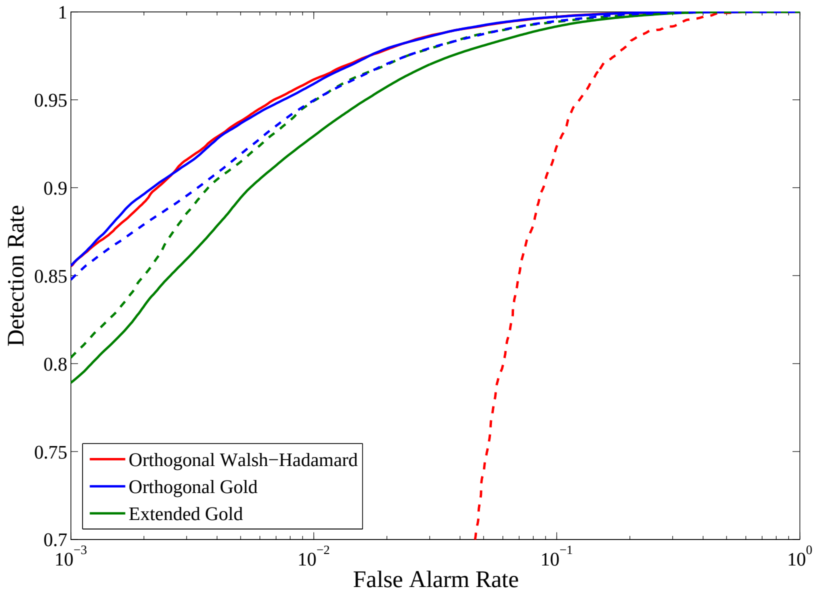

Figure 8.4: ROC for the tag detection in UWB backscatter system. Continuous lines (–) refer to the perfectly synchronous scenario, dashed lines (- -) refer to the asynchronous scenario due the presence of clock drift, with ideal code phase retrieving.

synchronous scenario.

It should be remarked that in this simulation near-far effects are negligible, as all the users were approximately placed at the same distance from the reader. To understand this problem, Fig. 8.5 shows the ROC when the useful tag is placed at 6 m from the reader, and 19 interfering tags are uniformly distributed between 2.8 m and 3.2 m. Orthogonal Gold codes are adopted, a synchronization offset of 500 ns, and a drift of 100 ppm are considered. The 16th bit of the transmitted preamble (a sequence of all '+1') is analyzed for detection purposes and the acquisition window is fixed to $40T_{\mathrm{p}}$ when performing synchronization. As clearly depicted in Fig. 8.5, the system suffers from near-far effects when a constant threshold over all the bins is considered (dashed lines). Thus a possible solution is represented by the adoption of a threshold which accounts for the interference effects, that is, a bin-dependent variable threshold computed such that, in the presence of interference, the PFA is constant for each bin. An empirical approach adopted for simulations considers a threshold reflecting the tag pathloss behavior until the tag energy, evaluated in T_{ED}, falls below the noise floor $N_0 W T_{\mathrm{ED}}$, then fixing the threshold to a constant value for the last bins. Figure 8.5 shows that, when the bin-dependent threshold is adopted (continuous lines), near-far effects are significantly mitigated and a detection rate higher than 0.8 with a false

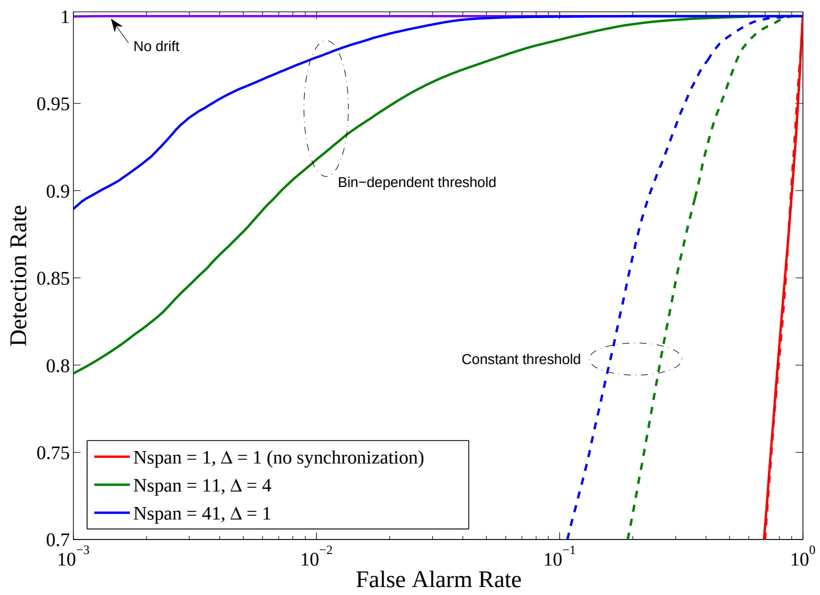

Figure 8.5: ROC for tag detection in presence of synchronization offset, clock drift and near-far interference effects. Continuous lines (–) refer to the bin-dependent threshold, dashed lines (- -) refer to the constant threshold.

alarm of 10^{-3} can be achieved when N_{span} is set to 41 to counteract the clock offset. Vice-versa, adopting $N_{\text{span}} = 11$, a lower detection rate is obtained since the synchronization scheme is less robust for the considered $N_{\text{c}} = 1024$. Fixing $N_{\text{span}} = 1$, that is, without code acquisition, no detection capabilities can be assured even when a bin-dependent threshold is chosen. Further results assessing the performance of the proposed bin-dependent threshold and comparing the effects of different code assignment strategies will be included in a following up publication [37].

8.6 Implementation Issues

We know report several implementation issues to be addressed for the practical realization of the system, as well as solutions to cope with these problems and impairments.

8.6.1 Receiver Dynamic Range

In practical implementation it is important to ensure a correct level of the received signal (both useful and interfering) in order to reduce the possibility of analog-to-digital converter (ADC) saturation or under quantization. For this reason it is important to analyze the characteristics of the signal expected at the reader receiving antenna. The overall signal present at the input of a specific reader is composed of different components:

- The signals backscattered by the tags related to the interrogation of the specific reader itself;
- The signals backscattered by the tags related to the interrogation signal of other readers (i.e., an interference component);
- Other readers direct interference, that is, the ensemble of signals emitted by other readers;
- The clutter, that is the signal emitted by the specific reader and reflected by the environment.

These components must be carefully considered, in order to define the dynamic range at the reader input port and possible issues related to it. For the sake of a complete characterization of the dynamic range, it is important to comprehend if the strongest received signal comes from an interfering reader, or it comes from the reflections of the environment, as well as the ratio between the strongest input signal and the tag backscattered signal (which is supposed to be strongly attenuated from the backscattering two-way channel).

The pathloss related to the different received signals, obtained adopting the free-space propagation model at a single central frequency, can be written as

$$PL^{r-t} = \frac{P_T}{P_R^t} = \left[G_{\mathrm{r}}^2 G_{\mathrm{t}}^2 \left(\frac{\lambda}{4\pi d^{r-t}} \right)^4 \right]^{-1}, \tag{8.41}$$

$$PL^{r-r} = \frac{P_T}{P_R^r} = \left[G_{\mathrm{r}}^2 \left(\frac{\lambda}{4\pi d^{r-r}} \right)^2 \right]^{-1}, \tag{8.42}$$

$$PL^{r-obj} = \frac{P_T}{P_R^{obj}} = \left[\sigma \, G_{\mathrm{r}}^2 \frac{\lambda^2}{(4\pi)^3} \left(\frac{1}{d^{r-t}} \right)^4 \right]^{-1} \tag{8.43}$$

where P_T is the transmitted power, P_R^t, P_R^r and P_R^{obj} are the received powers from tag, reader and objects, respectively, G_{r} the reader antenna gain, G_{t} the tag antenna gain, λ is the wavelength, d^{r-t} is the reader-tag distance, d^{r-r}

is the reader-reader distance.[21] The first term PL^{r-t} accounts for the useful reader-tag-reader backscattering information signal, that is the useful signal component of interest for detection, TOA estimation and packet demodulation. The second term, PL^{r-r} accounts for the direct path coming from an interfering reader: for a localization system we have in fact to deploy a network composed of at least three readers in order to perform trilateration once estimated the reader-tag distances. The last term PL^{r-obj} accounts for one of the clutter components, due to the reflection on a scatter with a radar cross section (RCS) σ (e.g., the object to which the tag is attached). In fact it is supposed that each tag is attached to a bigger object whose reflection properties, characterized by its RCS, could determine the presence of a strong clutter component having the same TOA of the useful signal. In particular, equations (8.41) and (8.43), that represent respectively the pathloss for tag and object backscattering, derive from the well known radar range equation. On the contrary, equation (8.42), that is the interfering signal coming from an other reader, is derived from the well known Friis formula.

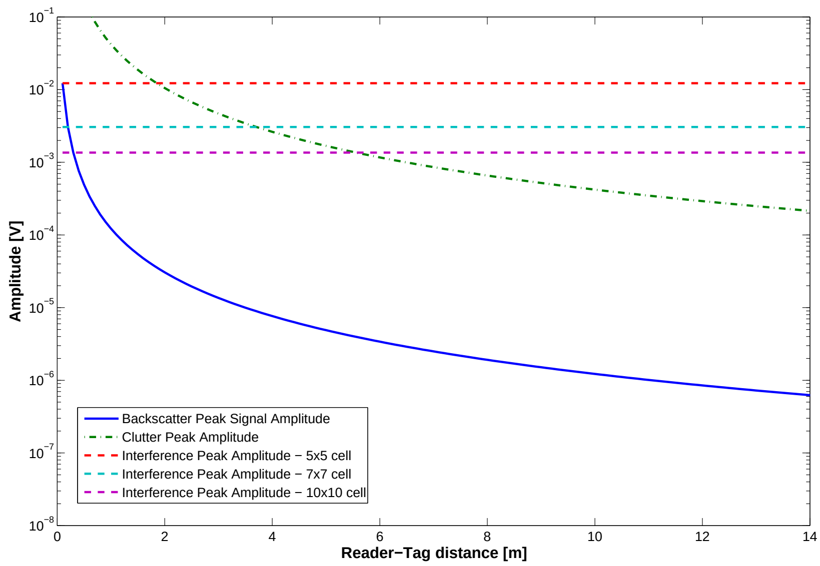

Figure 8.6: Typical dynamic range of a UWB-RFID system.

In Fig. 8.6, the peak of the received signals are reported considering three different reader-reader distances (i.e., three different square cell sizes), an object to which the tag is attached presenting the worst case RCS of a square

[21]For UWB signals all the terms should be characterized as function of the frequency. This is a central-frequency approximation useful for understanding the signal level at the receiver side.

metallic plate of $50 \times 50\,\text{cm}$.[22] The figure illustrates how the maximum received signal is usually the one coming from the opposite reader, depending on the cell dimensions. This means that the strongest signal at the reader input port is, in many situations, determined by the direct interference coming from the opposite reader.

8.6.2 Multi-Reader Interference

As already described, in the UWB-RFID network several readers (e.g., four as in the square cell scenario we are considering) are in charge of monitoring a determined area. It is clear how, in this manner, it is necessary to enable the possibility of accessing the same tag by multiple readers, with a potential problem of inter-reader interference.

For this analysis we consider the square scenario reported in Fig. 6.2 with the four readers placed at the corners of the cell. We now neglect the presence of obstacles, assuming that the greatest interference comes from the opposite reader in case of free-space propagation.[23] Focusing, whitout loss of generality, on the interference generated by Reader 3 (opposite Reader) and received by Reader 1, we can thus foresee three different situations:

1. The interfering signal is reflected (backscattered) by the useful tag (i.e., the tag which Reader 1 wants to detect or demodulate);
2. The direct path (or the multipath) between Reader 3 and Reader 1 (i.e., the already analyzed strongest interfering signal) exists;
3. The interfering signal is reflected by a tag different from the useful one.

We assume that the interrogation signals transmitted by Reader 3 and Reader 1 are generated adopting, respectively, the spreading codes $\left\{d_i^{(3)}\right\}$ and $\left\{d_i^{(1)}\right\}$, and that that the useful and the interfering tags have codes $\left\{c_i^{(u)}\right\}$ and $\left\{c_i^{(int)}\right\}$, respectively. To detect the presence of the useful tag, Reader 1 performs a de-spreading using the composed code $\left\{d_i^{(1)} \cdot c_i^{(u)}\right\}$, according to the procedure that described in detail in Chapter 7 and Sec. 8.4.

[22] Typical system parameters for antennas are accounted in the derivation. See, for a description, Sec. 8.5.1.

[23] In general we can assume a lower level for the interference of the two neighbor readers in the case of partial directive antennas at transmitting and/or receiving stage, while a higher level for the interference coming from the two neighbor readers in case of adoption of omnidirectional antennas.

As anticipated, the direct link between Reader 3 and Reader 1 represents the strongest interfering signal. Considering, in fact, the intended useful tag placed, for example, at the center of the square cell at distance $d = 7\,\mathrm{m}$ from the Reader 1, we have that the received tag backscatter signal scales with d^4, while the interfering Reader 3 direct signal scales with $(2d)^2$. It is immediate from free-space propagation equations (8.41) and (8.42) that the difference in the received power (in dB) between the interfering reader and the useful tag is given by

$$20\log(d) - 20\log\left(\frac{c}{2\pi f_{\mathrm{c}}}\right) \tag{8.44}$$

where c denotes the speed of light and f_{c} the signal central frequency, and where we have adopted, for simplicity, a unitary tag antenna gain. Substituting the value $d = 7\,\mathrm{m}$ we obtain a difference between the two received powers of about 55 dB. If a CDMA-based technique is adopted for readers MAC, even a very small de-spreading residual interference component can completely vanish the possibility of detecting and demodulating a tag signal. Moreover, as seen in Sec. 8.3, readers' code has to fulfill several requirements. In particular, relating to the previously presented three cases, the multi-reader interference is cancelled provided that the following three conditions are satisfied:

1. Cancellation of the multi-reader interference component modulated by the useful tag:

$$\sum_{i=1}^{N_{\mathrm{s}}} d_i^{(1)} c_i^{(u)} d_i^{(3)} c_i^{(u)} = \sum_{i=1}^{N_{\mathrm{s}}} d_i^{(1)} d_i^{(3)} = 0 \tag{8.45}$$

2. Cancellation of the direct reader-reader interference:

$$\sum_{i=1}^{N_{\mathrm{s}}} d_i^{(1)} d_i^{(3)} c_i^{(u)} = 0 \tag{8.46}$$

3. Cancellation of the multi-reader interference component modulated by an other tag:

$$\sum_{i=1}^{N_{\mathrm{s}}} d_i^{(1)} c_i^{(u)} d_i^{(3)} c_i^{(int)} = 0 \tag{8.47}$$

These stringent requirements[24] pose several challenges on readers' codes design, especially for the almost-ideal interference cancellation capability required. Moreover, the cancellation can be obtained by suitable orthogonal

[24]For example, the requirement 3 must be fulfill for all the possible tag sequences since it is necessary to remove the interference due to all the possible tags.

codes, but this fact poses further constraints on the synchronization level that the readers network has to provide.[25]

For this reason it is clear how a CDMA-based readers MAC scheme is critical, and simpler solutions, such as TDMA, have to be accounted at reader side, especially for low-complexity realizations. Specifically, it consists of alternating in a cyclic way the transmitting reader, with the other readers in receiving mode. Adopting TDMA the interference problem coming from other readers is completely avoided.

TDMA can be performed at different rates considering the alternation of the transmitting reader, for example, each symbol or each packet. Decreasing the switching rate between readers (e.g., implementing TDMA at packet level) allows preventing problems deriving from synchronization mismatches, whereas the main drawback is the reduction of the update rate and constraints on the maximum tags' allowed speed, when object tracking is performed.

It is worthwhile to highlight that even the MAC at reader level were TDMA-based, the access from each reader to multiple tags would be still CDMA-based.

8.6.3 Analog-to-Digital Conversion

The main reader functionality is to perform the signal de-spreading in order to detect and demodulate the tag signal, and to ensure the clutter cancellation. In principle this process can be performed in the analog or digital domain, as well as pre or post a matched filtering operation. If the de-spreading is realized in analog (both pre or post matched filtering and sampling), the output signal to be digital converted consists simply of the useful tag contribution and interference residual, as seen in Chapter 7 and Chapter 8. In this case the ADC dynamic can be adjusted on the maximum tag expected signal, considering, for example, a tag as close as much allowed to the reader.

Notice that, when a synchronization scheme is adopted exploiting the direct reader-to-reader UWB signals, or a multistatic WSR capability has to be guarantee, it is necessary to ensure that the interfering reader signal does not saturate the low-noise amplifier (LNA) at receiver side, also if TDMA is adopted as readers MAC. In this case a fixed amplifier gain is sufficient, since the signal amplitude is fixed once the cell size is defined. Vice versa, if readers' synchronization is not performed exploiting the UWB transceivers, multistatic techniques are not adopted, and TDMA is adopted as readers MAC, the input LNA can be designed in order to prevent saturation due to

[25]See Sec. 6.3.2.

the clutter. In this case a variable-gain amplifier (VGA) allows the system operation for different clutter levels of the environment (and different reflecting properties of objects where the tags are attached, in case these can be placed very close to the readers).

The number of quantization levels is then designed, as usual, for ensuring a satisfactory signal-to-quantization-noise ratio (SQNR) for what concerns a tag at the maximum allowed distance. Notice that, in this case, the number of quantization bits is in general higher than for a traditional one-way active communication due to the two-hop channel and its poor link budget.

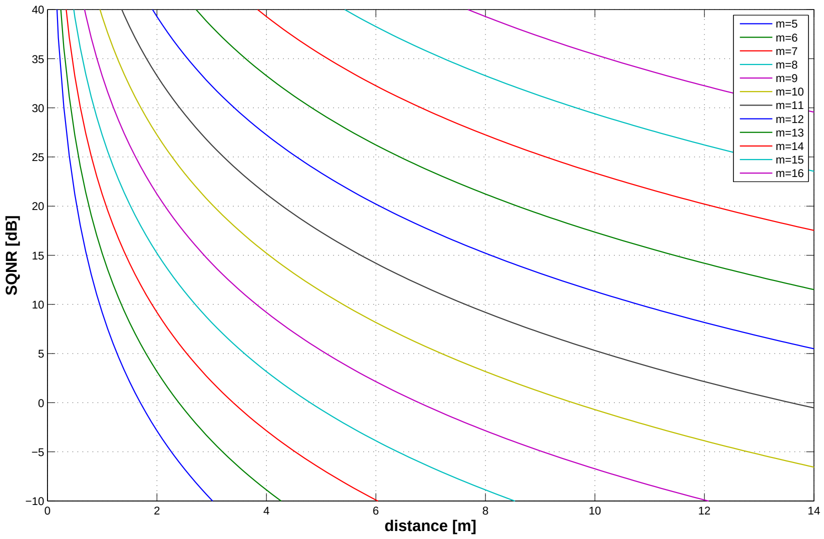

Figure 8.7: SQNR at the ADC output.

However, an analog implementation of the de-spreading process is often too complex for a practical realization, mainly due to the large signal bandwidth, so a digital realization is preferred.[26] In this case the clutter removal is performed on the digital domain so that, now, the ADC dynamic must be adjusted on the maximum expected signal at reader input port, that is, in absence of multi-reader interference, the clutter, as presented in Sec. 8.6.1. Furthermore, if readers synchronization is conducted exploiting UWB signals, as detailed in Sec 6.3.2, or if the reader MAC is CDMA-based, the ADC dynamics must be adjusted on the interfering reader signal amplitude. It is clear that this situation is strongly unfavorable due to the very high dynamic range at input port when a tag is far from the reader. Figure 8.7, as example, presents the SQNR obtained at the output of the ADC which

[26]Moreover, in order to prevent sampling at Nyquist rate, suboptimal techniques, such as the double quadrature receiver proposed in [299] can be adopted.

maximum dynamic is adjusted on the interfering opposite reader signal on a $10 \times 10\,\mathrm{m}$ square cell, as function of the reader-tag distance and for different number of quantization bits m, with $m = \log_2(L)$ and L the number of quantization levels. It is immediate to observe how, in this case, a very high number of bits is necessary in order to provide a satisfactory SQNR, for example a value so that the quantization noise is negligible with respect to the thermal noise. Fortunately, this requirement can be relaxed, by considering the presence of the digital de-spreading process, which can significantly help.

In fact, in Appendix 8.A it is shown that, in presence of low SNR conditions, as the case of the UWB-RFID system for the received tag signal, the process gain is beneficial not only for increasing the effective SNR but also for the SQNR. In particular, if N_s CRs are accumulated at receiver side, both the SNR and the SQNR are enhanced of a factor N_s with respect to the same quantities at the output of the ADC, prior the de-spreading stage. In this manner it is possible to significantly reduce the target SQNR at the output of the ADC, without suffering of quantization noise on the effective de-spreaded signal. The number of quantization bits can be in this manner significantly reduced.

8.7 Conclusion

In this chapter we have presented the UWB-RFID systems based on backscatter modulation, in presence of interference, wake-up synchronization offset and clock drift, considering a practical low-complexity tag detection scheme. Tag detection performance has been evaluated in terms of detection and false alarm probability, to analyze the robustness of different code families in different scenarios. It has been shown that the joint use of orthogonal Gold codes with proper low-complexity detection and code acquisition schemes involving bin-dependent thresholding is a promising solution to overcome implementation impairments and near-far effects. Several implementation issues have been analyzed and possible solutions to cope with problems of dynamic range, A/D conversion and multi reader interference proposed.

8.A Effect of De-Spreading on A/D Conversion

The purpose of this analysis is to derive the relationship between the SQNR at the output of the ADC and of the de-spreader as a function of the number of pulses N_s. Figure 8.8 shows the analyzed ADC and de-spreader, where

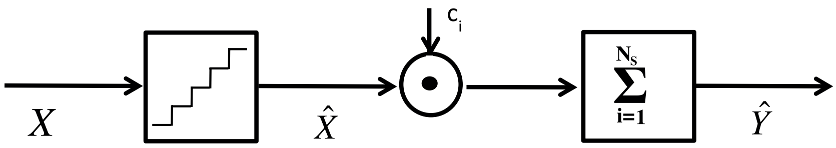

Figure 8.8: The considered scheme for the ADC and de-spreader.

the ADC output is multiplied by the tag code, and then it is accumulated for N_s times.
In particular, we can express the input signal X as:

$$X = x_u + x_c + n_i \tag{8.48}$$

where x_u is the useful signal component, x_c is the clutter/interference component (which mainly affects the upper bound of the dynamic range at the ADC input), and n_i is the additive thermal noise. The useful signal component and the clutter component are assumed uniformly distributed respectively in $[X_{min}, X_{max}]$ and $[-X_{c,max}, X_{c,max}]$, but they are considered both constant within a symbol time.

We can express $\hat{X}$ as

$$\hat{X} = x_u + x_c + n_i + \epsilon_x \tag{8.49}$$

where ϵ_x is the quantization noise error. We assume the quantization noise uniformly distributed in $[0, \delta]$, where δ corresponds to the quantization step amplitude.[27] Now, if we look at the output of the accumulator, we can express $\hat{Y}$ (under the hypothesis of zero mean code) as

$$\hat{Y} = N_\mathrm{s} \cdot x_u + n_{out} + \epsilon_y \tag{8.50}$$

where n_{out} is given by

$$n_{out} = \sum_{i=1}^{N_\mathrm{s}} c_i \cdot n_i \tag{8.51}$$

and c_i represents the i-th chip of the codeword.

The SQNRs $\mathrm{SQNR_{in}}$ and $\mathrm{SQNR_{out}}$, respectively, at the output of the ADC and of the accumulator are:

$$\mathrm{SQNR_{in}} = \frac{\mathbb{E}\left\{x_u^2\right\}}{\mathbb{E}\left\{\epsilon_x^2\right\}} \tag{8.52}$$

[27]Assuming that a sufficient high number of quantization bits is adopted and that the sum of signal and noise is above the quantization step.

and

$$\mathrm{SQNR}_{\mathrm{out}} = \frac{N_{\mathrm{s}}^2 \cdot \mathbb{E}\left\{x_u^2\right\}}{\mathbb{E}\left\{\epsilon_y^2\right\}} \tag{8.53}$$

In the following, we find the relationship between $\mathbb{E}\left\{\epsilon_y^2\right\}$ and $\mathbb{E}\left\{\epsilon_x^2\right\}$. In particular, we can write the second-order moment of ϵ_y as

$$\begin{aligned}
\mathbb{E}\left\{\epsilon_y^2\right\} &= \mathbb{E}\left\{\left(\sum_{i=1}^{N_{\mathrm{s}}} c_i \cdot \epsilon_{x_i}\right)^2\right\} \\
&= \mathbb{E}\left\{\sum_{i=1}^{N_{\mathrm{s}}} c_i^2 \cdot \epsilon_{x_i}^2 + 2 \cdot \sum_{i=1}^{N_{\mathrm{s}}-1} \sum_{j=i+1}^{N_{\mathrm{s}}} c_i \cdot \epsilon_{x_i} \cdot c_j \cdot \epsilon_{x_j}\right\}
\end{aligned} \tag{8.54}$$

We derive now (8.54) for two extreme cases: low SNR (where the thermal noise amplitude is larger than the quantization step and the useful signal amplitude), and high SNR (thermal noise negligible with respect to the useful signal and the quantization step). The first is the condition of interest for the UWB-RFID system, while the second is reported for sake of completeness.

Analysis at low SNR In this case, we can assume that ϵ_{x_i} and ϵ_{x_j} are independent (due to the Gaussian thermal noise), obtaining:

$$\mathbb{E}\left\{2 \cdot \sum_{i=1}^{N_{\mathrm{s}}-1} \sum_{j=i+1}^{N_{\mathrm{s}}} c_i \cdot \epsilon_{x_i} \cdot c_j \cdot \epsilon_{x_j}\right\} = 0 \tag{8.55}$$

and thus we can write

$$\begin{aligned}
\mathbb{E}\left\{\epsilon_y^2\right\} &= \mathbb{E}\sum_{i=1}^{N_{\mathrm{s}}} c_i^2 \cdot \epsilon_{x_i}^2 = \mathbb{E}\left\{\sum_{i=1}^{N_{\mathrm{s}}} c_i^2 \cdot \epsilon_{x_i}^2\right\} \\
&= \sum_{i=1}^{N_{\mathrm{s}}} c_i^2 \cdot \mathbb{E}\left\{\epsilon_{x_i}^2\right\} = N_{\mathrm{s}} \cdot \mathbb{E}\left\{\epsilon_x^2\right\}.
\end{aligned} \tag{8.56}$$

Finally we have the expression:

$$\mathrm{SQNR}_{\mathrm{out}} = \frac{N_{\mathrm{s}}^2 \cdot \mathbb{E}\left\{x_u^2\right\}}{N_{\mathrm{s}} \cdot \mathbb{E}\left\{\epsilon_x^2\right\}} = N_{\mathrm{s}} \cdot \mathrm{SQNR}_{\mathrm{in}} \tag{8.57}$$

where it is evident the processing gain of N_{s} shown also in Fig. 8.9. In the same figure, it is evident how five bits are not sufficient for the quantization, and thus there is no gain in the SQNR.

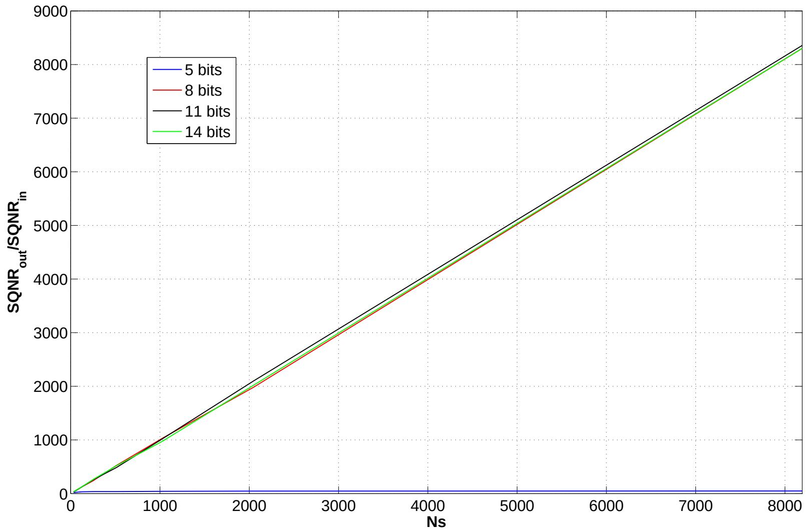

Figure 8.9: SQNR gain after de-spreading and accumulation.

Analysis at high SNR If we assume to work at high SNR, we can neglect n_i with respect to x_u. Consequently, equation (8.55) is no more valid, since ϵ_{x_i} and ϵ_{x_j} are not statistically independent (considering one observed bit, clutter is constant and the useful signal assumes only 2 values). Considering that ϵ_x depends only on the transmitted chip (+1 or -1), we can write (8.54) as:

$$\begin{aligned}\mathbb{E}\left\{\epsilon_y^2\right\} =&\mathbb{E}\left\{\sum_{i=1}^{\frac{N_\mathrm{s}}{2}} c_i^2 \cdot \epsilon_{x_i|+1}^2 + \sum_{i=\frac{N_\mathrm{s}}{2}+1}^{N_\mathrm{s}} c_i^2 \cdot \epsilon_{x_i|-1}^2 + \right. \\ &+2 \cdot \sum_{i=1}^{\frac{N_\mathrm{s}}{2}-1} \sum_{j=i+1}^{\frac{N_\mathrm{s}}{2}} c_i \cdot \epsilon_{x_i|+1} \cdot c_j \cdot \epsilon_{x_i|+1} + \\ &\left. +2 \cdot \sum_{i=\frac{N_\mathrm{s}}{2}+1}^{N_\mathrm{s}-1} \sum_{j=i+1}^{N_\mathrm{s}} c_i \cdot \epsilon_{x_i|-1} \cdot c_j \cdot \epsilon_{x_i|-1} \right\} \\ &= \mathbb{E}\left\{\epsilon_{x|+1}^2 \cdot \left(\sum_{i=1}^{\frac{N_\mathrm{s}}{2}} c_i\right)^2 + \epsilon_{x|-1}^2 \cdot \left(\sum_{i=\frac{N_\mathrm{s}}{2}+1}^{N_\mathrm{s}} c_i\right)^2\right\}\end{aligned} \tag{8.58}$$

where we assumed to have for simplicity a sequence of +1 until $\frac{N_\mathrm{s}}{2}$ and of -1 from $\left(\frac{N_\mathrm{s}}{2}+1\right)$ until N_s, and that $\epsilon_{x_i|+1}$ and $\epsilon_{x_i|-1}$ depends only on the transmitted chip (it means $\epsilon_{x_i|-1} = \epsilon_{x|-1}$ and $\epsilon_{x_i|+1} = \epsilon_{x|+1}$ for any i-th chip. Then we can write

$$\begin{aligned} \mathbb{E}\left\{\epsilon_y^2\right\} &= \mathbb{E}\left\{\left(\frac{N_\mathrm{s}}{2}\cdot\epsilon_{x|+1}\right)^2\right\} + \mathbb{E}\left\{\left(-\frac{N_\mathrm{s}}{2}\cdot\epsilon_{x|-1}\right)^2\right\} \\ &= \frac{N_\mathrm{s}^2}{4}\cdot\mathbb{E}\left\{\epsilon_{x|+1}^2\right\} + \frac{N_\mathrm{s}^2}{4}\cdot\mathbb{E}\left\{\epsilon_{x|-1}^2\right\} = \frac{N_\mathrm{s}^2}{2}\cdot\mathbb{E}\left\{\epsilon_x^2\right\} \end{aligned} \tag{8.59}$$

where

$$\mathbb{E}\left\{\epsilon_x^2\right\} = \frac{1}{2}\mathbb{E}\left\{\epsilon_{x|+1}^2\right\} + \frac{1}{2}\mathbb{E}\left\{\epsilon_{x|-1}^2\right\}. \tag{8.60}$$

We finally obtain the $\mathrm{SQNR_{out}}$ expression as

$$\mathrm{SQNR_{out}} = \frac{N_\mathrm{s}^2\cdot\mathbb{E}\left\{x_u^2\right\}}{\frac{N_\mathrm{s}^2}{2}\cdot\mathbb{E}\left\{\epsilon_x^2\right\}} = 2\cdot\mathrm{SQNR_{in}} \tag{8.61}$$

where no dependence on N_s is present, and the processing gain for the SQNR is 3 dB only.

Chapter 9

Theoretical Bounds on the Localization Accuracy

9.1 Motivations

One of the main motivations supporting the introduction of the UWB-RFID system is related to the possibility of performing, with the same network adopted for identification, high-accuracy localization. The aim of the following derivation is understanding the fundamental limits in the achievable position accuracy with such a kind of network. This provides an insight on how the different system parameters and the readers deployment play a role on the maximum localization performance. Moreover it allows the quantification of the benefits deriving from the exploitation of multistatic techniques for localization, as in WSRs. The comparison is obtained with the position error bound (PEB) introduced in [138] for active localization networks. In particular the derivation is valid not only for the UWB-RFID network object of this thesis, but also for WSR, also refereed to as RSN [287].

9.2 System Model

Both RFID networks and WSR networks are composed of transmitting entities, emitting the signals, tags or targets acting as reflectors, and receiving entities that detect the presence of the reflecting object and estimate the distance starting from the extraction of a feature from the received signal. The proposed performance bound is so applicable to both RFID networks and WSR networks. Due to the analogies in the backscatter processes, in the following we will refer to both tags and targets with the name *objects*.

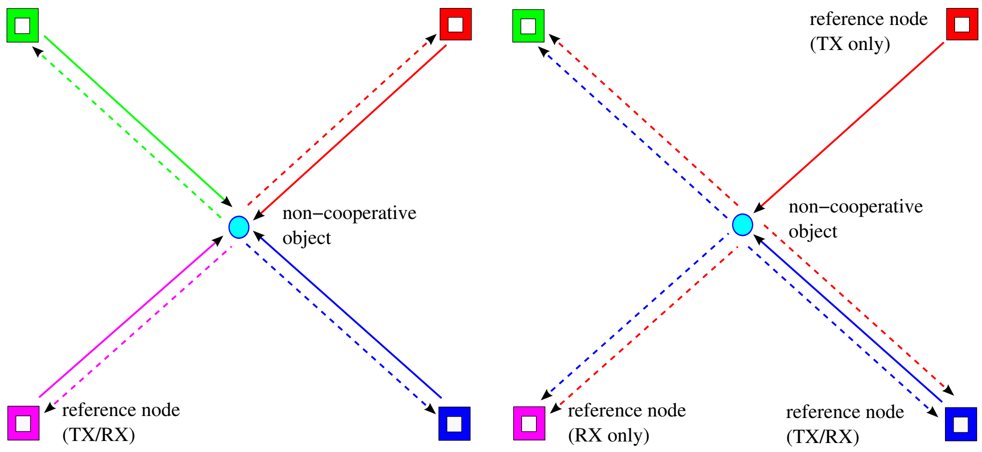

(a) Monostatic (b) Multistatic

Figure 9.1: Network configurations.

With reference to Fig. 9.1, we will analyze two different configurations for what the level of cooperation between reference nodes is regarded:

(a) *Monostatic networks*: N_r transceivers (i.e., co-located transmitters and receivers) are employed in known positions $\mathbf{p}_{\mathrm{R}i} = (x_{\mathrm{R}i}, y_{\mathrm{R}i})$, with $i = 1, 2, \ldots, N_\mathrm{r}$. Each reference node emits an interrogation signal and analyses the corresponding backscattered signals. This is the common operating mode proposed for RFID systems [50]. In this configuration, objects' position estimation is performed by exploiting $N = N_\mathrm{r}$ observations;

(b) *Multistatic networks*: the network is composed of N_t transmitters and N_r receivers located in known positions $\mathbf{p}_{\mathrm{T}j} = (x_{\mathrm{T}j}, y_{\mathrm{T}j})$ and $\mathbf{p}_{\mathrm{R}i} = (x_{\mathrm{R}i}, y_{\mathrm{R}i})$, respectively, with $j = 1, 2, \ldots, N_\mathrm{t}$, and $i = 1, 2, \ldots, N_\mathrm{r}$. Transmitters and receivers can be separated or co-located. Each receiver can potentially receive all the backscattered signals corresponding to the N_t transmitters. In this configuration up to $N = N_\mathrm{t} \times N_\mathrm{r}$ observations are exploited by the network for position estimation.

Hybrid solutions, where a receiver listens to a subset of the transmitted interrogation signals, are possible.[1] We want to underline that the adoption of multistatic RFID is a novelty for this kind of technology where transmitters and receivers are usually co-located [271, 50].

[1]See, as example, the case of one only transmitter and N_r receivers proposed for the WSR in [287].

9.2.1 Ranging Models and Localization

Since TOA estimation affects directly the performance theoretical bound, we define here the model adopted for the ranging error resulting from the processing operated on the de-spreaded signals analyzed in the previous chapters.

We assume tagged objects equipped with antennas presenting an omnidirectional radiation pattern (we neglect the angular dependency of the backscattered signal power) as well as we consider transmitter and receivers equipped with omnidirectional antennas.[2] Moreover, we account for LOS propagation in the distance estimates.[3]

Monostatic Networks

In this case transmitters and receivers are co-located. Since we have $j = i$, for simplicity we drop the index j considering the ranging estimates $r_i(\mathbf{p}_k) = r_{i,i}(\mathbf{p}_k)$. Denote $d_{\mathrm{R}i}$ the distance between the ith reference node and the object, and consider that at least three receivers have detected the target. In ideal conditions (perfect range estimates), object's position $\mathbf{p}_k$ is given by the intersection of circles centered in the reference nodes' positions with radius equal to the reference node-target distance (trilateration).[4]

Each distance measurement $r_i(\mathbf{p}_k)$ is assumed to be Gaussian distributed, that is, $r_i(\mathbf{p}_k) \sim \mathcal{N}(2d_{\mathrm{R}i}, \sigma_i(d_{\mathrm{R}i}))$, with $\sigma_i^2(d_{\mathrm{R}i})$ the estimation variance, which is a function of the target position $\mathbf{p}_k$ [134, 223, 138]. The factor 2 in the mean value accounts for the doubled estimated distance due to the two-hop link. Then, the distance estimation variance can be modeled, for example, according to the CRB, with $\sigma_i^2(d_{\mathrm{R}i}) = \sigma_0^2 d_{\mathrm{R}i}^{2\alpha}$, where σ_0^2 is the variance on ranging error of an object at distance $d_{\mathrm{R}i} = 1\,\mathrm{m}$ from the reference node and α is the pathloss exponent.[5] The exponent 2α accounts so for the two-hop link. This model is also suggested by the behavior of ML TOA estimators, considering the estimation variance as function of the SNR, that is, as function of the signal propagation distance [51].

---

[2]These assumptions can be also easily removed and different reflection behaviors or tag/target random orientations can be accounted for by including, for example, the derived PEB expressions in Monte Carlo simulations.

[3]The derivation can also be extended accounting for biases due to NLOS propagation as in [138].

[4]In presence of distance estimation errors several approaches con be found in the literature [24].

[5]Here and in the following we do not indicate the dependence on $\mathbf{p}_k$ of $d_{\mathrm{R}i}$ and r_i for convenience of notation.

Multistatic Networks

In this case N_t transmitters are present and N_r receivers perform demodulation of the backscatter signals. Denote $d_{\mathrm{T}j}$ the distance of the generic object from the jth transmitter and $d_{\mathrm{R}i}$ the distance from the ith receiver.

Now distance estimates through signal TOA are related to the sum $d_{\mathrm{T}j} + d_{\mathrm{R}i}$. Once this distance is estimated, in ideal conditions object's position can be obtained by the intersection of ellipses with foci on the jth transmitter and on the ith receiver [274]. If the transmitter and receiver are co-located, the ellipse collapses in a circumference as for the monostatic case and thus the position estimation relies on the intersection of both ellipses and circles (in particular, N_r circumferences and $N_\mathrm{r} \times (N_\mathrm{r} - 1)$ ellipses). In this scenario, we still model each distance measurement $r_{i,j}(\mathbf{p}_k)$, related to the ith receiver and the jth transmitter, according to a Gaussian distribution $r_{i,j}(\mathbf{p}_k) \sim \mathcal{N}(d_{\mathrm{T}j} + d_{\mathrm{R}i}, \sigma_{i,j}(d_{\mathrm{T}j}, d_{\mathrm{R}i}))$. The estimation variance can be modeled according to the CRB, with $\sigma^2_{i,j}(d_{\mathrm{T}j}, d_{\mathrm{R}i}) = \sigma_0^2 d^\alpha_{\mathrm{T}j} d^\alpha_{\mathrm{R}i}$, where σ_0^2 is, again, the variance for the distance estimation of an object at distance of 1 m from both the transmitter and the receiver. In this case both $d_{\mathrm{T}j}$ and $d_{\mathrm{R}i}$ are function of $\mathbf{p}_k$.[6]

9.2.2 Ranging Error and System Parameters

In order to compute the PEB it is necessary to model the ranging estimation variance at the reference distance σ_0^2. This can be related directly to system parameters considering the CRB bound of the distance estimator, once the estimator typology is defined. Considering, for example, TOA estimation, the expression for the CRB is [51][7]

$$\sigma_0^2 = \frac{c^2}{8\,\pi^2\,\beta^2\,\mathsf{SNR}_0} \tag{9.1}$$

where SNR_0 is the SNR of the received signal $p(t)$ at the reference distance $d_0 = 1$ m, c is the speed of light, β is the effective bandwidth of $p(t)$ defined in (3.23).

The SNR of the received signal can be obtained considering its PSD, the receiver noise and the number of coherently integrated pulses N_s as [274]

$$\mathsf{SNR}_0 = \frac{N_\mathrm{s} T_\mathrm{p}}{N_0} \int_{f_\mathrm{L}}^{f_\mathrm{U}} \frac{S_\mathrm{t}(f) G_\mathrm{r}^2(f) \sigma(f) c^2}{(4\pi)^3 f^2}\, df \tag{9.2}$$

[6]We do not indicate the dependence on $\mathbf{p}_k$ also of $d_{\mathrm{T}j}$ and $r_{i,j}$ for convenience of notation.

[7]See also (3.22) and Chapter 3.

for untagged objects (i.e., in WSR) and (8.36) considering $d = d_0$ for tagged objects (i.e., in RFID networks), where $S_{\mathrm{t}}(f)$ is the transmitted one-sided PSD, generally imposed by emission masks, $G_{\mathrm{r}}(f)$ is the antenna gain of transmitters and receivers, and f_{L}, f_{U} are, respectively, the lower and upper extreme of the signal bandwidth.

9.3 Localization Performance Bounds

The lower bound on the MSE of any position estimator $\widehat{\mathbf{p}}_k = (\widehat{x}_k, \widehat{y}_k)$ of $\mathbf{p}_k$ that exploits N distance observations[8] $\mathbf{r} = [r_1, r_2, \ldots, r_N]$ is given by the CRB [66][9]

$$\mathbb{E}_{\mathbf{r}} \left\{ (\mathbf{p}_k - \widehat{\mathbf{p}}_k)(\mathbf{p}_k - \widehat{\mathbf{p}}_k)^T \right\} \succeq \mathbf{J}^{-1}(\mathbf{p}_k) \tag{9.3}$$

where $\mathbb{E}_{\mathbf{r}}\{\cdot\}$ is the expectation with respect to the vector $\mathbf{r}$ and $\mathbf{J}(\mathbf{p}_k)$ is the Fisher information matrix (FIM) given by

$$\mathbf{J}(\mathbf{p}_k) = \mathbb{E}_{\mathbf{r}} \left\{ [\nabla_{\mathbf{p}_k} \ln(f(\mathbf{r}|\mathbf{p}_k))][\nabla_{\mathbf{p}_k} \ln(f(\mathbf{r}|\mathbf{p}_k))]^T \right\} \tag{9.4}$$

having indicated with $f(\mathbf{r}|\mathbf{p}_k)$ the p.d.f. of the observation vector $\mathbf{r}$ conditioned on $\mathbf{p}_k$. The PEB is then defined as [138]

$$\mathsf{PEB}(\mathbf{p}_k) \triangleq \sqrt{\mathrm{tr}\{\mathbf{J}^{-1}(\mathbf{p}_k)\}} \tag{9.5}$$

where $\mathrm{tr}\{\cdot\}$ is the trace of a square matrix. Considering the observations as independent we have[10]

$$f(\mathbf{r}|\mathbf{p}_k) = \prod_{i=1}^{N} f_i(r_i|\mathbf{p}_k) \tag{9.6}$$

where $f_i(r_i|\mathbf{p}_k)$ is the p.d.f. of the ith observation conditioned on $\mathbf{p}_k$. Considering that

$$\nabla_{\mathbf{p}_k} \ln(f(\mathbf{r}|\mathbf{p}_k)) = \sum_{i=1}^{N} \frac{1}{f_i(r_i|\mathbf{p}_k)} \begin{bmatrix} \frac{\partial f_i(r_i|\mathbf{p}_k)}{\partial x_k} \\ \frac{\partial f_i(r_i|\mathbf{p}_k)}{\partial y_k} \end{bmatrix} \tag{9.7}$$

[8] In Sec. 9.2 we defined $\mathbf{r}$ as a bidimensional vector for multistatic networks. For simplicity of notation here we consider a one dimensional vector containing all the $N = N_{\mathrm{t}} \times N_{\mathrm{r}}$ elements.

[9] $A \succeq B$ means that $A - B$ is non-negative definite.

[10] This is generically reasonable in the monostatic configuration. For multistatic networks it is still reasonable, for example, adopting the TDMA-based MAC for the N_{t} transmitters, if $N_{\mathrm{t}} > 1$.

we obtain

$$\mathbf{J}(\mathbf{p}_k)=$$
$$\mathbb{E}_{\mathbf{r}}\left\{\sum_{i=1}^{N}\sum_{j=1}^{N}\frac{1}{f_i(r_i|\mathbf{p}_k)}\frac{1}{f_j(r_j|\mathbf{p}_k)}\times\begin{bmatrix}\frac{\partial f_i(r_i|\mathbf{p}_k)}{\partial x_k}\frac{\partial f_j(r_j|\mathbf{p}_k)}{\partial x_k} & \frac{\partial f_i(r_i|\mathbf{p}_k)}{\partial x_k}\frac{\partial f_j(r_j|\mathbf{p}_k)}{\partial y_k}\\ \frac{\partial f_i(r_i|\mathbf{p}_k)}{\partial y_k}\frac{\partial f_j(r_j|\mathbf{p}_k)}{\partial x_k} & \frac{\partial f_i(r_i|\mathbf{p}_k)}{\partial y_k}\frac{\partial f_j(r_j|\mathbf{p}_k)}{\partial y_k}\end{bmatrix}\right\}. \tag{9.8}$$

As showed in [138] all terms in (9.8) for $i \neq j$ are 0 so that

$$\mathbf{J}(\mathbf{p}_k)=\mathbb{E}_{\mathbf{r}}\left\{\sum_{i=1}^{N}\frac{1}{f_i(r_i|\mathbf{p}_k)^2}\times\begin{bmatrix}\left(\frac{\partial f_i(r_i|\mathbf{p}_k)}{\partial x_k}\right)^2 & \frac{\partial f_i(r_i|\mathbf{p}_k)}{\partial x_k}\frac{\partial f_i(r_i|\mathbf{p}_k)}{\partial y_k}\\ \frac{\partial f_i(r_i|\mathbf{p}_k)}{\partial y_k}\frac{\partial f_i(r_i|\mathbf{p}_k)}{\partial x_k} & \left(\frac{\partial f_i(r_i|\mathbf{p}_k)}{\partial y_k}\right)^2\end{bmatrix}\right\}. \tag{9.9}$$

The PEB can be obtained by computing $\mathbf{J}(\mathbf{p}_k)$ using (9.9) for each network configuration, and then according to (9.5).

9.3.1 Monostatic Networks

In order to compute the FIM (9.9) it is necessary to derive the expression of $\frac{\partial f_i(r_i|\mathbf{p}_k)}{\partial x_k}$ and $\frac{\partial f_i(r_i|\mathbf{p}_k)}{\partial y_k}$. Considering that the p.d.f. of the distance estimate results

$$f_i(r_i|\mathbf{p}_k)=\frac{1}{\sqrt{2\pi\sigma_0^2 d_{\mathrm{R}i}^{2\alpha}}}\exp\left\{-\frac{(r_i-2d_{\mathrm{R}i})^2}{2\sigma_0^2 d_{\mathrm{R}i}^{2\alpha}}\right\} \tag{9.10}$$

we obtain

$$\frac{\partial f_i(r_i|\mathbf{p}_k)}{\partial x_k}=\frac{1}{\sqrt{2\pi\sigma_i^2}}\exp\left\{-\frac{\nu_i^2}{2\sigma_i^2}\right\}\left(\frac{\alpha\nu_i^2}{\sigma_i^2 d_{\mathrm{R}i}}+\frac{2\nu_i}{\sigma_i^2}-\frac{\alpha}{d_{\mathrm{R}i}}\right)\left(\frac{\partial}{\partial x_k}d_{\mathrm{R}i}\right), \tag{9.11}$$

$$\frac{\partial f_i(r_i|\mathbf{p}_k)}{\partial y_k}=\frac{1}{\sqrt{2\pi\sigma_i^2}}\exp\left\{-\frac{\nu_i^2}{2\sigma_i^2}\right\}\left(\frac{\alpha\nu_i^2}{\sigma_i^2 d_{\mathrm{R}i}}+\frac{2\nu_i}{\sigma_i^2}-\frac{\alpha}{d_{\mathrm{R}i}}\right)\left(\frac{\partial}{\partial y_k}d_{\mathrm{R}i}\right) \tag{9.12}$$

where $\nu_i=(r_i-2d_{\mathrm{R}i})$. We have also

$$\frac{\partial}{\partial x_k}d_{\mathrm{R}i}=\frac{x_k-x_i}{d_{\mathrm{R}i}}=\cos\theta_i\,, \tag{9.13}$$

$$\frac{\partial}{\partial y_k}d_{\mathrm{R}i}=\frac{y_k-y_i}{d_{\mathrm{R}i}}=\sin\theta_i \tag{9.14}$$

having indicated with θ_i the angle between the object and the ith receiver, measured with respect to the horizontal. We can now rewrite (9.9) as

$$\mathbf{J}(\mathbf{p}_k) = \sum_{i=1}^{N} \Gamma_i(d_{\mathrm{R}i}) \begin{bmatrix} \cos^2\theta_i & \cos\theta_i \sin\theta_i \\ \cos\theta_i \sin\theta_i & \sin^2\theta_i \end{bmatrix} \tag{9.15}$$

where $\Gamma_i(d_{\mathrm{R}i})$ accounts for the expectation in (9.9) and is given by

$$\Gamma_i(d_{\mathrm{R}i}) = \int_{-\infty}^{\infty} \frac{1}{f_i(r_i|\mathbf{p}_k)} g_i^2(\nu_i)\, d\nu_i \tag{9.16}$$

with

$$g_i(\nu_i) = \frac{1}{\sqrt{2\pi\sigma_i^2}} \exp\left\{-\frac{\nu_i^2}{2\sigma_i^2}\right\} \left(\frac{\alpha\nu_i^2}{\sigma_i^2 d_{\mathrm{R}i}} + \frac{2\nu_i}{\sigma_i^2} - \frac{\alpha}{d_{\mathrm{R}i}}\right). \tag{9.17}$$

Substituting (9.17) in (9.16) the integral results

$$\Gamma_i(d_{\mathrm{R}i}) = \frac{4}{\sigma_i^2} + \frac{2\alpha^2}{d_{\mathrm{R}i}^2}. \tag{9.18}$$

Moreover we can rewrite $\mathbf{J}$ in the form

$$\begin{aligned} \mathbf{J}(\mathbf{p}_k) &= \begin{bmatrix} \sum_{i=1}^N J_i^{(1)}(\mathbf{p}_k) & \sum_{i=1}^N J_i^{(2)}(\mathbf{p}_k) \\ \sum_{i=1}^N J_i^{(3)}(\mathbf{p}_k) & \sum_{i=1}^N J_i^{(4)}(\mathbf{p}_k) \end{bmatrix} = \\ &\begin{bmatrix} \sum_{i=1}^N \Gamma_i(d_{\mathrm{R}i}) \cos^2\theta_i & \sum_{i=1}^N \Gamma_i(d_{\mathrm{R}i}) \cos\theta_i \sin\theta_i \\ \sum_{i=1}^N \Gamma_i(d_{\mathrm{R}i}) \cos\theta_i \sin\theta_i & \sum_{i=1}^N \Gamma_i(d_{\mathrm{R}i}) \sin^2\theta_i \end{bmatrix}. \end{aligned} \tag{9.19}$$

The determinant of this matrix is given by

$$\begin{aligned} \det \mathbf{J}(\mathbf{p}_k) = &\left(\sum_{i=1}^N \Gamma_i(d_{\mathrm{R}i}) \cos^2\theta_i\right) \left(\sum_{i=1}^N \Gamma_i(d_{\mathrm{R}i}) \sin^2\theta_i\right) \\ &- \left(\sum_{i=1}^N \Gamma_i(d_{\mathrm{R}i}) \cos\theta_i \sin\theta_i\right)^2. \end{aligned} \tag{9.20}$$

Finally, it is so possible to derive $\mathbf{J}^{-1}$ as

$$\begin{aligned} \mathbf{J}^{-1}(\mathbf{p}_k) &= \frac{1}{\det \mathbf{J}(\mathbf{p}_k)} \\ &\times \begin{bmatrix} \sum_{i=1}^N \Gamma_i(d_{\mathrm{R}i}) \sin^2\theta_i & -\sum_{i=1}^N \Gamma_i(d_{\mathrm{R}i}) \cos\theta_i \sin\theta_i \\ -\sum_{i=1}^N \Gamma_i(d_{\mathrm{R}i}) \cos\theta_i \sin\theta_i & \sum_{i=1}^N \Gamma_i(d_{\mathrm{R}i}) \cos^2\theta_i \end{bmatrix} \end{aligned} \tag{9.21}$$

obtaining for the PEB the expression

$$\mathsf{PEB}(\mathbf{p}_k) =$$
$$\sqrt{\frac{\sum_{i=1}^{N}\Gamma_i(d_{\mathrm{R}i})}{\left(\sum_{i=1}^{N}\Gamma_i(d_{\mathrm{R}i})\cos^2\theta_i\right)\left(\sum_{i=1}^{N}\Gamma_i(d_{\mathrm{R}i})\sin^2\theta_i\right)-\left(\sum_{i=1}^{N}\Gamma_i(d_{\mathrm{R}i})\cos\theta_i\sin\theta_i\right)^2}}. \tag{9.22}$$

This expression is formally equal to the one derived in [138] for active localization networks, with a different expression for the terms in (9.18) characteristic of these passive localization networks.

9.3.2 Multistatic Networks

For convenience of notation we rewrite (9.9) by introducing a double sum accounting for the $N = N_\mathrm{t} \times N_\mathrm{r}$ observations due to the contribution of N_t transmitters and N_r receivers, that is

$$\mathbf{J}(\mathbf{p}_k) = \mathbb{E}_\mathbf{r}\left\{\sum_{i=1}^{N_\mathrm{r}}\sum_{j=1}^{N_\mathrm{t}}\frac{1}{f_{i,j}(r_{i,j}|\mathbf{p}_k)^2}\right.$$
$$\left.\times\begin{bmatrix}\left(\frac{\partial f_{i,j}(r_{i,j}|\mathbf{p}_k)}{\partial x_k}\right)^2 & \frac{\partial f_{i,j}(r_{i,j}|\mathbf{p}_k)}{\partial x_k}\frac{\partial f_{i,j}(r_{i,j}|\mathbf{p}_k)}{\partial y_k}\\ \frac{\partial f_{i,j}(r_{i,j}|\mathbf{p}_k)}{\partial y_k}\frac{\partial f_{i,j}(r_{i,j}|\mathbf{p}_k)}{\partial x_k} & \left(\frac{\partial f_{i,j}(r_{i,j}|\mathbf{p}_k)}{\partial y_k}\right)^2\end{bmatrix}\right\} \tag{9.23}$$

where $f_{i,j}(r_{i,j}|\mathbf{p}_k)$ is given by

$$f_{i,j}(r_{i,j}|\mathbf{p}_k)=\frac{1}{\sqrt{2\pi\sigma_0^2 d_{\mathrm{T}j}^\alpha d_{\mathrm{R}i}^\alpha}}\exp\left\{-\frac{(r_{i,j}-d_{\mathrm{T}j}-d_{\mathrm{R}i})^2}{2\sigma_0^2 d_{\mathrm{T}j}^\alpha d_{\mathrm{R}i}^\alpha}\right\}. \tag{9.24}$$

The partial derivatives in (9.23) can be easily computed obtaining

$$\frac{\partial f_{i,j}(r_{i,j}|\mathbf{p}_k)}{\partial x_k} = \frac{1}{\sqrt{2\pi\sigma_{i,j}^2}}\exp\left\{-\frac{\tilde{\nu}_{i,j}^2}{2\sigma_{i,j}^2}\right\}$$
$$\times\left[\left(\frac{\alpha\tilde{\nu}_{i,j}^2}{2\sigma_{i,j}^2 d_{\mathrm{T}j}}+\frac{\tilde{\nu}_{i,j}}{\sigma_{i,j}^2}-\frac{\alpha}{2d_{\mathrm{T}j}}\right)\left(\frac{\partial}{\partial x_k}d_{\mathrm{T}j}\right)\right.$$
$$\left.+\left(\frac{\alpha\tilde{\nu}_{i,j}^2}{2\sigma_{i,j}^2 d_{\mathrm{R}i}}+\frac{\tilde{\nu}_{i,j}}{\sigma_{i,j}^2}-\frac{\alpha}{2d_{\mathrm{R}i}}\right)\left(\frac{\partial}{\partial x_k}d_{\mathrm{R}i}\right)\right] \tag{9.25}$$

and

$$\frac{\partial f_{i,j}(r_{i,j}|\mathbf{p}_k)}{\partial y_k} = \frac{1}{\sqrt{2\pi\sigma_{i,j}^2}} \exp\left\{-\frac{\tilde{\nu}_{i,j}^2}{2\sigma_{i,j}^2}\right\}$$
$$\times \left[\left(\frac{\alpha\tilde{\nu}_{i,j}^2}{2\sigma_{i,j}^2 d_{\mathrm{T}j}} + \frac{\tilde{\nu}_{i,j}}{\sigma_{i,j}^2} - \frac{\alpha}{2d_{\mathrm{T}j}}\right)\left(\frac{\partial}{\partial y_k} d_{\mathrm{T}j}\right)\right.$$
$$\left. + \left(\frac{\alpha\tilde{\nu}_{i,j}^2}{2\sigma_{i,j}^2 d_{\mathrm{R}i}} + \frac{\tilde{\nu}_{i,j}}{\sigma_{i,j}^2} - \frac{\alpha}{2d_{\mathrm{R}i}}\right)\left(\frac{\partial}{\partial y_k} d_{\mathrm{R}i}\right)\right] \tag{9.26}$$

where $\tilde{\nu}_{i,j} = (r_{i,j} - d_{\mathrm{T}j} - d_{\mathrm{R}i})$. We have also

$$\frac{\partial}{\partial x_k} d_{\mathrm{T}j} = \frac{x_k - x_j}{d_{\mathrm{T}j}} = \cos\phi_j \,, \tag{9.27}$$

$$\frac{\partial}{\partial y_k} d_{\mathrm{T}j} = \frac{y_k - y_j}{d_{\mathrm{T}j}} = \sin\phi_j \tag{9.28}$$

having indicated with ϕ_j the angle between the jth transmitter and the object, measured with respect to the horizontal.

Considering the structure of the matrix $\mathbf{J}(\mathbf{p}_k)$ in (9.23)

$$\mathbf{J}(\mathbf{p}_k) = \begin{bmatrix} J_{1,1}(\mathbf{p}_k) & J_{1,2}(\mathbf{p}_k) \\ J_{2,1}(\mathbf{p}_k) & J_{2,2}(\mathbf{p}_k) \end{bmatrix} \tag{9.29}$$

we obtain the terms

$$J_{1,1}(\mathbf{p}_k) = \sum_{i=1}^{N_\mathrm{r}} \sum_{j=1}^{N_\mathrm{t}} \frac{1}{\sqrt{2\pi\sigma_{i,j}^2}} \int_{-\infty}^{\infty} \exp\left\{-\frac{\tilde{\nu}_{i,j}^2}{2\sigma_{i,j}^2}\right\}$$
$$\times \left(k_{\mathrm{T}j}\cos\phi_j + k_{\mathrm{R}i}\cos\theta_i\right)^2 \, d\tilde{\nu}_{i,j} \,, \tag{9.30}$$

$$J_{2,2}(\mathbf{p}_k) = \sum_{i=1}^{N_\mathrm{r}} \sum_{j=1}^{N_\mathrm{t}} \frac{1}{\sqrt{2\pi\sigma_{i,j}^2}} \int_{-\infty}^{\infty} \exp\left\{-\frac{\tilde{\nu}_{i,j}^2}{2\sigma_{i,j}^2}\right\}$$
$$\times \left(k_{\mathrm{T}j}\sin\phi_j + k_{\mathrm{R}i}\sin\theta_i\right)^2 \, d\tilde{\nu}_{i,j} \,, \tag{9.31}$$

$$J_{1,2}(\mathbf{p}_k) = J_{2,1}(\mathbf{p}_k) = \sum_{i=1}^{N_\mathrm{r}} \sum_{j=1}^{N_\mathrm{t}} \frac{1}{\sqrt{2\pi\sigma_{i,j}^2}} \int_{-\infty}^{\infty} \exp\left\{-\frac{\tilde{\nu}_{i,j}^2}{2\sigma_{i,j}^2}\right\}$$
$$\times \left(k_{\mathrm{T}j}\cos\phi_j + k_{\mathrm{R}i}\cos\theta_i\right)\left(k_{\mathrm{T}j}\sin\phi_j + k_{\mathrm{R}i}\sin\theta_i\right) \, d\tilde{\nu}_{i,j} \tag{9.32}$$

where

$$k_{\mathrm{T}j} = \left(\frac{\alpha \tilde{\nu}_{i,j}^2}{2\sigma_{i,j}^2 d_{\mathrm{T}j}} + \frac{\tilde{\nu}_{i,j}}{\sigma_{i,j}^2} - \frac{\alpha}{2d_{\mathrm{T}j}} \right) \tag{9.33}$$

and

$$k_{\mathrm{R}i} = \left(\frac{\alpha \tilde{\nu}_{i,j}^2}{2\sigma_{i,j}^2 d_{\mathrm{R}i}} + \frac{\tilde{\nu}_{i,j}}{\sigma_{i,j}^2} - \frac{\alpha}{2d_{\mathrm{R}i}} \right). \tag{9.34}$$

The integrals can be solved in closed form, obtaining:

$$\begin{aligned} &J_{1,1}(\mathbf{p}_k) = \\ &\sum_{i=1}^{N_\mathrm{r}} \sum_{j=1}^{N_\mathrm{t}} \left[\left(\frac{1}{\sigma_{i,j}^2} + \frac{\alpha^2}{2d_{\mathrm{T}j}^2} \right) \cos^2 \phi_j + \left(\frac{1}{\sigma_{i,j}^2} + \frac{\alpha^2}{2d_{\mathrm{R}i}^2} \right) \cos^2 \theta_i \right. \\ &\left. + \left(\frac{2}{\sigma_{i,j}^2} + \frac{\alpha^2}{d_{\mathrm{T}j} d_{\mathrm{R}i}} \right) \cos \phi_j \cos \theta_i \right], \end{aligned} \tag{9.35}$$

$$\begin{aligned} &J_{2,2}(\mathbf{p}_k) = \\ &\sum_{i=1}^{N_\mathrm{r}} \sum_{j=1}^{N_\mathrm{t}} \left[\left(\frac{1}{\sigma_{i,j}^2} + \frac{\alpha^2}{2d_{\mathrm{T}j}^2} \right) \sin^2 \phi_j + \left(\frac{1}{\sigma_{i,j}^2} + \frac{\alpha^2}{2d_{\mathrm{R}i}^2} \right) \sin^2 \theta_i \right. \\ &\left. + \left(\frac{2}{\sigma_{i,j}^2} + \frac{\alpha^2}{d_{\mathrm{T}j} d_{\mathrm{R}i}} \right) \sin \phi_j \sin \theta_i \right], \end{aligned} \tag{9.36}$$

$$\begin{aligned} &J_{1,2}(\mathbf{p}_k) = J_{2,1}(\mathbf{p}_k) = \sum_{i=1}^{N_\mathrm{r}} \sum_{j=1}^{N_\mathrm{t}} \left[\left(\frac{1}{\sigma_{i,j}^2} + \frac{\alpha^2}{2d_{\mathrm{T}j}^2} \right) \cos \phi_j \sin \phi_j \right. \\ &+ \left(\frac{1}{\sigma_{i,j}^2} + \frac{\alpha^2}{2d_{\mathrm{R}i}^2} \right) \cos \theta_i \sin \theta_i \\ &\left. + \left(\frac{1}{\sigma_i^2} + \frac{\alpha^2}{2d_{\mathrm{T}j} d_{\mathrm{R}i}} \right) \sin (\phi_j + \theta_i) \right]. \end{aligned} \tag{9.37}$$

We can now compute the PEB as

$$\mathsf{PEB}(\mathbf{p}_k) = \sqrt{\frac{J_{1,1}(\mathbf{p}_k) + J_{2,2}(\mathbf{p}_k)}{\det \mathbf{J}(\mathbf{p}_k)}}. \tag{9.38}$$

Notice that if the jth transmitter is co-located with the ith receiver (i.e., $i = j$, so with $d_{\mathrm{T}j} = d_{\mathrm{R}i}$ and $\phi_j = \theta_i$) we have that the ith contributions in (9.35), (9.36) and (9.37) degenerates, as expected, into the FIM elements already derived in (9.19).

9.4 Case Studies

We present, as case study, results in terms of the PEB derived in Sec. 9.3, related to TOA-based UWB-RFID localization. First we report, in Sec. 9.4.1, the system parameters considered in simulations necessary to determine the ranging error at reference distance σ_0^2. Numerical evaluation of the PEB has been carried out in a square cell of $(20 \times 20)\,\mathrm{m}^2$, with 4 reference nodes placed at the corners if not differently specified. Specifically, 5 different configurations are analyzed, showing as first the PEB in the 2D scenario (Sec. 9.4.2), and then the performance in terms of LEO (Sec. 9.4.3).

9.4.1 System Parameters

We consider a symbol composed of $N_\mathrm{s} = 8192$ pulses[11] with PRP $T_\mathrm{p} = 200\,\mathrm{ns}$. Transmitters and receivers have an antenna gain $G_\mathrm{r} = 2\,\mathrm{dBi}$, while tags are equipped with an antenna with gain $G_\mathrm{t} = 1\,\mathrm{dBi}$.[12] The backscattering modulation loss due to the presence of the switch in the tag is $L_\mathrm{t} = 2\,\mathrm{dB}$. The transmitted signal, adopting RRC pulses with pulse width parameter $T_\mathrm{w} = 1\,\mathrm{ns}$, roll-off factor $\nu = 0.6$, center frequency $f_\mathrm{c} = 4\,\mathrm{GHz}$, is compliant with the IEEE 802.15.4a emission mask in the $3.2-4.7\,\mathrm{GHz}$. The pathloss coefficient and the receiver noise figure are, respectively, $\alpha = 2$ and $F = 4\,\mathrm{dB}$.

9.4.2 PEB in the 2D Scenario

Here we report the PEB mapped in the cell for each analyzed configuration. Note that we assume the same omnidirectional antennas for each case, while these can be optimized for any specific configuration.

Configuration #1. Figure 9.2 presents the PEB contour plot in the 2D scenario adopting a monostatic configuration. It is interesting to notice the presence of a wide central area where the localization error is almost constant to values close to 40 cm, which is quite interesting for many potential applications.

Configuration #2. Figure 9.3 reports the PEB considering an ideal multistatic configuration, where each receiver is able to process the signal emitted by each transmitter. In this case the localization performance is obviously significantly improved with respect to the monostatic configuration, and the error presents a different distribution in the 2D scenario. The best perfor-

[11] This is a typical value for the number of pulses per symbol [37].
[12] We neglect frequency dependence as first approximation.

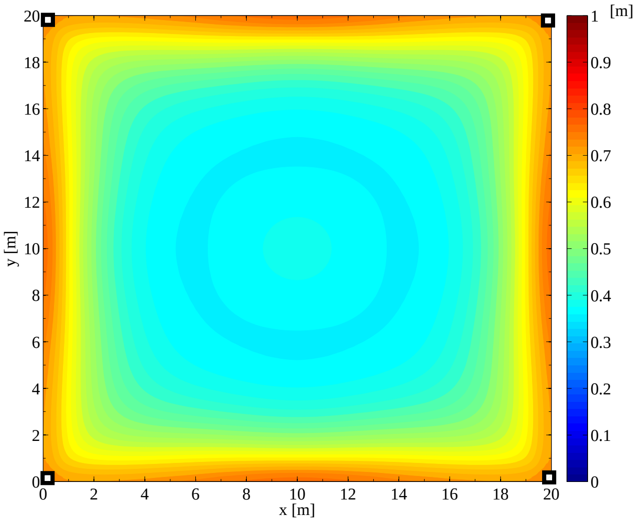

Figure 9.2: Configuration #1. PEB considering 4 reference nodes (transceivers) at the corners (monostatic).

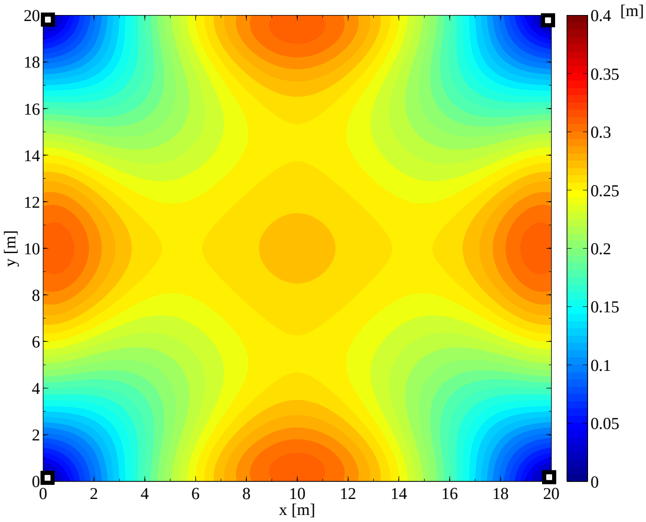

Figure 9.3: Configuration #2. PEB considering 4 reference nodes (transceivers) at the corners, each processing the signals of every transmitter (multistatic).

mance is guarantee in the areas close to the reference nodes.[13]

Configuration #3. A different configuration is examined in Fig. 9.4, where

[13]Note that in this figure the scale is limited in the interval $[0 - 0.4]$ m for a better visualization.

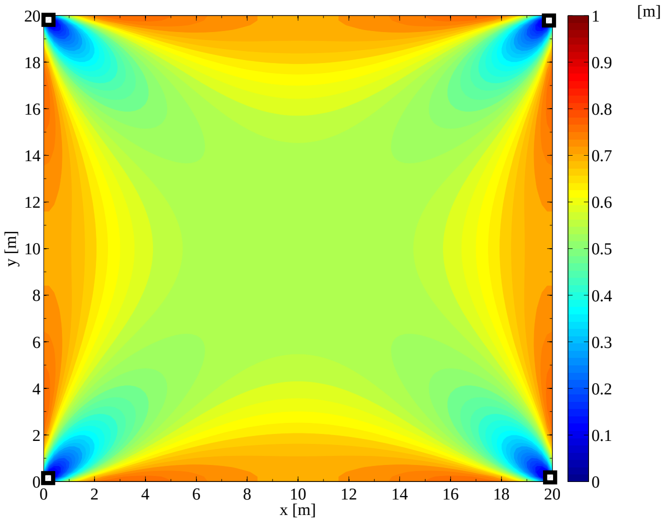

Figure 9.4: Configuration #3. PEB considering 2 transmitters in $[0, 0]$, $[20, 20]$, and 2 receivers in $[20, 0]$, $[0, 20]$ (multistatic).

two transmitters are placed in $[0, 0]$ and $[20, 20]$, and two receivers in the other two corners with coordinates $[20, 0]$ and $[0, 20]$. Each receiver processes the signal of both the transmitters, and the best coverage is again in the areas close to the reference nodes. Moreover, it is interesting to notice that there is no distinction, for what concern the localization capability, if a tagged object is close to a transmitter or to a receiver. The performance is in general worse than that in configurations #1 and #2 mainly because the number of transmitter and receivers is halved.

Configurations $\#4 - 5$. Other two multistatic configurations, with only one transmitter and 4 receivers, are investigated in Fig. 9.5 and Fig. 9.6. In configuration #4 the transmitter is co-located with the receiver in $[0, 0]$, whereas in configuration #5 the transmitter is placed in the center of the monitored area in $[10, 10]$. As will be quantified in the next section, configuration #5 is particularly attractive when a good compromise between the number of transmitters/receivers and localization coverage is desired.

9.4.3 Localization Error Outage

In order to compare the different topologies from the quantitative point of view, we now analyze the performance in terms of LEO. In particular, the LEO is defined as the probability that the expected localization accuracy, where the expectation is taken over all the possible time instants and lo-

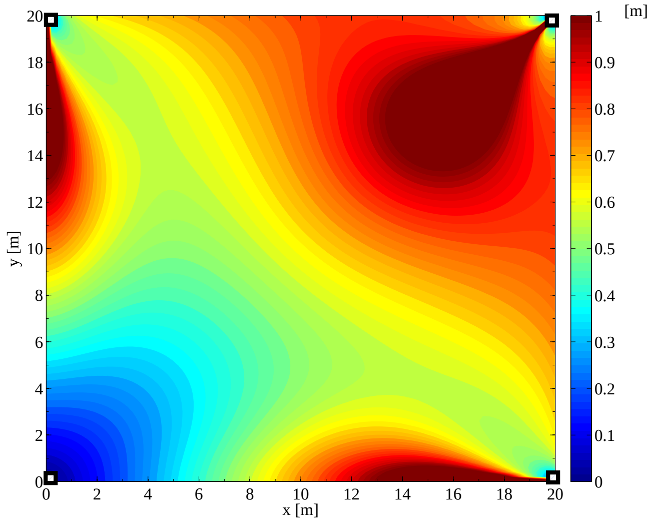

Figure 9.5: Configuration #4. PEB considering 1 transmitter, in $[0, 0]$, and 4 receivers at the corners (multistatic).

cations, does not satisfy a threshold accuracy level ϵ [52, 28]. Figure 9.7 reports the LEO as function of the target localization accuracy ϵ and for the different configurations investigated in Sec. 9.4.2. It is possible to notice how the multistatic configuration #2 with 4 transmitters and receivers ensures the highest performance in terms of outage achieving a target localization accuracy $< 30\,\text{cm}$ in almost all the locations of the area. The monostatic configuration #1 represents a trade-off among the investigated configurations, but cannot guarantee an error lower than about 35 cm in any location when our system parameters are considered. The adoption of more directive antennas can be an interesting solution for this specific case.

Differently, if we take into account configurations which employ a number of transmitters lower than 4, configuration #5 represents an interesting solution which guarantees performance close to that of configuration #2 with the advantage of a less power consuming network.

It is important to underline that the previous result did not account for the effective network localization update rate, that is the frequency at which the network is able to refresh the position estimate of a certain target object [52]. In fact, considering a network adopting N_t transmitters working with a TDMA-based MAC, to guarantee the absence of mutual interference between transmitters, a new target location estimate is available after a time not less than $N_\text{p}N_\text{s}N_\text{t}$ seconds, that is, the time to transmit N_t ranging packets each one composed of $N_\text{p}N_\text{s}$ pulses. If now we assume to work with a network

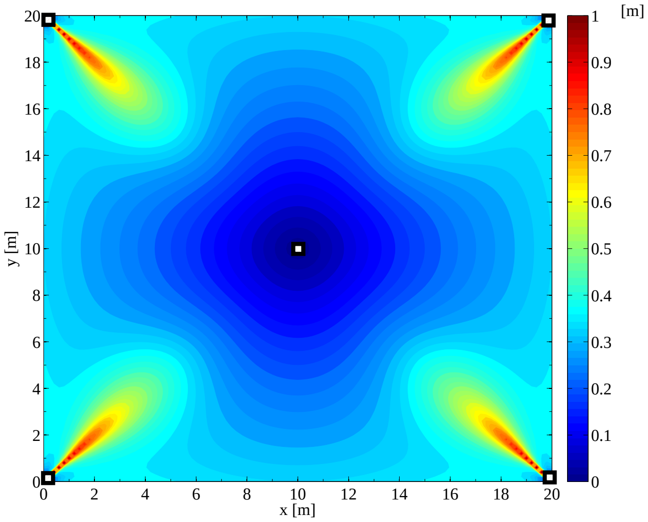

Figure 9.6: Configuration #5. PEB considering 1 transmitter in [10, 10], and 4 receivers at the corners (multistatic).

composed of a lower number of transmitters, as in configurations $\#3-5$, the same localization update rate can be guaranteed considering a symbol with a higher number of pulses N_s.[14] The corresponding increase of the effective SNR exploited by the receivers leads to a performance improvement. For a fair comparison between configurations, Fig. 9.8 shows the LEO considering the same setting as in Fig. 9.7, where results are obtained at constant update rate, that is, by considering $N_s = 2 \times 8192$ for configuration #3 and $N_s = 4 \times 8192$ for configurations $\#4 - 5$. In this setting, it is interesting to see how the multistatic configuration #5, with one only transmitter placed at the center of the cell, is able to outperform also the multistatic case #2 with 4 co-located transmitters and receivers. Moreover, all multistatic configurations outperform the monostatic configuration #1.

It has to be remarked that results provided so far are related to performance bounds which serve as benchmarks for any practical localization estimator as well as useful tools for identifying the best network deployment topology and configuration once the parameters are set as in Sec. 9.4.1. In practical setting, other issues must be taken into account, such as reference nodes synchronization, especially in multistatic configurations, and not omni-directional and frequency dependent object RCS. Reference nodes antennas gain and directivity play also an important role in the performance evaluation that needs to be investigated.

[14] We consider the ranging packet composed of a fixed number of symbols.

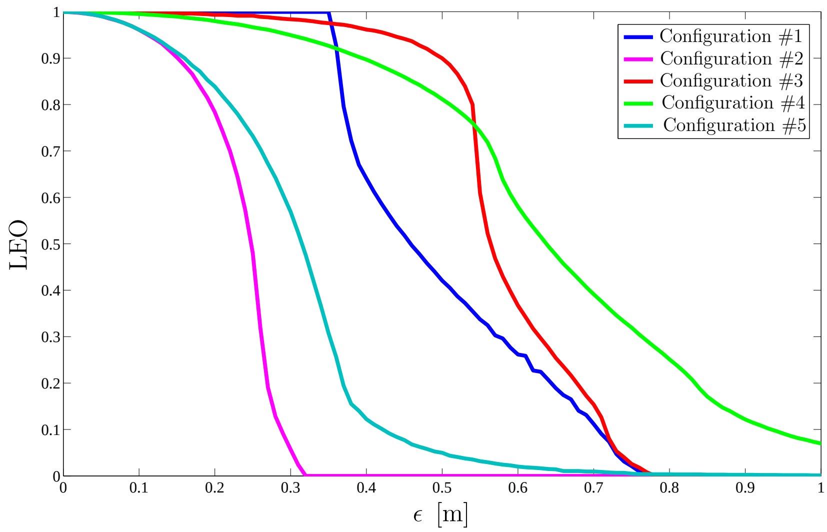

Figure 9.7: Localization error outage for different network configurations.

9.5 Conclusions

In this chapter theoretical bounds on the localization accuracy for non-cooperative objects (tagged and untagged) have been derived for monostatic and multistatic network configurations. These bounds are quite general and allow the investigation of the localization performance as a function of system parameters, network topology and configuration. The case studies analyzed have shown how the developed analytical framework is useful in identifying the best network topologies and configurations that maximize the localization coverage.

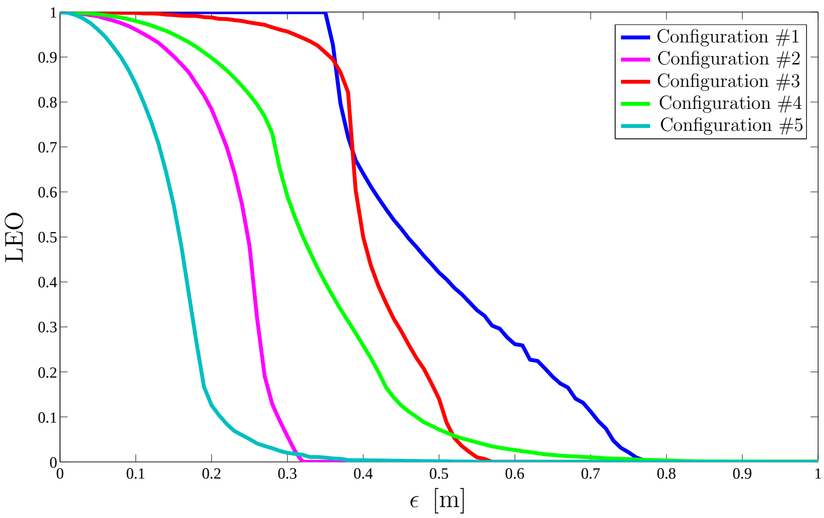

Figure 9.8: Localization error outage for different network configurations when fixing the localization update rate.

Conclusions

This thesis covered different topics related to *context-aware wireless networks*, that are networks capable to adapt their behavior to the context and to the application, thanks to the possibility of enabling communication, sensing and localization, even considering active nodes and/or (semi-)passive nodes (i.e., nodes not equipped with transmitters). Problems of signals demodulation, signal parameters estimation and localization have been addressed. In particular low complexity solutions for demodulation and time-of-arrival (TOA) estimation, also adopting ultrawide-band (UWB) signals, have been investigated. The localization problem has been addressed from a practical point of view, introducing solutions to cope with non-line-of-sight (NLOS) channel conditions. Novel radio-frequency identification (RFID) technologies have been investigated as case-study of context-aware wireless networks. Analytical methods have been exploited to derive theoretical bounds and analyze, in closed form, the performance of the proposed techniques. Experimentation has been adopted for characterizing the performance of real networks and to develop algorithms starting from real measured signals. Practical techniques and ad-hoc system designs have been devised to deal with implementation issues or demand of low-complexity realizations.

Specifically, in Chapter 1 a new blind method for the determination of the integration time in non-coherent UWB receivers has been proposed. It is based on information theoretic criteria (ITC) for model order selection problems, and it does not require any a priori knowledge or explicit features estimation from the propagation environment, as usual assumed with other techniques. This allows exploiting part of the multipath channel diversity without adopting complex receiver architectures. In Chapter 2 novel non-coherent receiver structures, called stop-and-go (SaG) receivers, have been introduced and analyzed. This SaG strategy, based on energy detection, can be adopted with transmitted-reference (TR)-autocorrelation receivers (AcRs) or energy detector receivers (EDRs), and it is able to further improve the signal demodulation performance with respect to conventional receivers in clustered multipath channels, also in presence of synchronization errors. Moreover different optimization techniques, requiring different complexity and enabling different receiver performance, have been proposed and characterized, providing closed-form expressions for the receiver bit error probability (BEP).

In Chapter 3 the problem of time delay estimation (TDE) (or TOA estimation) has been addressed from a theoretical point of view. This process is the key feature enabling network localization based on ranging measurements. Even if this issue has been widely investigate in the literature, no significant theoretical analyses are available in case of partial or no knowledge of the received signal waveform available. Along this direction, new fundamental bounds on TDE have been derived for different conditions, in particular in the case the received signal is partially known or totally unknown at receiver side, as often occurs in practice due to multipath propagation or due to the need of considering low-complexity estimators. Practical estimators, such as energy-based estimators, have been revised in the context of the novel theoretical derivation, and their performance compared with the new bounds. This comparison has highlighted how the new bounds are very tight for all SNRs of interest, providing a new design method previously not available due to the impossibility of defining the Cramér-Rao bound (CRB) in the case of unknown signals. Thanks to the presented derivation the estimator performance can be, in fact, characterized analytically. The obtained results represent also a more general outcome with applications to different signal processing problems involving audio processing, source localization, and synchronization.

In Chapter 4 an experimentation methodology for the characterization of cooperative localization networks in realistic indoor environments has been introduced. In the same chapter practical algorithms able to improve the accuracy in NLOS channel conditions have been proposed and tested on measurement databases realized during the experimentation. In particular it has been shown using experimental data how it is possible to detect the presence of LOS and NLOS channel conditions by a proper processing of the received waveform, and how this information, as well as the prior knowledge of the environment map, can improve the localization accuracy. With the purpose of enhancing the localization coverage seriously compromised by the presence of NLOS channel conditions, in Chapter 5 the idea of non-regenerative relaying for network localization has been introduced. A system analysis has been presented and ad hoc position estimation techniques, accounting for the presence of relay nodes in the network, have been devised. The case studies investigated have highlighted the significant localization coverage improvement achievable in NLOS conditions using the proposed low complexity relaying scheme.

In Chapter 6 the concept of UWB-RFID systems for detecting and locating semi-passive tags based on backscatter modulation has been introduced as example of context-aware wireless network. Performance analysis for what concerns signal demodulation in ideal conditions and with ideal hardware has been presented in Chapter 7, to assess the system feasibility. A deep study involving low-complexity receiver structures and with hardware constraints has been provided in Chapter 8. Specifically, receiver architectures able to work in realistic conditions and capable to deal with problems related to multi-tag interference, synchronization mismatches and clock drift have been introduced and characterized in terms of performance. Moreover the main design challenges and practical solutions for implementation concerning receiver dynamic range, A/D conversion, synchronization and multiple access have been investigated. Finally, theoretical bounds on the localization accuracy of RFID-UWB systems have been derived in Chapter 9. These bounds are useful to characterize not only the RFID-UWB network from the point of view of the localization accuracy, but can be also applied to other passive localization networks such wireless sensor radars (WSRs). In particular the behavior of different network configurations can be described, allowing the characterization of monostatic, bistatic and multistatic networks.

Several issues investigated in this thesis are under extension for further publications. In particular, for what concerns the problem of TDE, the introduction of non-idealities on the signal model, such as fading and interference effects will be considered in the future in the analysis of theoretical bounds. This allows describing in analytic form the behavior of non-coherent TOA estimators in presence of these effects. The introduction of the same non-idealities can be considered for deriving the BEP expressions characterizing the SaG receivers proposed in Chapter 2. In the field of location-awareness, novel experimental campaigns, started from the work carried out at MIT, are in preparation in order to test different localization algorithms in different operating scenarios under a common database. Moreover the feasibility of the relaying scheme will be proved with experimental measurements in realistic propagation conditions, in cooperation with CEA-LETI, a partner of the European project SELECT. The different components of the UWB-RFID system and the signal processing tasks introduced and analyzed are currently under development and a proof of concept of the feasibility of this system will be provided in the following months within the European project SELECT. The framework developed so far for passive localization can represent a starting point for further investigations on localization networks involving active and passive tags or offering WSR functionalities in conjunction with multistatic approaches. Finally, as introduced in Chapter 6, multistatic techniques can be investigated in the UWB-RFID system not only for tags localization, but also for enhanced detection and robust tag to reader communication.

Bibliography

[1] C. Floerkemeier, M. Langheinrich, E. Fleisch, F. Mattern, and S. E. Sarma, Eds., *The Internet of Things.* Springer, March. 2008.

[2] A. Iera, C. Floerkemeier, J. Mitsugi, and G. Morabito, “The Internet of Things,” *IEEE Wireless Communications*, vol. 17, no. 6, pp. 8 –9, Dec. 2010.

[3] J. Zheng, D. Simplot-Ryl, C. Bisdikian, and H. Mouftah, “The Internet of Things,” *IEEE Commun. Mag.*, vol. 49, no. 11, pp. 30 –31, Nov. 2011.

[4] K. Finkenzeller, *RFID Handbook: Fundamentals and Applications in Contactless Smart Cards and Identification.* Wiley, 2004.

[5] M. Weiser, “The computer for the 21st century,” *Scientific American*, vol. 265, no. 3, pp. 94–104, 1991.

[6] B. Schilit, N. Adams, and R. Want, “Context-aware computing applications,” in *First Workshop on Mobile Computing Systems and Applications.* IEEE, 1994, pp. 85–90.

[7] G. Chen and D. Kotz, “A survey of context-aware mobile computing research,” Technical Report TR2000-381, Dept. of Computer Science, Dartmouth College, Tech. Rep., 2000.

[8] V. Pejovic and E. Belding, “A context-aware approach to wireless transmission adaptation,” in *8th Annual IEEE Communications Society Conference on Sensor, Mesh and Ad Hoc Communications and Networks (SECON).* IEEE, 2011, pp. 592–600.

[9] A. Wood, J. Stankovic, G. Virone, L. Selavo, Z. He, Q. Cao, T. Doan, Y. Wu, L. Fang, and R. Stoleru, “Context-aware wireless sensor networks for assisted living and residential monitoring,” *IEEE Network*, vol. 22, no. 4, pp. 26–33, 2008.

[10] M. Covington, P. Fogla, Z. Zhan, and M. Ahamad, "A context-aware security architecture for emerging applications," in *18th Annual Computer Security Applications Conference*. IEEE, 2002, pp. 249–258.

[11] H. van Kranenburg, M. Bargh, S. Iacob, and A. Peddemors, "A context management framework for supporting context-aware distributed applications," *IEEE Communications Magazine*, vol. 44, no. 8, pp. 67–74, 2006.

[12] D. Bottazzi, A. Corradi, and R. Montanari, "Context-aware middleware solutions for anytime and anywhere emergency assistance to elderly people," *IEEE Communications Magazine*, vol. 44, no. 4, pp. 82–90, 2006.

[13] H. Pung, T. Gu, W. Xue, P. Palmes, J. Zhu, W. Ng, C. Tang, and N. Chung, "Context-aware middleware for pervasive elderly homecare," *IEEE Journal on Selected Areas in Communications*, vol. 27, no. 4, pp. 510–524, 2009.

[14] A. Krause, A. Smailagic, and D. Siewiorek, "Context-aware mobile computing: Learning context-dependent personal preferences from a wearable sensor array," *IEEE Transactions on Mobile Computing*, vol. 5, no. 2, pp. 113–127, 2006.

[15] Z. Yu, X. Zhou, Z. Yu, D. Zhang, and C. Chin, "An OSGi-based infrastructure for context-aware multimedia services," *IEEE communications Magazine*, vol. 44, no. 10, pp. 136–142, 2006.

[16] A. Smailagic and D. Kogan, "Location sensing and privacy in a context-aware computing environment," *IEEE Wireless Communications*, vol. 9, no. 5, pp. 10–17, 2002.

[17] T. Kanter, "Hottown, enabling context-aware and extensible mobile interactive spaces," *IEEE Wireless Communications*, vol. 9, no. 5, pp. 18–27, 2002.

[18] P. Bellavista, A. Corradi, and C. Giannelli, "A unifying perspective on context-aware evaluation and management of heterogeneous wireless connectivity," *IEEE Communications Surveys & Tutorials*, vol. 13, no. 3, pp. 337–357, 2011.

[19] K. Rehman, F. Stajano, and G. Coulouris, "An architecture for interactive context-aware applications," *IEEE Pervasive Computing*, vol. 6, no. 1, pp. 73–80, 2007.

[20] M. van Sinderen, A. van Halteren, M. Wegdam, H. Meeuwissen, and E. Eertink, "Supporting context-aware mobile applications: an infrastructure approach," *IEEE Communications Magazine*, vol. 44, no. 9, pp. 96–104, 2006.

[21] J. Garcia-luna aceves, M. Mosko, I. Solis, R. Braynard, and R. Ghosh, "Context-aware protocol engines for ad hoc networks," *IEEE Communications Magazine*, vol. 47, no. 2, pp. 142–149, 2009.

[22] P. Makris, D. Skoutas, and C. Skianis, "A survey on context-aware mobile and wireless networking: On networking and computing environments' integration," 2012.

[23] B. Schilit, D. Hilbert, and J. Trevor, "Context-aware communication," *IEEE Wireless Communications*, vol. 9, no. 5, pp. 46–54, 2002.

[24] D. Dardari, E. Falletti, and M. Luise, *Satellite and Terrestrial Radio Positioning Techniques - A signal processing perspective.* Elsevier Ltd, London, 2011.

[25] N. Decarli, A. Giorgetti, D. Dardari, and M. Chiani, "Blind integration time determination for UWB transmitted reference receivers," in *Proc. IEEE Global Telecomm. Conf.*, Dec. 2011, pp. 1 –5.

[26] N. Decarli, A. Giorgetti, D. Dardari, M. Chiani, and M. Z. Win, "Stop-and-go receivers for non-coherent UWB communication," *IEEE Trans. Wireless Commun.*, 2013, submitted.

[27] N. Decarli, D. Dardari, and M. Win, "Bounds on time-delay estimation of partially known and unknown signals," 2013, in preparation.

[28] A. Conti, M. Guerra, D. Dardari, N. Decarli, and M. Z. Win, "Network experimentation for cooperative localization," *IEEE J. Select. Areas Commun.*, vol. 30, no. 2, pp. 467–475, Feb. 2012.

[29] N. Decarli, D. Dardari, S. Gezici, and A. D'Amico, "LOS/NLOS detection for UWB signals: a comparative study using experimental data," in *IEEE International Symposium on Wireless Pervasive Computing (ISWPC 2010)*, Modena, Italy, May 2010.

[30] D. Dardari, N. Decarli, A. Guerra, and A. Conti, "Enhanced localization coverage with non-regenerative UWB relays," in *20th European Signal Processing Conference (EUSIPCO)*, Bucharest, Romania, Aug. 2012.

[31] N. Decarli, A. Guerra, A. Conti, R. D'Errico, A. Sibille, and D. Dardari, "Non-regenerative relaying for network localization," *IEEE Trans. Wireless Commun.*, 2013, submitted.

[32] N. Decarli, F. Guidi, A. Conti, and D. Dardari, "Interference and clock drift effects in UWB RFID systems using backscatter modulation," in *IEEE International Conference on Ultra-Wideband, ICUWB 2012*, Syracuse, USA, Sep. 2012, pp. 1–5.

[33] F. Guidi, N. Decarli, D. Dardari, C. Roblin, and A. Sibille, "Performance of UWB backscatter modulation in multi-tag RFID scenario using experimental data," in *IEEE International Conference on Ultra-Wideband, ICUWB 2011*, Bologna, Italy, Sep. 2011, pp. 1–5.

[34] R. D'Errico, M. Bottazzi, F. Natali, E. Savioli, S. Bartoletti, A. Conti, D. Dardari, N. Decarli, F. Guidi, F. Dehmas, L. Ouvry, U. Alvarado, N. Hadaschik, C. Franke, Z. Mhanna, M. Sacko, Y. Wei, and A. Sibille, "An UWB-UHF semi-passive RFID system for localization and tracking applications," in *IEEE International Conference on RFID-Technologies and Applications (RFID-TA)*, Nov. 2012, pp. 18 –23.

[35] N. Decarli and D. Dardari, "RFID and radar localization: A position error bound analysis," in *Proc. IEEE Int. Conf. on Commun.*, Jun. 2013.

[36] E. Savioli, M. Bottazzi, F. Natali, N. Decarli, F. Guidi, N. Hadaschik, R. D'Errico, and L. Ouvry, "Semi-passive UHF-UWB RFID: Architecture and localization performance," in *Proc. IEEE Int. Conf. on Commun.*, Jun. 2013.

[37] F. Guidi, N. Decarli, S. Bartoletti, A. Conti, and D. Dardari, "Robust detection of UWB backscatter signals in multi-tag environments," 2013, in preparation.

[38] N. Decarli, F. Guidi, and D. Dardari, "A novel joint RFID and radar sensor network for passive localization: Design and performance bounds," *IEEE J. Sel. Topics in Signal Processing*, 2013, submitted.

[39] "EUWB D2.2.2; Interference identification algorithms," Mar. 2010.

[40] "EUWB D2.4.2; Interference mitigation techniques algorithms," Jul. 2010.

[41] "NEWCOM DRB.4; Final report: seamless positioning techniques in wireless communications," Dec. 2011.

[42] "SELECT D2.1.1; Backscatter propagation modeling: interim report," Jul. 2011.

[43] "SELECT D2.2.1; Signal processing techniques: interim report," Jul. 2011.

[44] "SELECT D2.3.1; Multi-functional network design: intermediate system specification," Sep. 2011.

[45] "SELECT D2.2.2; Signal processing techniques: final report," Apr. 2012.

[46] "SELECT D2.3.2; Multi-functional network design: final system specification," Jun. 2012.

[47] M. Z. Win and R. A. Scholtz, "Impulse radio: How it works," *IEEE Commun. Lett.*, vol. 2, no. 2, pp. 36–38, Feb. 1998.

[48] ——, "Ultra-wide bandwidth time-hopping spread-spectrum impulse radio for wireless multiple-access communications," *IEEE Trans. Commun.*, vol. 48, no. 4, pp. 679–691, Apr. 2000.

[49] M. Win, D. Dardari, A. Molisch, W. Wiesbeck, and J. Zhang, "History and applications of UWB," *Proc. IEEE*, vol. 97, no. 2, pp. 198 –204, Feb. 2009.

[50] D. Dardari, R. D'Errico, C. Roblin, A. Sibille, and M. Z. Win, "Ultrawide bandwidth RFID: The next generation?" *Proceedings of the IEEE, Special Issue on RFID - A Unique Radio Innovation for the 21st Century.*, vol. 98, no. 9, pp. 1570 –1582, Sep. 2010.

[51] D. Dardari, A. Conti, U. Ferner, A. Giorgetti, and M. Win, "Ranging with ultrawide bandwidth signals in multipath environments," *Proceedings of the IEEE*, vol. 97, no. 2, pp. 404 –426, Feb. 2009.

[52] M. Z. Win, A. Conti, S. Mazuelas, Y. Shen, W. M. Gifford, D. Dardari, and M. Chiani, "Network localization and navigation via cooperation," *IEEE Commun. Mag.*, vol. 49, no. 5, pp. 56–62, May 2011.

[53] M. Z. Win and R. A. Scholtz, "On the robustness of ultra-wide bandwidth signals in dense multipath environments," *IEEE Commun. Lett.*, vol. 2, no. 2, pp. 51–53, Feb. 1998.

[54] ——, "On the energy capture of ultra-wide bandwidth signals in dense multipath environments," *IEEE Commun. Lett.*, vol. 2, no. 9, pp. 245–247, Sep. 1998.

[55] ——, "Characterization of ultra-wide bandwidth wireless indoor communications channel: A communication theoretic view," *IEEE J. Select. Areas Commun.*, vol. 20, no. 9, pp. 1613–1627, Dec. 2002, .

[56] D. Cassioli, M. Z. Win, and A. F. Molisch, "The ultra-wide bandwidth indoor channel: from statistical model to simulations," *IEEE J. Select. Areas Commun.*, vol. 20, no. 6, pp. 1247–1257, Aug. 2002.

[57] A. Molisch, "Ultra-wide-band propagation channels," *Proc. IEEE*, vol. 97, no. 2, pp. 353 –371, Feb. 2009.

[58] M. Win, G. Chrisikos, and N. Sollenberger, "Performance of RAKE reception in dense multipath channels: implications of spreading bandwidth and selection diversity order," *IEEE J. Select. Areas Commun.*, vol. 18, no. 8, pp. 1516 –1525, Aug. 2000.

[59] V. Lottici, A. D'Andrea, and U. Mengali, "Channel estimation for ultra-wideband communications," *IEEE J. Select. Areas Commun.*, vol. 20, no. 9, pp. 1638–1645, Dec. 2002.

[60] K. Witrisal, G. Leus, G. Janssen, M. Pausini, F. Troesch, T. Zasowski, and J. Romme, "Noncoherent ultra-wideband systems," *IEEE Signal Processing Magazine*, vol. 26, no. 4, pp. 48 –66, Jul. 2009.

[61] J. G. Proakis, *Digital Communications*, 4th ed. New York, NY, 10020: McGraw-Hill, Inc., 2001.

[62] D. Torrieri, *Principles of Spread Spectrum Communication Systems.* Springer, 2005.

[63] A. F. Molisch, *Wireless Communications*, 1st ed. Piscataway, New Jersey, 08855-1331: IEEE Press, J. Wiley and Sons, 2005.

[64] J. J. Stiffler, *Theory of Synchronous Communications*, 1st ed. Englewood Cliffs, New Jersey 07632: Prentice-Hall, 1971.

[65] B. Sklar, *Digital communications: fundamentals and applications*, ser. Prentice Hall Communications Engineering and Emerging Technologies Series. Prentice-Hall PTR, 2001.

[66] H. L. V. Trees, *Detection, Estimation, and Modulation Theory: Part I*, 2nd ed. New York, NY: John Wiley & Sons, Inc., 2001.

[67] C. K. Rushforth, "Transmitted-reference techniques for random or unknown channels," *IEEE Trans. Inform. Theory*, vol. 10, pp. 39 – 42, Jan. 1964.

[68] A. Polydoros and K. T. Woo, "LPI detection of frequency-hopping signals using autocorrelation techniques," *IEEE J. Select. Areas Commun.*, vol. 3, no. 5, pp. 714 – 726, Sep. 1985.

[69] J. D. Choi and W. E. Stark, "Performance of ultra-wideband communications with suboptimal receivers in multipath channels," *IEEE J. Select. Areas Commun.*, vol. 20, no. 9, pp. 1754–1766, Dec. 2002.

[70] Y.-L. Chao and R. A. Scholtz, "Ultra-wideband transmitted reference systems," *IEEE Trans. Veh. Technol.*, vol. 54, no. 5, pp. 1556–1569, Sep. 2005.

[71] S. Niranjayan and N. Beaulieu, "General performance analysis of TR UWB systems," *IEEE Trans. Wireless Commun.*, vol. 7, no. 12, pp. 5268 –5277, Dec. 2008.

[72] T. Q. S. Quek, M. Z. Win, and D. Dardari, "Unified analysis of UWB transmitted-reference schemes in the presence of narrowband interference," *IEEE Trans. Wireless Commun.*, vol. 6, no. 6, pp. 2126–2139, Jun. 2007.

[73] A. Rabbachin, T. Quek, P. Pinto, I. Oppermann, and M. Win, "Noncoherent UWB communication in the presence of multiple narrowband interferers," *IEEE Trans. Wireless Commun.*, vol. 9, no. 11, pp. 3365 –3379, Nov. 2010.

[74] T. Jia and D. I. Kim, "Multiple access performance of balanced UWB transmitted-reference systems in multipath," *IEEE Trans. Wireless Commun.*, vol. 7, no. 3, pp. 1084 –1094, Mar. 2008.

[75] D. Goeckel and Q. Zhang, "Slightly frequency-shifted reference ultra-wideband (UWB) radio," *IEEE Transactions on Communications*, vol. 55, no. 3, pp. 508 –519, Mar. 2007.

[76] A. D'amico and U. Mengali, "Code-multiplexed UWB transmitted-reference radio," *IEEE Transactions on Communications*, vol. 56, no. 12, pp. 2125 –2132, Dec. 2008.

[77] X. Dong, L. Jin, and P. Orlik, "A new transmitted reference pulse cluster system for UWB communications," *IEEE Trans. Veh. Technol.*, vol. 57, no. 5, pp. 3217 –3224, Sep. 2008.

[78] T. Quek, M. Win, and D. Dardari, "Unified analysis of UWB transmitted-reference schemes in the presence of narrowband interference," *IEEE Transactions on Wireless Communications*, vol. 6, no. 6, pp. 2126 –2139, Jun. 2007.

[79] S. Franz and U. Mitra, "Integration interval optimization and performance analysis for UWB transmitted reference systems," in *International Workshop on Ultra Wideband Systems, 2004.*, May 2004, pp. 26 – 30.

[80] Y.-L. Chao, "Optimal integration time for UWB transmitted reference correlation receivers," in *Conference Record of the Thirty-Eighth Asilomar Conference on Signals, Systems and Computers, 2004.*, vol. 1, 2004, pp. 647 – 651.

[81] M. Nemati, U. Mitra, and R. Scholtz, "Optimum integration time for UWB transmitted reference and energy detector receivers," in *IEEE Military Communications Conference, 2006. MILCOM 2006.*, 2006.

[82] C.-H. Hsieh, W-D.Wu, and C.-C. Chao, "Optimal channel energy capture for ultra-wideband transmitted reference systems in clustered channels," in *IEEE Wireless Communications and Networking Conference (WCNC), 2010*, 2010, pp. 1 –6.

[83] Y. Na and M. Saquib, "Analysis of the channel energy capture in ultra-wideband transmitted reference systems," *IEEE Transactions on Communications*, vol. 55, no. 2, pp. 262 –265, 2007.

[84] R. Zhang and X. Dong, "Synchronization and integration region optimization for UWB signals with non-coherent detection and auto-correlation detection," *IEEE Transactions on Communications*, vol. 56, no. 5, pp. 790 –798, May 2008.

[85] L. Jin, X. Dong, and Z. Liang, "Integration interval determination algorithms for ber minimization in UWB transmitted reference pulse cluster systems," *IEEE Transactions on Wireless Communications*, vol. 9, no. 8, pp. 2408 –2414, 2010.

[86] H. Urkowitz, "Energy detection of unknown deterministic signals," *Proceedings of the IEEE*, vol. 55, no. 4, pp. 523 – 531, 1967.

[87] P. Stoica and Y. Selen, "Model-order selection: a review of information criterion rules," *IEEE Signal Processing Mag.*, vol. 21, no. 4, pp. 36–47, 2004.

[88] M. Chiani and M. Win, "Estimating the number of signals observed by multiple sensors," in *2nd International Workshop on Cognitive Information Processing (CIP), 2010.* IEEE, 2010, pp. 156–161.

[89] A. Giorgetti and M. Chiani, "A new approach to time-of-arrival estimation based on information theoretic criteria," in *IEEE Int. Conf. on Ultra-Wideband (ICUWB 2011*, Bologna, Italy, Sep. 2011, pp. 1–5.

[90] K. M. L. Saxena and K. Alam, "Estimation of the non-centrality parameter of a Chi squared distribution," *The Annals of Statistics*, vol. 10, no. 3, pp. 1012–1016, 1982.

[91] H. Bozdogan, "Model selection and Akaike's information criterion (AIC): The general theory and its analytical extensions," *Psychometrika*, vol. 52, no. 3, pp. 345–370, 1987.

[92] A. Molisch, K. Balakrishnan, D. Cassioli, C.-C. Chong, S. Emami, A. Fort, J. Karedal, J. Kunisch, H. Schantz, U. Schuster, and K. Siwiak, "IEEE 802.15.4a channel model - final report," 2005.

[93] M. Sahin, I. Guvenc, and H. Arslan, "Optimization of energy detector receivers for UWB systems," in *IEEE 61st Vehicular Technology Conference, 2005. VTC 2005-Spring*, vol. 2, Jun. 2005, pp. 1386 – 1390.

[94] F. Wang, Z. Tian, and B. Sadler, "Weighted energy detection for noncoherent ultra-wideband receiver design," *IEEE Trans. Wireless Commun.*, vol. 10, no. 2, pp. 710 –720, Feb. 2011.

[95] A. D'Amico, U. Mengali, and E. Arias-de Reyna, "Energy-detection UWB receivers with multiple energy measurements," *IEEE Transactions on Wireless Communications*, vol. 6, no. 7, pp. 2652 –2659, Jul. 2007.

[96] G. Leus and A.-J. van der Veen, "A weighted autocorrelation receiver for transmitted reference ultra wideband communications," in *IEEE 6th Workshop on Signal Processing Advances in Wireless Communications*, Jun. 2005, pp. 965 – 969.

[97] J. Wu, H. Xiang, and Z. Tian, "Weighted noncoherent receivers for UWB PPM signals," *IEEE Communications Letters*, vol. 10, no. 9, pp. 655 –657, sept. 2006.

[98] D. Mu and Z. Qiu, "Weighted non-coherent energy detection receiver for UWB OOK systems," in *9th International Conference on Signal Processing, 2008. ICSP 2008*, Oct. 2008, pp. 1846 –1849.

[99] J. Romme and K. Witrisal, "Transmitted-reference UWB systems using weighted autocorrelation receivers," *IEEE Transactions on Microwave Theory and Techniques*, vol. 54, no. 4, pp. 1754 – 1761, Jun. 2006.

[100] D. Dardari, A. Giorgetti, M. Chiani, T. Quek, and M. Win, "A stop-and-go transmitted-reference UWB receiver," in *IEEE International Conference on Ultra-Wideband*, Sep. 2006, pp. 309 –314.

[101] T. Quek and M. Win, "Ultrawide bandwidth transmitted-reference signaling," in *IEEE International Conference on Communications*, vol. 6, Jun. 2004, pp. 3409 – 3413.

[102] ——, "Analysis of UWB transmitted-reference communication systems in dense multipath channels," *IEEE J. Select. Areas Commun.*, vol. 23, no. 9, pp. 1863 – 1874, 2005.

[103] A. D'Amico, U. Mengali, and L. Taponecco, "Synchronization for differential transmitted reference UWB receivers," *IEEE Trans. Wireless Commun.*, vol. 6, no. 11, pp. 4154 –4163, Nov. 2007.

[104] S. Franz, C. Carnonelli, and U. Mitra, "Joint semi-blind channel and timing estimation for generalized UWB transmitted reference systems," *IEEE Trans. Wireless Commun.*, vol. 6, no. 1, pp. 180 –191, Jan. 2007.

[105] A. F. Molisch, "Ultrawideband propagation channels-theory, measurements, and modeling," *IEEE Trans. Veh. Technol.*, vol. 54, no. 5, pp. 1528–1545, Sep. 2005.

[106] M. Abramowitz and I. A. Stegun, *Handbook of Mathematical Functions wih Formulas, Graphs, and Mathematical Tables.* Washington, D.C.: United States Department of Commerce, 1970.

[107] S. Dubouloz, B. Denis, S. de Rivaz, and L. Ouvry, "Performance analysis of LDR UWB non-coherent receivers in multipath environments," in *IEEE International Conference on Ultra-Wideband, 2005.*, Sep. 2005.

[108] H. Akaike, "A new look at the statistical model identification," *IEEE Trans. Automat. Contr.*, vol. 19, no. 6, pp. 716–723, Dec. 1974.

[109] J. Rissanen, "Modeling by shortest data description," *Automatica*, vol. 14, no. 5, pp. 465–471, 1978.

[110] A. Giorgetti and M. Chiani, "Time-of-arrival estimation based on information theoretic criteria," *IEEE Trans. on Signal Processing*, 2013.

[111] A. Mariani, A. Giorgetti, and M. Chiani, "Effects of noise power estimation on energy detection for cognitive radio applications," *IEEE Trans. Commun.*, vol. 59, no. 12, pp. 3410 –3420, Dec. 2011.

[112] G. Schwarz, "Estimating the dimension of a model," *The annals of statistics*, vol. 6, no. 2, pp. 461–464, 1978.

[113] "IEEE standard for information technology - telecommunications and information exchange between systems - local and metropolitan area networks - specific requirement part 15.4: Wireless medium access control (MAC) and physical layer (PHY) specifications for low-rate wireless personal area networks (WPANs)," *IEEE Std 802.15.4a-2007 (Amendment to IEEE Std 802.15.4-2006)*, pp. 1–203, 2007.

[114] A. F. Molisch, D. Cassioli, C.-C. Chong, S. Emami, A. Fort, B. Kannan, J. Karedal, J. Kunisch, H. Schantz, K. Siwiak, and M. Z. Win, "A comprehensive standardized model for ultrawideband propagation channels," *IEEE Trans. Antennas Propagat.*, vol. 54, no. 11, pp. 3151–3166, Nov. 2006, Special Issue on Wireless Communications.

[115] G. Carter, "Coherence and time delay estimation," *Proceedings of the IEEE*, vol. 75, no. 2, pp. 236–255, 1987.

[116] A. J. Weiss and E. Weinstein, "Fundamental limitations in passive time delay estimation - part I: Narrow-band systems," *IEEE Trans. Acoust., Speech, Signal Processing*, vol. ASP-31, no. 2, pp. 472–486, Apr. 1983.

[117] J. P. Iannello, "Large and small error performance limits for multipath time delay estimation," *IEEE Trans. Acoust., Speech, Signal Processing*, vol. ASSP-34, no. 2, pp. 245–251, Apr. 1986.

[118] J. Li and R. Wu, "An efficient algorithm for time delay estimation," *IEEE Trans. Signal Processing*, vol. 46, no. 8, pp. 2231–2235, Aug. 1998.

[119] T. Manickam, R. Vaccaro, and D. Tufts, "A least-squares algorithm for multipath time-delay estimation," *IEEE Trans. Signal Processing*, vol. 42, no. 11, pp. 3229–3233, 1994.

[120] J. Stuller and N. Hubing, "New perspectives for maximum likelihood time-delay estimation," *IEEE Transactions on Signal Processing*, vol. 45, no. 3, pp. 513–525, 1997.

[121] G. Jacovitti and G. Scarano, "Discrete time techniques for time delay estimation," *IEEE Transactions on Signal Processing*, vol. 41, no. 2, pp. 525–533, 1993.

[122] B. Sadler and R. Kozick, "A survey of time delay estimation performance bounds," in *Fourth IEEE Workshop on Sensor Array and Multichannel Processing*. IEEE, 2006, pp. 282–288.

[123] K. Gedalyahu and Y. Eldar, "Time-delay estimation from low-rate samples: A union of subspaces approach," *IEEE Transactions on Signal Processing*, vol. 58, no. 6, pp. 3017–3031, 2010.

[124] C. Knapp and G. Carter, "The generalized correlation method for estimation of time delay," *IEEE Transactions on Acoustics, Speech and Signal Processing*, vol. 24, no. 4, pp. 320–327, 1976.

[125] J. Krolik, M. Eizenman, and S. Pasupathy, "Time delay estimation of signals with uncertain spectra," *IEEE Transactions on Acoustics, Speech and Signal Processing*, vol. 36, no. 12, pp. 1801–1811, 1988.

[126] B. Yegnanarayana, S. Prasanna, R. Duraiswami, and D. Zotkin, "Processing of reverberant speech for time-delay estimation," *IEEE Transactions on Speech and Audio Processing*, vol. 13, no. 6, pp. 1110–1118, 2005.

[127] H. Urkowitz, C. Hauer, and J. Koval, "Generalized resolution in radar systems," *Proceedings of the IRE*, vol. 50, no. 10, pp. 2093–2105, 1962.

[128] M. Zakai and J. Ziv, "On the threshold effect in radar range estimation (corresp.)," *IEEE Transactions on Information Theory*, vol. 15, no. 1, pp. 167–170, 1969.

[129] G. Carter, "Time delay estimation for passive sonar signal processing," *IEEE Transactions on Acoustics, Speech and Signal Processing*, vol. 29, no. 3, pp. 463–470, 1981.

[130] A. Tajer, G. Jajamovich, X. Wang, and G. Moustakides, "Optimal joint target detection and parameter estimation by MIMO radar," *IEEE Journal of Selected Topics in Signal Processing*, vol. 4, no. 1, pp. 127–145, 2010.

[131] B. Friedlander, "An efficient parametric technique for doppler-delay estimation," *IEEE Transactions on Signal Processing*, vol. 60, no. 8, pp. 3953–3963, 2012.

[132] C. Carbonelli and U. Mengali, "Synchronization algorithms for UWB signals," *IEEE Transactions on Communications*, vol. 54, no. 2, pp. 329 – 338, Feb. 2006.

[133] C. Carbonelli, U. Mengali, and U. Mitra, "Synchronization and channel estimation for UWB signal," in *IEEE Global Telecommunications Conference, GLOBECOM*, vol. 2, Dec. 2003, pp. 764 – 768 Vol.2.

[134] S. Gezici, Z. Tian, G. B. Giannakis, H. Kobayashi, A. F. Molisch, H. V. Poor, and Z. Sahinoglu, "Localization via ultra-wideband radios: a look at positioning aspects for future sensor networks," *IEEE Signal Processing Mag.*, vol. 22, pp. 70–84, Jul. 2005.

[135] D. Dardari, C.-C. Chong, and M. Z. Win, "Threshold-based time-of-arrival estimators in UWB dense multipath channels," *IEEE Trans. Commun.*, vol. 56, 2008.

[136] Y. Shen and M. Z. Win, "Fundamental limits of wideband localization – Part I: A general framework," *IEEE Trans. Inform. Theory*, vol. 56, 2010.

[137] Y. Shen, H. Wymeersch, and M. Z. Win, "Fundamental limits of wideband localization – Part II: Cooperative networks," *IEEE Trans. Inform. Theory*, vol. 56, 2010.

[138] D. B. Jourdan, D. Dardari, and M. Z. Win, "Position error bound for UWB localization in dense cluttered environments," *IEEE Trans. Aerosp. Electron. Syst.*, vol. 44, no. 2, pp. 613–628, Apr. 2008.

[139] K. Yu and I. Oppermann, "An ultra wideband TAG circuit transceiver architecture," in *International Workshop on Ultra Wideband Systems. Joint UWBST and IWUWBS 2004.*, Kyoto, Japan, May 2004, pp. 258–262.

[140] S. Gezici, Z. Sahinoglu, H. Kobayashi, and H. V. Poor, *Ultrawideband Wireless Communications*. John Wiley & Sons, Inc., 2006, ch. Ultra Wideband Geolocation.

[141] J. Ianniello, "High-resolution multipath time delay estimation for broad-band random signals," *IEEE Transactions on Acoustics, Speech and Signal Processing*, vol. 36, no. 3, pp. 320–327, 1988.

[142] O. Bialer, D. Raphaeli, and A. Weiss, "Efficient time of arrival estimation algorithm achieving maximum likelihood performance in dense

multipath," *IEEE Transactions on Signal Processing*, vol. 60, no. 3, pp. 1241–1252, 2012.

[143] J.-Y. Lee and R. A. Scholtz, "Ranging in a dense multipath environment using an UWB radio link," *IEEE J. Select. Areas Commun.*, vol. 20, no. 9, pp. 1677–1683, Dec. 2002.

[144] I. Guvenc and Z. Sahinoglu, "Threshold-based TOA estimation for impulse radio UWB systems," in *Proc. IEEE Int. Conf. on Ultra-Wideband (ICUWB)*, Zurich, Switzerland, 2005, pp. 420–425.

[145] A. D'Amico, U. Mengali, and L. Taponecco, "Energy-based TOA estimation," *IEEE Transactions on Wireless Communications*, vol. 7, no. 3, pp. 838 –847, mar 2008.

[146] A. Rabbachin, I. Oppermann, and B. Denis, "ML time-of-arrival estimation based on low complexity UWB energy detection," in *Proc. IEEE Int. Conf. on Ultra-Wideband (ICUWB)*, Waltham, MA, Sep 2006, pp. 599–604.

[147] ——, "GML ToA estimation based on low complexity UWB energy detection," in *Proc. IEEE Int. Symp. on Personal, Indoor and Mobile Radio Commun.*, Sep. 2006, pp. 1 –5.

[148] Z. Lei, F. Chin, and Y.-S. Kwok, "UWB ranging with energy detectors using ternary preamble sequences," in *in Proc. of IEEE Wireless Communications and Networking Conference, WCNC 2006*, vol. 2, 2006, pp. 872–877.

[149] T. L. D'Amico A., Mengali U., "TOA estimation with pulses of unknown shape," in *in Proc. of IEEE International Conference on Communications, ICC '07*, Glasgow, UK, Jun. 2007, pp. 4287–4292.

[150] A. Sonnenschein and P. Fishman, "Radiometric detection of spread-spectrum signals in noise of uncertain power," *IEEE Transactions on Aerospace and Electronic Systems*, vol. 28, no. 3, pp. 654–660, 1992.

[151] R. Mills and G. Prescott, "A comparison of various radiometer detection models," *IEEE Transactions on Aerospace and Electronic Systems*, vol. 32, no. 1, pp. 467–473, 1996.

[152] V. Kostylev, "Energy detection of a signal with random amplitude," in *IEEE International Conference on Communications*, vol. 3. IEEE, 2002, pp. 1606–1610.

[153] D. Torrieri, "The radiometer and its practical implementation," in *Military communication conference*. IEEE, 2010, pp. 304–310.

[154] F. Digham, M. Alouini, and M. Simon, "On the energy detection of unknown signals over fading channels," *IEEE Transactions on Communications*, vol. 55, no. 1, pp. 21–24, 2007.

[155] V. Kostylev, "Characteristics of energy detection of quasideterministic radio signals," *Radiophysics and Quantum Electronics*, vol. 43, no. 10, pp. 833–839, 2000.

[156] J. Lehtomaki, M. Juntti, and H. Saarnisaari, "CFAR strategies for channelized radiometer," *IEEE Signal Processing Letters*, vol. 12, no. 1, pp. 13–16, 2005.

[157] R. Miller and C. Chang, "A modified Cramér-Rao bound and its applications (corresp.)," *IEEE Transactions on Information Theory*, vol. 24, no. 3, pp. 398–400, 1978.

[158] A. Catovic and Z. Sahinoglu, "The Cramer-Rao bounds of hybrid TOA/RSS and TDOA/RSS location estimation schemes," *IEEE Communications Letters*, vol. 8, no. 10, pp. 626–628, 2004.

[159] S. Gezici, H. Celebi, H. Poor, and H. Arslan, "Fundamental limits on time delay estimation in dispersed spectrum cognitive radio systems," *IEEE Transactions on Wireless Communication*, vol. 8, no. 1, pp. 78–83, 2009.

[160] Y. Karisan, D. Dardari, S. Gezici, A. D'Amico, and U. Mengali, "Range estimation in multicarrier systems in the presence of interference: Performance limits and optimal signal design," *IEEE Transactions on Wireless Communications*, vol. 10, no. 10, pp. 3321–3331, 2011.

[161] S. M. Kay, *Fundamentals of Statistical Processing: Estimation Theory*. Prentice-Hall Signal Processing Series, 1993, vol. 1.

[162] E. Weinstein and A. J. Weiss, "Fundamental limitations in passive time delay estimation - part II: Wide-band systems," *IEEE Trans. Acoust., Speech, Signal Processing*, vol. ASSP-32, no. 5, pp. 1064–1078, Oct. 1984.

[163] ——, "A general class of lower bounds in parameter estimation," *IEEE Trans. Inform. Theory*, vol. 34, no. 2, pp. 338–342, Mar. 1988.

[164] A. Zeira and P. M. Schultheiss, "Realizable lower bounds for time delay estimation," *IEEE Trans. Signal Processing*, vol. 41, no. 1, pp. 3102–3113, Nov. 1993.

[165] ——, "Realizable lower bounds for time delay estimation: Part 2-threshold phenomena," *IEEE Trans. Signal Processing*, vol. 32, no. 5, pp. 1001–1007, May 1994.

[166] J. Ziv and M. Zakai, "Some lower bounds on signal parameter estimation," *IEEE Trans. Inform. Theory*, vol. 15, no. 3, pp. 386–391, May 1969.

[167] S. Bellini and G. Tartara, "Bounds on error in signal parameter estimation," *IEEE Trans. Commun.*, vol. 22, no. 3, pp. 340–342, Mar. 1974.

[168] D. Chazan, M. Zakai, and J. Ziv, "Improved lower bounds on signal parameter estimation," *IEEE Trans. Inform. Theory*, vol. 21, no. 1, pp. 90–93, Jan. 1975.

[169] K. L. Bell, Y. Steinberg, Y. Ephraim, and H. L. V. Trees, "Extended Ziv-Zakai lower bound for vector parameter estimation," *IEEE Trans. Inform. Theory*, vol. 43, no. 2, pp. 624–637, Feb. 1997.

[170] D. Dardari, C.-C. Chong, and M. Z. Win, "Improved lower bounds on time-of-arrival estimation error in realistic UWB channels," in *Proc. IEEE Int. Conf. on Ultra-Wideband (ICUWB)*, Waltham, MA, Sep. 2006, pp. 531–537, .

[171] H. Anouar, A. M. Hayar, R. Knopp, and C. Bonnet, "Ziv-Zakai lower bound on the time delay estimation of UWB signals," in *in Proc. Int. Symposium on Commun., Control, and Signal Processing (ISCCSP)*, Marrakech, Morocco, Mar. 2006.

[172] B. M. Sadler, L. Huang, and Z. Xu, "Ziv-Zakai time delay estimation bound for ultra-wideband signals," in *IEEE International Conference on Acoustics, Speech and Signal Processing, 2007. ICASSP 2007*, vol. 3, Honolulu, HI, Apr. 2007, pp. 549–552.

[173] J. Zhang, R. A. Kennedy, and T. D. Abhayapala, "Cramer-Rao lower bounds for the time delay estimation of UWB signals," in *Proc. IEEE Int. Conf. on Commun.*, Paris, France, May 2004, pp. 3424–3428.

[174] Z. Xu and B. Sadler, "Time delay estimation bounds in convolutive random channels," *IEEE J. Sel. Topics in Signal Processing*, vol. 1, no. 3, pp. 418–430, Oct. 2007.

[175] D. Slepian, "On bandwidth," *Proc. IEEE*, vol. 64, no. 3, pp. 292–300, Mar. 1976.

[176] H. Landau and H. Pollak, "Prolate spheroidal wave functions, Fourier analysis and uncertainty: Part III," *Bell Sys. Tech. Journal*, vol. 41, pp. 1295–1336, 1962.

[177] L. Scharf and C. Demeure, *Statistical signal processing: detection, estimation, and time series analysis*, ser. Addison-Wesley Series in Electrical and Computer Engineering. Addison-Wesley Pub. Co., 1991.

[178] S. M. Kay, *Fundamentals of Statistical Processing: Detection Theory.* Prentice-Hall Signal Processing Series, 1993, vol. 2.

[179] B. Hu and N. Beaulieu, "Exact bit error rate analysis of TH-PPM UWB systems in the presence of multiple-access interference," *Communications Letters, IEEE*, vol. 7, no. 12, pp. 572–574, Dec. 2003.

[180] A. Giorgetti, M. Chiani, and M. Z. Win, "The effect of narrowband interference on wideband wireless communication systems," *IEEE Trans. Commun.*, vol. 53, no. 12, pp. 2139–2149, Dec. 2005.

[181] G. Corazza and R. Pedone, "Generalized and average likelihood ratio testing for post detection integration," *IEEE Transactions on Communications*, vol. 55, no. 11, pp. 2159–2171, 2007.

[182] C. W. Helstrom, *Statistical Theory of Signal Detection*, 2nd ed. Headington Hill Hall, Oxford: Pergamon Press, 1968.

[183] L. Scharf and B. Friedlander, "Matched subspace detectors," *IEEE Transactions on Signal Processing*, vol. 42, no. 8, pp. 2146 –2157, aug 1994.

[184] W. Davenport and W. Root, *An introduction to the theory of random signals and noise*, ser. Lincoln laboratory publications. IEEE Press, 1987.

[185] U. Grenander, H. Pollak, and D. Slepian, "The distribution of quadratic forms in normal variates: A small sample theory with applications to spectral analysis," *Journal of the Society for Industrial and Applied Mathematics*, vol. 7, no. 4, pp. 374–401, 1959.

[186] D. Slepian and H. Pollak, "Prolate spheroidal wave functions, Fourier analysis and uncertainty: Part I," *Bell Sys. Tech. Journal*, vol. 40, pp. 43–64, Jan. 1961.

[187] H. Landau and H. Pollak, "Prolate spheroidal wave functions, Fourier analysis and uncertainty: Part II," *Bell Sys. Tech. Journal*, vol. 40, pp. 65–84, Jan. 1961.

[188] D. Slepian and E. Sonnenblick, "Eigenvalues associated with prolate spheroidal wave functions of zero order," *Bell Sys. Tech. Journal*, vol. 44, 1965.

[189] D. Slepian, "Some comments on fourier analysis, uncertainty and modeling," *SIAM Review*, vol. 25, no. 3, pp. 379–393, Jul. 1983.

[190] C. E. Shannon, "Communications in the presence of noise," *Proc. IRE*, vol. 37, pp. 10–21, Jan. 1949.

[191] A. J. Jerri, "The Shannon sampling theorem – its various extensions and applications: A tutorial review," *Proc. IEEE*, vol. 65, no. 11, pp. 1565–1596, Nov. 1977.

[192] R. Gallager, *Principles of Digital Communication*. Cambridge University Press, 2008.

[193] M. Chiani, "Integral representation and bounds for Marcum Q-function," *Electronics Letters*, vol. 35, no. 6, pp. 445 –446, Mar. 1999.

[194] G. Corazza and G. Ferrari, "New bounds for the Marcum Q-function," *IEEE Transactions on Information Theory*, vol. 48, no. 11, pp. 3003 – 3008, Nov. 2002.

[195] P. Borjesson and C.-E. Sundberg, "Simple approximations of the error function Q(x) for communications applications," *IEEE Transactions on Communications*, vol. 27, no. 3, pp. 639 – 643, mar. 1979.

[196] W. Lindsey, "Error probabilities for rician fading multichannel reception of binary and N-ary signals," *IEEE Trans. Inform. Theory*, pp. 339 – 350, Oct. 1964.

[197] G. Watson, *A Treatise on the Theory of Bessel Functions*, ser. Cambridge Mathematical Library. Cambridge University Press, 1966.

[198] J. J. Caffery and G. L. Stuber, "Overview of radiolocation in CDMA cellular systems," *IEEE Commun. Mag.*, vol. 36, no. 4, pp. 38–45, Apr. 1998.

[199] K. Pahlavan, X. Li, and J.-P. Makela, "Indoor geolocation science and technology," *IEEE Commun. Mag.*, vol. 40, pp. 112–118, Feb. 2002.

[200] R. J. Fontana and S. J. Gunderson, "Ultra-wideband precision asset location system," *Proc. of IEEE Conf. on Ultra Wideband Systems and Technologies (UWBST)*, vol. 21, no. 1, pp. 147–150, May 2002.

[201] L. Stoica, A. Rabbachin, H. O. Repo, T. S. Tiuraniemi, and I. Oppermann, "An ultrawideband system architecture for tag based wireless sensor networks," *IEEE Trans. Veh. Technol.*, vol. 54, no. 5, pp. 1632–1645, Sep. 2005.

[202] K. Pahlavan, F. O. Akgul, M. Heidari, A. Hatami, J. M. Elwell, and R. D. Tingley, "Indoor geolocation in the absence of direct path," *IEEE Wireless Communications*, vol. 13, no. 6, pp. 50–58, Dec. 2006.

[203] I. Guvenc and C.-C. Chong, "A survey on TOA based wireless localization and NLOS mitigation techniques," *IEEE Communications Surveys Tutorials*, vol. 11, no. 3, pp. 107 –124, quarter 2009.

[204] S. Marano and, W. Gifford, H. Wymeersch, and M. Win, "NLOS identification and mitigation for localization based on UWB experimental data," *IEEE Journal on Selected Areas in Communications*, vol. 28, no. 7, pp. 1026 –1035, Sep. 2010.

[205] H. Chen, G. Wang, Z. Wang, H. So, and H. Poor, "Non-line-of-sight node localization based on semi-definite programming in wireless sensor networks," *IEEE Transactions on Wireless Communications*, vol. 11, no. 1, pp. 108 –116, Jan. 2012.

[206] H. Wymeersch, J. Lien, and M. Z. Win, "Cooperative localization in wireless networks," *Proc. IEEE*, 2009.

[207] A. Sendonaris, E. Erkip, and B. Aazhang, "User cooperation diversity. Part I. System description," *IEEE Trans. Commun.*, vol. 51, no. 11, pp. 1927–1938, Nov. 2003.

[208] J. Laneman, D. Tse, and G. Wornell, "Cooperative diversity in wireless networks: Efficient protocols and outage behavior," *IEEE Trans. Inform. Theory*, vol. 50, no. 12, pp. 3062–3080, Dec. 2004.

[209] A. Bletsas, H. Shin, and M. Z. Win, “Cooperative communications with outage-optimal opportunistic relaying,” *IEEE Trans. Wireless Commun.*, vol. 6, no. 9, pp. 3450–3460, Sep. 2007.

[210] M. Dohler, A. Gkelias, and A. Aghvami, “Capacity of distributed PHY-layer sensor networks,” *IEEE Transactions on Vehicular Technology*, vol. 55, no. 2, pp. 622 – 639, Mar. 2006.

[211] Y. Shen, S. Mazuelas, and M. Win, “Network navigation: Theory and interpretation,” *IEEE Journal on Selected Areas in Communications*, vol. 30, no. 9, pp. 1823 –1834, Oct. 2012.

[212] H. Hashemi, “The indoor radio propagation channel,” *Proc. IEEE*, vol. 81, no. 7, pp. 943–968, Jul. 1993.

[213] J.-F. Lemieux, M. El-Tanany, and H. Hafez, “Experimental evaluation of space /frequency /polarization diversity in the indoor wireless channel,” *IEEE Trans. on Veh. Technol.*, vol. 40, no. 3, pp. 569–574, Aug. 1991.

[214] J. B. Andersen, T. S. Rappaport, and S. Yoshida, “Propagation measurements and models for wireless communications channels,” *IEEE Commun. Mag.*, vol. 33, no. 1, pp. 42–49, Jan. 1995.

[215] F. van der Wijk, A. Kegel, and R. Prasad, “Assessment of a picocellular system using propagation measurements at 1.9 GHz for indoor wireless communications,” *IEEE Trans. on Veh. Technol.*, vol. 44, no. 1, pp. 155–162, Feb. 1995.

[216] I. Khan and P. S. Hall, “Experimental evaluation of MIMO capacity and correlation for narrowband body-centric wireless channels,” *IEEE Trans. Antennas Propagat.*, vol. 58, no. 1, pp. 195–202, Jan. 2010.

[217] Q. Spencer, B. Jeffs, M. Jensen, and A. Swindlehurst, “Modeling the statistical time and angle of arrival characteristics of an indoor multipath channel,” *IEEE J. Select. Areas Commun.*, vol. 18, no. 3, pp. 347–360, Mar. 2000.

[218] R. J.-M. Cramer, R. A. Scholtz, and M. Z. Win, “An evaluation of the ultra -wideband propagation channel,” *IEEE Trans. Antennas Propagat.*, vol. 50, no. 5, pp. 561–570, May 2002.

[219] C.-C. Chong and S. K. Yong, “A generic statistical-based UWB channel model for high-rise apartments,” *IEEE Trans. Antennas Propagat.*, vol. 53, no. 8, pp. 2389–2399, Aug. 2005.

[220] L. Yang and G. B. Giannakis, "Ultra-wideband communications: an idea whose time has come," *IEEE Signal Processing Mag.*, vol. 21, no. 6, pp. 26–54, Nov. 2004.

[221] L. Stoica, A. Rabbachin, and I. Oppermann, "A low-complexity noncoherent IR-UWB transceiver architecture with TOA estimation," *IEEE Trans. Microwave Theory Tech.*, vol. 54, no. 4, pp. 1637–1646, Jun. 2006.

[222] D. Dardari, "Pseudo-random active UWB reflectors for accurate ranging," *IEEE Commun. Lett.*, vol. 8, no. 10, pp. 608–610, Oct. 2004.

[223] C. Falsi, D. Dardari, L. Mucchi, and M. Z. Win, "Time of arrival estimation for UWB localizers in realistic environments," *EURASIP J. Appl. Signal Processing (Special Issue on Wireless Location Technologies and Applications)*, pp. 1–13, 2006.

[224] K. Yu and I. Oppermann, "Performance of UWB position estimation based on time-of-arrival measurements," in *International Workshop on Ultra Wideband Systems. Joint UWBST and IWUWBS 2004.*, Oulu, Finland, May 2004, pp. 400–404.

[225] B. Alavi and K. Pahlavan, "Modeling of the TOA-based distance measurement error using UWB indoor radio measurements," *IEEE Commun. Lett.*, vol. 10, no. 4, pp. 275–277, 2006.

[226] Y. Shen and M. Z. Win, "Energy efficient location-aware networks," in *Proc. IEEE Int. Conf. on Commun.*, Beijing, CHINA, May 2008, pp. 2995–3001.

[227] J. Schroeder, S. Galler, K. Kyamakya, and T. Kaiser, "Three-dimensional indoor localization in non line of sight UWB channels," in *IEEE International Conference on Ultra-Wideband, ICUWB 2007*, Singapore, Sep. 2007.

[228] D. Dardari, A. Conti, J. Lien, and M. Win, "The effect of cooperation in UWB based positioning systems using experimental data," *EURASIP Journal On Advances In Signal Processing*, 2008.

[229] A. Muqaibel, A. Safaai-Jazi, A. Bayeam, A. M. Attiya, and S. M. Riad, "Ultrawideband through-the-wall propagation," *IEE Proc. Microw. Antennas Propag.*, vol. 152, no. 6, pp. 581–588, Dec. 2005.

[230] P. Protiva, J. Mrkvica, and J. Machac, "Estimation of wall parameters from time-delay-only through-wall radar measurements," *IEEE Transactions on Antennas and Propagation*, vol. 59, no. 11, pp. 4268 –4278, Nov. 2011.

[231] S. Gezici, H. Kobayashi, and H. Poor, "Nonparametric non-line-of-sight identification," in *IEEE 58th Vehicular Technology Conference*, vol. 4, Oct. 2003.

[232] I. Guvenc, C.-C. Chong, and F. Watanabe, "NLOS identification and mitigation for UWB localization systems," in *in Proc. IEEE Wireless Commun. Networking Conf. (WCNC)*, Hong Kong, Mar. 2007.

[233] I. Guvenc, C.-C. Chong, F. Watanabe, and H. Inamura, "NLOS identification and weighted least-squares localization for UWB systems using multipath channel statistics," *EURASIP Journal on Advances in Signal Processing*, 2008.

[234] J. Borras, P. Hatrack, and N. B. Mandayam, "Decision theoritic framework for NLOS identification," in *Proc. 48th Annual Int. Veh. Technol. Conf.*, vol. 2, Ottawa, Canada, May 1998, pp. 1583–1587.

[235] A. Maali, A. Ouldali, H. Mimoun, and G. Baudoin, "Joint TOA estimation and NLOS identification for UWB localization systems," in *Third International Conference on Sensor Technologies and Applications*, Jun. 2009, pp. 212–216.

[236] M. Heidari, F. Akgul, and K. Pahlavan, "Identification of the absence of direct path in indoor localization systems," in *IEEE 18th International Symposium on Personal, Indoor and Mobile Radio Communications*, Sep. 2007, pp. 1–6.

[237] M. Heidari, F. Akgul, N. Alsindi, and K. Pahlavan, "Neural network assisted identification of the absence of direct path in indoor localization," in *IEEE Global Telecommunications Conference*, Nov. 2007, pp. 387–392.

[238] A. Maali, H. Mimoun, G. Baudoin, and A. Ouldali, "A new low complexity NLOS identification approach based on UWB energy detection," in *IEEE Radio and Wireless Symposium*, Jan. 2009, pp. 675–678.

[239] S. Venkatesh and R. Buehrer, "Non-line-of-sight identification in ultra-wideband systems based on received signal statistics," *Microwaves, Antennas & Propagation, IET*, vol. 1, no. 6, pp. 1120–1130, Dec. 2007.

[240] K. Yu and Y. Guo, "Non-line-of-sight detection based on TOA and signal strength," in *Personal, Indoor and Mobile Radio Communications, 2008. PIMRC 2008. IEEE 19th International Symposium on*, Sept. 2008, pp. 1–5.

[241] ——, "Statistical NLOS identification based on AOA, TOA, and signal strength," *Vehicular Technology, IEEE Transactions on*, vol. 58, no. 1, pp. 274–286, Jan. 2009.

[242] S. Marano, W. M. Gifford, H. Wymeersch, and M. Z. Win, "Nonparametric obstruction detection for UWB localization," in *IEEE Global Telecommunications Conference*, 2009.

[243] H. Wymeersch, S. Maranó, W. Gifford, and M. Win, "A machine learning approach to ranging error mitigation for uwb localization," *IEEE Transactions on Communications*, vol. 60, no. 6, pp. 1719 –1728, Jun. 2012.

[244] R. Pabst, B. Walke, D. Schultz, P. Herhold, H. Yanikomeroglu, S. Mukherjee, H. Viswanathan, M. Lott, W. Zirwas, M. Dohler, H. Aghvami, D. Falconer, and G. Fettweis, "Relay-based deployment concepts for wireless and mobile broadband radio," *IEEE Communications Magazine*, vol. 42, no. 9, pp. 80 – 89, Sep. 2004.

[245] J. Laneman and G. Wornell, "Distributed space-time-coded protocols for exploiting cooperative diversity in wireless networks," *IEEE Trans. Inform. Theory*, vol. 49, no. 10, pp. 2415–2425, Oct. 2003.

[246] G. Farhadi and N. Beaulieu, "On the ergodic capacity of multi-hop wireless relaying systems," *IEEE Transactions on Wireless Communications*, vol. 8, no. 5, pp. 2286 –2291, May. 2009.

[247] A. Sendonaris, E. Erkip, and B. Aazhang, "User cooperation diversity. Part I. system description," *IEEE Transactions on Communications*, vol. 51, no. 11, pp. 1927 – 1938, Nov. 2003.

[248] L. Reggiani, M. Rydstrom, E. Strom, and A. Svensson, "An algorithm for mapping the positions of point scatterers," in *5th IEEE Sensor Array and Multichannel Signal Processing Workshop*, Jul. 2008, pp. 63 –67.

[249] M. Rydstrom, E. Strom, A. Svensson, and L. Reggiani, "An algorithm for positioning relays and point scatterers in wireless systems," *IEEE Signal Processing Letters*, vol. 15, pp. 381 –384, 2008.

[250] L. Reggiani, M. Rydstrom, G. Tiberi, E. G. Strom, and A. Monorchio, "Ultra-wide band sensor networks for tracking point scatterers or relays," in *ISWCS'09*, 2009, pp. 1–5.

[251] P. Meissner, C. Steiner, and K. Witrisal, "UWB positioning with virtual anchors and floor plan information," in *7th Workshop on Positioning, Navigation and Communication*, Dresden, Germany, Mar. 2010, pp. 1–7.

[252] Z. Sahinoglu, "Method and system for target positioning and tracking in cooperative relay networks," U.S. Patent US 2010/0 177 681 A1, Jul. 15, 2010.

[253] L. W. Fullerton, M. D. Roberts, W. M. Einhorn, K. Loum, I. Dodoukh, and S. S. O'Hanian, "Method and system for extensible position location," U.S. Patent US 7,602,339 B2, Oct. 13, 2009.

[254] C. Villien and D. Norbert, "Systeme de radiolocalisation/posionment au moyen d'un resau ad hoc," France Patent 2 924 818/ 07 59 611, Jun. 12, 2009.

[255] M. D. Westrick and D. L. Sands, "RF passive repeater for a metal container," U.S. Patent US 2007/0 262 868, Nov. 15, 2007.

[256] N. E. Buris, R. S. Rachwalski, and W. J. Turney, "Passive repeater for radio frequency communications," U.S. Patent 7,429,953, Sep. 30, 2008.

[257] M. R. Nicholson, N. E. Jones, and E. A. Jesser, "RFID passive repeater system and apparatus," U.S. Patent 6,563,425, May 13, 2003.

[258] Y. Huang, N. Yi, and X. Zhu, "Investigation of using passive repeaters for indoor radio coverage improvement," in *Proc. of the IEEE Antennas and Propagation Society International Symposium, 2004*, vol. 2, Jun. 2004, pp. 1623 – 1626 Vol.2.

[259] M. Nakagawa, "UWB repeater with pulse delay and UWB communication system," U.S. Patent US 7,359,673 B2, Apr. 15, 2008.

[260] S. Niranjayan, A. Nallanathan, and B. Kannan, "Modeling of multiple access interference and BER derivation for TH and DS UWB multiple access systems," *IEEE Transactions on Wireless Communications*, vol. 5, no. 10, pp. 2794 –2804, Oct. 2006.

[261] I. Hosseini and N. Beaulieu, “Bit error rate of TH-BPSK UWB receivers in multiuser interference,” *IEEE Transactions on Wireless Communications*, vol. 8, no. 10, pp. 4916 –4921, Oct. 2009.

[262] P. Pinto, A. Giorgetti, M. Win, and M. Chiani, “A stochastic geometry approach to coexistence in heterogeneous wireless networks,” *IEEE Journal on Selected Areas in Communications*, vol. 27, no. 7, pp. 1268 –1282, Sep. 2009.

[263] D. Dardari, A. Giorgetti, and M. Z. Win, “Time-of-arrival estimation of UWB signals in the presence of narrowband and wideband interference,” in *Proc. IEEE Int. Conf. on Ultra-Wideband (ICUWB)*, Singapore, Sep. 2007.

[264] “Ubisense limited,” *www.ubisense.net.*

[265] R. A. Horn and C. R. Johnson, *Matrix Analysis*, 1st ed. Cambridge: Cambridge University Press, 1990.

[266] J. Langley, P. Hall, and P. Newham, “Balanced antipodal Vivaldi antenna for wide bandwidth phased arrays,” *IEE Proc. on Microwave and Antennas Propagation*, vol. 143, no. 2, Apr. 1996.

[267] S. Bories, C. Delaveaud, and H. Jacquinot, “Low profile and directive UWB antenna,” in *3rd European Conference on Antennas and Propagation, 2009*, Mar. 2009, pp. 1632 –1635.

[268] A. Waadt, A. Burnic, D. Xu, C. Kocks, S. Wang, and P. Jung, “Analysis of RSSI based positioning with multiband OFDM UWB,” in *Future Network and Mobile Summit, 2010*, Jun. 2010, pp. 1 –8.

[269] B. Dewberry and W. Beeler, “Increased ranging capacity using ultrawideband direct-path pulse signal strength with dynamic recalibration,” in *Position Location and Navigation Symposium*, Apr. 2012, pp. 1013 –1017.

[270] J. Mentzer, W. DeWitt, J. Keebler, S. Min, N. Nix, C. Smith, and Z. Zacharia, “Defining supply chain management,” *Journal of Business logistics*, vol. 22, no. 2, pp. 1–25, 2001.

[271] D. Dardari and R. D’Errico, “Passive Ultrawide Bandwidth RFID,” in *Proc. IEEE Global Telecomm. Conf.*, Dec. 2008, pp. 1 –6.

[272] D. Arnitz, U. Muehlmann, and K. Witrisal, “UWB ranging in passive UHF RFID: proof of concept,” *Electronics Letters*, vol. 46, no. 20, pp. 1401 –1402, 30 2010.

[273] N. Patwari and J. Wilson, “RF sensor networks for device-free localization: Measurements, models, and algorithms,” *Proc. IEEE*, vol. 98, no. 11, pp. 1961 –1973, Nov. 2010.

[274] E. Paolini, A. Giorgetti, M. Chiani, R. Minutolo, and M. Montanari, “Localization capability of cooperative anti-intruder radar systems,” *EURASIP Journal on Advances in Signal Processing, Special Issue on Cooperative Localization in Wireless Ad Hoc and Sensor Networks*, 2008.

[275] J. Liang and Q. Liang, “Design and analysis of distributed radar sensor networks,” *IEEE Trans. on Parallel and Distributed Systems*, vol. 22, no. 11, pp. 1926 –1933, Nov. 2011.

[276] M. Arik and O. Akan, “Collaborative mobile target imaging in UWB wireless radar sensor networks,” *IEEE J. Select. Areas Commun.*, vol. 28, no. 6, pp. 950 –961, Aug. 2010.

[277] J. Li, Z. Zeng, J. Sun, and F. Liu, “Through-wall detection of human being’s movement by UWB radar,” *IEEE Geoscience and Remote Sensing Letters*, vol. 9, no. 6, pp. 1079 –1083, Nov. 2012.

[278] A. Yarovoy, L. Ligthart, J. Matuzas, and B. Levitas, “UWB radar for human being detection,” *IEEE Aerospace and Electronic Systems Mag.*, vol. 21, no. 3, pp. 10 – 14, Mar. 2006.

[279] V. Casadei, N. Nanna, and D. Dardari, “Experimental study in breath detection and human target ranging in the presence of obstacles using ultra-wideband signals,” *International Journal of Ultra Wideband Communications and Systems - Special Issue on Applications of Ultra Wideband Technology in Healthcare*, vol. 2, no. 2, pp. 116–123, 2011.

[280] I. Immoreev, S. Samkov, and T.-H. Tao, “Short-distance ultra wideband radars,” *IEEE Aerospace and Electronic Systems Magazine*, vol. 20, no. 6, pp. 9–14, Jun. 2005.

[281] R. Zetik, J. Sachs, and R. Thoma, “UWB short-range radar sensing - the architecture of a baseband, pseudo-noise UWB radar sensor,” *IEEE Instrumentation & Measurement Magazine*, vol. 10, no. 2, pp. 39–45, Apr. 2007.

[282] S. Bartoletti, A. Conti, and A. Giorgetti, “Analysis of UWB radar sensor networks,” in *Proc. IEEE Int. Conf. on Commun.*, May 2010, pp. 1 –6.

[283] R. D’Errico, “An indoor backscattering channel characterization for UWB passive RFID applications,” in *European Conf. on Antennas and Prop.*, Mar. 2012, pp. 1169 –1173.

[284] A. Sibille, M. Sacko, Z. Mhanna, F. Guidi, and C. Roblin, “Joint antenna-channel statistical modeling of UWB backscattering RFID,” in *IEEE International Conference on Ultra-Wideband*, Sep. 2011, pp. 474 –478.

[285] D. Dardari, F. Guidi, C. Roblin, and A. Sibille, “Ultra-wide bandwidth backscatter modulation: Processing schemes and performance,” *EURASIP Journal on Wireless Communications and Networking*, vol. 2011, no. 1, 2011.

[286] S. Bartoletti and A. Conti, “Passive network localization via UWB wireless sensor radars: The impact of TOA estimation,” in *Proc. IEEE Int. Conf. on Ultra-Wideband (ICUWB)*, Sep. 2011, pp. 258 –262.

[287] M. Chiani, A. Giorgetti, M. Mazzotti, R. Minutolo, and E. Paolini, “Target detection metrics and tracking for UWB radar sensor networks,” in *Proc. IEEE Int. Conf. on Ultra-Wideband (ICUWB)*, 2009, pp. 469–474.

[288] H. M. M. T. Raza, A. H. Akbar, S. A. Chaudhry, G. Bag, S.-W. Yoo, and K.-H. Kim, “A yaw rate aware sensor wakeup protocol (YAP) for target prediction and tracking in sensor networks,” in *Proc. Military Commun. Conf.*, Oct. 2007, pp. 1 –7.

[289] I. Bradaric, G. Capraro, D. Weiner, and M. Wicks, “Multistatic radar systems signal processing,” in *IEEE Conference on Radar*, Apr. 2006.

[290] F. Muller, R. Farias, C. Sobrinho, and V. Dmitriev, “Multistatic radar with ultra-wideband pulses: FDTD simulation,” in *International Conference on Microwave and Optoelectronics*, Jul. 2005, pp. 574 – 577.

[291] C. Berger, B. Demissie, J. Heckenbach, P. Willett, and S. Zhou, “Signal processing for passive radar using OFDM waveforms,” *IEEE J. Sel. Topics in Signal Processing*, vol. 4, no. 1, pp. 226 –238, Feb. 2010.

[292] F. Guidi, D. Dardari, C. Roblin, and A. Sibille, "Backscatter communication using ultrawide bandwidth signals for RFID applications," in *20th Tyrrhenian Workshop on Digital Communications*, Pula, Sardinia, ITALY, Sep. 2009.

[293] Federal Communications Commission, "Revision of part 15 of the commission's rules regarding ultra-wideband transmission systems, first report and order (ET Docket 98-153)," Adopted Feb. 14, 2002, Released Apr. 22, 2002.

[294] C. Xu and C. L. Law, "TOA estimator for UWB backscattering RFID system with clutter suppression capability," *EURASIP Journal on Wireless Communications and Networking*, 2010.

[295] V. Heiries, K. Belmkaddem, F. Dehmas, B. Denis, L. Ouvry, and R. D'Errico, "UWB backscattering system for passive RFID tag ranging and tracking," in *Proc. IEEE Int. Conf. on Ultra-Wideband (ICUWB)*, Sep. 2011, pp. 489 –493.

[296] F. Guidi, M. Sacko, A. Sibille, and C. Roblin, "Analysis of UWB RFID tag backscattering in the presence of scatterers," in *General Assembly and Scientific Symposium*, Aug. 2011, pp. 1 –4.

[297] D. Sarwate and M. Pursley, "Crosscorrelation properties of pseudorandom and related sequences," *Proceedings of the IEEE*, vol. 68, no. 5, pp. 593 – 619, May 1980.

[298] P. Fan, "Spreading sequence design and theoretical limits for quasisynchronous CDMA systems," *EURASIP Journal on Wireless Communications and Networking*, vol. 2004, no. 1, 2004.

[299] D. Lachartre, B. Denis, D. Morche, L. Ouvry, M. Pezzin, B. Piaget, J. Prouve, and P. Vincent, "A 1.1nJ/b 802.15.4a-Compliant Fully Integrated UWB Transceiver in 0.13 μm CMOS," in *Proc. of the ISSCC 2009*, San Francisco, Feb. 2009.

[300] H. Donelan and T. O'Farrell, "Method for generating sets of orthogonal sequences," *Electronics Letters*, vol. 35, no. 18, pp. 1537 –1538, Sep. 1999.

[301] R. De Gaudenzi, C. Elia, and R. Viola, "Bandlimited quasi-synchronous CDMA: a novel satellite access technique for mobile and personal communication systems," *IEEE Journal on Selected Areas in Communications*, vol. 10, no. 2, pp. 328 –343, Feb. 1992.

Acknowledgments

At the end of this PhD I'd like to thank all the people who made it possible.

First of all prof. Davide Dardari for his support and his daily presence in my work, and prof. Marco Chiani for his suggestions and the possibility of this experience.

I'd like to give special thanks to Andrea (Mario) and Francesco (Guido), who shared with me these years of work, and much more. What a team!

Thanks to my colleagues at Cesena, Simone, Vincenzo, Anna, Matteo, Enrico, Andrea G. and the others who cooperated with me, in particular Andrea C. and the partners of SELECT project.

Thanks to prof. Moe Win for the great opportunity of visiting MIT, for his kind hospitality and the fruitful discussions. Thank you to my lab-mate, Henghui, and to the other colleagues, Ae, Alberto, Santi, Yuan, Jowoon, Jemin, Tianheng, Wenhan, Steven, Andrew, Dongwoo and Shervin.

A big thanks to my family, Rosi and all my fantastic friends who shared and share their life with me, making every day exciting and wonderful.